



2009

# EXPERIMENTAL AND MOLECULAR DYNAMICS SIMULATION STUDIES OF PARTITIONING AND TRANSPORT ACROSS LIPID BILAYER MEMBRANES

Ravindra Wadhupal Tejawani

*University of Kentucky*, [tejwanir@gmail.com](mailto:tejwanir@gmail.com)

**[Click here to let us know how access to this document benefits you.](#)**

---

## Recommended Citation

Tejawani, Ravindra Wadhupal, "EXPERIMENTAL AND MOLECULAR DYNAMICS SIMULATION STUDIES OF PARTITIONING AND TRANSPORT ACROSS LIPID BILAYER MEMBRANES" (2009). *University of Kentucky Doctoral Dissertations*. 738.

[https://uknowledge.uky.edu/gradschool\\_diss/738](https://uknowledge.uky.edu/gradschool_diss/738)

This Dissertation is brought to you for free and open access by the Graduate School at UKnowledge. It has been accepted for inclusion in University of Kentucky Doctoral Dissertations by an authorized administrator of UKnowledge. For more information, please contact [UKnowledge@lsv.uky.edu](mailto:UKnowledge@lsv.uky.edu).

ABSTRACT OF DISSERTATION

Ravindra Wadhupal Tejwani

The Graduate School  
University of Kentucky

2009

EXPERIMENTAL AND MOLECULAR DYNAMICS SIMULATION STUDIES OF  
PARTITIONING AND TRANSPORT ACROSS LIPID BILAYER MEMBRANES

---

ABSTRACT OF DISSERTATION

---

A dissertation submitted in partial fulfillment of the  
requirements for the degree of Doctor of Philosophy in the  
College of Pharmacy  
at the University of Kentucky

By  
Ravindra Wadhupal Tejwani  
Lexington, Kentucky

Director: Dr. Bradley D. Anderson, Professor of Pharmaceutical Sciences  
Lexington, Kentucky

2009

Copyright © Ravindra W. Tejwani 2009

## ABSTRACT OF DISSERTATION

### EXPERIMENTAL AND MOLECULAR DYNAMICS SIMULATION STUDIES OF PARTITIONING AND TRANSPORT ACROSS LIPID BILAYER MEMBRANES

Most drugs undergo passive transport during absorption and distribution in the body. It is desirable to predict passive permeation of future drug candidates in order to increase the productivity of the drug discovery process. Unlike drug-receptor interactions, there is no receptor map for passive permeability because the process of transport across the lipid bilayer involves multiple mechanisms. This work intends to increase the understanding of permeation of drug-like molecules through lipid bilayers.

Drug molecules in solution typically form various species due to ionization, complexation, etc. Therefore, species specific properties must be obtained to bridge the experiment and simulations. Due to the volume contrast between intra- and extraventricular compartments of liposomes, minor perturbations in ionic and binding equilibria become significant contributors to transport rates. Using tyramine as a model amine, quantitative numerical models were developed to determine intrinsic permeability coefficients. The microscopic ionization and binding constants needed for this were independently measured. The partition coefficient in 1,9-decadiene was measured for a series of compounds as a quantitative surrogate for the partitioning into the hydrocarbon region of the bilayer. These studies uncovered an apparent long-range interaction between the two polar substituents that caused deviations in the microscopic pKa values and partition coefficient of tyramine from the expected values. Additionally the partition coefficients in the preferred binding region of the bilayer were also measured by equilibrium uptake into liposomes.

All-atom molecular dynamics simulations of lipid bilayers containing tyramine, 4-ethylphenol, or phenylethylamine provided free energies of transfer of these solutes from water to various locations on the transport path. The experimentally measured partition coefficients were consistent with the free energy profiles in showing the barrier in the hydrocarbon region and preferred binding region near the interface. The substituent contributions to these free energies were also quantitatively consistent between the experiments and simulations. Specific interactions between solutes and the bilayer suggest that amphiphiles are likely to show preferred binding in the head group region and that the most of hydrogen bonds involving solutes located inside the bilayer are with

water molecules. Solute re-orientation inside the bilayer lowers the partitioning barrier by allowing favorable interactions.

**KEYWORDS:** Permeability Coefficient, Partition Coefficient, Molecular Dynamics Simulation, Lipid Bilayer, Ionization Constant

---

Student's Signature

---

Date

EXPERIMENTAL AND MOLECULAR DYNAMICS SIMULATION STUDIES OF  
PARTITIONING AND TRANSPORT ACROSS LIPID BILAYER MEMBRANES

By

Ravindra Wadhupal Tejawani

---

Director of Dissertation

---

Director of Graduate Studies

---

Date



DISSERTATION

Ravindra Wadhupal Tejwani

The Graduate School

University of Kentucky

2009



EXPERIMENTAL AND MOLECULAR DYNAMICS SIMULATION STUDIES OF  
PARTITIONING AND TRANSPORT ACROSS LIPID BILAYER MEMBRANES

---

DISSERTATION

---

A dissertation submitted in partial fulfillment of the  
requirements for the degree of Doctor of Philosophy in the  
College of Pharmacy  
at the University of Kentucky

By  
Ravindra Wadhupal Tejwani

Lexington, Kentucky

Director: Dr. Bradley D. Anderson, Professor of Pharmaceutical Sciences

Lexington, Kentucky

2009

Copyright © Ravindra W. Tejwani 2009

*For Amrita and Monica, in the loving memory of my parents*

## Acknowledgements

While computers and the internet have shrunk the long distances, working with long distance students can be a challenge. I appreciate the open mindedness of the UKY faculty and especially Dr. Anderson in working with this unconventional arrangement. I am grateful to Dr. Anderson for his guidance throughout the last six years, his teaching of the technical knowledge that I am proud of, and his patience in working with my erratic productivity due to my part time commitment. I am thankful to him for letting me be a part of the research group that is exceptionally bright and knowledgeable.

I am grateful to Terry Stouch for teaching the fundamentals of computer simulations and converting a novice such as me to run large scale MD simulation studies. Initiating and completing three large scale simulations lasting almost three years could not have been possible without Terry's enthusiasm and expertise. An undertaking this big can only be tackled with programming and the bugs would have kept me at the keyboard a great deal longer if it wasn't for help from Malcolm Davis. I am indebted to him for teaching me Pearl scripts.

Thanks are due to the dissertation committee: Drs. Bummer, Spielmann, Xiang, and Li for their sincere critique of the dissertation and being available for periodic data review meetings through these years. Their patience as well as the time is sincerely appreciated.

The multidisciplinary nature of the dissertation topic has required me to tap into expertise of several individuals. In this respect, I would like to thank Dr. Xiang for being available to tap into his knowledge of lipid bilayer related experiments, William Pitts for answering questions regarding chemical syntheses, Greg Stiegler and Saverio Vacca for

computer hardware related help, John Carpenter and Steve Plimpton for Lammgs software, Sharon Callahan and Sarah Traeger for answering questions regarding NMR instrumentation, and Catina Rossoll for her help with the graduate school paperwork.

I am grateful to my mentors at the Bristol-Myers Squibb Company for continuously encouraging me to obtain the doctoral degree. In particular, thanks are due to Drs. Nancy Barbour, Abu Serajuddin, Sailesh Varia, and Joseph Bogardus for writing testimonials for the admission and fellowship applications. I am particularly thankful to Dr. Srinivasan Venkatesh for suggesting UKY for the degree and for crystallizing the necessary initial steps for obtaining the approvals. I am thankful to the Bristol-Myers Squibb Company for the Doctoral Fellowship and to Dr. Scott Biller for his guidance and support in requesting for the same. Finally I am thankful to the supervisors at the company, specifically Jatin Patel and Omar Sprockel for allowing me to take vacations and leaves whenever the needs arose.

Appreciation is due to the extended family and friends who frequently inquired about the progress of my research and shared their good wishes and offered support during difficult times.

Most important of all I am sincerely thankful to Monica and Amrita, for their unconditional love. They waited for me when I worked late, and were there whenever I wanted to take a break from office or graduate school work. Without their firm support, the combined stress of work and study would have been impossible to handle.

## Table of Contents

Acknowledgements	iii
List of Tables	vii
List of Figures	viii
Chapter One: Introduction	1
Background and significance	1
Solubility diffusion theory and the need for identification of a barrier domain	2
Non-classical hydrophobicity	4
Intrinsic and apparent permeability coefficients	4
Lipid bilayers as drug delivery devices	5
Molecular level understanding of the transport and the retention	5
Chapter Two: Statement of aims	10
Chapter Three: Influence of intravesicular pH drift and membrane binding on the liposomal release of a model amine containing permeant	12
Introduction	12
Materials and methods	13
Theoretical	19
Results	25
Discussion	30
Conclusion	39
Chapter Four: Substituent effects on solute ionization, partitioning into hydrocarbon, and binding to the lipid bilayer membranes. Electrostatic effects dependent on conformation	66
Introduction	66
Materials and methods	70
Results and discussion	76
Conclusion	86
Chapter Five: Partitioning of solute from water to various locations in the lipid bilayer: A comparison of results from the simulation and the experiment	113
Introduction	113
Methods and theoretical	117
Results and discussion	125
Conclusion	140

Chapter Six: Specific intermolecular solute-bilayer interactions as determined by MD simulations: Factors responsible for the locations of the transport barrier and the preferred binding regions	171
Introduction	171
Methods and theoretical	175
Results	178
Discussion	184
Conclusion	191
Chapter Seven: Conclusions and future directions	248
Experimental models for permeation and partitioning	248
Molecular dynamics simulations for partitioning into DOPC bilayers	250
Appendices	
Appendix One: Additional notes on the volume contrast between intravesicular and extravesicular compartments	254
Appendix Two: Alternative hypotheses evaluated in chapter three	259
References and bibliography	263
Vita	292

## List of Tables

Table 3-1.	Microscopic and macroscopic ionization constants for tyramine (Figure 3-2). Values in parentheses are standard deviations.	41
Table 3-2.	Summary of intrinsic permeability coefficients and fitting statistics obtained from nonlinear regression analyses of the combined data for tyramine transport employing various models	42
Table 4-1.	Chemical structures, negative logarithms of the (microscopic) ionization constants, logarithms of liposome/water partition coefficients ( $K_{lipo}$ ), and logarithms of intrinsic 1,9-decadiene/water partition coefficients ( $K_{o/w}$ ) of the respective neutral species of compounds I-VII. The ionization constants of monoionizable compounds IV-VII are listed in columns that correspond to the appropriate microscopic ionization constants defined in Figure 4-1.	88
Table 5-1.	Free energies of transfer of solutes and functional groups. Values less than zero indicate that the transfer is favored. Superscripts and footnotes indicate the source experiment or simulation of the value. When superscripts appear on solutes the free energy values have been calculated from partition coefficients from two different studies and differ in the solvents employed.	143

## List of Figures

Figure 3-1.	Structural formula of bretylium	43
Figure 3-2.	Ionization of tyramine	44
Figure 3-3.	Fraction of tyramine species: cation (□), zwitterion (◆), neutral (—), and anion (○), as a function of pH.	45
Figure 3-4.	1,9-Decadiene-water partition coefficient of tyramine as a function of pH. The points are single determinations and the line is the best fit to Equation 3-4.	46
Figure 3-5.	Permeability of D-mannitol (○) and bretylium (◆) across DOPC and permeability of D-mannitol across egg phosphatidylcholine bilayers (Δ, data from Mayer et al). Error bars (sometimes smaller than symbols) represent standard deviations and lines represent the average of the points.	47
Figure 3-6.	Equilibrium unbound extravesicular tyramine concentration as a function of total tyramine concentration at pH 2 (◆), 3 (○), and 4 (Δ) in liposomal dispersions (13.5 mM lipid) at 25 °C. Symbols at three conditions overlap suggesting pH independence.	48
Figure 3-7.	Representative profile for tyramine efflux from DOPC vesicles at initial pH 3.77 and initial intravesicular tyramine concentration of 10 mM. Lines reflect best fits according to the conventional model (Equation 3-6, --) and comprehensive model (Equations 3-17 to 3-19,—) developed in this study.	49
Figure 3-8.	Representative profile for tyramine efflux from DOPC vesicles at initial pH pH 4.15 and initial intravesicular tyramine concentration of 3 mM. Lines reflect best fits according to the conventional model (Equation 3-6, --) and comprehensive model (Equations 3-17 to 3-19,—) developed in this study.	50
Figure 3-9.	Representative profile for tyramine efflux from DOPC vesicles at initial pH 3.31 and initial intravesicular tyramine concentration of 1 mM. Lines reflect best fits according to the conventional model (Equation 3-6, --) and comprehensive model (Equations 3-17 to 3-19,—) developed in this study.	51
Figure 3-10.	Plot of log P <sub>app</sub> vs. pH for tyramine determined using either the conventional model (Δ, Equation 3-6) or the comprehensive model (○, Equations 3-17 to 3-19) at initial intravesicular tyramine concentration of 1 mM. Error bars indicate standard	



- deviations and may be smaller than symbols. Lines are drawn to indicate approximate slopes. 52
- Figure 3-11. Plot of  $\log P_{app}$  vs. pH for tyramine determined using either the conventional model ( $\Delta$ , Equation 3-6) or the comprehensive model ( $\circ$ , Equations 3-17 to 3-19) at initial intravesicular tyramine concentration of 3 mM. Error bars indicate standard deviations and may be smaller than symbols. Lines are drawn to indicate approximate slopes. 53
- Figure 3-12. Plot of  $\log P_{app}$  vs. pH for tyramine determined using either the conventional model ( $\Delta$ , Equation 3-6) or the comprehensive model ( $\circ$ , Equations 3-17 to 3-19) at initial intravesicular tyramine concentration of 10 mM. Error bars indicate standard deviations and may be smaller than symbols. Lines are drawn to indicate approximate slopes. 54
- Figure 3-13. Simulation of the expected pH-permeability profile for a weak base with  $pK_a=10$  and intrinsic permeability coefficients of  $3 \times 10^{-2}$  and  $3 \times 10^{-11}$  cm/s for the neutral and ionized forms, respectively. 55
- Figure 3-14. Plot illustrating simulations according to Equation 3-13 for the effect of pH-independent membrane binding on liposomal release profiles as a function of time for a weakly basic permeant having a  $pK_a$  of 10 at pH 3.25. Membrane binding constants assumed were  $1 \times 10^{-6} M^{-1}$  ( $\blacklozenge$ ),  $30 M^{-1}$  ( $\Delta$ ), and  $100 M^{-1}$  ( $\circ$ ) to reflect negligible, low, and moderate binding of the permeant, respectively. The initial intravesicular solute concentration (bound + free) was assumed to be 0.01 M, lipid concentration was 0.0015 M, 1% volume enclosed (sink conditions), and the intrinsic permeability coefficient was 0.0316 cm/s. 56
- Figure 3-15. Plot illustrating simulations according to Equation 3-13 for the effect of pH-independent membrane binding on unbound permeant concentration gradients as a function of time for a weakly basic permeant having a  $pK_a$  of 10 at pH 3.25. Membrane binding constants assumed were  $1 \times 10^{-6} M^{-1}$  ( $\blacklozenge$ ),  $30 M^{-1}$  ( $\Delta$ ), and  $100 M^{-1}$  ( $\circ$ ) to reflect negligible, low, and moderate binding of permeant. The initial intravesicular solute concentration (bound + free) was assumed to be 0.01 M, lipid concentration was 0.0015 M, 1% volume enclosed (sink conditions), and the intrinsic permeability coefficient was 0.0316 cm/s. 57
- Figure 3-16. Results of simulations using Equation 3-14 and 3-16 to determine the change in intravesicular pH resulting from the

liposomal efflux of a weakly basic amine ( $pK_a = 10$ ) initially present at an intravesicular concentration of 0.01 M. An intrinsic permeability coefficient of 0.03 cm/s was assumed for the amine along with a negligible binding constant. The initial intravesicular pH was buffered (40 mM buffer) at 2.25 and ( $pH - pK_a$ ) was 0.5 ( $\blacklozenge$ ) or -0.5( $\circ$ ). 58

Figure 3-17. Results of several simulations using Equation 3-14 and 3-16 to determine the change in intravesicular pH resulting from the liposomal efflux of a weakly basic amine ( $pK_a = 10$ ) initially present at an intravesicular concentration of 0.01 M. An intrinsic permeability coefficient of 0.03 cm/s was assumed for the amine along with a negligible binding constant. The initial intravesicular pH was buffered (40 mM buffer) at 4.25 and ( $pH - pK_a$ ) was 0.5 ( $\blacklozenge$ ) or -0.5( $\circ$ ). 59

Figure 4-1. Ionization of p-(aminoethyl)phenol showing four species in aqueous solutions: cation ( $BH^+$ ), neutral (BN), zwitterion (Bz), and anion ( $B^-$ ). The compounds are: Tyramine (I):  $R_1=R_2=H$ , N-methyltyramine (II):  $R_1=CH_3$  and  $R_2=H$ , N,N-dimethyltyramine (III):  $R_1=R_2=CH_3$ . The four equilibria representing respective interconversions are labeled with corresponding microscopic ionization constants,  $k_1$ ,  $k_2$ ,  $k_{12}$ , and  $k_{21}$ . The fifth possible interconversion between zwitterion and neutral forms is independent of pH (shown as  $K_z$ ) as no protons are added or removed during the conversion. A simple pH-volumetric titration shows two apparent ionization constants  $K_1$  and  $K_2$  that are a composite of two of the four microscopic ionization constants. A spectrometric titration demonstrates only two distinct species related to the ionization state of the phenol group. 90

Figure 4-2. The UV absorbance spectra of tyramine solutions prepared at varying pH. The numbers in the legend indicate pH of each solution. 91

Figure 4-3. A representative plot of pH as a function of volume. 92

Figure 4-4. Representative plot of UV absorbance as a function of pH. 93

Figure 4-5. Fraction of various species of p-(aminoethyl)phenol in solution as function of pH. Structures of cation ( $BH^+$ ,  $\text{— — —}$ ), zwitterion (Bz,  $\text{— — —}$ ), neutral (BN,  $\text{- - -}$ ), and anion ( $B^-$ ,  $\text{— - —}$ ) are shown in Figure 4-1. 94

Figure 4-6. Effect of successive methylation on ionization constant of each amine. R= methyl- ( $\blacklozenge$ ), phenethyl- ( $\Delta$ ), p-methoxyphenethyl-

- ( $\times$ ), p-hydroxyphenethyl- ( $\circ$ ). Values are plotted from Table 4-1 and literature. 95
- Figure 4-7. Apparent partition coefficient of compounds I ( $\Delta$ ,  $\blacktriangle$ ), II ( $\circ$ ), and III ( $\blacklozenge$ ) is shown as a function of pH. Lines show best fit to Equation 4-4. The partition coefficient for compound I was determined at total concentration of 0.05 mM (closed symbols) or at 1 mM (open symbols). 96
- Figure 4-8. Contribution of the amine group to the transfer free energy,  $\Delta(\Delta G^0)_{H \rightarrow NH_2}$  ( $\circ$ , plotted on the left axis), along with pKa of the corresponding amine ( $\square$ , plotted on the right axis). The hydrocarbon water partition coefficient values were taken from Table 4-1 or literature. Error bars indicate the range of determinations. 97
- Figure 4-9. Contribution of first methylation  $\Delta(\Delta G^0)_{RNH_2 \rightarrow RNHCH_3}$  (solid bars) and second methylation  $\Delta(\Delta G^0)_{RNHCH_3 \rightarrow RN(CH_3)_2}$  (shaded bars) to the free energy of transfer of the amines from water to hydrocarbon for three different series. Partition coefficients of A (methylamine), B (dimethylamine), and C (trimethylamine) were obtained from the literature. Roman numerals correspond to the solutes shown in Table 4-1. 98
- Figure 4-10. Contribution of hydroxyl group removal,  $\Delta(\Delta G^0)_{ROH \rightarrow RH}$  (shaded bars) or its methylation,  $\Delta(\Delta G^0)_{ROH \rightarrow ROCH_3}$  (open bars) to the free energy of transfer of solute from water to hydrocarbon. A = H, B = -CH<sub>2</sub>CH<sub>3</sub>, C = -CH<sub>2</sub>CH<sub>2</sub>NH<sub>2</sub>, D = -CH<sub>2</sub>CH<sub>2</sub>NHCH<sub>3</sub>, Error bars indicate the range of determinations. 99
- Figure 4-11. The folded gauche conformer of p-(aminoethyl)phenol (left) and the putative water adduct (right). All heavy atoms are dark colored and hydrogens are light colored. The nitrogen and oxygen atoms have been labeled as N and O, respectively. 100
- Figure 4-12. Partition coefficient of tyramine in liposomes. Diamonds = pH 2, squares = pH 3, and triangles = pH 4. 101
- Figure 4-13. Partition coefficient of N-methyltyramine in liposomes. Diamonds = pH 2, squares = pH 3, and triangles = pH 4. 102
- Figure 4-14. Partition coefficient of dimethyltyramine in liposomes. Diamonds = pH 2, squares = pH 3, and triangles = pH 4. 103

Figure 5-1.	Chemical structures of the three solutes used in this study	145
Figure 5-2.	Chemical structure of 1,2-dioleoyl- <i>sn</i> -glycero-3-phosphocholine (DOPC).	146
Figure 5-3.	Structure of the simulated lipid bilayer. Carbon atoms are green, hydrogen atoms are white, oxygen atoms are red, nitrogen atoms are blue, and phosphorous atoms are purple.	147
Figure 5-4.	Illustration showing the use of a quadratic biasing potential in an MD simulation designed to determine a free energy profile. The upper pair of plots shows the energy profiles of two systems: the first has an underlying free energy profile with no slope (left plot, □) and the second has an underlying linear free energy profile with positive slope (right plot, □). A quadratic potential centered at $z=1$ (—) is applied to each system and the resulting energy profile takes the shape shown (■) in each plot. The probability distributions of the states for each of the two cases are shown with similar symbols in the lower two plots, the unconstrained system exhibits the probability distribution shown by □ symbol and the constrained system exhibits the probability distribution shown by ■ symbol. The benefit of applying the quadratic constraint is apparent in the lower right hand side plot where an otherwise low probability of occurrence ( $z = 0.75$ to $1$ ) has been improved significantly. In this case the constraint could be relocated to $z = 1.25$ to further improve sampling of lower probability states on the right side.	148
Figure 5-5.	Average distribution of the atoms of various elements along the depth of the DOPC bilayer. ■: phosphorus, □: nitrogen, ×: carbonyl groups, Δ: oxygen of water. The y-axis on the right hand side has been used for the distribution of the oxygen atoms of water molecules.	149
Figure 5-6.	Thickness of the simulated lipid bilayer as measured by the distance between the average location of phosphorus atoms in the two leaflets over time.	150
Figure 5-7.	The order parameters of the two oleoyl chains in the DOPC molecules of the lipid bilayer containing phenethylamine: □ = oleoyl chain at the second carbon of the glycerol, ■ = oleoyl chain at the third carbon of the glycerol. The profiles for the lipid bilayer containing no solute or any of the other two solutes are nearly superimposable with this profile. The experimentally measured order parameters for the oleoyl chain of POPC bilayer are plotted as Δ (Seelig and Waespe-Sarcevic, 1978). Average	

- order parameters for both oleoyl chains of DOPC from the MD simulation of Mashl et al are shown as ● (Mashl et. al, 2001). 151
- Figure 5-8. The order parameters of the two oleoyl chains in the DOPC molecules of the lipid bilayer without solutes (○, □) and that containing phenethylamine (●, ■) as a function of carbon number. The oleoyl chain attached at the second carbon of glycerol is shown as (□, ■) and the chain attached at the third carbon of glycerol is shown as (○, ●). 152
- Figure 5-9. Average number of oleoyl chain torsions in the *gauche* conformation as a function of simulation time. Upper (dark) and lower (grey) bands are from the simulations for the neat bilayer and that containing tyramine, respectively. 153
- Figure 5-10. Average angle of the P→N vector with the bilayer normal as a function of simulation time. 154
- Figure 5-11. Number of times tyramine was observed in a given 0.3 angstrom slice of the bilayer as a function of the distance of the mid point of the slice from the center of the bilayer during a representative MD simulation. A solute copy was considered to be present in a 0.3 angstrom slice when the aromatic carbon atom attached to the ethyl chain (the atom closest to the center of mass) was found at this location. 155
- Figure 5-12. A representative convergence plot of the evolution of free energy of transfer of phenethylamine from water to the preferred binding region (at about 12 angstroms from the center of bilayer) as data are accumulated during the course of the simulation (— —). Error bars indicate the standard error of the estimate. The decrease in the standard error of estimate as the simulation progresses is shown on the right hand side y-axis (- - - -). 156
- Figure 5-13. Free energy of transfer of tyramine from water to various locations within the bilayer, calculated using population density analysis method. Location of tyramine is determined by the location of the aromatic carbon atom attached to the ethyl chain. 157
- Figure 5-14. Free energy of transfer of solute from water to various locations within the bilayer; ••••• = tyramine, - - - - = phenethylamine, — — = 4-ethylphenol. The solute position was defined by the location of the aromatic carbon attached to the ethyl chain. Therefore, the solutes, due to their own size, can span a region of approximately 2 to 5 angstroms on each side of the location indicated on the graph. 158

- Figure 5-15. Effect of slab thickness used for the force integration calculation (0.3 Angstrom = ••••, 5 Angstrom = - - - -, 10 Angstrom = —) on the free energy profile of phenylethylamine. Location of the aromatic carbon attached to ethyl chain is taken as the location of the solute. 159
- Figure 5-16. Hydroxyl (—) and amino (- - -) group contributions to the free energy of solute transfer from water to various locations within the lipid bilayer. The lines were calculated by taking the difference between the profiles of respective solutes from the Figure 5-14. The solute position was defined by the location of the aromatic carbon attached to the ethyl chain. Therefore, the solutes, due to their own size, can span a region of approximately 2 to 5 angstroms on each side of the location indicated on the graph. 160
- Figure 6-1. The unit normal vector (vertical arrow) and the unit longitudinal vector of the solute (arrow with label R) at an angle  $\theta$ . R is the radius of the sphere and the spherical cap specified by the rotation of the solute vector around the normal vector is shown with dots. 194
- Figure 6-2. Free energy of solute transfer from water to various locations within the bilayer; •••• = tyramine, - - - = phenylethylamine, — = 4-ethylphenol. 195
- Figure 6-3. Distribution of the lipid bilayer functional groups: — = carbonyl oxygen, - - - = phosphoryl oxygen, - - - = choline nitrogen, - • - • - = water. The average number of functional units found in each 0.3 angstrom slice is shown. The left plot shows the presence of carbonyl groups and water near the center of the bilayer. The plateau level of water in the center corresponds to approximately 1/10000 of the concentration in bulk water. 196
- Figure 6-4. Simulation unit cell with the atoms colored by partial charge. Parts of the lipid and water molecules extending out of the unit cell were *relocated* from the opposite face of the unit cell to maintain integrity of the molecules for visualization. The color scale at the bottom has a negative partial charge on the left and positive on the right extreme. 197
- Figures 6-5 through 6-15: Average number of hydrogen bonds per solute functional group as a function of the distance from the center of the bilayer.
- Figure 6-5. All hydrogen bonds 198

Figure 6-6.	Hydrogen bonds with the outer phosphoether oxygen atom	199
Figure 6-7.	Hydrogen bonds with the phosphoryl oxygen atom	200
Figure 6-8.	Hydrogen bonds with the inner phosphoether oxygen atom	201
Figure 6-9.	Hydrogen bonds with the ether oxygen atom of the 2-oleoyl chain	202
Figure 6-10.	Hydrogen bonds with the carbonyl oxygen atom of the 2-oleoyl chain	203
Figure 6-11.	Hydrogen bonds with the ether oxygen atom of the 1-oleoyl chain	204
Figure 6-12.	Hydrogen bonds with the carbonyl oxygen atom of the 1-oleoyl chain	205
Figure 6-13.	Hydrogen bonds with the oxygen atom of water	206
Figure 6-14.	Hydrogen bonds with the hydrogen atom of water	207
Figure 6-15.	Configurations without any hydrogen bonds	208
Figure 6-16 through 6-25	Average distances between the heavy (non-hydrogen) atoms of the interacting functional groups of the lipid bilayer and the solute.	
Figure 6-16.	All hydrogen bonds	209
Figure 6-17.	Hydrogen bonds with the outer phosphoether oxygen atom	210
Figure 6-18.	Hydrogen bonds with the phosphoryl oxygen atom	211
Figure 6-19.	Hydrogen bonds with the inner phosphoether oxygen atom	212
Figure 6-20.	Hydrogen bonds with the ether oxygen atom of the 2-oleoyl chain	213
Figure 6-21.	Hydrogen bonds with the carbonyl oxygen atom of the 2-oleoyl chain	214
Figure 6-22.	Hydrogen bonds with the ether oxygen atom of the 1-oleoyl chain	215
Figure 6-23.	Hydrogen bonds with the carbonyl oxygen atom of the 1-oleoyl chain	216
Figure 6-24.	Hydrogen bonds with the oxygen atom of water	217

Figure 6-25.	Hydrogen bonds with the hydrogen atom of water	218
Figure 6-26.	Relative distribution of orientations of 4-ethylphenol versus distance from the center of the bilayer	219
Figure 6-27.	Relative distribution of orientations of phenylethylamine versus distance from the center of the bilayer	220
Figure 6-28.	Relative distribution of orientations of tyramine versus distance from the center of the bilayer	221
Figure 6-29.	Two representative trajectories from the simulation of 4-ethylphenol. Top panels show the location of solute from relative to the center of the bilayer versus the simulation time. Bottom panels show the corresponding orientation angle of the solute versus the same time step in the simulation.	222
Figure 6-30.	Various conformers of tyramine based on the rotation of the first dihedral of the ethylamine chain. The numerical labels assigned for these conformers have been used in the subsequent figures.	223
Figure 6-31.	Equilibrium distribution of the various conformers of 4-ethylphenol based on the rotation of the first dihedral of the ethyl chain. The conformation labels are as shown in Figure 6-29.	224
Figure 6-32.	Equilibrium distribution of the various conformers of phenylethylamine based on the rotation of the first dihedral of the ethylamine chain. The conformation labels are as shown in Figure 6-29.	225
Figure 6-33.	Equilibrium distribution of the various conformers of tyramine based on the rotation of the first dihedral of the ethylamine chain. The conformation labels are as shown in Figure 6-29.	226
Figure 6-34.	Conformers of tyramine based on the rotation of the second dihedral of the ethylamine chain. The numerical labels assigned for these conformers have been used in the subsequent figures.	227
Figure 6-35.	Equilibrium distribution of the various conformers of 4-ethylphenol based on the rotation of the second dihedral of the ethyl chain. The conformation labels are as shown in Figure 6-33.	228
Figure 6-36.	Equilibrium distribution of the various conformers of phenylethylamine based on the rotation of the second dihedral of the ethylamine chain. The conformation labels are as shown in Figure 6-33.	229



- Figure 6-37. Equilibrium distribution of the various conformers of tyramine based on the rotation of the second dihedral of the ethylamine chain. The conformation labels are as shown in Figure 6-33. 230
- Figure 6-38. Snapshot of a tyramine molecule located in water. Tyramine and the water molecules hydrogen bonded to it are shown as sticks; all other molecules are shown as lines. The dotted lines show the hydrogen bonds detected by the visualization software. The molecules in the water network on the distal side of the benzene ring appear to be missing some of their hydrogen bonds due to the presence of the hydrophobic solute molecule. The faint gray straight lines going through the image are the edges of the unit cell. Atoms are colored by element type: hydrogen=white, carbon=grey, nitrogen = blue, and oxygen = red. 231
- Figure 6-39. Snapshot of a phenylethylamine molecule located in water that does not appear to have any hydrogen bonds with water molecules. The network of water molecules forms an empty cavity around the solute. Distances of the solute atoms from the nearby water molecules that are missing some of their hydrogen bonds are shown as solid lines. Water molecules from the proximal and distal side of the plane of the picture were removed for visualization. 232
- Figure 6-40. Snapshot of a tyramine molecule located on the water side of the water/headgroup interface, viewed from inside the bilayer. Each side of the benzene ring is close to choline methyl groups as if it were solvated by the latter in this relatively polar environment. The phenol group is close to a phosphonyl group (which has been removed for visibility). In the upper image the atoms are colored by element type where all element colors are as before and the phosphorus atoms are orange. In the lower image the atoms are colored by their partial charges. The color scale at the bottom has a negative partial charge on the left and a positive partial charge on the right. 233
- Figure 6-41. Snapshot of a phenylethylamine molecule at the water/headgroup interface as its hydrophobic portion is shielded from water by the choline methyl groups. The solid lines with numbers are the distance measurements and the dotted lines indicate hydrogen bonds among various molecules detected by the visualization software. The atoms are colored by element type. 235
- Figure 6-42. Snapshot of a tyramine molecule located at the interface of the bilayer and water. The polar groups are hydrogen bonded with the nearby water molecules. Faces of the benzene ring are close to a water molecule on the proximal side and a choline methyl

- group on the distal side. The lines with numbers are the measured distances in angstroms. In the upper image the atoms are colored by element type and in the lower image the atoms are colored by their partial charges. The color scale at the bottom has a negative partial charge on the left and a positive partial charge on the right. 236
- Figure 6-43. Snapshot of a phenylethylamine molecule located on the head group side of the water/head group interface where it forms a hydrogen bond with a nearby water molecule. The line with a number is the distance in angstroms. 238
- Figure 6-44. Snapshot of a tyramine molecule near the center of the bilayer. The molecules of interest are shown with stick models; others are shown with lines, and the terminal methyl of the oleoyl chains are shown as balls. The lines with numbers are the distance measurements. In the upper image the atoms are colored by element type and in the lower image the atoms are colored by their partial charges. The color scale at the bottom has a negative partial charge on the left and a positive charge on the right. 239
- Figure 6-45. Snapshot of a tyramine molecule located at approximately 5 angstroms from the central plane of the bilayer. In the left hand image, lines with numbers show the distance measurements in angstroms. In the right hand image, the dotted lines indicate hydrogen bonds among various molecules detected by the visualization software. 240
- Figure 6-46. Snapshot of a tyramine molecule located at approximately 10 angstroms from the center of the bilayer. While the phenol group appears to participate in the hydrogen bonded network of the water molecules, the ethylamine chain of tyramine located in the hydrocarbon region is in a folded conformation. In the left hand image, lines with numbers are the distance measurements in angstroms. In the right hand image, the dotted lines indicate hydrogen bonds among various molecules detected by the visualization software. 241
- Figure 6-47. Free energy of transfer of water from bulk water to various locations within the simulation cell. The profiles were obtained from the MD simulations of the lipid bilayer containing: 4-ethylphenol (—), phenylethylamine (— —), or tyramine (---). The profiles were computed using the probability density method of post-processing. The lack of a significant number of observations near the center of the bilayer increases the uncertainty in that region. The profile shown with circular

symbols (•) has been redrawn from the work of Shinoda and coworkers (Shinoda et. al, 2004) for the transfer of water into a DPPC bilayer.

242

## CHAPTER ONE: Introduction

### Background and Significance

Among various others, one *modus operandi* in a rational drug discovery program is to modulate function of a receptor or a molecular drug target. Two factors contribute to the success in terms of the activity of the drugs: 1. binding of the drug candidate to the receptor, and 2. concentration of the drug candidate near the receptor. The first factor, *activity*, is unique to a given discovery program whereas the second, *delivery*, is universal to a majority of drugs. Activity of a candidate is typically optimized through receptor mapping and similar techniques where the *required features*, or the least common denominator, of the structure of the drug (SAR(Lien, 1987)) are first determined and subsequently become the guidepost for the search. The delivery of the drug however is a complex sequence of temporally overlapping events. Irrespective of the mode of administration, first is the dissolution of the drug to a molecular solution followed by the absorption and distribution in the body. A significant body of knowledge has been amassed in the pharmaceutical literature on the solubility and dissolution of drugs (Grant and Higuchi, 1990) that has been applied to the understanding of drug delivery. The absorption, however, involves the transport of the drug to various tissues of the body (distribution) and several barriers may be encountered in the process. Therefore, it is important to know how drugs transport and where they are retained. While molecular transporters participate in the translocation of some of drugs, most enter cells or cross biological membranes via passive permeability. Empirical approaches to the prediction of passive intestinal permeability have had limited success due to the difficulty in pinpointing (Sugano et al., 2002) the structural features of the compounds to be optimized for this purpose. As a result, permeability measurements across surrogate membranes are generally employed.

Since the lipid bilayer is the primary component of the cell and organelle membranes, understanding transport across this barrier is imperative to the understanding of absorption and distribution. While significant research has been published describing interactions of various types of molecules (solutes) with lipid bilayer membranes, more

may be needed to describe the “least common denominator” for passive permeability. Unlike drug activity, receptor mapping for lipid bilayer transport is not possible because of the inherent dynamics of the process and the diversity of the chemical nature of the drug candidates the transport and retention behavior of which must be predicted. Nevertheless, it may be possible to develop a relationship between the chemical structure of the solutes and their ability to be retained in or transport across the lipid bilayer membranes.

### **Solubility diffusion theory and the need for identification of a barrier domain**

Passive permeability (P) can be described using solubility diffusion theory (Finkelstein and Cass, 1968) which suggests that the permeability of a solute across a uniform or isotropic membrane is a function of its partition coefficient ( $K_{m/w}$ ) between water and the membrane and its diffusion (D) coefficient as shown in the following equation:

$$P = \frac{K_{m/w}D}{h} \quad (1-1)$$

where h is the thickness of the isotropic membrane. Since lipid bilayer membranes are quite heterogeneous along the transport path, Diamond and Katz (Diamond and Katz, 1974) derived a related expression that treats the transport similar to resistances in series. In its general form it is given as

$$\frac{1}{P} = \sum_i \frac{h_i}{K_i^{m/w} D_i} \quad (1-2)$$

where the subscript *i* refers to the chemically distinct environments along the path of transport. The continuous form of this equation is given as

$$\frac{1}{P} = \int \frac{dh}{K_{m/w}(h)D(h)} \quad (1-3)$$

Since Equation 1-2 is a sum of the resistances across various regions of the bilayer, it is possible that one of the terms is sufficiently large to be the primary determinant of the net result (i.e. the barrier domain). Similarly, in the continuous case (Equation 1-3), there may be regions that contribute much less than the others to the final result. It is therefore possible to identify a barrier region for a set of molecules such that the entire summation is again not necessary. This has been shown to be the case with a few different series of carboxylic acids where the permeability coefficients for similarly sized molecules across liquid crystalline bilayers are collinear with the partition coefficients in 1,9-decadiene (Xiang and Anderson, 1994b, Mayer et al., 2000) exhibiting slopes of approximately one. While the heterogeneous solubility diffusion theory relates the attributes of the solutes to their permeability coefficients, the only parameter that describes the membrane is its thickness. Identification of the ordered chain region as the barrier domain inside the lipid bilayer in the above described studies further allows one to relate the permeability coefficient to a key attribute of the membrane (i.e. the chain ordering within the bilayer). This barrier domain solubility diffusion model (Xiang and Anderson, 1997, Xiang et al., 1998) is described by the following equation

$$P = f * P_0 = f \frac{K_{m/w} D}{h} \quad (1-4)$$

where a permeability decrement factor,  $f$ , has been introduced that depends on the degree of chain ordering within the barrier - such as a gel phase or a liquid crystalline phase membrane and the size of the permeant. The symbols  $P$  and  $P_0$  represent the actual intrinsic permeability coefficient and the permeability coefficient of the solute predicted by classical solubility-diffusion theory; all other terms are the same as before.

In the above work (Xiang et al., 1998) it has been established that the lipid bilayer barrier domain varies with the phase structure of the barrier, and with the solute structure. Extending the chemical series to a broader set, including small peptide chains, it has been shown that the above model continues to predict the permeability coefficients (Mayer et al., 2003, Cao et al., 2008) using partition coefficients based on the 1,9-decadiene / water system.

## **Non-classical hydrophobicity**

While effect of solute size on the diffusion coefficient is relatively easily perceived, the same effect on the partition coefficient has also been noted in the experiments of this (Xiang and Anderson, 1994a, Xiang and Anderson, 1997) and other laboratories (Seelig and Ganz, 1991, Wimley and White, 1993, DeVido et al., 1998). These studies observed that the partition coefficients in the lipid bilayers exhibit higher selectivity for the size of solutes than that expected from the hydrocarbon water partition coefficients. This size dependence of the partition coefficient into the lipid bilayer has been suggested to be due to the exclusion effect of the chain ordering in the lipid bilayers akin to that in polymer solutions (Flory, 1953). As a result, lattice theory has been used in attempts to rationalize and quantitate the observations. Nonetheless, the effect has been termed “non-classical hydrophobicity” or the “bilayer effect”. This term has been used throughout the subsequent chapters with brief explanation.

## **Intrinsic and apparent permeability coefficients**

While studies involving the lipid bilayer membrane have typically reported species specific permeability coefficients for the solutes, the databases used for the development of numerical models for passive membrane permeability in general have not consistently done this. This could be due to the fact that the observed passive permeability is generally at certain biorelevant conditions (Sugano et al., 2002, Sugano et al., 2003, Stenberg et al., 1999) and the intrinsic permeability coefficients specific to single species were not available. One of the works concludes that while the computational power available for predicting the permeabilities almost doubles every 18 months, the rate limiting step remains the development of efficient software to utilize such resources and quality data to base the numerical models on (Stenberg, 2001). In order to address this, it must be recognized that one must understand all the phenomena underlying the measurement so that the experimental values obtained are intrinsic to a single species that is being included in a given model. If there are processes other than ionization, such as complexation, binding, partitioning, etc. they must be accounted for as well. One of the significant reasons for the scatter in the published comparisons of

experimental permeability coefficients to those derived from the predictive models above may be the use of apparent permeability coefficients.

### **Lipid bilayers as drug delivery devices**

Other than their biological importance in drug transport (for absorption) and drug distribution, lipid bilayers have also been used in drug delivery systems (liposomes). Due to their versatility and the availability of extensive literature, liposomes remain an attractive drug delivery system to address any shortcomings of therapeutic agents such as extension of circulation half life for a metabolically unstable drug, targeted distribution of an anticancer agent to a specific tissue etc. Very few regulatory approvals have, however, been achieved for the liposome based drug formulations. The reasons for fewer approvals include the lack of quantitative mechanism-based approaches for describing these formulations and issues in scale up (Joguparthi, 2007) among others. In order to overcome such hurdles one must understand the mechanism of loading of the active moiety into the liposomes (whether unilamellar or multilamellar) and any mechanism of extending the time of its retention, as these may in effect constitute the patent claims of the drug delivery system.

### **Molecular level understanding of transport from and retention in liposomes**

This work seeks to increase understanding by addressing some of the questions raised above in the context of the transport and retention of drug candidates in lipid bilayers. While some numerical models are available for prediction of these properties, a complete synthetic basis of the parameters used in these models is only pending. For example one study reported that taking into account the number of hydrogen bond acceptor and donor groups helps to improve permeability prediction (Huque et al., 2004), yet the rationale for the use of such parameters is nebulous. What structural features of a solute determine its relative free energies in various regions of the bilayer and the locations of the preferred regions for retention and the barrier domain in the lipid bilayer remain to be uncovered. That is, an equivalent of *receptor mapping* is still incomplete in the case of structure- lipid bilayer permeability relationships.



Some molecular level mechanistic understanding has recently been obtained using molecular dynamics studies (Xiang and Anderson, 2006) which have raised awareness regarding the heterogeneity of the lipid bilayer membrane (Marrink and Berendsen, 1994) and have provided molecular level visualization of the transport and retention of some solutes. With an increase in computing power such studies have proliferated, but only a few present a parallel experimental measurement and a simulation study that would assure accuracy of the latter by way of comparison to reinforce the microscopic picture derived from the same.

This work utilizes the above framework to conduct experimental measurements and molecular dynamics (MD) simulations and molecular dynamics simulations on similar systems in order to attempt answering some of the unsolved questions. The specific aims of this work are described in the subsequent chapter.

## References

- CAO, Y., XIANG, T.-X. & ANDERSON, B. D. (2008) Development of structure-lipid bilayer permeability relationships for peptide-like small organic molecules. *Molecular Pharmaceutics*, 5, 371-88.
- DEVIDO, D. R., DORSEY, J. G., CHAN, H. S. & DILL, K. A. (1998) Oil/water partitioning has a different thermodynamic signature when the oil solvent chains are aligned than when they are amorphous. *Journal of Physical Chemistry B*, 102, 7272-7279.
- DIAMOND, J. M. & KATZ, Y. (1974) Interpretation of nonelectrolyte partition coefficients between dimyristoyl lecithin and water. *Journal of Membrane Biology*, 17, 121-54.
- FINKELSTEIN, A. & CASS, A. (1968) Permeability and electrical properties of thin lipid membranes. *Journal of General Physiology*, 52, 145.

- FLORY, P. J. (1953) *Principles Of Polymer Chemistry*, Ithaca, NY, Cornell University Press.
- GRANT, D. J. W. & HIGUCHI, T. (1990) *Solubility Behavior of Organic Compounds*, New York, Wiley.
- HUQUE, F. T. T., BOX, K., PLATTS, J. A. & COMER, J. (2004) Permeability through DOPC/dodecane membranes: measurement and LFER modelling. *European Journal of Pharmaceutical Sciences*, 23, 223-232.
- JOGUPARTHI, V. (2007) Physicochemical Approaches To Enhance The Liposomal Loading And Retention Of Hydrophobic Weak Acids. PhD Thesis. College of Pharmacy, The University of Kentucky, Lexington, KY.
- LIEN, E. J. (1987) *SAR: Side Effects And Drug Design*, New York, NY, Marcel Dekker, Inc.
- MARRINK, S.-J. & BERENDSEN, H. J. C. (1994) Simulation of water transport through a lipid membrane. *Journal of Physical Chemistry*, 98, 4155-4168.
- MAYER, P., XIANG, T.-X. & ANDERSON, B. (2000) Independence of substituent contributions to the transport of small-molecule permeants in lipid bilayer. *The AAPS Journal*, 2, 40-52.
- MAYER, P. T., XIANG, T.-X., NIEMI, R. & ANDERSON, B. D. (2003) A hydrophobicity scale for the lipid bilayer barrier domain from peptide permeabilities: Nonadditivities in residue contributions. *Biochemistry*, 42, 1624-1636.
- SEELIG, J. & GANZ, P. (1991) Nonclassical hydrophobic effect in membrane binding equilibria. *Biochemistry*, 30, 9354-9359.
- STENBERG, P. (2001) Computational Models For The Prediction Of Intestinal Membrane Permeability. PhD Thesis. Pharmaceutics, Uppsala University, Uppsala, Sweden.

- STENBERG, P., LUTHMAN, K., ELLENS, H., LEE, C. P., SMITH, P., LAGO, A., ELLIOTT, J. D. & ARTURSSON, P. (1999) Prediction of the intestinal absorption of endothelin receptor antagonists using three theoretical methods of increasing complexity. *Pharmaceutical Research*, 16, 1520-1526.
- SUGANO, K., NABUCHI, Y., MACHIDA, M. & ASO, Y. (2003) Prediction of human intestinal permeability using artificial membrane permeability. *International Journal of Pharmaceutics*, 257, 245.
- SUGANO, K., TAKATA, N., MACHIDA, M., SAITOH, K. & TERADA, K. (2002) Prediction of passive intestinal absorption using bio-mimetic artificial membrane permeation assay and the paracellular pathway model. *International Journal of Pharmaceutics*, 241, 241.
- WIMLEY, W. C. & WHITE, S. H. (1993) Membrane partitioning: distinguishing bilayer effects from the hydrophobic effect. *Biochemistry*, 32, 6307-12.
- XIANG, T.-X. & ANDERSON, B. D. (1994a) The relationship between permeant size and permeability in lipid bilayer membranes. *Journal of Membrane Biology*, 140, 111-22.
- XIANG, T.-X. & ANDERSON, B. D. (1994b) Substituent contributions to the transport of substituted *p*-toluic acids across lipid bilayer membranes. *Journal of Pharmaceutical Sciences*, 83, 1511-18.
- XIANG, T.-X. & ANDERSON, B. D. (1997) Permeability of acetic acid across gel and liquid-crystalline lipid bilayers conforms to free-surface-area theory. *Biophysical Journal*, 72, 223-237.
- XIANG, T.-X. & ANDERSON, B. D. (2006) Liposomal drug transport: A molecular perspective from molecular dynamics simulations in lipid bilayers. *Advanced Drug Delivery Reviews*, 58, 1357-1378.

XIANG, T.-X., XU, Y. H. & ANDERSON, B. D. (1998) The barrier domain for solute permeation varies with lipid bilayer phase structure. *Journal of Membrane Biology*, 165, 77-90.

Copyright © Ravindra W. Tejwani 2009

## CHAPTER TWO: Statement of Aims

In order to address the questions raised in the previous chapter regarding the underlying mechanism of the permeation and retention of drugs in lipid bilayer membranes, a set of solutes was chosen such that all atom molecular dynamics simulations of a reasonable length could be conducted in parallel with experimental measurement. The three solutes chosen were such that a comparison of group contributions to the free energies of solute transfer for the hydroxyl and amino functional groups from water to various regions of the bilayer would also be possible both experimentally and in the simulations. The solutes chosen were tyramine, phenylethylamine, and 4-ethylphenol. The specific aims for the achievement of the above objectives were:

***1. Develop a quantitative physical model to generate intrinsic permeability coefficients and extend the validation of experimental methods to amine containing compounds.***

Since previous work with lipid bilayer membranes in this laboratory involved carboxylic acids, measurements for amines involve studies to be conducted in a new pH range. As a result, a validation of the barrier properties of the lipid bilayer model was required. Various speciation effects including ionization, binding to the lipid bilayer, dimerization of the permeant were examined for their impact on the apparent permeability coefficients. Additionally, an effect of concentration of the amine on the transport was also studied in order to understand the impact of high concentration drug loading on the transport characteristics.

***2. Determine partition coefficients of the amine containing solutes between selected regions of the lipid bilayer and water. Determine free energies of transfer of the model solutes from water to the barrier and retention regions in order to generate functional group contributions for amino and phenolic hydroxyl functional groups***

Since direct measurement of partition coefficients in selected regions of the lipid bilayer membrane may not be possible, species-specific (intrinsic) partition coefficients of the selected solutes were measured in established surrogate media: 1,9-decadiene for

the barrier domain and the lipid bilayer itself for the preferred binding domain. Since species-specific partition coefficients for each solute will be needed, the microscopic ionization constants that are self consistent and accurate had to be determined.

***3. Using molecular dynamics simulations generate free energy profiles of the three model solutes to verify the location of the barrier and the retention regions. Predict partition coefficients at each of the locations; predict the free energies of transfer of the functional groups to each of these locations; and compare all of these against the experimental results.***

While the parameters for the molecular models for lipid bilayer and water have been established, a model of the lipid bilayer was built and its properties were verified against those established by the experiment. Subsequently MD simulations of sufficient length were conducted for each of the three model solutes to obtain free energy profiles to provide the free energies of transfer of solutes to those bilayer regions of interest. The locations of the barrier and the retention regions for each solute were determined for each of the three model solutes and the respective transfer free energies were compared against the experimental values obtained for the same set of the solutes. The functional group contributions (for amino and phenolic hydroxyl groups) to the free energies of transfer were also compared between the experiment and the simulation.

***4. Using the molecular dynamics simulations investigate the intermolecular interactions and other driving factors that govern the transport and retention of solutes in the lipid bilayer membrane.***

Once the lipid bilayer validation was established and the free energies of transfer verified, an analysis of the trajectory data was conducted for each solute to explore the specific interactions of each solute with its environment along the depth of the bilayer. The analyses were designed so as to uncover the underlying causes of the shapes of the free energy profiles, so that a relationship can be linked to the chemical structure of the solute.

## **CHAPTER THREE: Influence of intravesicular pH drift and membrane binding on the liposomal release of a model amine containing permeant**

### **Introduction**

Models to predict passive membrane permeability are of significance in drug discovery, development, and in liposomal drug delivery applications. Predictive models are typically based on statistical correlations of passive permeability data to other physicochemical properties or structural descriptors. It is critical that such models are built from accurate intrinsic permeability coefficients (i.e., values typically representing the neutral, unbound permeant species) so that the effects of other variables (e.g., pH, protein or lipid binding, etc.) can be properly incorporated into the models. Linear free energy relationships between membrane permeability coefficients and properties such as bulk solvent-water partition coefficients that are not based on species-specific information for both properties are likely to be unreliable when extrapolated beyond the conditions upon which the relationships are derived.

Predictive relationships between lipid bilayer membrane transport, permeant structure, and bilayer composition may ultimately be valuable tools for predicting drug transport across biomembranes, inasmuch as the lipid bilayer is a primary component of such membranes. More directly, such relationships are critical to an understanding of the loading, retention, and release of drugs from liposomes or other similar drug delivery systems. Several popular techniques for loading drugs into liposomes (Nichols and Deamer, 1976, Mayer et al., 1986, Mayer et al., 1985) such as those that rely on pH, salt or charge gradients are usually applied empirically because comprehensive quantitative theoretical treatments are unavailable. These applications typically use high concentrations of solute to maximize loading and thus deviations from ideal behavior may be the norm. Kinetic studies of drug efflux from such delivery systems usually provide only apparent transport rates due to simplifying assumptions that are made in treating the data combined with the lack of complete information on the underlying equilibria that determine the concentration gradients that provide the driving force for efflux. Drug ionization, surface adsorption, protein and lipid binding, complexation or

self-association, partitioning, and precipitation are among the equilibria that may need to be quantified in order to obtain reliable intrinsic permeability coefficients.

A large number of studies in the literature have shown that for weak electrolytes, the neutral form is generally the species responsible for transport across lipid bilayers. This gives rise to classical pH-permeability profiles characterized by a region in which the ionized permeant species predominates in aqueous solution and the logarithm of the permeability coefficient is directly proportional to pH, as demonstrated previously in numerous studies of a variety of carboxylic acids at low concentrations (Walter and Gutknecht, 1984, Walter et al., 1982, Mayer et al., 2003, Mayer et al., 2000, Xiang et al., 1998). Once reliable intrinsic permeability coefficients became available, linear free energy relationships such as those correlating lipid bilayer permeability coefficients with hydrocarbon/water partition coefficients emerged (Walter and Gutknecht, 1984, Xiang and Anderson, 1994, Mayer et al., 2000).

In this study the above methodologies have been extended to a model amine-containing permeant, tyramine, under conditions similar to a liposome loading or release experiment in which high solute concentrations may be utilized. Deviations from the classical (i.e., expected) pH-permeability profiles were found to occur at relatively high loading. This study examines the potential factors contributing to these deviations by investigating the solution equilibria (e.g., ionization, membrane binding, etc.) and kinetic processes that may alter apparent drug permeability and incorporating these phenomena into kinetic models to obtain the true intrinsic permeability coefficient.

## **Materials and Methods**

### ***Materials***

1,2-Dioleoyl-*sn*-glycero-3-phosphocholine (DOPC) and sodium 1,2-dioleoyl-*sn*-glycero-3-phosphate (DOPA) were purchased from Avanti Polar Lipids, Inc. (Alabaster, AL). The former was obtained as a 20 mg/mL solution in chloroform and the latter was obtained as a lyophilized powder. Both were used as obtained. Tyramine, bretylium (Figure 3-1) tosylate and manganese (II) bromide, each 99% or greater, were purchased



from Sigma-Aldrich Corporation (St. Louis, MO). 1,9-Decadiene was purchased from either Sigma-Aldrich Corporation, or TCI America, Inc. (Tokyo, Japan), and was >98% pure by GC. <sup>14</sup>C-Mannitol was purchased as a 0.1 mCi per mL (50 to 60 mCi per mmol) solution in Sterile Water for Injection from American Radiolabelled Chemicals (St. Louis, MO). All other reagents and materials were of analytical grade.

### *Determination of ionization constants*

A semi-micro ROSS® combination electrode attached to an Orion model 611 meter (Thermo Electron Corporation, Beverly, MA) was calibrated using pH 7 and 10 standard buffers (VWR Scientific, West Chester, PA) under a stream of nitrogen while gently stirring at 25±0.5°C. Tyramine was dissolved in deionized water (0.03 M) containing an equivalent amount of HCl and a sufficient amount of sodium chloride such that the ionic strength at the half-neutralization point was 0.1. The solution was stirred under nitrogen in a temperature-controlled reservoir at 25±0.5°C and circulated through a flow-cell in a UV-visible spectrophotometer (Waters 486 Tunable absorbance detector, Waters Corporation, Milford, MA), with water containing sodium chloride as a blank. The solution in the reservoir was titrated with 1 N sodium hydroxide solution while the solution pH and the UV-absorbance were recorded. All data were fitted simultaneously to Equations 3-1 and 3-2 to obtain the microscopic ionization constants for tyramine,  $k_1$ ,  $k_2$ ,  $k_{12}$ , and  $k_{21}$ , as defined in Figure 3-2.

$$\frac{B_0 V_b}{V_0 + V_b} + \left( \frac{[H^+]^2 - k_1 k_{12}}{D} \right) \times \frac{pC_0 V_0}{V_0 + V_b} - \frac{K_w}{[H^+]} = 0 \quad (3-1)$$

$$\frac{A}{C_0} = \frac{\varepsilon_A ([H^+]^2 + [H^+] k_2) + \varepsilon_C (k_1 [H^+] + k_1 k_{12})}{D} \quad (3-2)$$

where,

$$D = [H^+]^2 + [H^+] (k_1 + k_2) + k_1 k_{12} \quad (3-3)$$

$[H^+]$  represents the hydrogen ion concentration,  $K_w$  represents the ion product of water,  $V_0$  is the initial solution volume,  $V_b$  is the volume of titrant added,  $B_0$  is the normality of

the sodium hydroxide titrant,  $C_0$  and  $p$  are the tyramine concentration and purity, respectively,  $A$  is the measured absorbance, and  $\epsilon_A$  and  $\epsilon_B$  refer to the molar extinction coefficients of the phenol and phenolate species, respectively.

### ***Determination of partition coefficients***

The 1,9-decadiene/water partition coefficients were determined at 25°C using the shake flask method (Leo et al., 1971). 1,9-Decadiene was pre-washed with 0.1 M sulfuric acid, water, 0.1 M sodium hydroxide, and twice with water, then washed and pre-equilibrated with the corresponding buffer (tris-HCl or carbonate, 0.04 M, ionic strength=0.1) before the experiment. The two phases after equilibration were either diluted or concentrated appropriately for HPLC analysis. The solutions were concentrated by extracting 10 volumes of oil phase using 1 volume of 1N sulfuric acid. Typically two successive extracts combined together were found to provide adequate mass balance.

Apparent partition coefficients ( $K_{o/w}^{apparent}$ ) generated at varying pH (8.3 to 9.3) were used to calculate the intrinsic partition coefficient for the neutral species, ( $K_{o/w}^{B_N}$ ), using the following equation which assumes that only the neutral (non-zwitterionic) form of tyramine,  $B_N$  (Figure 3-2), partitions into decadiene:

$$K_{o/w}^{apparent} = \frac{B_N(oil)}{B_w^T} = K_{o/w}^{B_N} f_{B_N} \quad (3-4)$$

where  $B_w^T$  represents the total tyramine concentration in the aqueous phase, and  $f_{B_N}$  is the fraction of neutral form in the aqueous phase.

### ***LUV preparation and characterization***

The LUVs were prepared as reported earlier (Xiang et al., 1998) and briefly described here. Accurately weighed quantities of DOPC and DOPA (96:4 mole ratio, 25 mM) were dissolved in chloroform. Aliquots of this solution were transferred to glass vials (0.6 mL) and evaporated under a stream of nitrogen to obtain a dry lipid film. The

tubes were further dried at 40°C for a few hours to remove any traces of solvent. An aqueous permeant solution at a known concentration (1, 3, or 10 mM, 1 mL) in 40 mM buffer (phosphate, formate or acetate) at ionic strength of 0.1 (adjusted with sodium chloride) was added to the film to prepare a 15 mM lipid dispersion. The lipid dispersion was vortexed repeatedly for 5 minutes until a uniform dispersion was obtained, then extruded (17 times) through a 0.1  $\mu$  pore size polycarbonate membrane (Nuclepore, Pleasanton, CA) to obtain LUVs. Particle size and size distribution of the resulting vesicles were measured using dynamic light scattering (Horiba LA-920 particle size distribution analyzer, Horiba International Corporation, Irvine, CA) after appropriately diluting the vesicles in the matching buffer.

The average number of bilayers for the LUVs was determined as described previously (Xiang and Anderson, 1995).  $^{31}\text{P}$ -NMR measurements were carried out using an Eclipse+ 400 spectrometer from JEOL-USA, Incorporated (Peabody, MA) operated at 161.83 MHz. Spectra were accumulated over 14000 scans by employing a 45 degree pulse over a 32.47 kHz spectral width with gated proton decoupling, an acquisition time of 0.68 s and a relaxation delay of 4 s. A line-broadening of 100 Hz was applied prior to Fourier transformation and phasing of the spectra.

A 0.07 mL aliquot of  $\text{D}_2\text{O}$  was added to 0.7 mL of the LUV (30 mM) dispersion as an internal signal lock reagent. An initial  $^{31}\text{P}$ -NMR spectrum was obtained on this sample as described above. After obtaining the first spectrum, 0.07 mL of 0.1 M manganese (II) bromide was added to the sample tube to obtain a second spectrum. The relative percentage loss in the signal ( $\eta$ ) due to addition of  $\text{Mn}^{+2}$  was calculated from the peak areas of the two spectra. The average number of bilayers was calculated as  $100R/2\eta$  where R is the ratio of the outer to inner surface area calculated from the particle size measurements of the vesicles and assuming a bilayer thickness of 3.6 nm.

#### ***Equilibrium uptake of tyramine into the LUVs***

LUVs were prepared as described above in 0.04 M phosphate, formate, or acetate buffers with ionic strength adjusted to 0.1. A series of tyramine stock solutions from 3.7 to 100 mM were prepared in buffers matching those of three different LUV dispersions.

Aliquots from these stock solutions were added to the corresponding vesicle dispersions to obtain a lipid concentration of 13.5 mM and tyramine concentrations of 3.7-10 mM. The resulting dispersions were equilibrated at 25°C for 24 to 48 hours. After equilibration, the dispersions were filtered through Centricon-100 (nominal molecular weight limit = 100,000 g/mol) filters (Millipore Corporation, Bedford, MA) to obtain the extravesicular solution which was subsequently analyzed by HPLC for permeant concentration after appropriate dilution. The total concentration of tyramine in the dispersion was determined after lysing the vesicles by diluting them 1:2 in 1% Triton X-100 solution (prepared in HPLC mobile phase) and analyzing the clear solution by HPLC.

#### *Determination of apparent permeability coefficients*

A 0.6 mL aliquot of the LUVs (in 0.04 M formate or acetate buffer with ionic strength adjusted to 0.1 M) obtained from the extrusion process described above was applied to a PD-10 Sephadex G-25M column (Amersham Biosciences, Piscataway, NJ) preequilibrated with the matching buffer and eluted with the same buffer under gravity to remove untrapped permeant. The vesicles containing permeant were collected in the void volume of the column and were used for subsequent transport studies. Besides clearing the extravesicular volume of the permeant, the size exclusion process can also result in slight loss and dilution of the vesicles. The loss and dilution factor (yield factor) was estimated from the expected (calculated) and actual total permeant concentration in the dispersion after size exclusion. Actual total permeant concentration was obtained from HPLC analysis of the vesicle lysate prepared by diluting the vesicle dispersion with Triton X-100 solution in HPLC mobile phase. The concentration of the amine in lysate and the yield factor were subsequently used to estimate the lipid concentration, fraction volume enclosed, and amine mass balance in the post size exclusion vesicles.

The LUV dispersion obtained from the size exclusion column was placed in a 25 °C incubator and sampled at specific time intervals. The extravesicular solution was separated from vesicles at each time interval by ultrafiltration through Centricon-100 (nominal molecular weight limit = 100,000 g/mol, Millipore Corporation, Bedford, MA)

filters. Permeant concentration in this extravascular solution was then measured by HPLC or by scintillation counting (for  $^{14}\text{C}$ -mannitol). Data for tyramine were fitted as described in the theory section and those for bretylium and mannitol were fitted to the following equation to obtain  $P_{\text{app}}$ , the apparent permeability coefficient:

$$\left(C_{\text{filtrate}}^{\infty} - C_{\text{filtrate}}^t\right) = \left(C_{\text{filtrate}}^{\infty} - C_{\text{filtrate}}^0\right) e^{-6P_{\text{app}} t / d} \quad (3-5)$$

where  $C_{\text{filtrate}}$  represents the extravascular permeant concentration, superscripts 0 and  $\infty$  represent the initial and equilibrium concentrations, respectively,  $t$  represents the sampling time and  $d$  represents the vesicle hydrodynamic diameter. The equilibrium concentration was confirmed by analyzing a lysate of vesicles (lysed by diluting with an equal volume of 2% Triton X-100 solution in the HPLC mobile phase).

### ***HPLC analyses***

Tyramine was analyzed by reversed phase HPLC with UV detection at 280 nm. A 3  $\mu$ , 15 cm long, 4.6 mm inner diameter YMC-ODS-AQ C18 column (Waters Corp., Milford, MA) was employed for samples from experiments at 3 mM and 10 mM initial amine concentrations. A linear mobile phase gradient was used starting with a 20 mM pH 4.5 ammonium acetate buffer containing 1 mM octanesulfonate and increasing the acetonitrile percentage to 30% over 15 minutes, followed by a 5 minute equilibration at the initial conditions prior to the subsequent injection. A 3  $\mu$ , 50 mm long, 2 mm inner diameter Phenomenex Luna phenyl-hexyl column (Torrance, CA) was used for quantitation of samples from experiments at 1 mM initial amine concentration. The mobile phase consisted of 95% aqueous component (20 mM pH 4.5 ammonium acetate buffer containing 1 mM octanesulfonate) with 5% acetonitrile which was pumped at a flow rate of 0.3 mL/min.

Analyses of samples for bretylium concentration utilized the YMC-ODS-AQ C18 column described above and a linear mobile phase gradient from 0.05% TFA in deionized water to 25% acetonitrile:water also containing 0.05% TFA over a 20 minute period. UV detection was employed at 271 nm.

## Theoretical

### *Conventional approach to determine intrinsic permeability coefficient from pH-permeability profiles*

The rate of change of extravascular permeant concentration (i.e., ultrafiltrate concentration) in a liposomal dispersion,  $dB_{T(\text{ext})}/dt$ , containing a weak base is typically represented by the following rate law:

$$\frac{dB_{T(\text{ext})}}{dt} = \frac{6P_{\text{app}}V_{\text{int}}}{V_{\text{ext}}d} (B_{T(\text{int})} - B_{T(\text{ext})}) \quad (3-6)$$

where  $B_{T(\text{int})}$  and  $B_{T(\text{ext})}$  represent the total concentrations of permeant (i.e., neutral and ionized species) in the intravesicular and extravascular aqueous compartments, respectively, having volumes  $V_{\text{int}}$  and  $V_{\text{ext}}$ ,  $d$  is the vesicle diameter, and  $P_{\text{app}}$  and  $t$  are the apparent permeability coefficient and time, respectively.

If lipid bilayer transport can be attributed solely to the neutral species,  $P_{\text{app}}$  is related to the intrinsic permeability coefficient for the neutral species by the following:

$$P_{\text{app}} = f_B P \quad (3-7)$$

where  $f_B$  is the fraction of total solute in neutral form ( $f_B = K_a/(H^+ + K_a)$ ) where  $K_a$  is the ionization constant of the weak base). The validity of this assumption is typically verified by conducting multiple experiments at varying pH. Under acidic conditions ( $H^+ \gg K_a$ ) the above relationships suggest a linear relationship between  $\log(P_{\text{app}})$  and pH with a slope of 1.

Deviations in the slope of the plot of  $\log(P_{\text{app}})$  versus pH from a value of one or an incorrect value of the intrinsic permeability coefficient may occur due to several factors (e.g., permeant binding to the liposomal membrane, pH drift in either the intravesicular or extravascular compartments, etc.) that are not considered in the conventional model described above. The effects of membrane binding as influenced by pH, changes in internal or external pH due to permeant or buffer transport or flip-flop of acidic lipid

components, and the effects of pH drift on transport can be incorporated into the conventional model, as described below. Effects of some of these phenomena are magnified in the case of liposomal transport compared to those in the case of planar lipid membrane. This occurs due to significant volume differences between the two compartments as explained in detail in Appendix 1. Additional phenomena not covered in this theoretical section: transport of a permeable ion pair and the transport of a permeable dimer of the amine have been discussed in Appendix 2.

***Incorporation of the effect of membrane binding on the transport model***

Binding or complexation of a weakly basic amine must consider the binding of both neutral and charged species. The apparent binding constant,  $K_D^{app}$  can be defined as:

$$K_D^{app} = \frac{BHL + BL}{(BH^+ + B)L} \quad (3-8)$$

where B and BH<sup>+</sup> are the unbound neutral and protonated amine concentrations, respectively, and BL and BHL are the bound neutral and protonated amine concentrations, respectively. L is the lipid concentration available for binding (i.e., unbound concentration).

Total permeant concentration, B<sub>T</sub> is given as a sum of concentration of all species in solution. The fraction of neutral unbound amine,  $f_{B,unbound}$  can be obtained as follows:

$$f_{B,unbound} = \frac{B}{B_T} = \frac{B}{B + BH + BL + BHL} \quad (3-9)$$

Substituting the apparent binding constant gives:

$$f_{B,unbound} = \frac{K_a}{(H^+ + K_a)(1 + K_D^{app}L)} = f_B \left( \frac{1}{1 + K_D^{app}L} \right) = f_B f_{unbound} \quad (3-10)$$

where  $f_B$  is same as for Equation 3-7. The superscript *app* is omitted in the remainder of the text for simplicity and only  $K_D$  is used to represent the constant.

The above complexation model implies that a correction for unbound lipid concentration may be necessary. Accordingly, the following equation can be utilized for this purpose:

$$L = \frac{L_T}{1 + K_D(BH^+)} = \frac{L_T}{1 + K_D f_{BH} f_{unbound} B_T} \quad (3-11)$$

In practice, correcting for unbound lipid concentration may be unnecessary providing that the total lipid concentration,  $L_T$ , is in excess of the drug concentration. Under these circumstances, the complexation model becomes equivalent to a model which assumes that the drug can partition into the lipid membrane “pseudophase”.

To properly account for drug binding in a liposomal dispersion, it is important to distinguish between the effective intravesicular and extravesicular lipid concentrations or phase volumes to which the drug has access. Intravesicular drug binding may be significantly enhanced due to the elevated effective lipid concentration in the liposome interior. The total mass of lipid in the intravesicular and extravesicular compartments can be considered to be proportional to the surface areas of the inner and outer bilayer leaflets. The lipid concentrations in these compartments are therefore obtained from the vesicle radius ( $r$ ), lipid bilayer thickness ( $\lambda$ ) and total lipid concentration ( $L_T$ ) as follows:

$$L_{T(int)} = \frac{L_T V_T}{V_{int}} \frac{(r - \lambda)^2}{[(r)^2 + (r - \lambda)^2]} \quad (3-12)$$

$$L_{T(ext)} = \frac{L_T V_T}{V_{ext}} \frac{(r)^2}{[(r)^2 + (r - \lambda)^2]}$$

where  $V_T$ ,  $V_{int}$ , and  $V_{ext}$  represent the total, intravesicular, and extravesicular aqueous volumes, respectively.

Once the fraction of unbound neutral amine is estimated in both compartments, the rate law for efflux is then as follows:

$$\frac{dB_{T(ext)}}{dt} = \frac{6V_{int}}{V_{ext}d} P_{app} (f_{unbound(int)} B_{T(int)} - f_{unbound(ext)} B_{T(ext)}) \quad (3-13)$$



where the coefficients and constants were defined previously. The free fraction of intravesicular solute may be significantly reduced by the elevated lipid concentration to which the permeant is exposed in this compartment. On the other hand, nearly all of the extravesicular solute may be unbound due to the relatively low lipid concentration to which extravesicular permeant is exposed.

### ***Incorporation of intravesicular pH drift into the transport model***

Starting from equal pH in the two compartments, efflux of the unionized free base form of an amine-containing permeant can lead to significant acidification of the intravesicular compartment. This drift occurs due to the small volume of the intraliposomal aqueous core and is especially large when the buffer capacity is low. The pH of the extravesicular compartment would likely be unaffected by this process due to its much larger volume (~100 fold) and therefore insignificant perturbation in its proton concentration.

The increase in intravesicular  $H^+$  concentration as amine transport progresses is partially compensated by permeation of acidic buffer species. For the ensuing calculations, low molecular weight carboxylic acids employed as buffers are assumed to be freely permeable in their protonated form and impermeable as anions.

Combining Equations 3-6 and 3-7 and accounting for differing values for the fractions of free amine in the intravesicular ( $f_{B(int)}$ ) and extravesicular ( $f_{B(ext)}$ ) compartments in the presence of potential pH gradients, we obtain:

$$\frac{dB_{T(ext)}}{dt} = \frac{6V_{int}}{V_{ext}d} P \left( f_{B(int)} B_{T(int)} - f_{B(ext)} B_{T(ext)} \right) \quad (3-14)$$

At any given time,  $t$ , the intravesicular pH can be obtained from the charge balance equation with the condition that electroneutrality is maintained:

$$OH^-(0) - OH^-(t) + A^-(0) - A^-(t) = H^+(0) - H^+(t) + BH^+(0) - BH^+(t) \quad (3-15)$$

where the intraliposomal concentrations initially and at a later time are shown.  $A^-$  represents the concentration of buffer anion. Since the extravesicular compartment volume is large, extravesicular concentrations are minimally perturbed. Also, the HA species concentration is assumed to remain equal and invariant in the two compartments, given that the neutral species of buffer is freely permeable. Under acidic conditions where  $OH^-$  is negligible, Equation 3-15 thus becomes:

$$H_{int}^+(0) - H_{int}^+(t) = \left( B_{T(int)}(0) f_{BH(int)}(0) - B_{T(int)}(t) f_{BH(int)}(t) \right) + \left( A_{int}^-(0) - HA \frac{K_{buf}}{H_{int}^+} \right) \quad (3-16)$$

where  $K_{buf}$  is the acid ionization constant for the buffer. The charge balance can be solved to obtain a quadratic equation for proton concentration and intravesicular pH. Equation 3-14 can be numerically integrated, solving Equation 3-16 at each time step to fit one or more kinetic data sets simultaneously to obtain an intrinsic permeability coefficient when intraliposomal pH drift occurs due to efflux of free base.

### ***Effect of other acid/base carriers on the pH drift***

The ionizable lipid components of lipid bilayer membranes, such as phosphatidylglycerols or phosphatidic acid, have also been shown to distribute asymmetrically between the two leaflets in response to a pH gradient. (Hope and Cullis, 1987, Hope et al., 1989, Redelmeier et al., 1990) In the present studies, 4 mole percent of DOPA was incorporated into the liposomal membranes in order to impart physical stability to the vesicles (Cevc et al., 1988). DOPA is a weak acid that undergoes lipid bilayer flip-flop in response to a pH gradient and in the process act as a proton carrier between the compartments. This transport of DOPA between the two leaflets dissipates part of the pH gradient that caused it. Therefore, DOPA permeability across the lipid bilayer vesicles was also included in the rate law as follows.

$$\frac{dDOPA_{T(ext)}}{dt} = \frac{6V_{int}}{V_{ext}d} P_{DOPA} \left( DOPA_{T(int)} \left( \frac{H_{int}^+}{K_a^{DOPA} + H_{int}^+} \right) - DOPA_{T(ext)} \left( \frac{H_{ext}^+}{K_a^{DOPA} + H_{ext}^+} \right) \right) \quad (3-17)$$

where  $DOPA_T$  is the total intravesicular or extravesicular concentration of DOPA calculated as the mass of DOPA on the inner or outer leaflet divided by the intravesicular or extravesicular aqueous compartment volumes.  $P_{DOPA}$  is the intrinsic permeability coefficient of the neutral (protonated) form of DOPA ( $6.14 \times 10^{-6}$  cm/s) which was calculated from the rate constant reported by Eastman and coworkers (Eastman et al., 1991). The value of  $K_a^{DOPA}$ , the ionization constant of membrane bound DOPA reported by Eastman and coworkers ( $10^{-3}$  M) (Eastman et al., 1991) was assumed in these studies.

With this additional contribution, Equation 3-16 can be modified as follows:

$$H_{int}^+(0) - H_{int}^+(t) = \left( B_{T(int)}(0) f_{BH(int)}(0) - B_{T(int)}(t) f_{BH(int)}(t) \right) + \left( A_{int}^-(0) - HA \frac{K_{buf}}{H_{int}^+} \right) + \left( DOPA_{int}^-(0) - DOPA_{T(int)}(t) \frac{K_a^{DOPA}}{H_{int}^+(t) + K_a^{DOPA}} \right) \quad (3-18)$$

When DOPA is present, Equations 3-14 and 3-17 can be numerically integrated, solving Equation 3-18 at each time step to fit one or more kinetic data sets simultaneously to obtain an intrinsic permeability coefficient when intraliposomal pH drift occurs due to efflux of free base.

For an accurate calculation of pH drift, one must account for the transport of each species in solution capable of transporting protons back and forth across the membrane. For rapidly permeable species (such as the neutral buffer species employed in this study) including a term in the charge balance is sufficient. However if the flux of such a species is on the same time-scale as or slower than the transport of the amine, an additional rate equation such as Equation 3-17 must also be included and integrated simultaneously with the rate equation for amine transport.

### ***Combined model accounting for pH drift, complexation, and DOPA asymmetry***

In order to evaluate the simultaneous role of all processes described above (permeant ionization, membrane binding, pH drift and DOPA redistribution), Equation 3-14 must be modified as follows:

$$\frac{dB_{T(ext)}}{dt} = \frac{6V_{int}}{V_{ext}d} P \left( f_{unbound(int)} f_{B(int)} B_{T(int)} - f_{unbound(ext)} f_{B(ext)} B_{T(ext)} \right) \quad (3-19)$$

This equation and Equation 3-17 were used in their differential form and integrated numerically and the charge balance Equation 3-18 was solved at each time step. These equations were used to fit one or more kinetic data sets simultaneously by non-linear least-squares regression analysis (Micromath Scientist (Micromath, 1995)) to obtain an intrinsic permeability coefficient.

## Results

### *Determination of tyramine ionization constants*

Tyramine was chosen for this study as the first in a series of compounds to be examined for the construction of structure-transport relationships for amine-containing drugs. The aim was to select amine-containing compounds having a second polar functional group well isolated from the amine and similar minimum cross-sectional areas as other series of compounds previously studied in the authors' laboratories (Xiang and Anderson, 1994). Since tyramine and compounds structurally related to tyramine were available commercially, it was selected for this study.

Due to the closely spaced ionization constants of the phenol and primary amino functional groups, four tyramine species are possible in an aqueous solution (Figure 3-2). Detailed treatments of the equilibria and computation of individual species concentrations can be found in several papers (Riegelman et al., 1962, Martin, 1971, Armstrong and Barlow, 1976, Peinhardt and Wiese, 2001, Nagy and Takacs-Novak, 2004). However, due to conflicting data in the literature, all microconstants were estimated experimentally as needed under conditions similar to those employed in the permeability experiments.

Tyramine has four microscopic ionization states due to the ionization constants for the phenolic and amine groups which appear as two inflection points in a pH titration. Since phenol ionization is solely responsible for changes in the UV spectrum with pH, the spectrometric titration shows only one inflection point. Simultaneous fitting of both

the pH-titration curve and the UV spectral changes with pH to Equations 3-1, 3-2, and 3-3 yielded the microconstants listed in Table 3-1.

Figure 3-3 shows the fraction of each species in solution as a function of pH. At low pH the cationic species (charge = +1) dominates while at high pH the anionic species (charge = -1) is dominant. The neutral and zwitterionic forms reach their highest concentrations at ~ pH 10. The ratio of the zwitterionic to neutral form (referred to as the zwitterionic constant,  $K_z$ ) remains constant at all pH conditions. The fraction neutral calculated using Equation 3-7 gives the sum of neutral and zwitterion species. Given that the zwitterion fraction ( $f_{Bz}$ ) is significant for tyramine, one must calculate and use the fraction of neutral species ( $f_B$ ) estimated using  $K_z$  in order to calculate the intrinsic permeability of the neutral form. The microscopic ionization constants obtained above were used without correction for ionic strength. Since all studies employing these constants are also carried out at comparable ionic strengths, such conversion would cancel in calculations of the neutral species fraction.

***1,9-Decadiene-water partition coefficient and predicted permeability coefficient for tyramine***

The apparent partition coefficient of tyramine as a function of pH is shown in Figure 3-4. The log(intrinsic partition coefficient) obtained using Equation 3-4 is  $-1.33 \pm 0.015$  (SD).

Previous studies have established a correlation between the permeability coefficients for two series of carboxylic acids (Mayer et al., 2000, Xiang and Anderson, 1994) across liquid crystalline phosphatidylcholine bilayers and their 1,9-decadiene-water partition coefficients as follows:

$$\log(P) = 0.99 * \log(K_{o/w}) - 0.17 \quad (3-20)$$

The intrinsic permeability coefficient for tyramine can be predicted from this equation to be  $3.25 \times 10^{-2} \text{ cm/s} \pm 0.1 \times 10^{-3}$  (SD) corresponding to a log(intrinsic permeability) of  $-1.49 \pm 0.014$ .

### *Characterization of the lipid bilayer vesicles and pH dependence of barrier properties*

The transport models employed for obtaining the intrinsic permeability coefficient from the data generated in this study assume unilamellar vesicles and require a value for the vesicle diameter. For each of the several batches of vesicles used in this study, the vesicle diameter determined by laser light scattering was found to be  $\sim 200$  nm and similar to previously published results from the authors' laboratories.

While most of the experiments in the authors' laboratories in the past have utilized unilamellar vesicles, these studies were generally at a higher pH than the pH window for this study (Mayer et al., 2003, Mayer et al., 2000). Consequently, lamellarity (average number of lipid bilayers per vesicle) was verified at two extremes of pH. The vesicles prepared at pH 2 and 6 were found to contain averages of 1.15 and 1.0 bilayers, respectively, with an approximate error estimated from the baseline noise of the spectra of approximately  $\pm 0.3$ . This large error of estimation was due to the long acquisition time for spectra which in turn was due to the slow relaxation rates of the phosphorus atoms in the lipid bilayers compared to typical nuclei in solution.

The apparent permeability coefficients for mannitol and bretylium across DOPC bilayers as a function of pH (this study) along with values for mannitol across egg phosphatidylcholine (EPC) vesicles at 25°C measured previously (Mayer et al., 2000) are shown in Figure 3-5. EPC bilayers are comparable in chemical composition and phase structure to the DOPC bilayers and the permeability coefficient obtained for mannitol in this study ( $9 \times 10^{-11}$  cm/s) agreed well with that reported previously in EPC ( $1.0 \times 10^{-10}$  cm/s). An average permeability coefficient of  $3 \times 10^{-11}$  cm/s was obtained for bretylium. Since bretylium is a quaternary ammonium compound and mannitol a nonelectrolyte, neither undergoes pH-dependent ionization. As a result, their apparent permeability coefficients would not be expected to change with pH unless the barrier itself exhibited pH-dependence. The horizontal pH-permeability profiles exhibited by both permeants indicate that the barrier properties did not vary with pH. A similar conclusion was reached previously based on the lack of variation in the permeability coefficient for

acetamide (average  $2.9 \times 10^{-4}$  cm/s) as a function of pH across planar lipid bilayer (EPC) membranes between pH 3 to 8 (Xiang et al., 1992).

### ***Equilibrium uptake of tyramine into the lipid bilayer vesicles***

Tyramine-liposome binding experiments were conducted over the pH window (pH 2-4) along with experiments to ensure that tyramine binding to ultrafiltration filters and tubes was negligible (results not shown) as a function of pH and concentration. Figure 3-6 shows that approximately 80% of the total tyramine concentration in the presence of liposomes (13.5 mM lipid) is unbound at pH 2, 3, and 4. The absence of curvature in the plots at each pH suggests the absence of saturable binding (Austin et al., 1998) or other phenomena that might lead to a concentration dependence in binding over the relevant concentration range. Consequently, the extent of tyramine binding at pH 2, 3, and 4 was considered to be independent of pH for subsequent calculations. The equilibrium uptake data obtained at all pH conditions were combined and fit to a model that considered both binding and the potential intravesicular pH drift that might accompany uptake of the neutral (basic) tyramine molecule (see methods section). A binding constant,  $K_D$ , of  $24.1 \pm 1.2$  (SD)  $M^{-1}$  was obtained.

### ***Vesicle efflux and the pH-permeability profile for tyramine***

Representative profiles for tyramine efflux from DOPC vesicles at varying initial pH and starting intravesicular concentrations of permeant are shown in Figures 3-7, 3-8, and 3-9. While initial conditions dictate that the extravesicular concentration is zero at the start of experiment, due to practical reasons an initial delay of a few minutes is unavoidable. While this initial release has no effect on the sink conditions, the integrated form of the conventional transport model (Equation 3-5) allows for including the initial permeant release to be subtracted from each time point. However since the remaining rate laws (Equations 3-13, 3-14, 3-17 and 3-19) require time dependent terms other than concentration (fraction unbound, pH, fraction of neutral permeant, DOPA concentration and fraction ionized), all these terms must be calculated using the concentration of solute released at the initial time point. Therefore all applicable equilibria (binding, ionization, pH drift, DOPA) for a given model were solved to

correspond with the small amount of solute released and appropriate values were used as initial conditions in Equations 3-13, 3-14, 3-17 and 3-19 for the numerical integration.

As transport progresses, the extravesicular amine concentration approaches a plateau value depending on the initial concentration of the amine. This equilibrium concentration was typically found to be less than that determined after surfactant lysis of the vesicles (i.e., when fraction = 1 in Figures 3-7, 3-8, and 3-9), suggesting incomplete liposomal release despite maintenance of a significant concentration gradient.

Fits of the data in Figures 3-7, 3-8, and 3-9 to the conventional model (dashed lines, Equation 3-6) and the comprehensive model (solid lines, Equations 3-17, 3-18, and 3-19) are also shown. The apparent permeability coefficients obtained by fitting the data to Equation 3-6 (conventional model) for initial amine concentrations of 1 mM, 3 mM, and 10 mM are plotted as a function of the initial buffer pH in Figures 3-10, 3-11, and 3-12. Whereas a slope of 1 is predicted from Equation 3-7, the slopes of the  $\log(P_{app})$  vs. pH plots were found to be less than one and decreasing with increasing initial concentration of tyramine (i.e., 0.91, 0.69, and 0.44, for 1 mM, 3 mM, and 10 mM initial amine concentrations). Moreover, the scatter in the data appeared to increase with an increase in the initial amine concentration. The intrinsic  $\log(\text{Permeability coefficient})$  obtained from the combined fits of all the data from these three sets was -2.14 ( $\pm 0.023$ ) which did not agree with the value predicted (-1.49) using Equation 3-20.

The comprehensive model shown in Equations 3-17, 3-18, and 3-19 was used to fit data from each kinetic curve to obtain an intrinsic permeability coefficient for each. Each intrinsic permeability coefficient was then used to calculate an apparent permeability coefficient at the initial pH of the corresponding experiment and subsequently used to construct a pH profile to demonstrate the effect of the comprehensive model on the slope of the pH profile. The reconstructed profiles along with those obtained from the conventional model are shown in Figures 3-10, 3-11, and 3-12 for 1 mM, 3 mM, and 10 mM initial amine concentrations. Slopes of the  $\log(P_{app})$  vs. pH profiles were found to be much closer to the theoretical expectation of 1.0 (i.e., 0.86, 0.88, and 1.07, for 1 mM, 3 mM, and 10 mM initial amine concentrations,



respectively). An additional change realized from the use of the comprehensive model was an upward shift of all three profiles, indicating a higher value for the calculated intrinsic permeability coefficient. A value of -1.39 ( $\pm 0.019$ ) was obtained for the intrinsic log(Permeability coefficient) from the combined fit of all the data from these three sets, which is closer to the value predicted using Equation 3-20.

## **Discussion**

### ***Characterization of LUVs and validation of the barrier properties at low pH***

While DOPC:DOPA lipid bilayer membranes or vesicles have been employed in previous transport studies at relatively high pH, (Mayer et al., 2000, Mayer et al., 2003) the effect of an acidic pH on their barrier properties has not been established to the authors' knowledge. Considering that the first pKa of liposomally bound phosphatidic acid is  $\sim 3$  (Eastman et al., 1991), verification of barrier integrity in the vicinity of pH 3 was considered essential. The lack of any significant change in the permeability coefficients of mannitol and bretylium in the pH 2-4 range (Figure 3-5) suggests that the state of ionization of DOPA had a minimal effect on barrier properties. This observation may have been due to the fact that DOPA accounted for only 4% of the total lipid in the bilayer, with the major component, DOPC, being zwitterionic over the entire pH range examined.

Hydrolysis of saturated or unsaturated phosphatidylcholines may also occur at low pH to form lysophosphatidylcholine. Grit and coworkers (Grit and Crommelin, 1992) have shown that the initial (up to 50 hours) leakage rate of calcein in 10% hydrolyzed egg phosphatidylcholine vesicles was similar to or slightly lower than that of fresh vesicles. Therefore, the barrier properties of EPC bilayers appear to change minimally with up to 10 percent hydrolysis. A series of systematic studies reported for various phosphatidylcholine (Grit and Crommelin, 1993) vesicles indicated the existence of a "V" shaped pH-stability profile with maximum stability between pH 6 and 7. The water, proton and hydroxyl ion catalyzed rate constants for hydrolysis at 70 °C were reported to be  $6.2 \times 10^{-8} \text{ s}^{-1}$ ,  $1.6 \times 10^{-2} \text{ M}^{-1} \text{ s}^{-1}$ , and  $2.7 \times 10^{-1} \text{ M}^{-1} \text{ s}^{-1}$ , respectively. Assuming a 2 fold decrease in rate constant per 10 °C change in temperature, approximately 10

percent reaction would be expected in 10 hours at pH 2 and 25°C. For this reason, the duration of our experiments at low pH was less than 8 hours. The assumption of a 2-fold decrease in rate constant is likely to result in an overestimate of the extent of reaction under the conditions of this study.

***Predicted value for the lipid bilayer permeability coefficient of tyramine***

According to the bulk solubility-diffusion theory, (Finkelstein, 1976, Xiang and Anderson, 1997) the passive permeability coefficient,  $P_o$ , for a molecule across a lipid bilayer membrane can be determined from its membrane/water partition coefficient,  $K$ , and diffusion coefficient,  $D$ , in the membrane, assuming that the membrane behaves as a homogeneous bulk solvent:

$$P_o = \frac{KD}{h} \quad (3-21)$$

where  $h$  is the thickness of the membrane. Treatments that recognize the well-known heterogeneity of lipid bilayer membranes account for the resistance to transport (i.e., the inverse of permeability ( $1/P$ )) in terms of the additive contributions of a series of domains (Diamond and Katz, 1974). If the contribution of a single region (the rate-limiting barrier) to the overall resistance is significantly larger than the rest, it can be shown that the overall permeability is the same as the permeability across this domain. The recently proposed barrier domain model (Xiang and Anderson, 1998) suggests that the barrier region for the transport of relatively polar molecules across lipid bilayers is the hydrocarbon chain region and that the permeability coefficient ( $P_m$ ) is determined by the product of the bulk-solubility diffusion model-predicted permeability coefficient ( $P_o$ ) and a correction factor ( $f$ ) to account for the additional contribution of chain ordering to barrier properties (i.e.,  $P_m = f*P_o$ ). The permeability decrement factor ( $f$ ) was shown to be a function of the free surface area of the bilayer and the minimum cross-sectional area of the permeant.

Equation 3-20, generated from previous work in the authors' laboratories for two different series of carboxylic acids having similar minimum cross-sectional areas,

indicates that the permeability coefficients across liquid crystalline lipid bilayer membranes is a linear function of the 1,9-decadiene/water partition coefficient, consistent with the view that the barrier domain is the hydrocarbon chain region (Mayer et al., 2000). Since the bilayer composition employed in the present study is similar to that used in the previous work and the minimum cross-sectional area for tyramine is comparable to those of the permeants upon which Equation 3-20 is based, the correlation described by Equation 3-20 was used to predict the intrinsic permeability coefficient of the neutral form of tyramine from its 1,9-decadiene/water partition coefficient, which was generated from the data shown in Figure 3-4.

#### ***Expected pH profile for tyramine transport across lipid bilayer membranes***

According to the pH-partition hypothesis, the permeability of weak electrolytes across lipid bilayer membranes is proportional to the fraction of the neutral form in solution, as described for a monovalent weak base by Equation 3-7. According to Equation 3-7, a linear pH-permeability profile with slope of 1 is expected when  $\text{pH} \ll \text{pK}_a$ , as illustrated in Figure 3-13. A plateau should occur at high pH where the neutral form is dominant in solution while deviations from linearity at low pH may reflect a contribution to transport from the ionized species.

The log (Papp) vs. pH profiles for tyramine shown in Figures 3-10, 3-11, and 3-12 based on the use of the conventional model (Equation 3-6) to generate values of Papp from efflux data did not conform to the expectations of pH-partition theory described above. Whereas the slope of the profile at an initial intravesicular tyramine concentration of 1 mM was close to 1, the slopes of the profiles at 3 mM and 10 mM tyramine were significantly less than 1. The intrinsic permeability coefficient calculated using the conventional model (Table 3-2) also appeared to be significantly lower than the value predicted from Equation 3-6.

Gutknecht and coworkers (Gutknecht and Walter, 1981) found that non-linearity in pH profiles reported by Bean and coworkers (Bean et al., 1968) was related to unstirred water layer effects. While unstirred water layers are frequently a rate-limiting concern for studies in planar lipid bilayer systems, the unstirred water layers in the case

of liposomes (approximately 200 nm diameter) are much thinner (Higuchi and Hiestand, 1963) and were ruled out as a contributing factor in the present studies.

In addition to the observation that the slopes of  $\log(P_{app})$  vs. pH were non-unity (Figures 3-10, 3-11, and 3-12), a closer examination of the efflux profiles (Figures 3-7, 3-8, and 3-9) revealed several unusual findings. First, the extent of tyramine release from the vesicles was less than 100% at the completion of the efflux process, despite the continuing presence of a tyramine concentration gradient favoring further release. Second, plots of extraventricular fraction vs. time (Figures 3-7, 3-8, 3-9) exhibited greater curvature than could be accommodated by the conventional model (Equation 3-6).

Several possible causes of these discrepancies were considered. They included membrane binding of tyramine enhanced by the high local lipid concentration in the vesicle interior and various factors that might lead to the development of pH gradients between the internal and extraventricular compartments. These factors are discussed in the following sections.

#### ***Equilibrium uptake of tyramine and the effect of membrane binding***

The equilibrium uptake of tyramine into liposomes at a lipid concentration of 13.5 mM in the pH 2-4 region was shown to account for approximately 20% of the total tyramine in solution, independent of pH and concentration (Figure 3-6). Both hydrophobic and electrostatic components may contribute to the binding of solutes to lipid bilayers. Usually, electrostatic interactions are saturable due to charge repulsion produced by the increasing surface concentration of the bound solute (if ionized) (Baeuerle and Seelig, 1991). This effect is frequently modeled using Gouy-Chapman theory which accounts for a reduced interfacial concentration of ions due to charge accumulation (Aveyard and Haydon, 1973). The absence of pH dependent binding in Figure 3-6 in the pH range where the protonated amine is the dominant species suggests that the protonated amine may be the major species bound in the pH range of interest. The lack of significant curvature in the binding isotherms rules out potential saturation due to charge effects. This apparent contradiction may be due to the fact that the interfacial binding is driven primarily by hydrophobic contributions with the charged

amino group located further from the interface and solvated by water and oppositely charged counterions. Molecular dynamics simulations of tyramine have shown that near the membrane-water interface tyramine tends to orient in a manner perpendicular to the membrane interface with the phenolic-OH pointing towards the membrane and the amine group solvated in water (Tejwani et al., 2004).

The equilibrium uptake experiments described above have been interpreted solely in terms of membrane binding without taking into account possible changes in the thermodynamic activity coefficient of protonated tyramine in the intraliposomal compartment that are unrelated to membrane binding. For example, the surface charge on the inner bilayer leaflet and the cloud of oppositely charged ions that concentrate at the membrane water interface to dissipate this charge may influence the activity coefficient of protonated tyramine if a significant fraction of entrapped tyramine molecules in the aqueous core are in sufficiently close proximity to the bilayer membrane surface. In a 0.1 M monovalent salt solution these effects would be largely dissipated over a distance of approximately 1 nm (Bockris and Reddy, 1998), however, and should have little influence on the overall thermodynamic activity of protonated tyramine in the aqueous compartment of a 200 nm diameter vesicle. If present, any effects on thermodynamic activity coefficients apart from membrane binding are incorporated into the membrane binding term in this study.

Data for binding to lipid bilayers can be treated mathematically by partitioning models (Macdonald and Seelig, 1988, Austin et al., 1998, Rogers and Davis, 1980) or by complexation or Langmuir-type adsorption models where each lipid molecule is considered to be a binding site (Martin et al., 1993). While the two are mathematically equivalent in non-saturating conditions, the latter allows for saturation. Since tyramine binding (Figure 3-6) did not exhibit significant curvature, the partitioning and complexation approaches are equivalent in the present case.

The effect of pH-independent membrane binding on liposomal efflux was simulated for the cases of negligible ( $K_d = 1 \times 10^{-6} \text{ M}^{-1}$ ), low ( $K_d = 30 \text{ M}^{-1}$ ), and moderate ( $K_d = 100 \text{ M}^{-1}$ ) binding using Equation 3-13 as illustrated in Figures 3-14 and 3-15.

Figure 3-14 displays the fraction of drug released while Figure 3-15 shows the unbound concentration gradient vs. time. Since membrane binding reduces permeant flux, any membrane binding that is not properly taken into account can lead to a significant underestimation of permeability coefficients. The influence of pH-independent membrane binding on the log apparent permeability coefficient vs. pH profile (e.g., Figure 3-10, 3-11, and 3-12) would be to shift the entire profile downward, due to consistent underestimation of the apparent permeability coefficients at various pH conditions.

For tyramine, the resulting logarithm of the intrinsic permeability coefficient obtained after applying the binding correction to all of the kinetic profiles is  $-1.76 \pm 0.02$  cm/s (Table 3-2). The correction still appeared to underestimate the permeability coefficient compared with that predicted using Equation 3-20, and the slopes of the pH profiles at higher initial tyramine concentrations (plots not shown) remained significantly less than unity.

#### *Effect of pH drift and the role of other acid/base carriers*

Weak electrolytes are known to distribute asymmetrically across semi-permeable membranes in response to a pH gradient (Deamer et al., 1972, Nichols and Deamer, 1976). This behavior occurs when the neutral form is the permeable species and therefore the pH-partition hypothesis is applicable while the ionic equilibria on either side of the membrane **are** governed by the Henderson-Hasselbalch relation. For monoamines, the following relation was derived (Deamer et al., 1972) using the Henderson-Hasselbalch relation assuming that the neutral species equilibrates across the membrane.

$$\frac{H_{don}^+}{H_{rec}^+} = \frac{BH_{don}^+}{BH_{rec}^+} \quad (3-22)$$

Equation 3-22 is frequently employed with  $^{14}\text{C}$ -labelled amines or amine spin probes for measurement of transmembrane pH gradients in liposomes. The movement of amines in response to a pH gradient has been used in pH-gradient loading of liposomes containing a pre-established pH gradient (generated by one of several other means). The

technique is known to achieve significantly high concentrations of solutes inside liposomes (Mayer et al., 1986, Mayer et al., 1990, Lasic et al., 1995) for drug delivery applications.

Since pH gradients of 2 to 4 units are neutralized by the loading of amines into the liposomes, it is expected that solute release from these systems would also lead to the generation of a pH gradient (See Appendix 1 for a detailed description of pH gradient generation in response to amine transport). While permeant uptake and release both involve the generation or dissipation of pH gradients, kinetic studies of such systems frequently assume that the pH in the donor and receiver compartments is equal and constant with respect to time for calculating the rate constants (Harrigan et al., 1993, Boman et al., 1993). This assumption can lead to errors in the intrinsic permeability coefficients that are determined from the rate constants. Further, an incomplete understanding of the speciation and pH conditions can complicate drug delivery system design as this information may be necessary to optimize other aspects of such dosage forms.

Ceh and Lasic (Ceh and Lasic, 1995) derived predictive equations describing the equilibrium concentrations of several species, including the expected final pH gradient due to the remote loading of liposomes. However, since kinetic expressions involving the development of pH gradients are difficult to solve analytically, a fixed pH gradient was assumed to integrate the relatively complex rate law (Ceh and Lasic, 1998). Due to the difficulty of analytically integrating equations describing a continuous change in pH with time, one must employ numerical integration with the appropriate rate laws to carry out regression analyses.

Ignoring the pH drift that may occur during liposomal transport studies involving weak acids or bases may contribute to non-conformity with the theoretical pH profiles. Lee and coworkers (Lee et al., 1998) measured the release of carboxyfluorescein from folate-PEG-liposomes as a function of pH. While they did not report the apparent rate constants, the slopes of linear release profiles indicated only a 3-fold increase in rate constant for a one unit decrease in pH, instead of the theoretically expected 10-fold

change. Similarly, the time course of vincristine uptake as a function of pH reported by Boman et al (Boman et al., 1993) showed a significantly lower slope in the pH profile than that expected theoretically.

Since the release of a weak base from vesicles leads to a decrease in intravesicular pH (as derived in the theoretical section), the instantaneous flux continuously decreases with time. Evidence for this phenomenon can be seen in Figures 3-7 to 3-9, where the curvature for the experimental profiles was found to be greater than could be predicted by the conventional transport model due (possibly) to a continuous decrease in pH. A consequence of intraliposomal pH drift for both weakly basic and weakly acidic permeants is that the conventional model would underestimate the permeability coefficient. This self-inhibiting bias increases with liposomal drug loading as the pH drift is quantitatively linked to the amount of solute transferred. This can be seen in Figures 3-10 to 3-12 where the deviation in the slope of the log  $P_{app}$  vs. pH profile from a value of one is greater for the higher initial amine concentration.

Shown in Figures 3-16 and 3-17 are the results of several simulations using Equations 3-14 and 3-16 to determine the change in intravesicular pH resulting from the liposomal efflux of a weakly basic amine ( $pK_a = 10$ ) initially present at an intravesicular concentration of 0.01 M (Additional simulations are given in Appendix 1). An intrinsic permeability coefficient of 0.03 cm/s was assumed for the amine along with a negligible binding constant. The initial intravesicular pH was buffered (40 mM buffer) at either 2.25 or 4.25 and buffer  $pK_a$  was varied from 1.75 to 4.75. For these simulations the buffer species (HA) was assumed to be rapidly permeable, similar to the case of acetate or formate relative to apparent permeability coefficients of tyramine. For the same quantity of permeant transported, the pH drift was found to be greater at the higher initial pH. Thus, the efflux of 0.01 M of amine at initial pH 4.25 resulted in a pH drift of  $> 1$  unit in the low buffer capacity situation (buffer  $pK_a$  of 4.75) whereas the same transport at initial pH 2.25 led to a pH change of  $< 0.3$  units (buffer  $pK_a$  of 2.75).

This dependence of the pH drift on the initial intravesicular pH can lead to a reduction in the slope of a plot of log  $P_{app}$  vs. pH, since the permeability at a higher



initial intravesicular pH is inhibited more by the greater pH drift that occurs. This effect, combined with the effect of the initial solute concentration described above, is seen in the conventional pH-permeability profiles for tyramine shown in Figures 3-10 to 3-12 where the deviation from a slope of one is the largest at 0.01 M tyramine while the slope in the 0.001 M tyramine experiments is nearly one.

In the simulations described above (and also in the experiments) the buffer concentration was at least 4-fold higher than the permeant concentration and the intravesicular pH was within 0.5 pH units of the buffer pKa. Nevertheless, the pH drift in some cases was substantial, particularly when the initial intravesicular pH was below the pKa of the buffer, as the pH decrease that occurred with loss of the weakly basic permeant was also accompanied by a reduction in buffer capacity. This is illustrated in Figures 3-16 and 3-17 by the significantly greater pH drift that occurred at an initial pH of 4.25 when the buffer pKa was 4.75 compared to when it was 3.75. Variation in the magnitude of pH drift therefore depends on the setting of the initial intravesicular pH relative to the buffer pKa (initial pH such that  $\text{pH} - \text{pKa} > \text{or} < 0$ ) and may result in an increase in the scatter of pH permeability profiles when the conventional model is used for determining permeability coefficients.

In the development of the comprehensive model described by Equations 3-17, 3-18, and 3-19, the neutral buffer species (HA) was assumed to be rapidly permeable, such that the concentration of HA remained equal on both sides of the membrane at all times. If a buffer species were to be slowly permeable over the time scale of the experiment, efflux of the weakly basic permeant would produce a steeper initial pH gradient because the compensation effect of buffer co-transport would be delayed. DOPA, one of the potential buffer species present in the membrane, may be an example of a buffer species that exhibits slow equilibration in response to a developing pH-gradient. The rate of DOPA flip-flop in response to a pH gradient at various pH conditions has been previously studied (Eastman et al., 1991) and this phenomenon was therefore incorporated into the model.

The permeability coefficients obtained by fitting the various models described above to the combined experimental data are shown in Table 3-2 along with other statistical measures of the quality of fit such as the model selection criterion (MSC, a statistical parameter useful in comparing models with a different number of fitted parameters) (Micromath, 1995), and the corresponding sum of squared deviations between the observed and calculated data. Higher values of MSC and lower sums of squared deviations are associated with improved fits. Since all models utilized the experimentally determined ionization constants while those models invoking membrane binding also used experimental values, the only fitted parameter was the intrinsic permeability coefficient. Thus, the sum of squared deviations can be compared as an indicator of goodness of fit. The improved fit for the comprehensive model that considered intravesicular pH-drift (including DOPA flip-flop) and membrane binding of the permeant along with the similarity of the resulting value for the log of intrinsic permeability to that predicted (-1.49) from Equation 3-20 underscores the importance of accounting for these phenomena when they are likely to be important.

### **Conclusion**

The agreement of the experimental intrinsic permeability value of tyramine to that predicted from solubility diffusion theory when a comprehensive model was used to analyze the transport data suggests that the most critical phenomena causing errors in determining accurate intrinsic permeability coefficients have been addressed. Very weak binding of tyramine to the lipid bilayer membrane was found to shift the apparent permeability coefficients significantly, suggesting that membrane binding should be taken into account even for solutes that bind only moderately. The pH gradient effects, most frequently encountered in drug delivery applications, can also significantly alter the apparent intrinsic permeability coefficients and thereby affect the predictability of release rates. In contrast to membrane binding, pH drift can potentially alter the slopes of pH profiles as well as shift them upward or downward. The development of unintended pH gradients in liposomal drug delivery systems may also be a concern from other points of view such as drug stability. Mathematical models presented in this study show a means to estimate and correct for such gradients.

A less obvious consequence of pH-drift in liposomal transport studies is the scatter that it may produce due to variability in the relative values of the initial intravesicular pH and the pKa of the buffer being employed to control pH. This effect combined with the effects of other acid/base carriers that may be present can further complicate the situation, which in certain cases can lead to pH-profiles that deviate significantly from the classical behavior.

It is interesting to note that the phenomena described herein may have only minor effects on experiments conducted in classical diffusion-cells. However, the large disparity in volumes between the intraliposomal and receiver compartments can magnify both binding effects and pH-drift to such an extent that the reliable estimation of intrinsic permeability coefficients may be impossible without the appropriate models.

**Table 3-1.** Microscopic and macroscopic ionization constants for tyramine (Figure 3-2). Values in parentheses are standard deviations.

Constant	This study	Literature values
pk <sub>1</sub>	9.62 (0.01)	9.61 <sup>i</sup> , 10.30 <sup>ii</sup> , 9.59 <sup>iii</sup>
pk <sub>2</sub>	10.01 (0.02)	10.06 <sup>i</sup> , 9.72 <sup>ii</sup> , 9.66 <sup>iii</sup>
pk <sub>12</sub>	10.62 (0.02)	10.53 <sup>i</sup> , 9.48 <sup>ii</sup> , 10.03 <sup>iii</sup>
pk <sub>21</sub>	10.23	10.08 <sup>i</sup> , 10.06 <sup>ii</sup> , 9.97 <sup>iii</sup>
K <sub>z</sub>	2.43	2.82 <sup>i</sup> , 1.18 <sup>iii</sup>
pK <sub>1</sub>	9.47	9.48 <sup>i</sup> , 9.38 <sup>ii,a</sup> , 9.37 <sup>iii,b</sup>
pK <sub>2</sub>	10.77	10.66 <sup>i</sup> , 10.40 <sup>ii,a</sup> , 10.70 <sup>iii,b</sup>
Ionic strength	0.1	0.15 <sup>ii</sup> , 0.1 <sup>iii</sup>
Temperature (°C)	25	25 <sup>i</sup> , 25 <sup>ii</sup>

i. Value reported by Peinhardt et al (Peinhardt and Wiese, 2001)

ii. Value reported by Nagy et al (Nagy and Takacs-Novak, 2004)

iii. Value reported by Riegelman et al (Riegelman et al., 1962)

<sup>a</sup>Values of pK<sub>1</sub> and pK<sub>2</sub> calculated using microconstants reported in the same study are 9.62 and 10.16, respectively.

<sup>b</sup>Values of pK<sub>1</sub> and pK<sub>2</sub> calculated using microconstants reported in the same study are 9.32 and 10.30, respectively.

**Table 3-2.** Summary of intrinsic permeability coefficients and fitting statistics obtained from nonlinear regression analyses of the combined data for tyramine transport employing **various** models

<b>Model</b>	<b>Log(Intrinsic Permeability, cm/s)</b>	<b>Lower 95% C.I.<sup>a</sup></b>	<b>Upper 95% C.I.<sup>a</sup></b>	<b>MSC<sup>b</sup></b>	<b>Sum of Squared Deviations</b>
Conventional	-2.14	-2.18	-2.09	2.91	3.26E-09
Binding	-1.76	-1.80	-1.72	3.22	2.39E-09
pH-drift with DOPA	-1.96	-1.99	-1.91	3.47	1.74E-09
Comprehensive	-1.39	-1.42	-1.35	4.15	9.28E-10

<sup>a</sup>C.I. = confidence interval

<sup>b</sup>MSC = Model Selection Criterion is a modified Akaike information criterion (AIC) that provides largest number for the most appropriate model (Micromath, 1995).

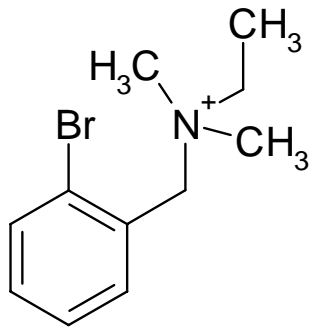


Figure 3-1. Structural formula of bretylium

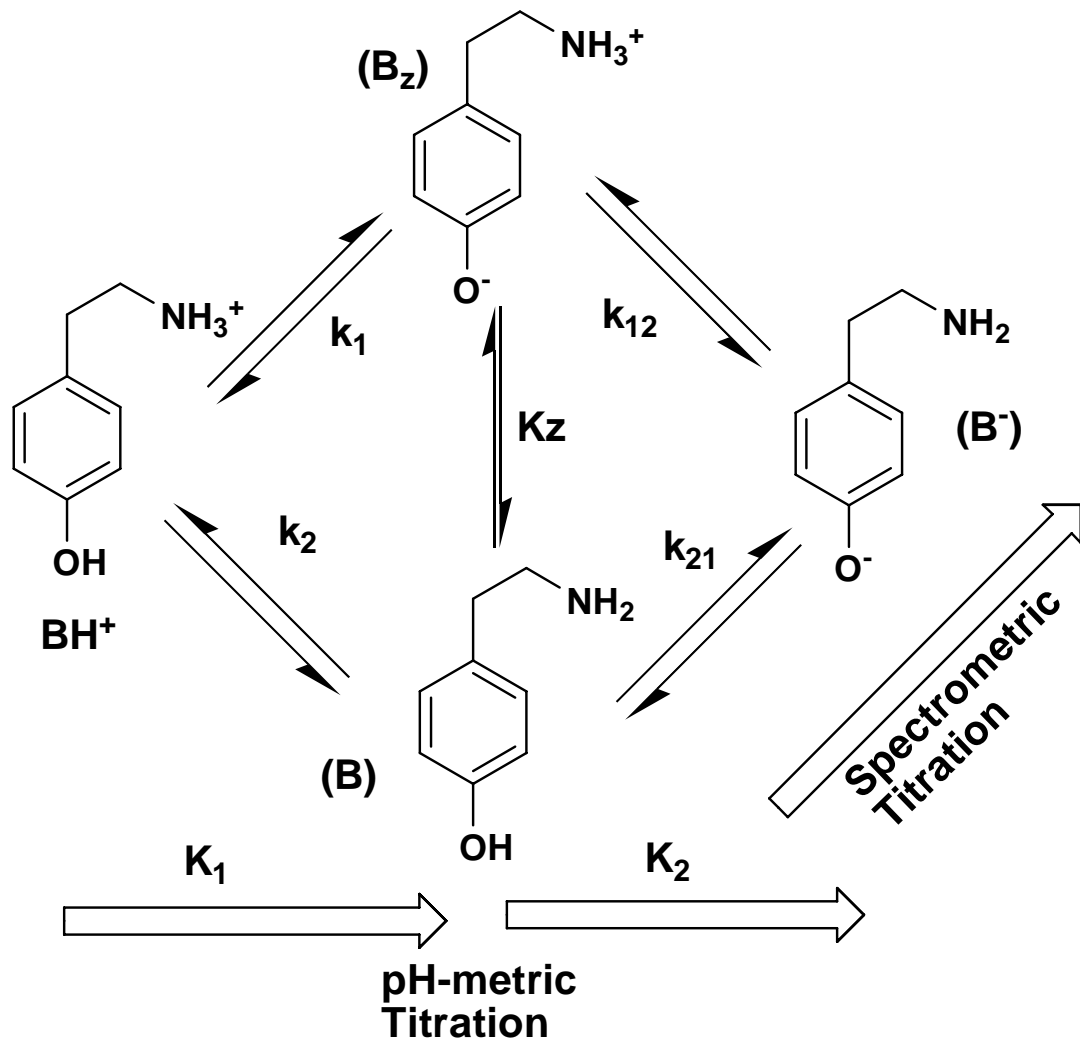


Figure 3-2. Ionization of tyramine

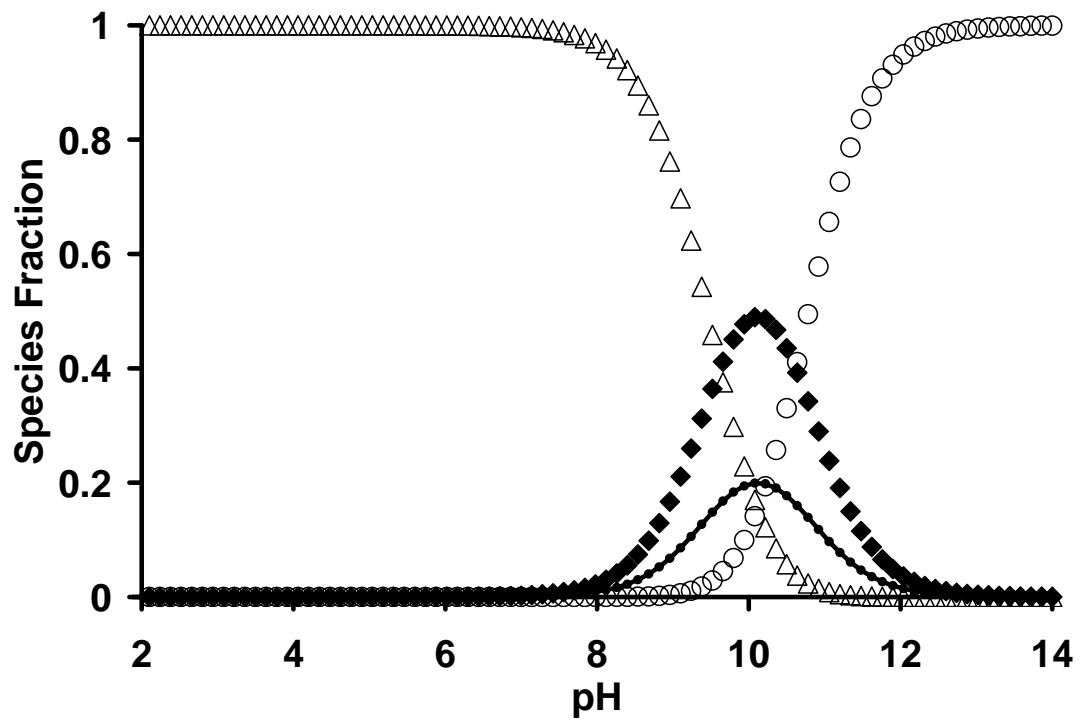


Figure 3-3. Fraction of tyramine species: cation (  $\Delta$  ), zwitterion (  $\blacklozenge$  ), neutral (—), and anion (  $\circ$  ), as a function of pH.



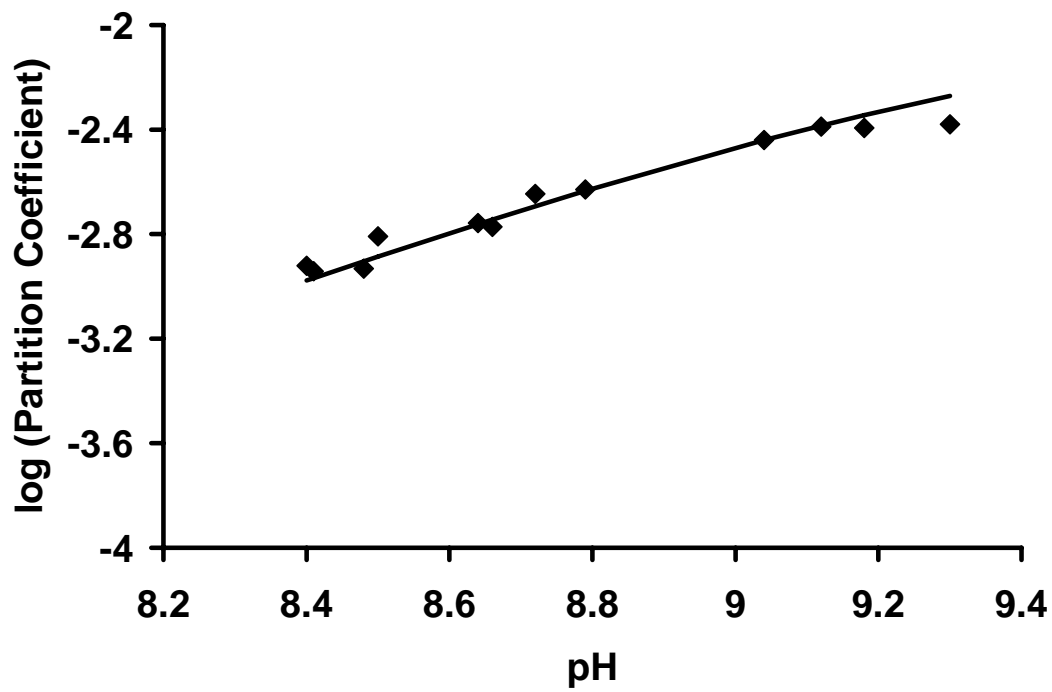


Figure 3-4. 1,9-Decadiene-water partition coefficient of tyramine as a function of pH. The points are single determinations and the line is the best fit to Equation 3-4.

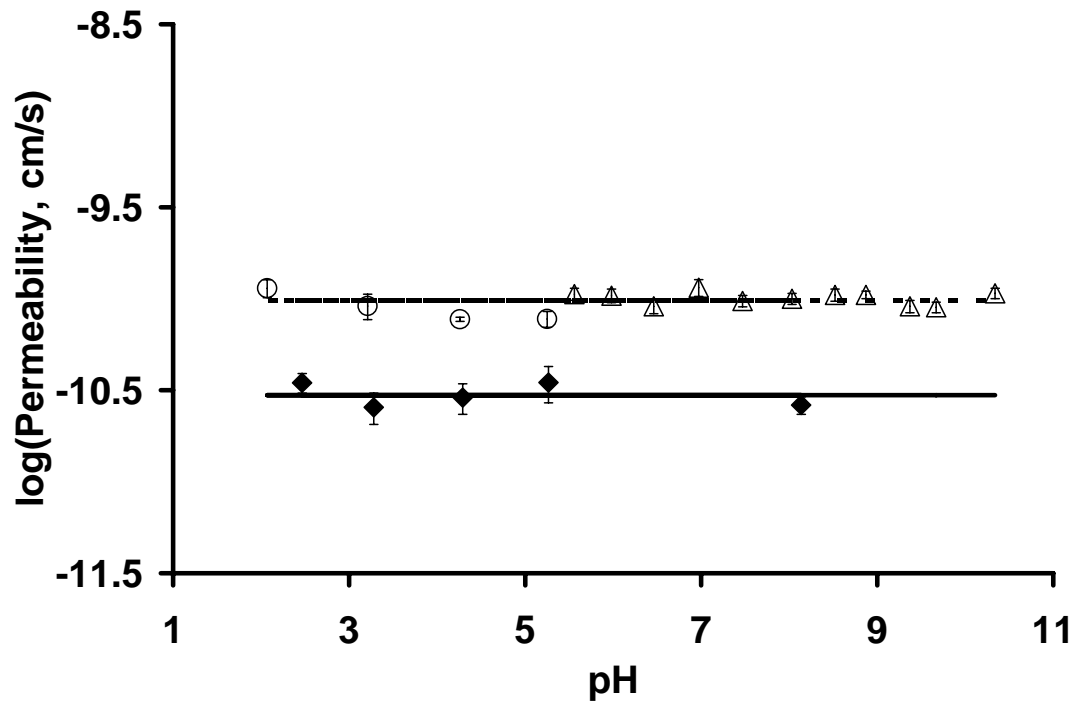


Figure 3-5. Permeability of D-mannitol (○) and bretylium (◆) across DOPC and permeability of D-mannitol across egg phosphatidylcholine bilayers (Δ, data from Mayer et al (Mayer et al., 2000)). Error bars (sometimes smaller than symbols) represent standard deviations and lines represent the average of the points.

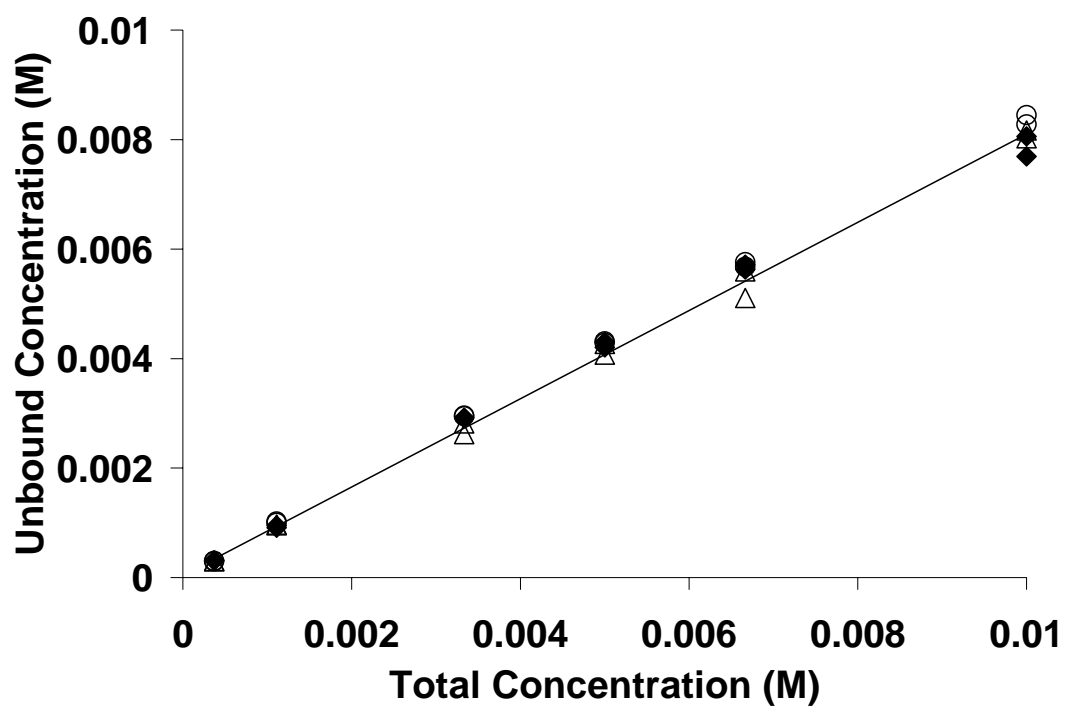


Figure 3-6. Equilibrium unbound extravascular tyramine concentration as a function of total tyramine concentration at pH 2 ( $\blacklozenge$ ), 3 ( $\circ$ ), and 4 ( $\Delta$ ) in liposomal dispersions (13.5 mM lipid) at 25 °C. Symbols at three conditions overlap suggesting pH independence.

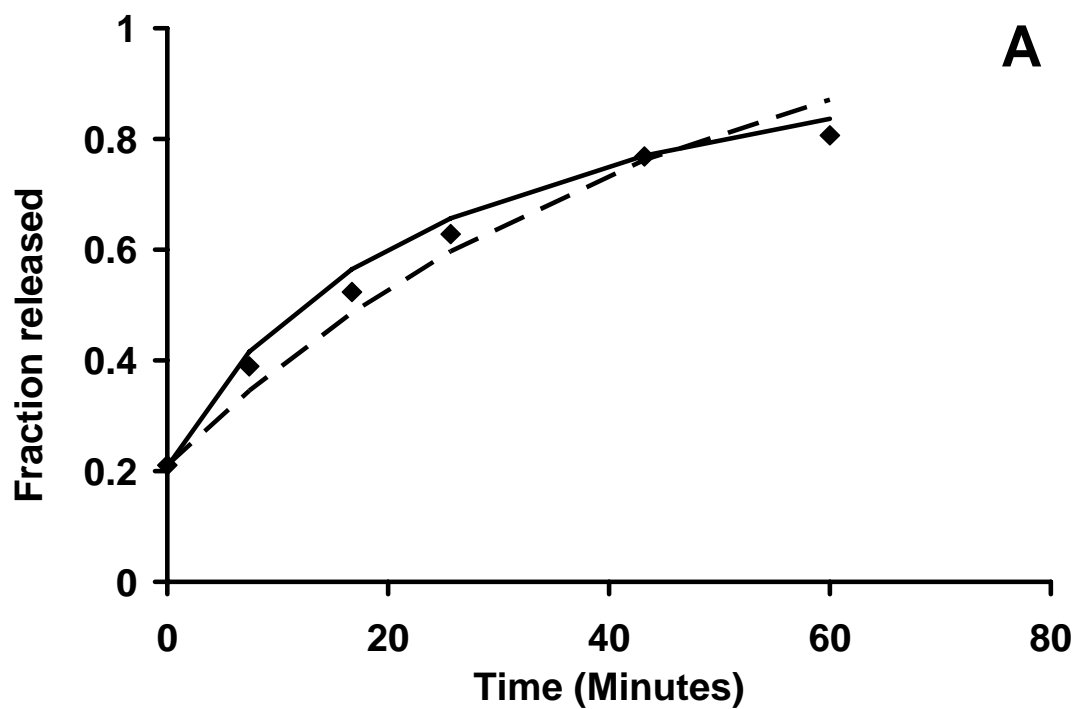


Figure 3-7. Representative profile for tyramine efflux from DOPC vesicles at initial pH 3.77 and initial intravesicular tyramine concentration of 10 mM. Lines reflect best fits according to the conventional model (Equation 3-6, --) and comprehensive model (Equations 3-17 to 3-19,—) developed in this study.

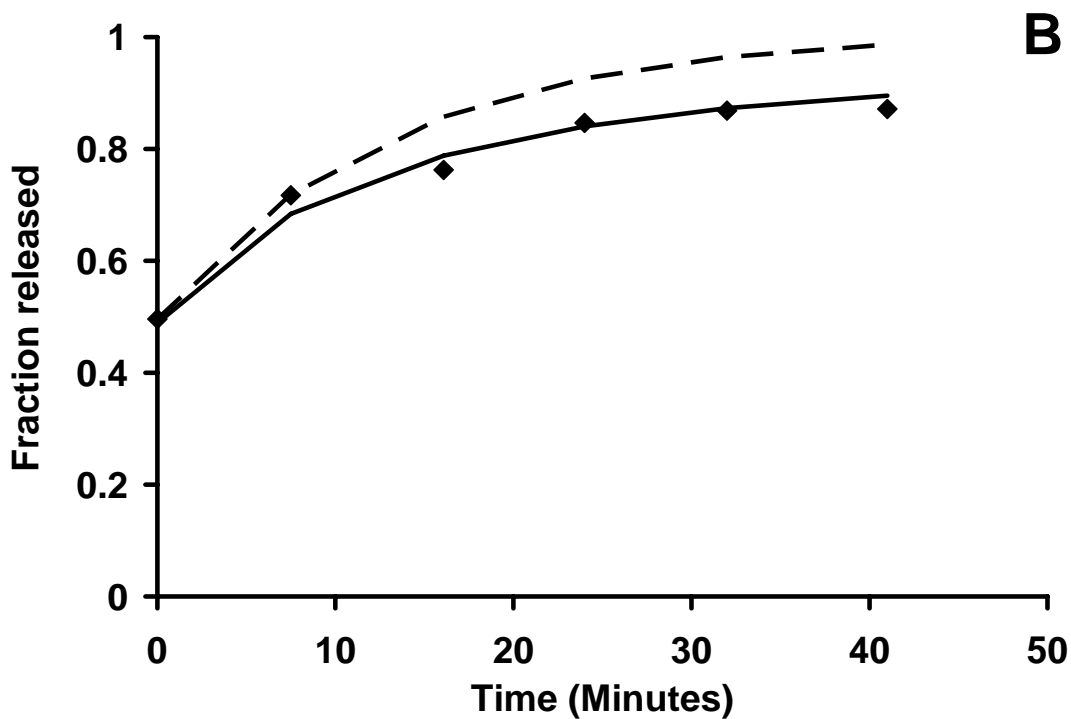


Figure 3-8. Representative profile for tyramine efflux from DOPC vesicles at initial pH 4.15 and initial intravesicular tyramine concentration of 3 mM. Lines reflect best fits according to the conventional model (Equation 3-6, --) and comprehensive model (Equations 3-17 to 3-19, —) developed in this study.

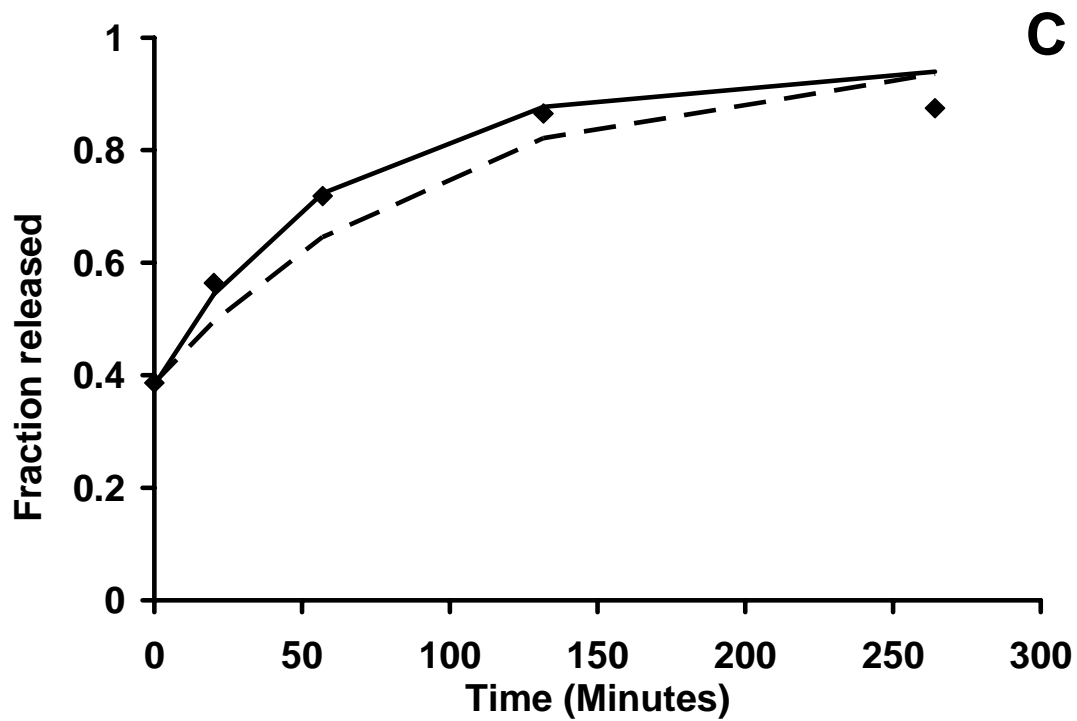


Figure 3-9. Representative profile for tyramine efflux from DOPC vesicles at initial pH 3.31 and initial intravesicular tyramine concentration of 1 mM. Lines reflect best fits according to the conventional model (Equation 3-6, --) and comprehensive model (Equations 3-17 to 3-19, —) developed in this study.

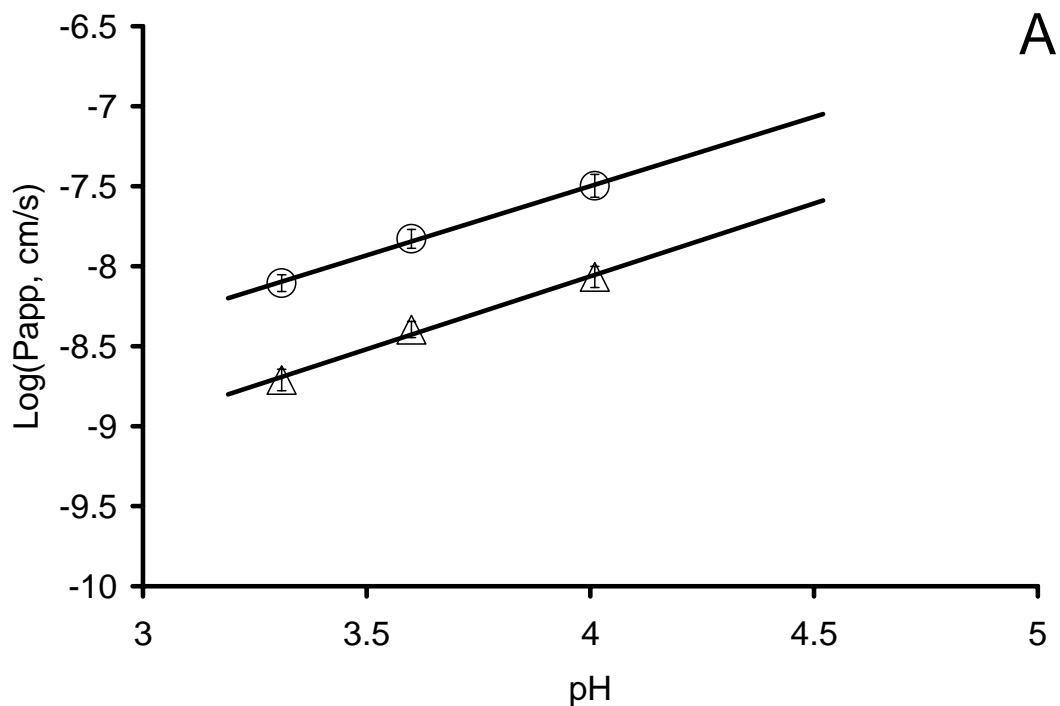


Figure 3-10. Plot of  $\log P_{app}$  vs. pH for tyramine determined using either the conventional model ( $\Delta$ , Equation 3-6) or the comprehensive model ( $\circ$ , Equations 3-17 to 3-19) at initial intravesicular tyramine concentration of 1 mM. Error bars indicate standard deviations and may be smaller than symbols. Lines are drawn to indicate approximate slopes.

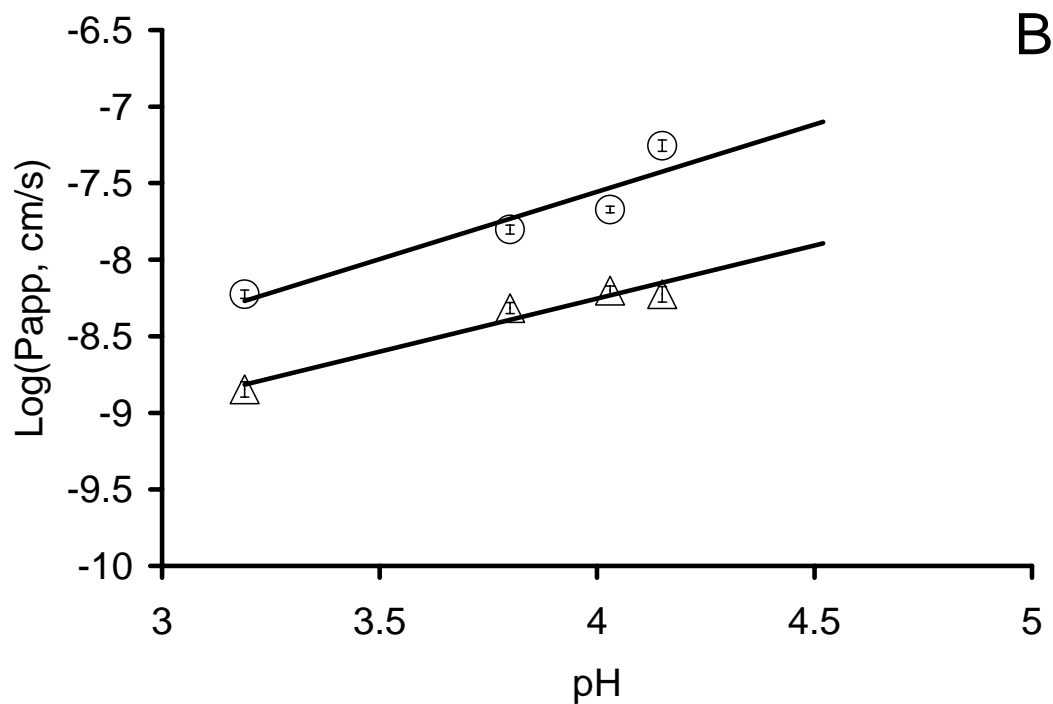


Figure 3-11. Plot of  $\log P_{app}$  vs. pH for tyramine determined using either the conventional model ( $\Delta$ , Equation 3-6) or the comprehensive model ( $\circ$ , Equations 3-17 to 3-19) at initial intravesicular tyramine concentration of 3 mM. Error bars indicate standard deviations and may be smaller than symbols. Lines are drawn to indicate approximate slopes.



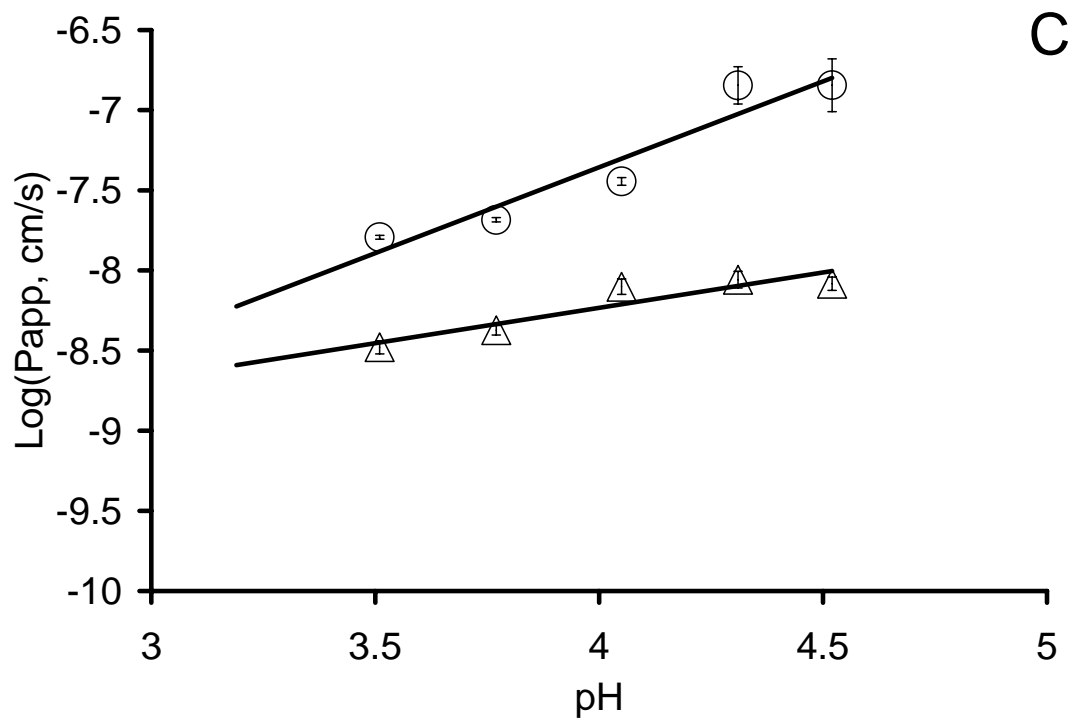


Figure 3-12. Plot of  $\log P_{app}$  vs. pH for tyramine determined using either the conventional model ( $\Delta$ , Equation 3-6) or the comprehensive model ( $\circ$ , Equations 3-17 to 3-19) at initial intravesicular tyramine concentration of 10 mM. Error bars indicate standard deviations and may be smaller than symbols. Lines are drawn to indicate approximate slopes.

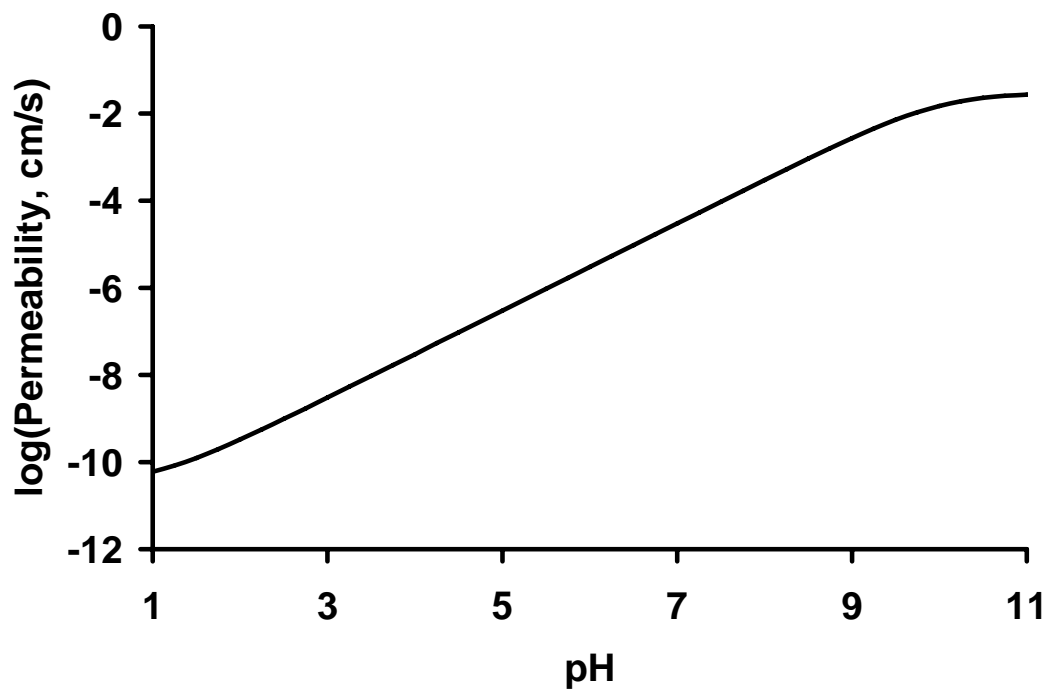


Figure 3-13. Simulation of the expected pH-permeability profile for a weak base with  $pK_a=10$  and intrinsic permeability coefficients of  $3 \times 10^{-2}$  and  $3 \times 10^{-11}$  cm/s for the neutral and ionized forms, respectively.

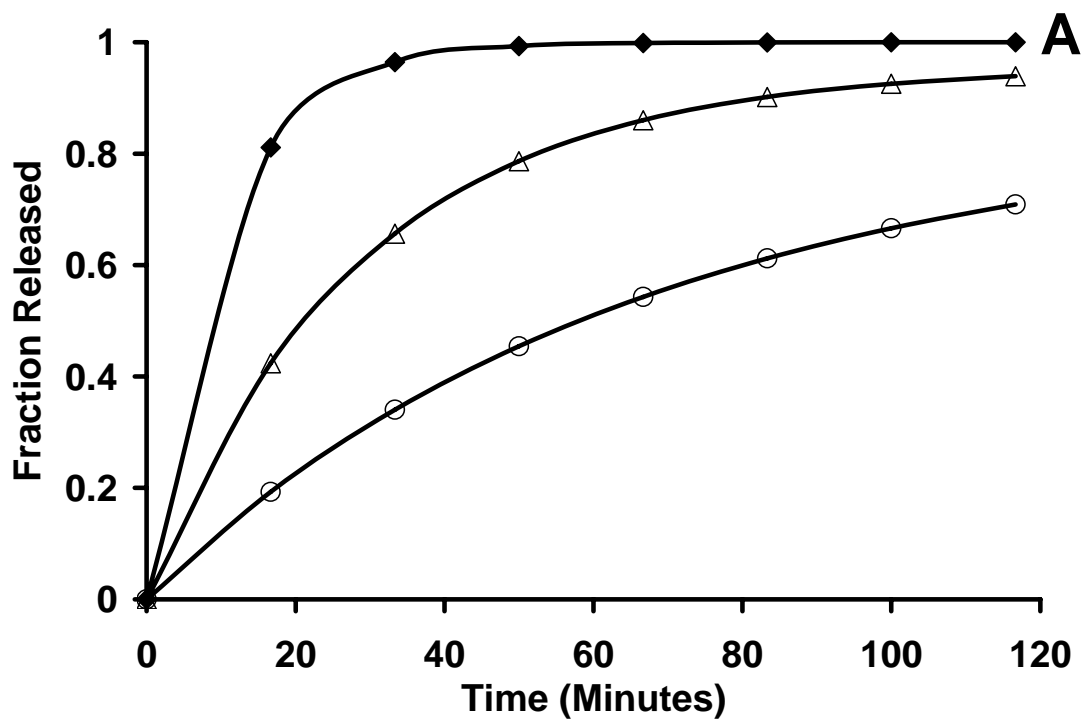


Figure 3-14. Plot illustrating simulations according to Equation 3-13 for the effect of pH-independent membrane binding on liposomal release profiles as a function of time for a weakly basic permeant having a pKa of 10 at pH 3.25. Membrane binding constants assumed were  $1 \times 10^{-6} \text{ M}^{-1}$  ( $\blacklozenge$ ),  $30 \text{ M}^{-1}$  ( $\Delta$ ), and  $100 \text{ M}^{-1}$  ( $\circ$ ) to reflect negligible, low, and moderate binding of the permeant, respectively. The initial intravesicular solute concentration (bound + free) was assumed to be 0.01 M, lipid concentration was 0.0015 M, 1% volume enclosed (sink conditions), and the intrinsic permeability coefficient was 0.0316 cm/s.

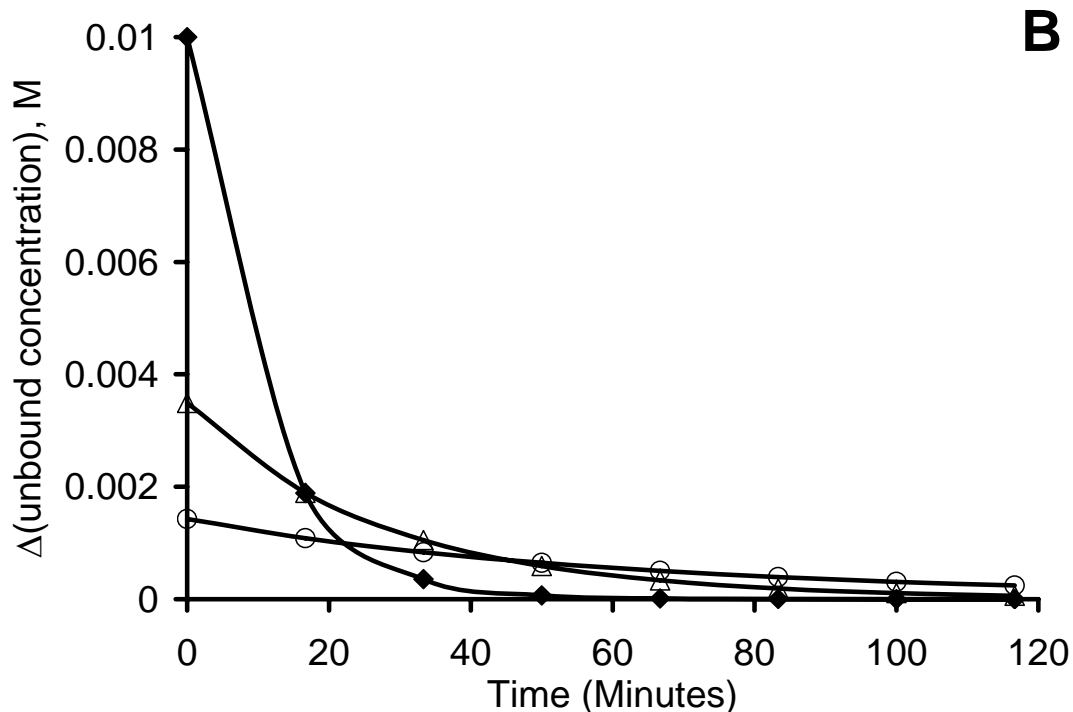


Figure 3-15. Plot illustrating simulations according to Equation 3-13 for the effect of pH-independent membrane binding on unbound permeant concentration gradients as a function of time for a weakly basic permeant having a pKa of 10 at pH 3.25. Membrane binding constants assumed were  $1 \times 10^{-6} \text{ M}^{-1}$  (◆),  $30 \text{ M}^{-1}$  (Δ), and  $100 \text{ M}^{-1}$  (○) to reflect negligible, low, and moderate binding of permeant. The initial intravesicular solute concentration (bound + free) was assumed to be 0.01 M, lipid concentration was 0.0015 M, 1% volume enclosed (sink conditions), and the intrinsic permeability coefficient was 0.0316 cm/s.

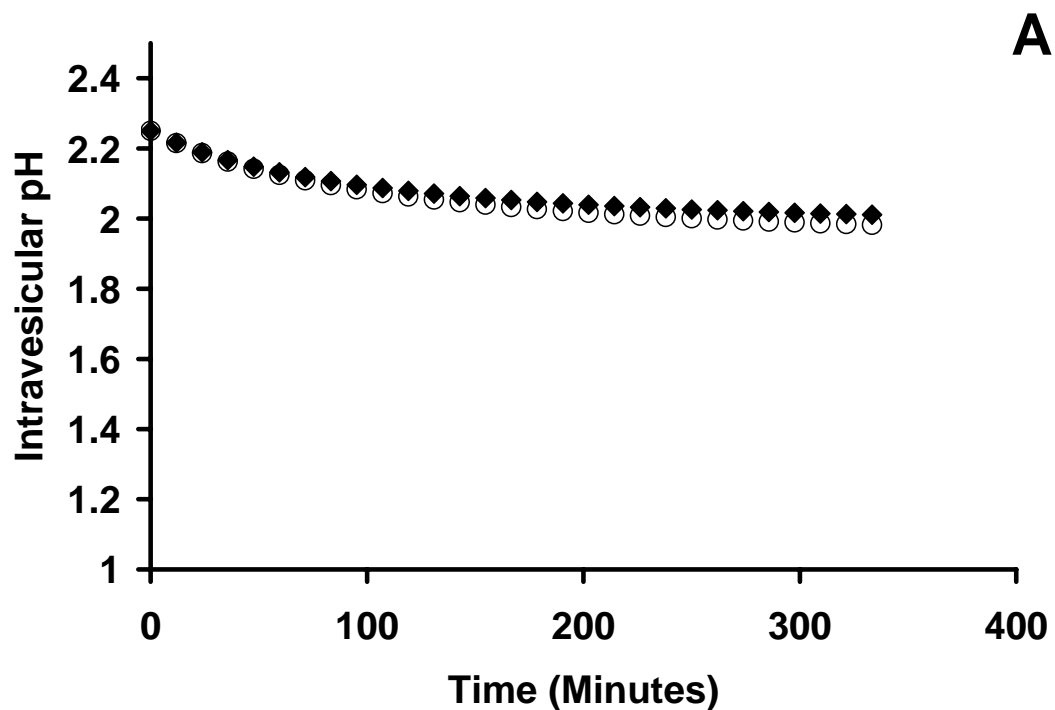


Figure 3-16. Results of simulations using Equation 3-14 and 3-16 to determine the change in intravesicular pH resulting from the liposomal efflux of a weakly basic amine ( $pK_a = 10$ ) initially present at an intravesicular concentration of 0.01 M. An intrinsic permeability coefficient of 0.03 cm/s was assumed for the amine along with a negligible binding constant. The initial intravesicular pH was buffered (40 mM buffer) at 2.25 and ( $pH - pK_a$ ) was 0.5 (◆) or -0.5(○).

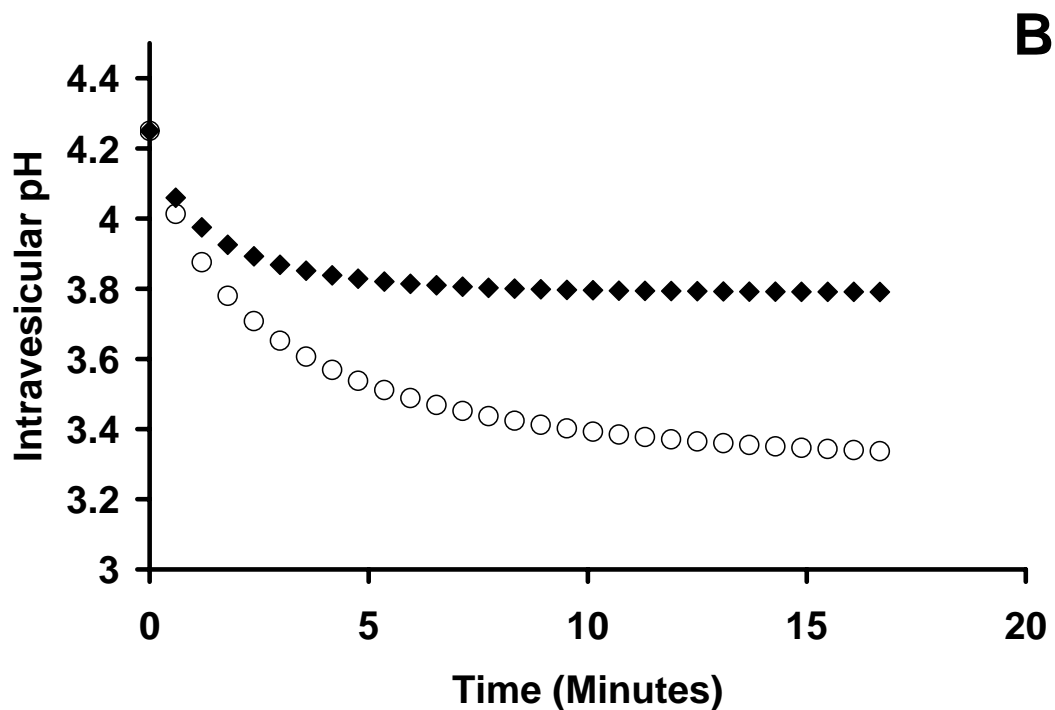


Figure 3-17. Results of several simulations using Equation 3-14 and 3-16 to determine the change in intravesicular pH resulting from the liposomal efflux of a weakly basic amine ( $pK_a = 10$ ) initially present at an intravesicular concentration of 0.01 M. An intrinsic permeability coefficient of 0.03 cm/s was assumed for the amine along with a negligible binding constant. The initial intravesicular pH was buffered (40 mM buffer) at 4.25 and ( $pH - pK_a$ ) was 0.5 (◆) or -0.5(○).

## References

- ARMSTRONG, J. & BARLOW, R. B. (1976) The ionization of phenolic amines, including apomorphine, dopamine, and catecholamines and an assessment of zwitterion constants. *British Journal of Pharmacology*, 57, 501-16.
- AUSTIN, R. P., BARTON, P., DAVIS, A. M., MANNERS, C. N. & STANSFIELD, M. C. (1998) The effect of ionic strength on liposome-buffer and 1-octanol-buffer distribution coefficients. *Journal of Pharmaceutical Sciences*, 87, 599-607.
- AVEYARD, R. & HAYDON, D. A. (1973) *An Introduction To The Principles Of Surface Chemistry*, Cambridge, UK, Cambridge University Press.
- BAEUERLE, H. D. & SEELIG, J. (1991) Interaction of charged and uncharged calcium channel antagonists with phospholipid membranes. Binding equilibrium, binding enthalpy, and membrane location. *Biochemistry*, 30, 7203-11.
- BEAN, R. C., SHEPHERD, W. C. & CHAN, H. (1968) Permeability of lipid bilayer membranes to organic solutes. *Journal of General Physiology*, 52, 495-508.
- BOCKRIS, J. O. M. & REDDY, A. K. N. (1998) *Modern Electrochemistry*, New York, Plenum Publishing Corporation.
- BOMAN, N. L., MAYER, L. D. & CULLIS, P. R. (1993) Optimization of the retention properties of vincristine in liposomal systems. *Biochimica et Biophysica Acta, Biomembranes*, 1152, 253-8.
- CEH, B. & LASIC, D. D. (1995) A rigorous theory of remote loading of drugs into liposomes. *Langmuir*, 11, 3356-68.
- CEH, B. & LASIC, D. D. (1998) Kinetics of accumulation of molecules into liposomes. *Journal of Physical Chemistry B*, 102, 3036-3043.

- CEVC, G., SEDDON, J. M., HARTUNG, R. & EGGERT, W. (1988) Phosphatidylcholine-fatty acid membranes. I. Effects of protonation, salt concentration, temperature and chain-length on the colloidal and phase properties of mixed vesicles, bilayers and nonlamellar structures. *Biochimica et Biophysica Acta, Biomembranes*, 940, 219-40.
- DEAMER, D. W., PRINCE, R. C. & CROFTS, A. R. (1972) Response of fluorescent amines to pH gradients across liposome membranes. *Biochimica et Biophysica Acta, Biomembranes*, 274, 323-35.
- DIAMOND, J. M. & KATZ, Y. (1974) Interpretation of nonelectrolyte partition coefficients between dimyristoyl lecithin and water. *Journal of Membrane Biology*, 17, 121-54.
- EASTMAN, S. J., HOPE, M. J. & CULLIS, P. R. (1991) Transbilayer transport of phosphatidic acid in response to transmembrane pH gradients. *Biochemistry*, 30, 1740-5.
- FINKELSTEIN, A. (1976) Water and nonelectrolyte permeability of lipid bilayer membranes. *Journal of General Physiology*, 68, 127-35.
- GRIT, M. & CROMMELIN, D. J. A. (1992) The effect of aging on the physical stability of liposome dispersions. *Chemistry and Physics of Lipids*, 62, 113-22.
- GRIT, M. & CROMMELIN, D. J. A. (1993) Chemical stability of liposomes: Implications for their physical stability. *Chemistry and Physics of Lipids*, 64, 3-18.
- GUTKNECHT, J. & WALTER, A. (1981) Histamine, theophylline and tryptamine transport through lipid bilayer membranes. *Biochimica et Biophysica Acta*, 649, 149-54.
- HARRIGAN, P. R., WONG, K. F., REDELMEIER, T. E., WHEELER, J. J. & CULLIS, P. R. (1993) Accumulation of doxorubicin and other lipophilic amines into large



unilamellar vesicles in response to transmembrane pH gradients. *Biochimica et Biophysica Acta, Biomembranes*, 1149, 329-38.

HIGUCHI, W. I. & HIESTAND, E. N. (1963) Dissolution rates of finely divided drug powders. I. Effect of a distribution of particle sizes in a diffusion-controlled process. *Journal of Pharmaceutical Sciences*, 52, 67-71.

HOPE, M. J. & CULLIS, P. R. (1987) Lipid asymmetry induced by transmembrane pH gradients in large unilamellar vesicles. *Journal of Biological Chemistry*, 262, 4360-6.

HOPE, M. J., REDELMEIER, T. E., WONG, K. F., RODRIGUEZA, W. & CULLIS, P. R. (1989) Phospholipid asymmetry in large unilamellar vesicles induced by transmembrane pH gradients. *Biochemistry*, 28, 4181-7.

LASIC, D. D., CEH, B., STUART, M. C. A., GUO, L., FREDERIK, P. M. & BARENHOLZ, Y. (1995) Transmembrane gradient driven phase transitions within vesicles: lessons for drug delivery. *Biochimica et Biophysica Acta, Biomembranes*, 1239, 145-56.

LEE, R. J., WANG, S., TURK, M. J. & LOW, P. S. (1998) The effects of pH and intraliposomal buffer strength on the rate of liposome content release and intracellular drug delivery. *Bioscience Reports*, 18, 69-78.

LEO, A., HANSCH, C. & ELKINS, D. (1971) Partition coefficients and their uses. *Chemical Reviews (Washington, DC, United States)*, 71, 525-616.

MACDONALD, P. M. & SEELIG, J. (1988) Anion binding to neutral and positively-charged lipid membranes. *Biochemistry*, 27, 6769-75.

MARTIN, A. N., BUSTAMANTE, P. & CHUN, A. H. (1993) Interfacial Phenomena. IN MARTIN, A. N. (Ed.) *Physical Pharmacy*. 4 ed., 362-392.

- MARTIN, R. B. (1971) Zwitterion formation upon deprotonation in L-3,4-dihydroxyphenylalanine and other phenolic amines. *Journal of Physical Chemistry*, 75, 2657-61.
- MAYER, L. D., BALLY, M. B. & CULLIS, P. R. (1986) Uptake of adriamycin into large unilamellar vesicles in response to a pH gradient. *Biochimica et Biophysica Acta, Biomembranes*, 857, 123-6.
- MAYER, L. D., BALLY, M. B., HOPE, M. J. & CULLIS, P. R. (1985) Uptake of dibucaine into large unilamellar vesicles in response to a membrane potential. *Journal of Biological Chemistry*, 260, 802-8.
- MAYER, L. D., TAI, L. C. L., BALLY, M. B., MITILENES, G. N., GINSBERG, R. S. & CULLIS, P. R. (1990) Characterization of liposomal systems containing doxorubicin entrapped in response to pH gradients. *Biochimica et Biophysica Acta, Biomembranes*, 1025, 143-51.
- MAYER, P., XIANG, T.-X. & ANDERSON, B. D. (2000) Independence of substituent contributions to the transport of small molecule permeants in lipid bilayers. *AAPS PharmSci*, 2(2) article 14 (<http://www.pharmsci.org/>), 1-13.
- MAYER, P. T., XIANG, T.-X., NIEMI, R. & ANDERSON, B. D. (2003) A hydrophobicity scale for the lipid bilayer barrier domain from peptide permeabilities: Nonadditivities in residue contributions. *Biochemistry*, 42, 1624-1636.
- MICROMATH, I. (1995) Micromath Scientist for Windows. 2.01 Compiled 7/21/1995 1:55 PM ed. Saint Louis, Missouri, 63144, Micromath Scientific Software.
- NAGY, P. I. & TAKACS-NOVAK, K. (2004) Tautomeric and conformational equilibria of biologically important (hydroxyphenyl)alkylamines in the gas phase and in aqueous solution. *Physical Chemistry Chemical Physics*, 6, 2838-2848.

- NICHOLS, J. W. & DEAMER, D. W. (1976) Catechol amine uptake and concentration by liposomes maintaining pH gradients. *Biochimica et Biophysica Acta, Biomembranes*, 455, 269-71.
- PEINHARDT, G. & WIESE, M. (2001) Microionization constants: novel approach for the determination of the zwitterionic equilibrium of hydroxyphenylalkylamines by photometric titration. *International Journal of Pharmaceutics*, 215, 83-89.
- REDELMEIER, T. E., HOPE, M. J. & CULLIS, P. R. (1990) On the mechanism of transbilayer transport of phosphatidylglycerol in response to transmembrane pH gradients. *Biochemistry*, 29, 3046-53.
- RIEGELMAN, S., STRAIT, L. A. & FISCHER, E. Z. (1962) Acid dissociation constants of phenylalkanolamines. *Journal of Pharmaceutical Sciences*, 51, 129-33.
- ROGERS, J. A. & DAVIS, S. S. (1980) Functional group contributions to the partitioning of phenols between liposomes and water. *Biochimica et Biophysica Acta, Biomembranes*, 598, 392-404.
- TEJWANI, R. W., DAVIS, M. M. & STOUCH, T. R. (2004) Large scale molecular dynamics simulation of a drug like molecule in 1,2-dioleoyl-*sn*-glycero-3-phosphocholine (DOPC) bilayer. *The AAPS Journal*, 6, T2271.
- WALTER, A. & GUTKNECHT, J. (1984) Monocarboxylic acid permeation through lipid bilayer membranes. *Journal of Membrane Biology*, 77, 255-64.
- WALTER, A., HASTINGS, D. & GUTKNECHT, J. (1982) Weak acid permeability through lipid bilayer membranes. Role of chemical reactions in the unstirred layer. *Journal of General Physiology*, 79, 917-33.
- XIANG, T.-X. & ANDERSON, B. D. (1994) Substituent contributions to the transport of substituted *p*-toluic acids across lipid bilayer membranes. *Journal of Pharmaceutical Sciences*, 83, 1511-18.

- XIANG, T.-X. & ANDERSON, B. D. (1995) Development of a combined NMR paramagnetic ion-induced line-broadening/dynamic light scattering method for permeability measurements across lipid bilayer membranes. *Journal of Pharmaceutical Sciences*, 84, 1308-15.
- XIANG, T.-X. & ANDERSON, B. D. (1997) Permeability of acetic acid across gel and liquid-crystalline lipid bilayers conforms to free-surface-area theory. *Biophysical Journal*, 72, 223-237.
- XIANG, T.-X. & ANDERSON, B. D. (1998) Influence of chain ordering on the selectivity of dipalmitoylphosphatidylcholine bilayer membranes for permeant size and shape. *Biophysical Journal*, 75, 2658-2671.
- XIANG, T.-X., CHEN, X. & ANDERSON, B. D. (1992) Transport methods for probing the barrier domain of lipid bilayer membranes. *Biophysical Journal*, 63, 78-88.
- XIANG, T.-X., XU, Y. H. & ANDERSON, B. D. (1998) The barrier domain for solute permeation varies with lipid bilayer phase structure. *Journal of Membrane Biology*, 165, 77-90.

## **CHAPTER FOUR: Substituent effects on solute ionization, partitioning into hydrocarbon, and binding to the lipid bilayer membranes. Electrostatic effects dependent on conformation**

### **Introduction**

The example of the model amine in the previous chapter illustrates the possibility that the lipid bilayer membrane can present a barrier to the transport of a solute that is concomitantly bound to it (has a relatively high partition coefficient). For the bilayer membrane to be rate limiting for the transport, heterogeneous solubility diffusion theory (Diamond and Katz, 1974) requires a region of the lipid bilayer where the partition coefficient of the solute is low. For example, the permeability coefficient for tyramine is orders of magnitude smaller than would be predicted from its diffusion coefficient and the barrier thickness alone. As a result, at least two regions having distinctly different partition coefficients exist for this compound. Since a direct measurement of partition coefficient in each of the two regions of the lipid bilayer can be experimentally difficult, in this chapter we use alternative methods to determine the same.

It has been established by the previous work in this laboratory that the chemical selectivity of the barrier region in liquid crystalline bilayers is represented by 1,9-decadiene/water partition coefficients (Xiang et al., 1998). This measurement was used as a primary means to estimate the barrier domain / water partition coefficients for the solutes of interest. From these functional group contributions for the amino, methylamino, dimethylamino, aromatic hydroxyl, and aromatic methoxy groups were also determined in order to extend the existing database of values generated in this laboratory.

The octanol/water partition coefficient has been suggested to mimic the lipid bilayer membrane interface in recent molecular dynamics simulations comparing the free energies of transfer of amino acid side chain solutes (MacCallum et al., 2008). Data from the experimental studies by Wimley and coworkers have however found that the solvation parameters estimated from the measurements of partition coefficients of amino

acid residues in octanol and in the bilayer surface differ from each other (Wimley et al., 1996, Wimley and White, 1996). Since it is possible to directly measure liposome/water partition coefficients, these are preferable as measures of the extent of binding in the preferred binding region over a surrogate. The solutes used in this study show sufficient binding that the expected concentration in the binding region overwhelms the contributions from other regions with low partition coefficients. As a result, a partition coefficient in the lipid bilayer represents the partition coefficient in the preferred binding region. Therefore, liposome/water partition coefficients for the solutes of interest were measured to generate functional group free energy contributions that can be used towards the broader aim of comparison with the MD simulations in a subsequent chapter.

Capacity factors calculated from the immobilized artificial membrane (IAM) chromatography are an additional means of obtaining liposome water partition coefficients. The capacity factors are not exactly the partition coefficients; however they are related to the partition coefficients via the phase volumes in a given chromatography experiment. Since phase volumes in chromatography may be difficult to estimate, and vary among the laboratories, the calculation of functional group contributions eliminates this effect. Studies have been conducted with multiple organic molecules that allow calculation of several functional group contributions (Valko et al., 2000, Lazaro et al., 2005, Barbato et al., 2004) to the transfer of solutes from water to the preferred binding region.

Since the solutes used in this study are ionizable, accurate ionization constants are needed in order to derive species specific partition coefficients. While ionization constants of monoionized molecules are easily available in the literature, significant disagreement was found for the microscopic ionization constants of p(aminoethyl)-phenols. Therefore, the microscopic ionization constants for the p-(aminoethyl)-phenols used in this work were determined and their corresponding structure-property relationships were evaluated to ensure self-consistency and accuracy. Based on the hydrocarbon/water partition coefficients and the ionization constants, the assumption of independence of the contributions of the apparently well isolated polar functional groups

(amino and phenol) to the free energies of ionization and solute transfer from water to hydrocarbons have been evaluated.

### ***Background on the substituent effects and pKa prediction***

Computational methods to predict physicochemical properties of drug molecules such as pKa values, partition coefficients, etc., are increasingly attractive due to the large number of molecules that are typically considered in the early stages of drug discovery and lead optimization (van de Waterbeemd and Gifford, 2003). Predictive methods based on linear free energy relationships (LFERs) have been widely employed for such purposes (ACD-pKa, 1994-2007). Typically, the average deviations of predicted values from experimental ionization constants and partition coefficients reported in such predictions are on the order of 0.5 to 1 log units (Platts et al., 2000, Zhang et al., 2006). LFERs rely largely on the principles of independence and additivity of the contributions of various structural components or fragments in each molecule to determine the overall free energy, although correction factors to account for conjugation, steric, and polar interactions between functional groups in close proximity may also be required (Perrin et al., 1981). Molecules containing multiple ionizable functional groups pose additional challenges to the computational approaches because the strength and therefore significance of intramolecular interactions may depend on the state of ionization of each group and the conformational flexibility of the molecule. Due to neglect of such interactions, the pKa values of carboxyl and amino groups of  $\epsilon$ -aminohexanoic acid (4.37 and 10.80 (Brandariz et al., 1993)) are estimated by a fragment based approach to be 4.68 and 10.63, respectively (ACD-pKa, 1994-2007).

Further complicating the situation when multiple ionizable groups have similar ionization tendencies is the difficulty in correctly assigning microscopic ionization constants to specific functional groups using the macroscopic pKa values generated in pH-titration measurements. There are numerous examples of drugs, biomolecules, and other pharmaceutically relevant molecules having pKa values that may be difficult to predict based on a fragment based calculation alone due to such ionization behavior. Examples of these include fluoroquinolone antibacterials (Takacs-Novak et al., 1990,

Langlois et al., 2005), imatinib (Szakacs et al., 2005), peptides (N. Gulyaeva, 2003), penicillin derivatives, p-aminosalicylic acid, terbutaline, methyldopa, glutathione (Noszal and Szakacs, 2003), EDTA, and various others. Predictions (ACD-pKa, 1994-2007) for terbutaline, dopamine, and methyldopa based on a fragment based approach lead to sets of microscopic ionization constants that are not self-consistent (let alone comparable with the experimental values) and point to the need to further explore additional contributing factors to the LFERs in these compounds. Tyramine and other structurally related aminoalkyl phenols provide a simple framework for this type of study. For these compounds, one might comfortably assume that direct intramolecular interactions such as hydrogen bonding between the terminal amino and phenolic –OH groups can be ignored since they are separated by a distance of approximately 8 Å in the fully extended conformation and the aromatic ring prevents folded conformations that would permit intramolecular hydrogen bonding between the polar substituents. Long-range polar substituent effects may still be possible, however, aided by electron delocalization via resonance through the aromatic ring and partial folding of the ethylamine chain.

#### ***Microscopic ionization constants of p-(aminoethyl)phenols***

Ionization of the phenol and amine groups in tyramine and other structurally similar aminoalkyl phenols results in the existence of four different species in an aqueous solution, the interconversion of which can be described with four microscopic ionization constants (Figure 4-1). Several publications have reported microscopic ionization constants for such compounds (Riegelman et al., 1962, Peinhardt and Wiese, 2001, Nagy and Takacs-Novak, 2004, Martin, 1971, Kappe and Armstrong, 1965, Armstrong and Barlow, 1976, Granot, 1976), however, the various reported values do not agree. Even quite recent publications such as the work by Nagy and Takacs-Novak (Nagy and Takacs-Novak, 2004), and Peinhardt and Weise (Peinhardt and Wiese, 2001) report widely disparate values for the microscopic ionization constants for tyramine when compared with each other, and both conflict with earlier work such as that by Riegelman et al. (Riegelman et al., 1962) or those predicted by a fragment based approach (ACD-pKa, 1994-2007). These discrepancies, up to 1 pKa unit, are larger than the typical variation in reported pKa values generated for the same compound in multiple labs, and



may be due to various reasons including incorrect assignment of the microscopic constants, experimental error, or other factors. Due to the uncertainties in the values of microscopic ionization constants, the species-specific partitioning data in hydrocarbon/water systems are also scarce for the bifunctional *p*-(aminoethyl)phenols.

As a part of this chapter the microscopic ionization constants for tyramine and other N-methylated *p*-(aminoethyl)phenol analogs have been measured and the assignments verified by their self-consistency within structurally relevant groupings. Hydrocarbon (i.e., 1,9-decadiene)/water partition coefficients of these compounds are also reported as a function of pH to estimate the intrinsic partition coefficients for the neutral species. The assumption of independence of the contributions of the apparently well isolated polar functional groups (amino and phenol) to the free energies of ionization and solute transfer from water to hydrocarbon has been evaluated.

## **Materials and Methods**

Macroscopic and microscopic ionization constants of compounds I-III (see Table 4-1 for structures) in aqueous solution and intrinsic partition coefficients (1,9-decadiene/water and liposome/water) of the neutral forms were determined at 0.1 M ionic strength (adjusted with sodium chloride) and 25°C.

### ***Materials***

Tyramine (*p*-(aminoethyl)phenol, *p*-hydroxyphenethylamine, I), *p*-methoxyphenylethylamine (IV), phenethylamine (VI), and 1,9-decadiene were purchased from Sigma-Aldrich (Saint Louis, MO). 4-Ethylphenol (VII) was purchased from CHEMService (West Point, PA). N-methyl-O-methyltyramine (V) and N-methyltyramine (II) were synthesized using procedures described in the literature (Kiefer, 1972, Borgman et al., 1973) as described below. Dimethyltyramine (III) sulfate was purchased from TCI, Inc. (Tokyo, Japan). 1,2-Dioleoyl-*sn*-glycero-3-phosphocholine (DOPC) and sodium 1,2-dioleoyl-*sn*-glycero-3-phosphate (DOPA) were purchased from Avanti Polar Lipids, Inc. (Alabaster, AL). The former was obtained as a 20 mg/mL

solution in chloroform and the latter was obtained as a lyophilized powder. All other reagents and materials were of analytical grade.

### 1. Synthesis and characterization of N-methyl-p-methoxyphenylethylamine hydrochloride

N-methyl-*p*-methoxyphenylethylamine (V) hydrochloride was prepared from *p*-methoxyphenylethylamine as described by Kiefer et al (Kiefer, 1972). Benzene in the published method was replaced with toluene as the operating solvent. Two grams of *p*-methoxyphenylethylamine was added to 2 mL of toluene and 1.4 g of benzaldehyde and heated under reflux using a Dean-Stark trap until no more water was present in the condensate. Then without cooling, a solution of 1.64 g methylsulfate in 4 mL toluene was added at a rate such as to maintain reflux (about 15 minutes). Resulting two phase liquid was heated for 90 minutes, cooled slightly and treated with 4 mL of water, then heated for another 20 minutes and finally cooled in ice. The aqueous layer was isolated and washed twice with diethylether and then made strongly basic with 50% aqueous sodium hydroxide to separate out the amine layer. Two diethylether washings of aqueous phase were added to the amine layer which was subsequently allowed to dry in the hood. The amine was then dissolved in 20% ethanol/ether (10 mL), and 1 mL of concentrated HCl was added (dropwise) to obtain the HCl salt. The white solid was washed twice with cold ethanol/ether mixture and dried first in the hood and then at 60 °C for 30-60 minutes to obtain 1.4 grams of solid. Melting onset and maximum (using a TA Instruments differential scanning calorimeter operated at 10 °C per minute with sample in an aluminum pan) were found to be 169 and 177 °C respectively. <sup>1</sup>H-NMR spectra (at 500.16 MHz using Eclipse+ 500 spectrometer) were obtained in a 10% TFA(<sup>2</sup>H) in D<sub>2</sub>O solution prepared at 1 mM. (<sup>1</sup>H-NMR peaks for starting material: 2.5,t,2.00; 2.8,t,1.98; 3.4,s,2.99; 6.6,d,1.96; 6.9,d,1.93; and for the product: 0.8,t,2.95; 2.3,s,3.00; 2.6,t,2.03; 2.9,t,2.00; 3.2,q,2.00; 3.4,s,3.07; 6.6,d,2.08; 6.9,d,2.07).

### 2. Synthesis and characterization of N-methyltyramine

N-methyltyramine (II) was prepared from N-methyl-*p*-methoxyphenylethylamine (V) according to the procedure used by Borgman et al (Borgman et al., 1973). To 1.23 g

of N-methyl-p-methoxyphenylethylamine HCl prepared above, 7 mL of 48% aqueous HBr was added. The flask was flushed with N<sub>2</sub> for 30 minutes and then heated to 125 °C for 2 hours. The reaction progress was monitored by taking <sup>1</sup>H-NMR of a small sample dissolved in 10% TFA(<sup>2</sup>H) in D<sub>2</sub>O. Excess acid was removed at 60 °C under reduced pressure with a cold trap and the concentrate obtained was dissolved in methanol and rotoevaporated to obtain a moist solid which was stored under vacuum over phosphorous pentoxide to obtain 1.3 g of dry product. <sup>1</sup>H-NMR spectra: 2.3s,2.96; 2.6t,2.04; 2.9t,2.00; 6.5d,2.05; 6.8d,2.11.

### ***HPLC Analyses***

All amines were analyzed by reversed phase HPLC using a 3 μm, 15 cm x 4.6 mm inner diameter YMC-ODS-AQ C18 column (Waters Corp., Milford, MA). A linear mobile phase gradient was used starting with solvent A and changing to solvent B over 15 minutes followed by 5 minute equilibration at initial conditions for the subsequent run. In the foregoing, solvent A was 1 mM sodium octanesulfonate dissolved in 20 mM pH 4.5 ammonium acetate buffer; and solvent B was 30% acetonitrile in solvent A. A UV detector operated at 280-, 274-, or 257-nm for tyramines (I, II, III), O-methyl tyramines (IV, V), or phenylethylamine (VI), respectively, was used for all quantitations.

4-Ethylphenol (VII) was analyzed by reversed phase HPLC using the same column as above. A linear gradient from 0.05% TFA in water to 0.05% TFA in acetonitrile was run over 20 minutes and UV spectra (resolution = 3.6nm) were obtained between 210 to 310 nm. The chromatograms extracted at 278nm were integrated to quantitate 4-ethylphenol.

### ***Macroscopic and Microscopic Ionization Constants***

The ionization scheme for compounds I, II, and III in Figure 4-1 shows the four different species that exist in the aqueous solutions. The four species interconvert as a function of pH and the equilibrium constants  $k_1$ ,  $k_2$ ,  $k_{12}$ , and  $k_{21}$  are referred to as the microscopic ionization constants. A simple volumetric titration may only show two *macroscopic* K<sub>a</sub> values shown as K<sub>1</sub> and K<sub>2</sub> in Figure 4-1, each of which is a composite of two of the four microscopic constants mentioned above.

The macroscopic and microscopic ionization constants of compounds I-III in aqueous solutions were determined using a combined spectroscopic/volumetric pH-titration method. A semi-micro ROSS® combination electrode attached to an Orion model 611 meter (Thermo Electron Corporation, Beverly, MA) was calibrated using pH 7 and 10 standard buffers (VWR Scientific, West Chester, PA) under a stream of nitrogen while gently stirring at 25±0.5°C. The solution in the titration reservoir was stirred under nitrogen in a temperature-controlled reservoir at 25±0.5°C and circulated through a flow-cell in a UV-visible spectrophotometer (Waters 486 Tunable absorbance detector, Waters Corporation, Milford, MA), which had water containing sodium chloride as a blank.

The UV absorbance measurement allows the estimation of phenol/phenolate species whereas the pH-volumetric method allows the estimation of the macroscopic ionization. A pre-experiment was conducted in order to determine the appropriate wavelength of the UV light to be used in the experiment. The UV absorbance spectra of the solutions of the compound in a series of buffers were measured and are shown in Figure 4-2. The wavelength was chosen such as to stay within the linear range of the instrument at the concentrations of the titration and away from the isosbestic points.

During titration, an equimolar amount of hydrochloric acid was included in solutions of I as it was obtained as a free base whereas compounds II and III were used without added acid as they were obtained as salts. A 0.03 M aqueous solution of the compound, containing sodium chloride to adjust the ionic strength to 0.1 M at the half neutralization point, was equilibrated under a stream of nitrogen in a reservoir maintained at 25 ± 0.5 °C and circulated through a flow-cell in a UV-visible spectrophotometer. Small increments of 1N sodium hydroxide solution were added to the solute solution as its pH and the UV absorbance at 300 nm were recorded. The UV absorbance and the pH data from each titration (Figures 4-3 and 4-4) were fitted simultaneously to the following equations to obtain three of the four microscopic ionization constants defined in Figure 4-1 ( $k_1$ ,  $k_{12}$ ,  $k_2$ ,  $k_{21}$ ). The remaining microscopic constant was determined using the relationship  $k_1k_{12} = k_2k_{21}$ .

$$\frac{B_0 V_b}{V_0 + V_b} + \left( \frac{[H^+]^2 - k_1 k_{12}}{D} \right) \times \frac{p C_0 V_0}{V_0 + V_b} - \frac{K_w}{[H^+]} = 0 \quad (4-1)$$

$$\frac{A}{C_0} = \frac{\varepsilon_A ([H^+]^2 + [H^+] k_2) + \varepsilon_B (k_1 [H^+] + k_1 k_{12})}{D} \quad (4-2)$$

$$D = [H^+]^2 + [H^+] (k_1 + k_2) + k_1 k_{12} \quad (4-3)$$

where  $[H^+]$  is the hydrogen ion concentration,  $K_w$  is the ion product of water,  $V_0$  is the initial solution volume,  $V_b$  is the volume of sodium hydroxide titrant (having a molarity of  $B_0$ ),  $C_0$  and  $p$  are the concentration and purity of analyte, respectively,  $A$  is the measured absorbance at the wavelength of interest, and  $\varepsilon_A$  and  $\varepsilon_B$  refer to the molar extinction coefficients of the phenol and phenolate species at that wavelength, respectively.

#### ***Partition coefficients in 1,9-decadiene***

The apparent partition coefficients between 1,9-decadiene and aqueous buffer at varying pH and 0.1 M ionic strength were determined by the shake flask method at 25°C as described in detail previously (Tejwani and Anderson, 2008). The aqueous and organic phases were mutually saturated prior to initiation of the experiment. A 1 mM or lower concentration of solute was prepared in the aqueous phase and shaken with the organic phase for 12-24 hours using a vortex shaker at 25 °C. Subsequent to separation by centrifugation, for quantitation of the solute, the aqueous phase was diluted as needed whereas the organic phase was extracted using 1N aqueous sulfuric acid solution. The concentration in each phase was then determined using a reversed phase HPLC method described above. The operating concentration of 1 mM or lower was chosen for all the solutes to avoid possible contributions of self associated species (Anderson et al., 1980, Anderson et al., 1979, Rytting et al., 1978a, Anderson et al., 1978, Anderson et al., 1975) to the measurement.

The apparent partition coefficients of compounds I-VII vary as a function of the neutral species concentration in the aqueous solution. Intrinsic partition coefficients

( $K_{o/w}^{B_N}$ ) for the neutral (non-zwitterionic) species of compounds I-III were estimated using non-linear least squares fits of the apparent partition coefficients ( $K_{o/w}^{apparent}$ ) to the following equations.

$$K_{o/w}^{apparent} = \frac{B_N(oil)}{B_w^T} = K_{o/w}^{B_N} f_{B_N} \quad (4-4)$$

$$f_{B_N} = \frac{k_2[H^+]}{[H^+]^2 + [H^+](k_1 + k_2) + k_1k_{12}} \quad (4-5)$$

where  $B_w^T$  represents the total solute concentration in the aqueous phase,  $B_N(oil)$  is the concentration of solute in the non-aqueous phase, and  $f_{B_N}$  is the fraction of neutral form in the aqueous phase. For the monofunctional bases or acids Equation 4-5 was replaced with either Equation 4-6 or 4-7, respectively.

$$f_{B_N} = \frac{K_a}{[H^+] + K_a} \quad (4-6)$$

$$f_{B_N} = \frac{[H^+]}{[H^+] + K_a} \quad (4-7)$$

where  $K_a$  is the ionization constant of the compound.

### ***Partition coefficients in the large unilamellar vesicles (liposomes) of DOPC***

#### ***1. Preparation of large unilamellar vesicles (LUVs)***

Accurately weighed quantities of DOPC and DOPA (96:4 mole ratio, 25 mM) were dissolved in chloroform. Aliquots of this solution were transferred to glass vials (0.6 mL) and evaporated under a stream of nitrogen to obtain a dry lipid film. The tubes were further dried at 40°C for a few hours to remove any traces of solvent. An aqueous 40 mM buffer (phosphate, formate or acetate) at ionic strength of 0.1 (adjusted with sodium chloride) was added to the film to prepare a 15 mM lipid dispersion. The lipid dispersion was vortexed repeatedly for 5 minutes until a uniform dispersion was

obtained, then extruded (17 times) through a 0.1  $\mu\text{m}$  pore size polycarbonate membrane (Nuclepore, Pleasanton, CA) to obtain LUVs. Particle size and size distribution of the resulting vesicles were measured using dynamic light scattering (Horiba LA-920 particle size distribution analyzer, Horiba International Corporation, Irvine, CA) after appropriately diluting the vesicles in the matching buffer.

## *2. The partitioning experiment*

Large unilamellar vesicles (LUVs) were prepared in 0.04 M phosphate, formate, or acetate buffers with ionic strength adjusted to 0.1. A series of stock solutions of tyramine, N-methyltyramine, and dimethyltyramine from 3.7 to 100 mM were prepared in buffers matching those of three different LUV dispersions. Aliquots from these stock solutions were added to the corresponding vesicle dispersions to obtain a lipid concentration of 13.5 mM and the amine concentrations of 3.7-10 mM. The resulting dispersions were equilibrated at 25°C for 24 to 48 hours. After equilibration, the dispersions were filtered through Centricon-100 (nominal molecular weight limit = 100,000 g/mol) filters (Millipore Corporation, Bedford, MA) to obtain the extravesicular solution which was subsequently analyzed by HPLC for permeant concentration after appropriate dilution. The total concentration of the amine in the dispersion was determined after lysing the vesicles by diluting them 1:2 in 1% Triton X-100 solution (prepared in HPLC mobile phase) and analyzing the clear solution by HPLC. For the purpose of calculating the partition coefficient of the solute in moles per liter units, the specific gravity of DOPC was taken as 1 (Rogers and Davis, 1980).

## **Results and Discussion**

### *Assignment and verification of the microscopic ionization constants*

The microscopic ionization constants of I, II, and III resulting from non-linear least squares fitting of the titration data are shown in Table 4-1. The concentration fractions of each species in a solution of I as a function of pH are shown in Figure 4-5. Compounds II and III exhibited similar profiles for the four species in solution. While the cation and the anion fractions dominate at low and high pH, respectively, the neutral

and the zwitterionic forms exhibit maxima near a pH of 10. The ratio of the concentrations of the neutral form to that of the zwitterion, sometimes referred to as the zwitterion constant ( $K_z = k_1/k_2$ ), remains unchanged with pH.

Among the four microscopic ionization constants of I,  $pk_2$  (10.01, Table 4-1) is the closest to the pKa value of phenethylamine (VI) and *p*-methoxyphenethylamine (IV). Similarly, the microscopic constant  $pk_{21}$  (10.23, Table 4-1) is the closest to the pKa value of 4-ethylphenol (VII). Compound II also displays similar features and the corresponding microscopic ionization constants were assigned. On the other hand, the remaining two constants for the phenol and amine ionization equilibria involving the zwitterion do not have corresponding monovalent compounds for comparison.

Table 4-1 also lists the microscopic ionization constants calculated for each of the solutes using ACD/pKa dB (ACD-pKa, 1994-2007) with those from the literature. The predicted microscopic ionization constants for I are close to the observed values, however some of the constants for II and III deviate by up to 0.4 units from those observed. While the similarity in the microscopic ionization constants for the amine and phenol groups in compound I to the corresponding pKa values of the monovalent compounds, phenethylamine (VI) and 4-ethylphenol (VII), provides some assurance that the assignments are correct, the conflicting literature values for  $pk_1$ ,  $pk_2$ ,  $pk_{12}$ , and  $pk_{21}$ , examples of which are listed in Table 4-1, suggest that further verification would be advisable to confirm these assignments. Therefore, the trend in amine microscopic ionization constants with successive N-methylation was explored.

Successive methylation of alkyl amines is known to cause a predictable shift in the ionization constant. It has been established that the gas phase proton affinities in alkyl amines increase ( $R_3N > R_2NH > RNH_2 > NH_3$ ) with successive methylation (Munson, 1965). However, for amines dissolved in water (Hall and Sprinkle, 1932, Harned and Owen, 1930, Harned and Robinson, 1928) or non-protic solvents (Coetzee and Padmanabhan, 1965), the order of basicities differs ( $R_3N \ll R_2NH > RNH_2 > NH_3$ ). For example, methylation of ammonia favors protonation by  $\sim 2$  kcal/mole, the second methylation has a minimal effect, and the final methylation favors de-protonation by  $\sim 1$



kcal/mol (Brown et al., 1944). This anomalous order of amine basicities in aqueous solutions with successive methylation (Aue et al., 1976, Bowers et al., 1971, Arnett et al., 1972, Aue et al., 1972, Henderson et al., 1972) can also be demonstrated in the phenethylamine, *p*-hydroxyphenethylamine (i.e., compounds I-III), and methoxyphenethylamine series of compounds (Figure 4-6). The retention of the same anomalous order in the microscopic ionization constants of compounds I, II, and III with successive methylation confirms that the microscopic constants  $pk_2$  and  $pk_{12}$  are associated with the ionization of the amine group and the remaining two constants are associated with the phenol ionization.

### ***Substituent Effects on Microscopic Ionization Constants***

Substituent effects on pKa values are typically described using linear free energy relationships taking the form of the Hammett equation (Hammett, 1937, Taft, 1953) which attribute pKa changes to the product of a substituent constant ( $\sigma$ ) and a reaction constant ( $\rho$ ). Because the  $-NH_2$  and phenolic  $-OH$  groups are separated by a distance of approximately 8 Å in the fully extended conformation in tyramine (I) and are further shielded by two methylene groups separating the amino from the aromatic portion of the molecule, it would appear that long-range interactions between these groups could be neglected.

The microscopic ionization constants for deprotonation of the cation of I to its neutral form are consistent with the above expectation. Thus, as illustrated in Table 4-1, the value of 10.01 for  $pk_2$  (Table 4-1) is close to that of phenethylamine (pKa = 9.9) and *p*-methoxyphenethylamine (pKa = 9.96) which lack a phenolic OH. Similarly, the microscopic ionization constants for deprotonation of the neutral forms of I, II, and III to their respective anions ( $pk_{21}$  = 10.23, 10.35, and 10.17, respectively) are quite similar to that of 4-ethylphenol (pKa = 10.21).

On the other hand, the ionization constants involving the zwitterionic forms ( $pk_1$  and  $pk_{12}$ ) are shifted by approximately 0.6 units relative to the corresponding neutral forms of I, II, and III. Thus, the phenol group is 0.6 pH units more acidic and the amine group is 0.6 units more basic when the opposing functional group is ionized indicating

that the ionization of one functional group favors the ionization of the other. While equal magnitudes of pK shift are required to balance the thermodynamic square ( $k_1k_{12} = k_2k_{21}$ ), these results are clearly indicative of an amplified long-range interaction when the substituents are ionized. The direction of the shift and its magnitude remain approximately the same for the primary, secondary, and tertiary amine-containing compounds I, II, and III (Table 4-1).

In contrast to the above group of compounds, the pK<sub>a</sub> value for the phenolic -OH in *p*-hydroxyphenylalkanoic acids (when two or more methylene groups separate the phenyl and carboxyl) is 10.14 (Ishimitsu et al., 1979) which is close to that of 4-ethylphenol (pK<sub>a</sub>=10.21). The ionization of the carboxyl group in this case has a nearly negligible effect on the phenol ionization constant. In a separate instance, the pK<sub>a</sub> value of 4-ethylaniline is 5.06 (Demirelli and Koeseoglu, 2004) whereas the pK<sub>a</sub> value of aniline in 4-(2-aminoethyl)-aniline is 4.41 (Tejwani and Anderson, 2004). In this case, the protonated ethylamine weakens the basicity of the aniline by approximately 0.7 units.

It appears that the long-range substituent effects caused by electrostatic interactions become significant when the substituent on the ethyl chain is positively charged. The effect is negligible in the corresponding molecules where the substituent on the ethyl chain is negatively charged.

#### ***Field effect of a charged group on ionization***

Bjerrum (Bjerrum, 1923) invoked Coulomb's law in calculating the effect of an existing charged group of a given molecule on the ionization of second functional group in the same molecule. The electrostatics dictate that greater energy is required to remove a proton from a negatively charged molecule as compared to that from a neutral one. The converse is true in case of a molecule that bears a positive charge. Based on these considerations, Bjerrum proposed a relationship between the pK<sub>a</sub> resulting from this effect ( $\Delta\log K$ ) and the distance between the two interacting groups (*r*, in Angstroms). This relationship in its simplest form at 25 °C, is shown below

$$\Delta \log K = \frac{241.86}{D \cdot r} \quad (4-8)$$

where D is the dielectric constant of the medium, and the quantity in the numerator is the result of multiplication of several physical constants in appropriate units. Edsall (Edsall et al., 1958), based on the formulation by Kirkwood and Westheimer (Kirkwood and Westheimer, 1938, Westheimer and Kirkwood, 1938), calculated the effective dielectric for the interaction between tyrosine hydroxyl and amino groups in water to be 58. Using this value for the effective dielectric constant, a  $\Delta pK_a$  value of 0.6 to 0.7 observed for I, II, III, and 4-(2-aminoethyl)-aniline corresponds to a distance of about 6 Angstroms. This calculated distance is considerably shorter than that for a fully extended *trans* conformation and corresponds better with the relatively folded, *gauche* conformer of the ethylamine chain.

While disagreements still remain regarding the appropriate level of generalization (Ehrenson, 1976) that should be used in the Kirkwood-Westheimer approach, it is reasonable to expect that for a given series of molecules where r remains unchanged, the value of  $\Delta pK_a$  should hold. Similarly, the conclusion regarding the molecular conformation holds even if the electron pair of the phenolate ion is considered to delocalize over the benzene ring.

#### ***Partition coefficients in hydrocarbon***

The apparent 1,9-decadiene/water partition coefficients of compounds I, II, and III as a function of pH are shown in Figure 4-7. As expected, the apparent partition coefficients for each of the three compounds increase with an increase in pH from 8 to 9.5, corresponding to increases in the neutral fraction (Figure 4-5). While the partition coefficient measurements were carried out at very low concentrations (less than  $10^{-3}$  moles/liter) to prevent the possible participation of self association, the goodness of fit of Equation 4-4 to the data provides an additional evidence for the absence of such an effect (Anderson et al., 1980, Anderson et al., 1979, Rytting et al., 1978a, Anderson et al., 1978, Anderson et al., 1975). Moreover, as shown in Figure 4-7, no difference was seen in the tyramine partition coefficients at two different aqueous concentrations of 1 mM and 0.05

mM. The resulting intrinsic values for the neutral form of each compound explored are shown in Table 4-1.

***Functional group contributions derived from the partition coefficients***

The contribution of a functional group (X) to the free energy of solute transfer from water to hydrocarbon is given as

$$\Delta(\Delta G^0)_{RH \rightarrow RX} = -RT \ln \left( \frac{K_{o/w}^{RX}}{K_{o/w}^{RH}} \right) \quad (4-9)$$

where  $K_{o/w}^{RX}$  and  $K_{o/w}^{RH}$  are the hydrocarbon/water partition coefficients of the compound with and without the functional group X.

A fragment based approach to the prediction of permeability coefficients across lipid bilayers as well as partition coefficients in the 1,9-decadiene/water system has been developed in this laboratory (Cao, 2008). This approach considers that the functional group contribution to solvation consists of a polar and a non-polar component (Mayer et al., 2003, Wimley et al., 1996, S. H. Yalkowsky, 1976). The non-polar component can be described as the multiple of the solvation parameter (free energy per unit non-polar surface area of the molecule,  $\sigma_{np}$ ) and the sum of the surface areas of all the non-polar constituents of the functional group, corrected for the surface area of the reference compound ( $\Delta A_{np}$ ). The polar component on the other hand can be described as the sum of the free energy contributions of all the polar functional groups ( $\Delta(\Delta G^0)_p$ ). The resulting total free energy contribution of the molecular fragment can be given as

$$\Delta(\Delta G^0)_X = \sigma_{np} \sum \Delta A_{np} + \sum \Delta(\Delta G^0)_p \quad (4-10)$$

Based on the non-polar surface areas and functional group contributions previously calculated (Cao, 2008), the partition coefficients of the compounds in this study were predicted. The estimates are shown along with the experimentally measured partition coefficients in Table 4-1. The estimates for 4-ethylphenol and phenylethylamine, the monofunctional molecules, are predicted to within a few hundred

calories per mole. The estimates for several bifunctional molecules however deviate by a larger margin and could be due to the indirect calculation of the functional group contribution of amine used for the prediction. Due to absence of the amine functional group contribution in the existing database, it was calculated from a linear combination of other functional group contributions (-CON<, -COO-, and -O-). The contributions for the first and second amine protons were similarly derived from the amide protons. The weakness of the predictions suggests that the experimentally determined contributions for these functional groups may be needed before predictions can be tested for these compounds. A more robust functional group contribution for the amino group transfer from water to the hydrocarbon was determined using the aqueous and heptane solubility data from Rytting et al (Rytting et al., 1978b). The calculated free energy of transfer of alkyl amino group from this study is 5 kcal per mole favoring the aqueous phase.

The functional group contribution for the amino group calculated from the partition coefficients of 4-ethylphenol and tyramine is 2.8 kcal per mole. This value, along with the similarly calculated transfer free energy for the incorporation of the -NH<sub>2</sub> substituent in phenethylamine and *p*-methoxyphenethylamine displayed in Figure 4-8 indicate that significant disparities exist in the value of  $\Delta(\Delta G^0)_{H \rightarrow NH_2}$  depending on the nature of the substituent at the *para* position of the aromatic ring. While incorporation of an amino group significantly disfavors partitioning into 1,9-decadiene by ~3-4 kcal/mol, this unfavorable effect is significantly reduced in tyramine, suggesting that a long-range interaction between the amine and phenolic -OH may occur in the hydrocarbon phase.

Additional evidence for an amplified long-range substituent effect favoring the partitioning of tyramine is provided by the functional group contributions of successive N-methylation,  $\Delta(\Delta G^0)_{RNH_2 \rightarrow RNHCH_3}$  and  $\Delta(\Delta G^0)_{RNHCH_3 \rightarrow RN(CH_3)_2}$ , to the free energy of solute transfer from water to hydrocarbon shown in Figure 4-9. The first N-methylation of tyramine (I) decreases its partition coefficient by three-fold while the second methylation increases it by six-fold. Successive methylations of methylamine to form dimethyl- and trimethylamine, however, show consistently negative values. The

anomalous effect of the first N-methylation in tyramine is not seen when the phenolic -OH is replaced with phenolic -OCH<sub>3</sub> (i.e., comparing compounds IV & V).

The same effect is apparent when the functional group contributions for removal of the phenolic -OH,  $\Delta(\Delta G^0)_{ROH \rightarrow RH}$ , and for O-methylation,  $\Delta(\Delta G^0)_{ROH \rightarrow ROCH_3}$ , are compared as shown in Figure 4-10. Both contributions are significantly (~ 1 kcal/mol) smaller in I as compared to those in the other series.

### ***The NH- $\pi$ effect and water adduct hypotheses***

Based on spectroscopic studies of phenethylamine and related compounds (Robertson et al., 2001, Melandri and Maris, 2004, Richardson et al., 2004) the folded *gauche* conformer of the ethylamine chain (Figure 4-11) has the lowest energy in the gas phase for these compounds. This is attributed to a charge interaction between the partially positively charged N-H proton and the  $\pi$  ring system (electron rich). Similar interactions in a hydrocarbon solvent may favor the partitioning of tyramine in both its neutral and zwitterionic forms. Alternatively, the availability of water molecules may facilitate partitioning through formation of water adducts as depicted in Figure 4-11, which could involve either the neutral drug molecule or an internal ion pair. The role of residual water in the oil phase in altering the partitioning of solutes has been documented previously (Cao et al., 2004).

### ***Partition coefficients in the preferred binding domain of the lipid bilayer membrane***

The lipid bilayer / water partition coefficients of tyramine, N-methyltyramine and dimethyltyramine as a function of aqueous phase concentration (0.0003 to 0.0085 moles per liter) determined in various pH buffers are shown in Figures 4-12, 4-13, and 4-14, respectively. The concentration independence suggests the absence of saturable binding (Baeuerle and Seelig, 1991) or any other phenomena that can affect the partitioning or binding estimates. An independent control experiment established that binding to the ultrafiltration filters and tubes was non-detectable (results not shown). As a result, the binding of solutes to the lipid bilayer membrane was taken to be independent of pH and

concentration. All the data were combined to determine  $\log(K_{\text{liposome/water}})$  for each of the three solutes. For tyramine, N-methyltyramine, and dimethyltyramine, it was found to be 1.24, 1.04, and 1.05, respectively.

Both hydrophobic and electrostatic components may contribute to the binding (or surface partitioning) of solutes to lipid bilayers. Usually, electrostatic interactions are saturable due to charge repulsion produced by the increasing surface concentration of the bound solute. This effect is frequently modeled using Gouy-Chapman theory which accounts for a reduced interfacial concentration of ions due to charge accumulation (Aveyard and Haydon, 1973). The absence of pH dependent binding in the pH range where the protonated amine is the dominant species suggests that the protonated amine may be the major species bound in the pH range of interest. The lack of significant curvature in the binding isotherms rules out potential saturation due to charge effects. This apparent contradiction may be due to the fact that the interfacial binding is driven primarily by hydrophobic contributions with the charged amino group located further from the interface and solvated by water and oppositely charged counterions. Molecular dynamics simulations of tyramine have shown that near the membrane-water interface tyramine tends to orient in a manner perpendicular to the membrane interface with the phenolic-OH pointing towards the membrane and the amine group solvated in water (chapters 5 and 6).

#### *Functional group contributions derived from the lipid bilayer partition coefficients*

White and coworkers (Wimley and White, 1996) measured the surface binding of a series of peptides and determined the free energy contributions for transfer of each of the amino acid residues from the lipid bilayer surface to water. The functional group contributions for transfer of amino, hydroxyl, and phenolic hydroxyl from water to the lipid bilayer surface calculated from their database are 1.3, -0.04, and 0.19 kcal per mole, respectively. The liposome/water partition coefficients of tyramine and 4-ethylphenol yield a value of 2 kcal per mole for the transfer of the amino group which is close to the value obtained from the amino acid data.

Immobilized artificial membrane chromatography has been employed to determine the liposome water partition coefficients of a variety of compounds. The chromatographic capacity factor,  $k'$ , is related to the partition coefficient in the stationary phase by the following relationship

$$k' = \frac{t_R - t_0}{t_0} = \frac{V_S}{V_m} K_{s/m} \quad (4-11)$$

Here,  $t_R$  and  $t_0$  are the retention time of the solute and a non-retained solute in a given chromatographic experiment;  $V_S$  and  $V_m$  are the volume of the stationary phase and the retention volume of the solute, and  $K_{s/m}$  is the partition coefficient between the stationary and mobile phases. While possible, the determination of the volumes in Equation 4-11 is relatively difficult and tends to vary between experimental runs as well as laboratories. However, if one calculates the free energy contributions for the capacity factors from a single experimental set up, the volume terms cancel and the free energy contributions are the same as those for the partition coefficient. It should be noted that the properties obtained in IAM chromatography are similar to the shake flask partition coefficient determinations in the liposome/water system. Whether they correspond to the partition coefficient on the surface or the hydrocarbon region of the bilayer depends on the nature of the solute. For example, only amphiphilic solutes may have a propensity to partition into the interface and complete hydrophobes may partition into the hydrocarbon region of the bilayer.

A compilation of the retention factors of several organic compounds in an IAM column with similar head groups as that of DOPC has been prepared by Barbato et al (Barbato et al., 2004), Lazaro et al (Lazaro et al., 2005), and Abraham and coworkers (Valko et al., 2000). The last two of these report capacity factors for phenol and resorcinol<sup>‡</sup> that result in -0.4 kcal per mole for transfer of the phenolic hydroxyl to the interface. This value is not too distant from the interface transfer value of the same group

---

<sup>‡</sup> The corresponding Hammett sigma ( $\sigma$ ) value for the *meta*-hydroxyl group is 0.12 and the Hammett rho ( $\rho$ ) is 0.8 to 1.8 (HINE, J. S. (1975) Equilibrium in hydrogen bonding. *Structural Effects On Equilibria In Organic Chemistry*. New York, John Wiley & Sons, Inc., 200.). The corresponding change in the free energy contribution is +0.1 to +0.2 kcal per mole.



(-0.2 kcal per mole) calculated from the partition coefficients of tyrosine and phenylalanine determined by Wimley and coworkers (Wimley and White, 1996) using partition coefficients of a pentapeptide. It is interesting that the transfer of the phenolic hydroxyl to the interface costs almost nothing in terms of the free energy when compared with the transfer to the hydrocarbon where the energetic cost is almost 4 kcal per mole (Figure 4-10). The preferred binding region of these compounds is certainly different in its solvation properties compared to the hydrocarbon region. However, the low transfer free energy of the polar groups reinforces the idea that the driving force for binding may still be the hydrophobic effect.

Changes to the polar functional groups, such as methylation of the amino group were also calculated. The free energy contribution for first and second methylation of the amine nitrogen yields -0.3 and 0.01 kcal per mole. The first methylation value obtained from the IAM capacity factors ranges from -0.04 to 0.14 kcal based on the values for N-methylphenylethylamine and phenylethylamine (Barbato et al., 2004) which is similar to the one determined in this study. If hydrophobic effect was the driving force for the binding of these solutes to the lipid bilayer membrane, methylation should show an increase in the binding. While the changes in the quantities are small for a positive verification, they seem to trend in the direction predicted.

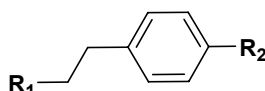
## Conclusion

This study highlights the potential importance of apparent “long-range” interactions between substituents that would typically be assumed to be “well isolated” in standard LFER applications. Our results show that interactions between the ionized phenolic and amine groups in p-(aminoethyl)-phenols result in significant shifts in their microscopic ionization constants in water. This effect is quantitatively consistent among several compounds, including those that bear an aniline group instead of a phenol. The resulting shift in the pKa values points to a significant contribution by the folded conformation of the ethylamine chain likely due to electrostatic stabilization by the second functional group. The conformation effectively provides a significant *through-space* interaction between groups that would be considered “long-range” in terms of

either intra-molecular “through-bond” distance or the *through-space* distance observed in an extended conformation. A similar apparent long-range interaction is revealed in comparisons of the 1,9-decadiene/water partition coefficients of I with those of structurally similar compounds. An interaction between the phenolic –hydroxyl and ethylamino groups in I or internal ion pair formation in the hydrocarbon solvent (either of which may include water molecules) results in an enhanced partition coefficient for I beyond that predicted from a consideration of individual functional group contributions to the free energy of transfer from water to hydrocarbon.

Besides the group contributions for transfer to the barrier region, the same for the preferred binding region were also calculated. The free energy contributions to the transfer of the amphiphilic solutes to the preferred binding domain were found to correlate with those obtained from the immobilized artificial membrane chromatography. From the magnitude of the free energy contributions it appears that the partition coefficients in the preferred binding region are relatively less sensitive to the addition of hydroxyl or amino groups to the molecules. Further, the methylation of amine nitrogen shows changes that are small albeit consistent with those expected from the hydrophobic effect.

**Table 4-1.** Chemical structures, negative logarithms of the (microscopic) ionization constants, logarithms of liposome/water partition coefficients (K<sub>lipo</sub>), and logarithms of intrinsic 1,9-decadiene/water partition coefficients (K<sub>o/w</sub>) of the respective neutral species of compounds I-VII. The ionization constants of monoionizable compounds IV-VII are listed in columns that correspond to the appropriate microscopic ionization constants defined in Figure 4-1.



Solute	R1	R2	Negative Log of Ionization Constant ( $\pm$ SD)				LogK <sub>lipo</sub>	LogK <sub>o/w</sub>
			Pk <sub>1</sub>	pk <sub>2</sub>	pk <sub>12</sub>	pk <sub>21</sub>		
I	NH <sub>2</sub>	OH	9.62 (0.01)	10.01 (0.02)	10.62 (0.02)	10.23 (0.05)	1.24 (0.11)	-1.35 (0.02)
			9.61 <sup>i</sup>	10.06 <sup>i</sup>	10.53 <sup>i</sup>	10.08 <sup>i</sup>		-2.26 <sup>ii</sup>
			10.30 <sup>iii</sup>	9.72 <sup>iii</sup>	9.48 <sup>iii</sup>	10.06 <sup>iii</sup>		
			9.70 <sup>iv</sup>	10.09 <sup>iv</sup>	10.72 <sup>iv</sup>	10.33 <sup>iv</sup>		
			9.51 <sup>v</sup>	10.13 <sup>v</sup>	10.49 <sup>v</sup>	10.07 <sup>v</sup>		
II	NHCH <sub>3</sub>	OH	9.62 (0.01)	10.08 (0.04)	10.81 (0.02)	10.35 (0.07)	1.04 (0.20)	-1.75 (0.03)
			9.86 <sup>v</sup>	10.43 <sup>v</sup>	10.67 <sup>v</sup>	10.09 <sup>v</sup>		-2.62 <sup>ii</sup>
III	N(CH <sub>3</sub> ) <sub>2</sub>	OH	9.56 (0.02)	9.53 (0.02)	10.15 (0.03)	10.17 (0.07)	1.05 (0.11)	-0.9 (0.01)
			9.57 <sup>v</sup>	9.51 <sup>v</sup>	9.69 <sup>v</sup>	10.05 <sup>v</sup>		-1.84 <sup>ii</sup>
IV	NH <sub>2</sub>	OCH <sub>3</sub>		9.92 <sup>v</sup>				0.65 (0.01)
							2.04 <sup>ii</sup>	
V	NHCH <sub>3</sub>	OCH <sub>3</sub>		10.04 <sup>vi</sup>				1.12 (0.05)
				10.52 <sup>v</sup>			-0.94 <sup>ii</sup>	
VI	NH <sub>2</sub>	H		9.9 <sup>v,viii</sup>				0.62 (0.03)
				9.88 <sup>vii</sup>			0.57 <sup>ii</sup>	
				9.83 <sup>ix</sup>				

Solute	R1	R2	Negative Log of Ionization Constant ( $\pm$ SD)				LogK <sub>lipo</sub>	LogK <sub>o/w</sub>
			Pk <sub>1</sub>	pk <sub>2</sub>	pk <sub>12</sub>	pk <sub>21</sub>		
VII	H	OH				10.21 <sup>x</sup> 10.26 <sup>v</sup>	2.75 <sup>xi</sup>	0.71 (0.01) 0.93 <sup>ii</sup>

- i. Microscopic ionization constants from Peinhardt et al (Peinhardt and Wiese, 2001)
- ii. Predicted using the hydrophobicity scale from Cao et al (Cao, 2008)
- ii. Microscopic ionization constants from Nagy et al (Nagy and Takacs-Novak, 2004)
- iii. Obtained from Yamazaki et al (Yamazaki et al., 1965)
- iv. Calculated using ACD-pKa v.10 (ACD-pKa, 1994-2007)
- v. Obtained from Armstrong et al (Armstrong and Barlow, 1976)
- vi. Obtained from Kappe et al (Kappe and Armstrong, 1965)
- vii. Obtained from Mack et al (Mack and Boenisch, 1979)
- viii. Obtained from Gluck et al (Gluck and Cleveland, 1994)
- ix. Obtained from Wehry et al (Wehry and Rogers, 1965)
- x. Obtained from Rogers et al (Rogers and Davis, 1980)

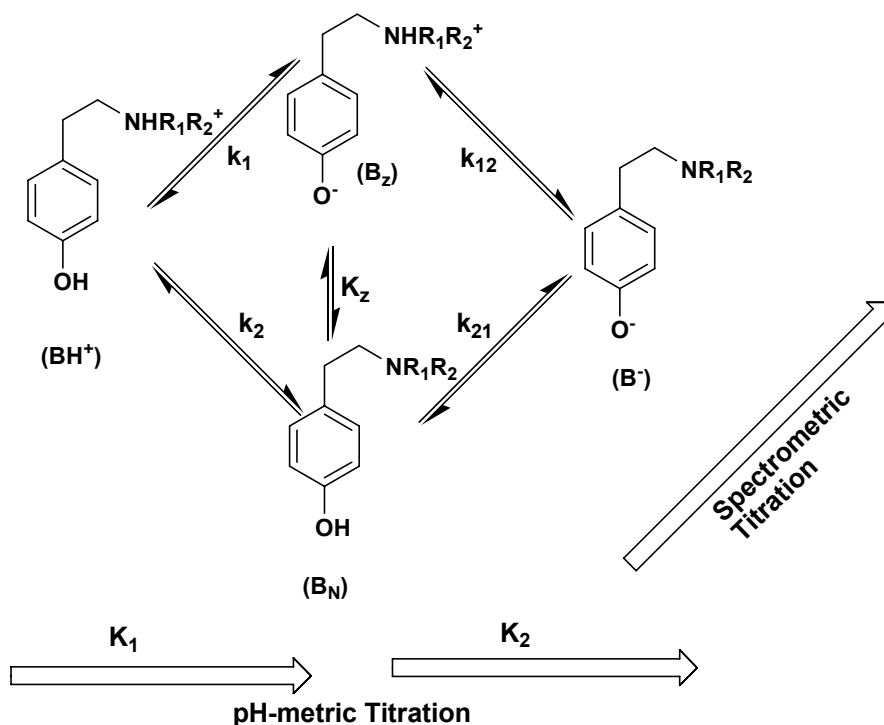


Figure 4-1. Ionization of *p*-(aminoethyl)phenol showing four species in aqueous solutions: cation (BH<sup>+</sup>), neutral (B<sub>N</sub>), zwitterion (B<sub>Z</sub>), and anion (B<sup>-</sup>). The compounds are: Tyramine (I): R<sub>1</sub>=R<sub>2</sub>=H, N-methyltyramine (II): R<sub>1</sub>=CH<sub>3</sub> and R<sub>2</sub>=H, N,N-dimethyltyramine (III): R<sub>1</sub>=R<sub>2</sub>=CH<sub>3</sub>. The four equilibria representing respective interconversions are labeled with corresponding microscopic ionization constants, *k*<sub>1</sub>, *k*<sub>2</sub>, *k*<sub>12</sub>, and *k*<sub>21</sub>. The fifth possible interconversion between zwitterion and neutral forms is independent of pH (shown as K<sub>Z</sub>) as no protons are added or removed during the conversion. A simple pH-volumetric titration shows two apparent ionization constants K<sub>1</sub> and K<sub>2</sub> that are a composite of two of the four microscopic ionization constants. A spectrometric titration demonstrates only two distinct species related to the ionization state of the phenol group.

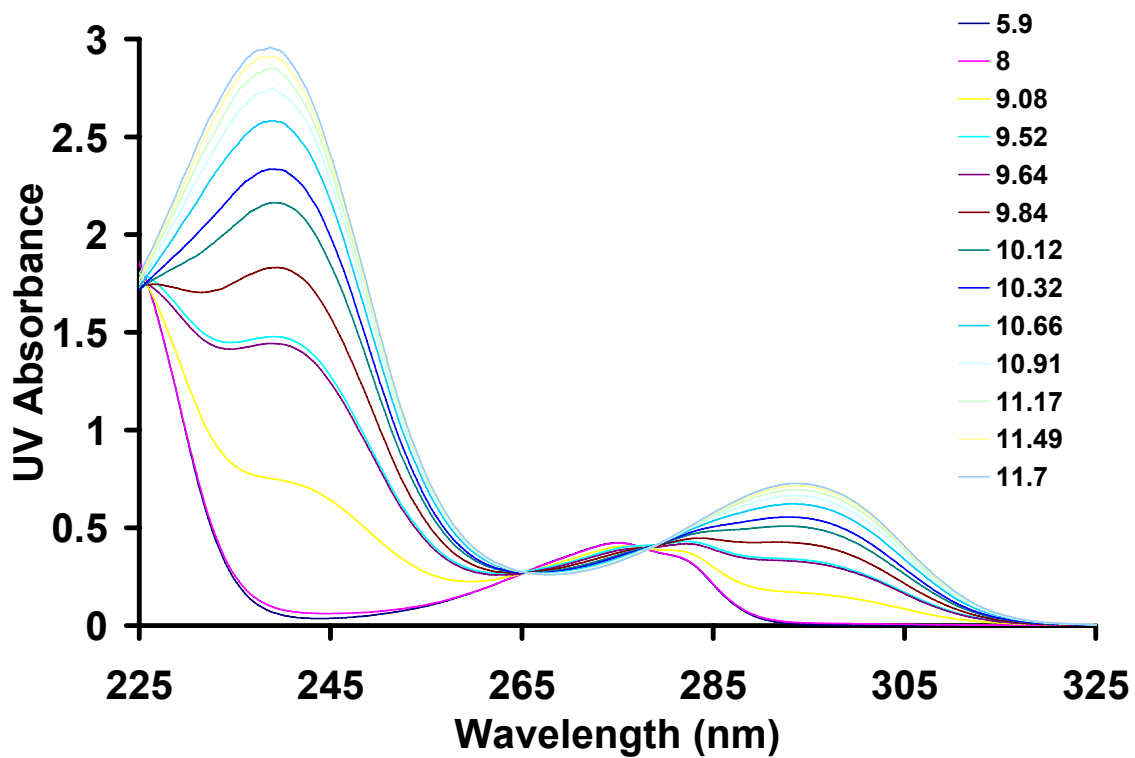


Figure 4-2. The UV absorbance spectra of tyramine solutions prepared at varying pH. The numbers in the legend indicate pH of each solution.

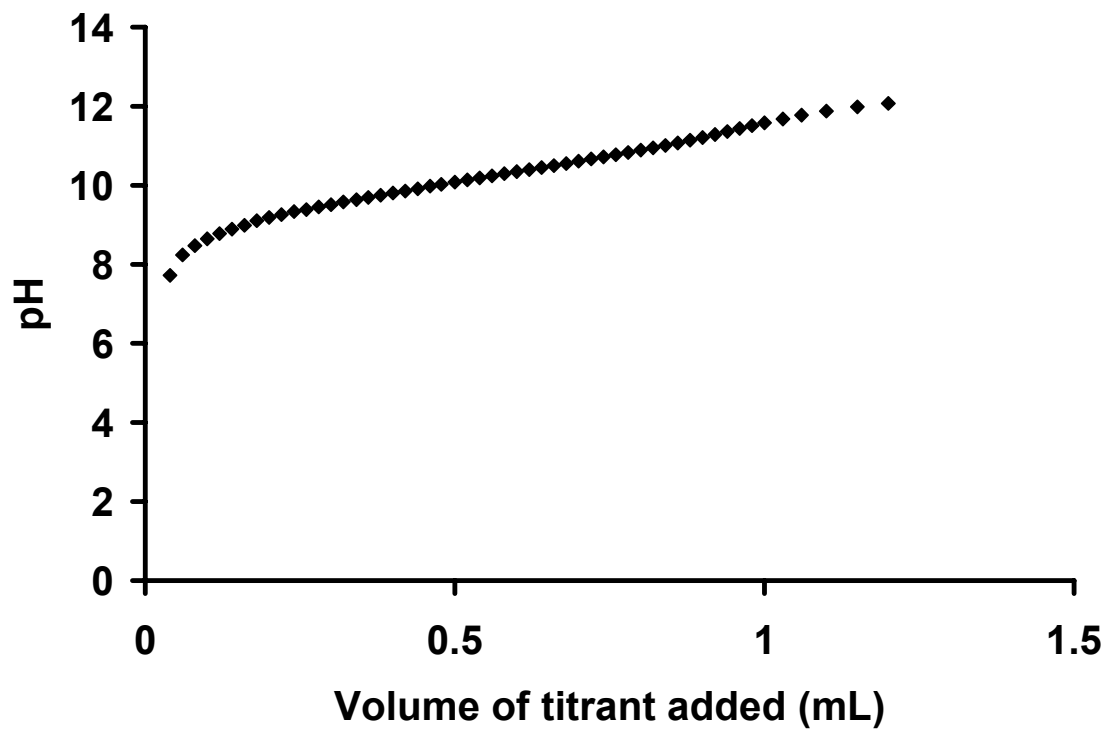


Figure 4-3. Plot of pH of tyramine solution (0.03 M, 16 mL) as a function of volume of 1N sodium hydroxide.

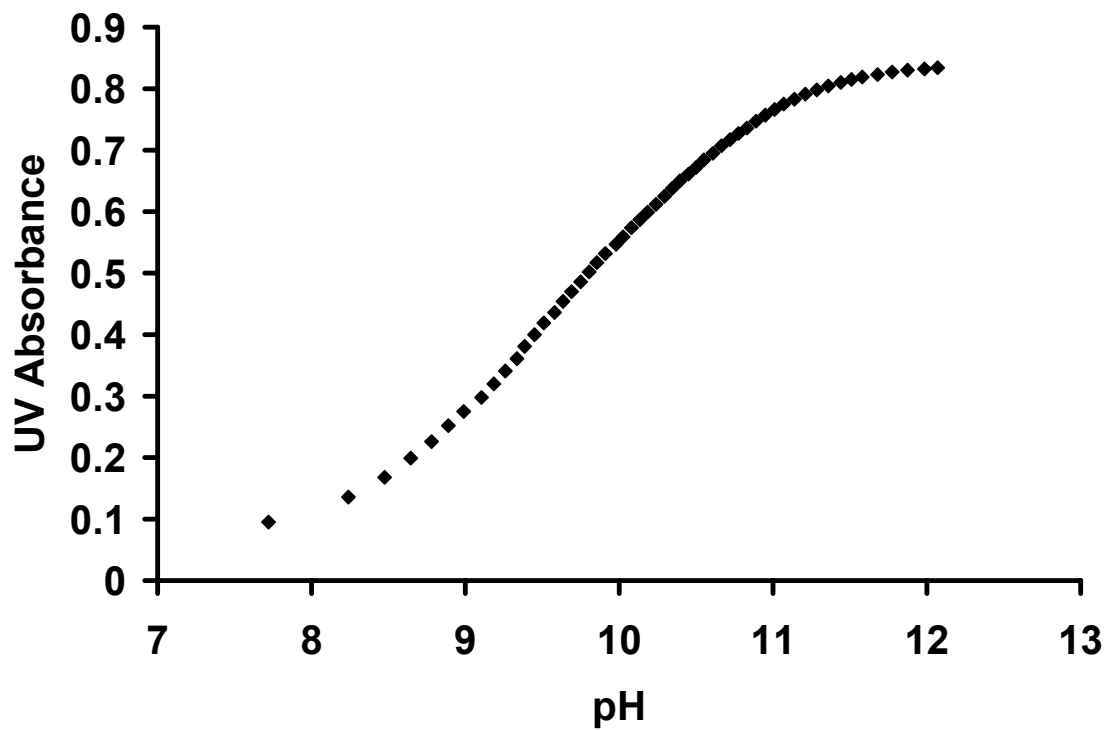


Figure 4-4. Plot of UV absorbance (320 nm) of the tyramine solution for which titration is shown in Figure 4-3.



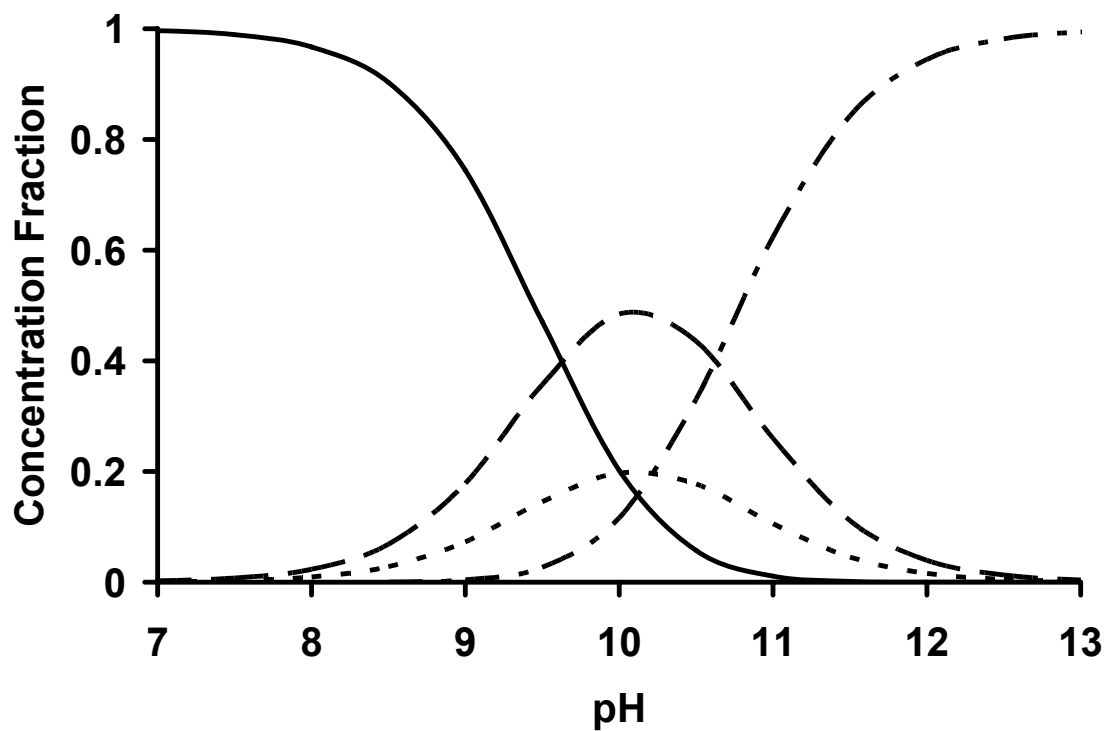


Figure 4-5. Fraction of various species of *p*-(aminoethyl)phenol in solution as function of pH. Structures of cation (BH<sup>+</sup>, ———), zwitterion (B<sub>z</sub>, — —), neutral (B<sub>N</sub>, - - -), and anion (B<sup>-</sup>, — - —) are shown in Figure 4-1.

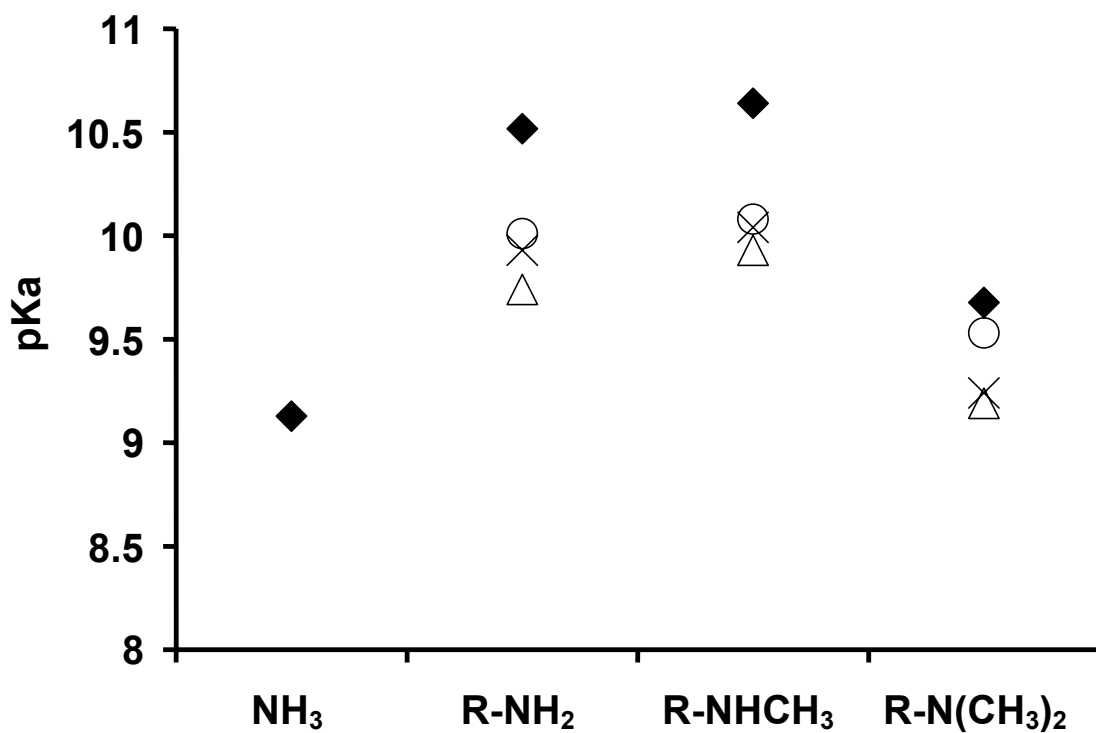


Figure 4-6. Effect of successive methylation on ionization constant of each amine. R= methyl- (♦), phenethyl- ( $\Delta$ ), *p*-methoxyphenethyl- ( $\times$ ), *p*-hydroxyphenethyl- ( $\circ$ ). Values are plotted from **Table 4-1** and literature (Aue et al., 1976, Armstrong and Barlow, 1976).

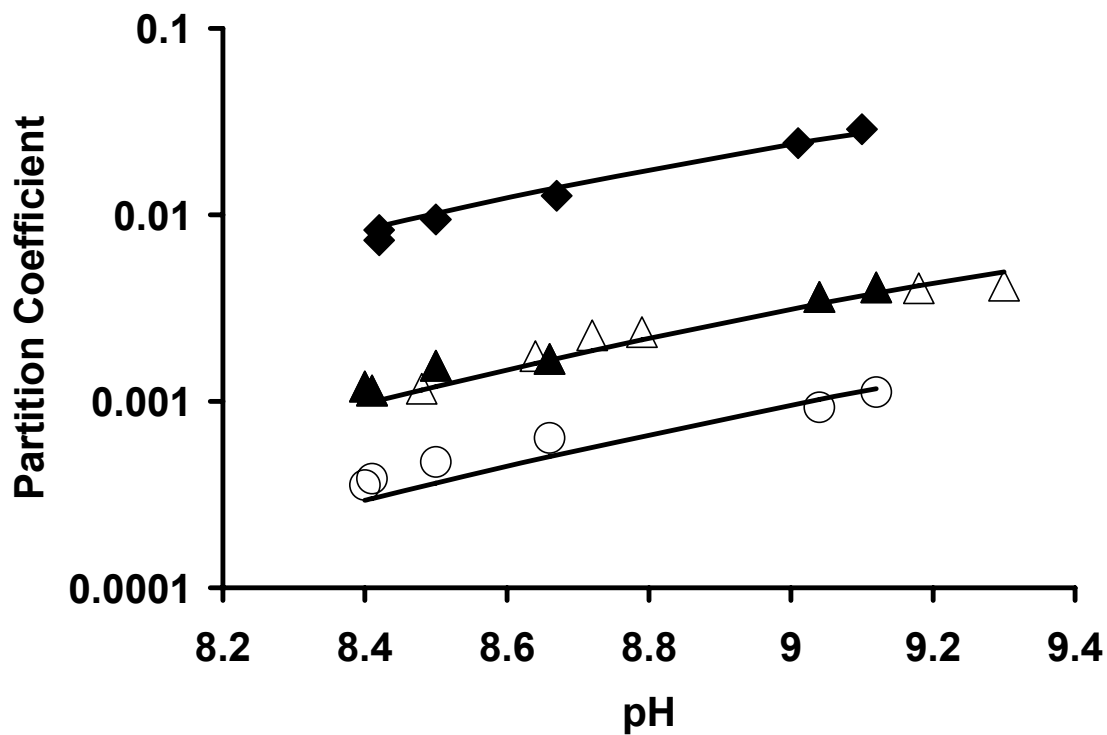


Figure 4-7. Apparent partition coefficients of compounds I ( $\Delta$ ,  $\blacktriangle$ ), II ( $\circ$ ), and III ( $\blacklozenge$ ) are shown as a function of pH. Lines show best fits to Equation 4-4. The partition coefficient for compound I was determined at a total concentration of 0.05 mM ( $\blacktriangle$ ) or at 1 mM ( $\Delta$ ).

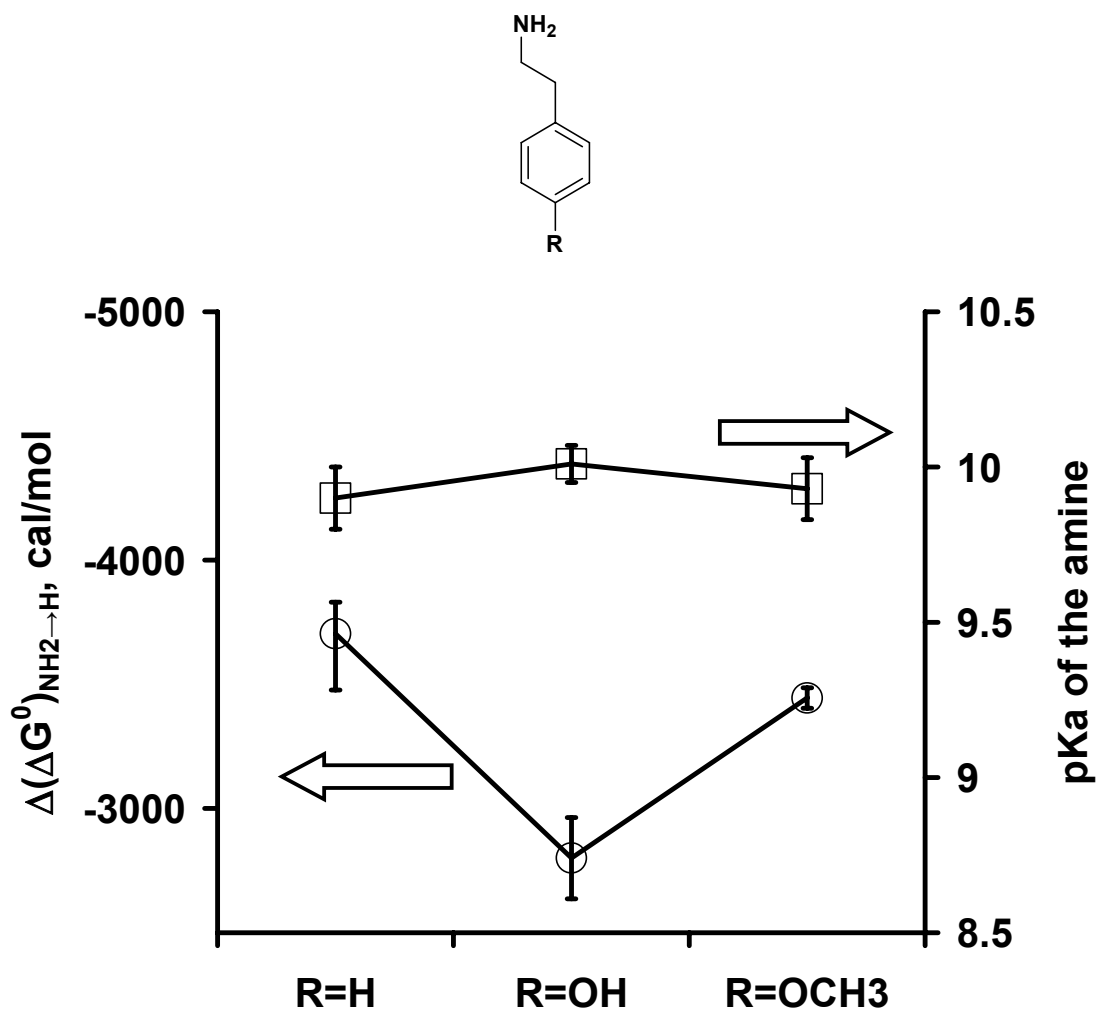


Figure 4-8. Contribution of the amine group to the transfer free energy,  $\Delta(\Delta G^0)_{H \rightarrow \text{NH}_2}$  (○, left axis), along with pKa of the corresponding amine (□, right axis). The hydrocarbon water partition coefficient values were taken from **Table 4-1** or literature (Lambert et al., 1990, Abraham et al., 1994). Error bars indicate the range of determinations.

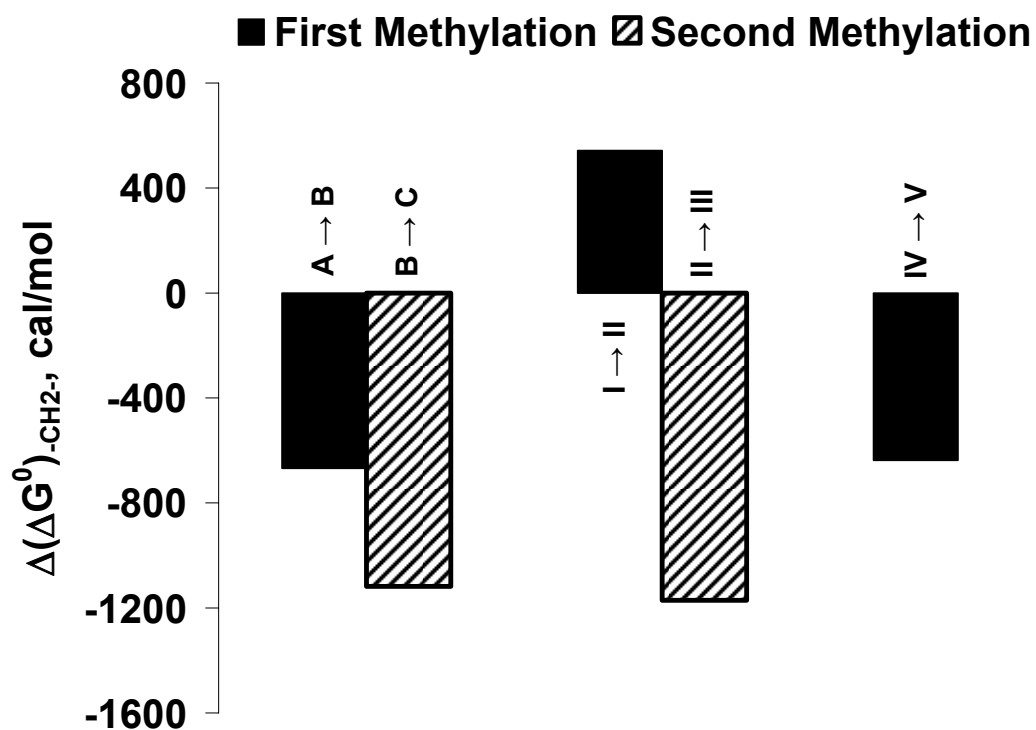


Figure 4-9. Contribution of first methylation  $\Delta(\Delta G^0)_{RNH_2 \rightarrow RNHCH_3}$  (solid bars) and second methylation  $\Delta(\Delta G^0)_{RNHCH_3 \rightarrow RN(CH_3)_2}$  (shaded bars) to the free energy of transfer of the amines from water to hydrocarbon for three different series. Partition coefficients of A (methylamine), B (dimethylamine), and C (trimethylamine) were obtained from the literature (Abraham et al., 1994). Roman numerals correspond to the solutes shown in Table 4-1.

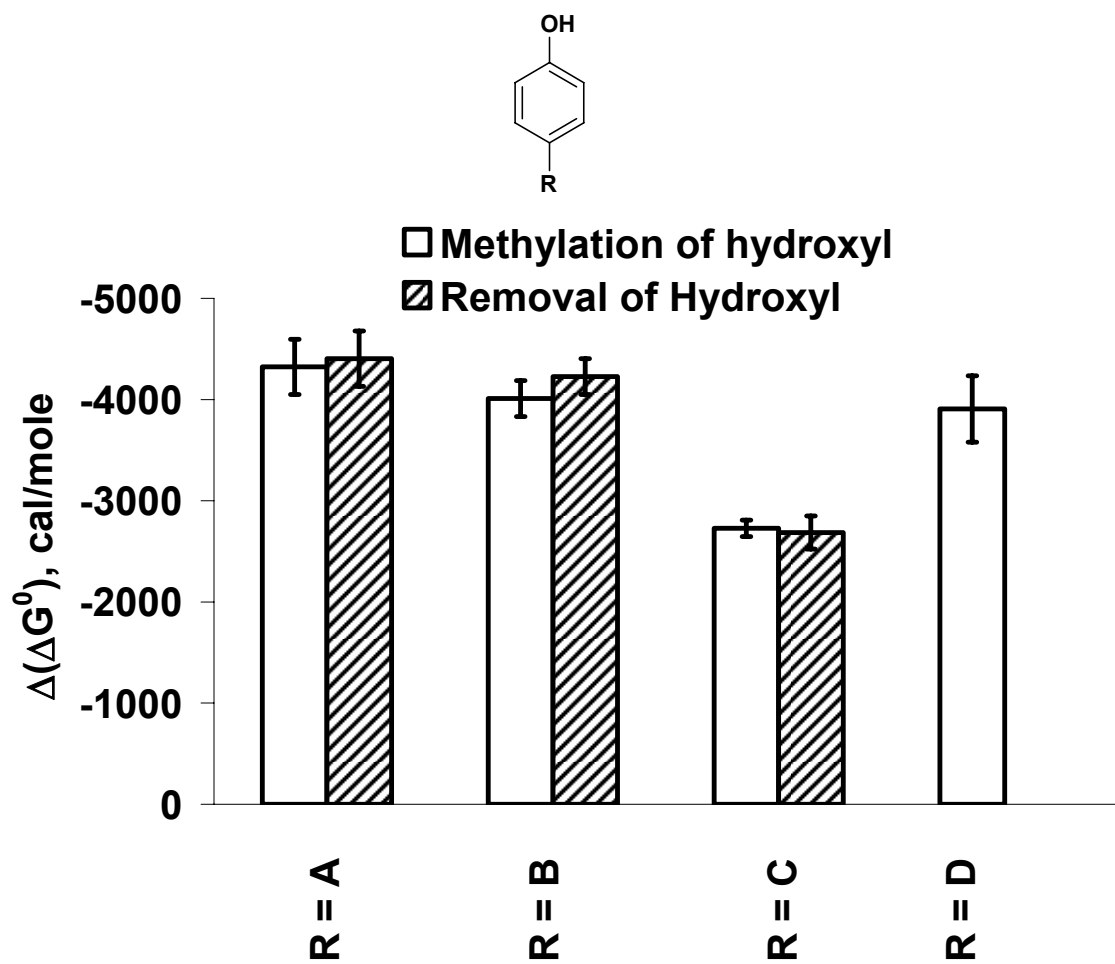


Figure 4-10. Contribution of hydroxyl group removal,  $\Delta(\Delta G^0)_{ROH \rightarrow RH}$  (shaded bars) or its methylation,  $\Delta(\Delta G^0)_{ROH \rightarrow ROCH_3}$  (open bars) to the free energy of transfer of solute from water to hydrocarbon. A = H, B =  $-\text{CH}_2\text{CH}_3$ , C =  $-\text{CH}_2\text{CH}_2\text{NH}_2$ , D =  $-\text{CH}_2\text{CH}_2\text{NHCH}_3$ , Error bars indicate the range of determinations.

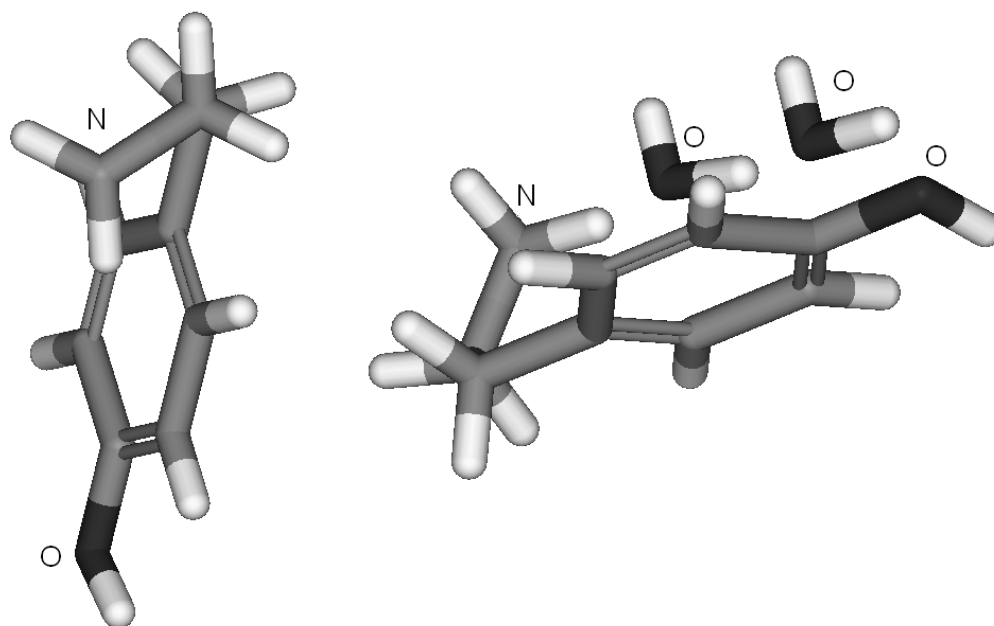


Figure 4-11. The folded *gauche* conformer (Robertson et al., 2001) of *p*-(aminoethyl)phenol (left) and the putative water adduct (right). All heavy atoms are dark colored and hydrogens are light colored. The nitrogen and oxygen atoms have been labeled as N and O, respectively.

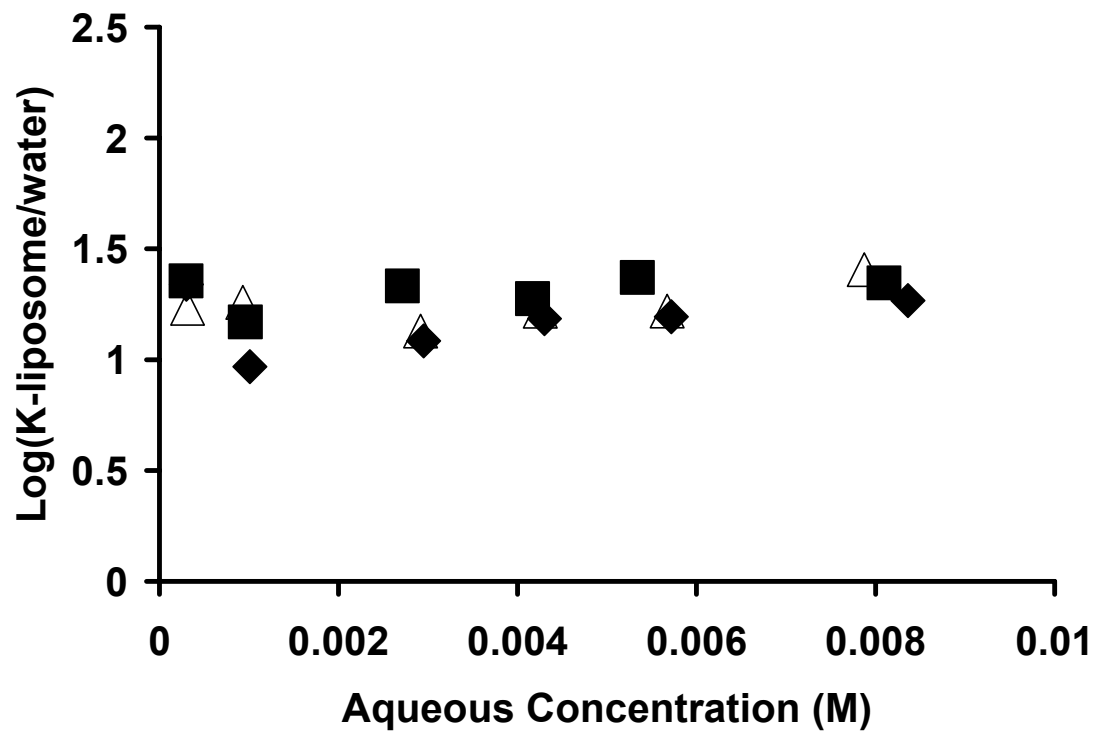


Figure 4-12. Partition coefficient of tyramine in liposomes. ♦ = pH 2, ■ = pH 3, and Δ = pH 4.



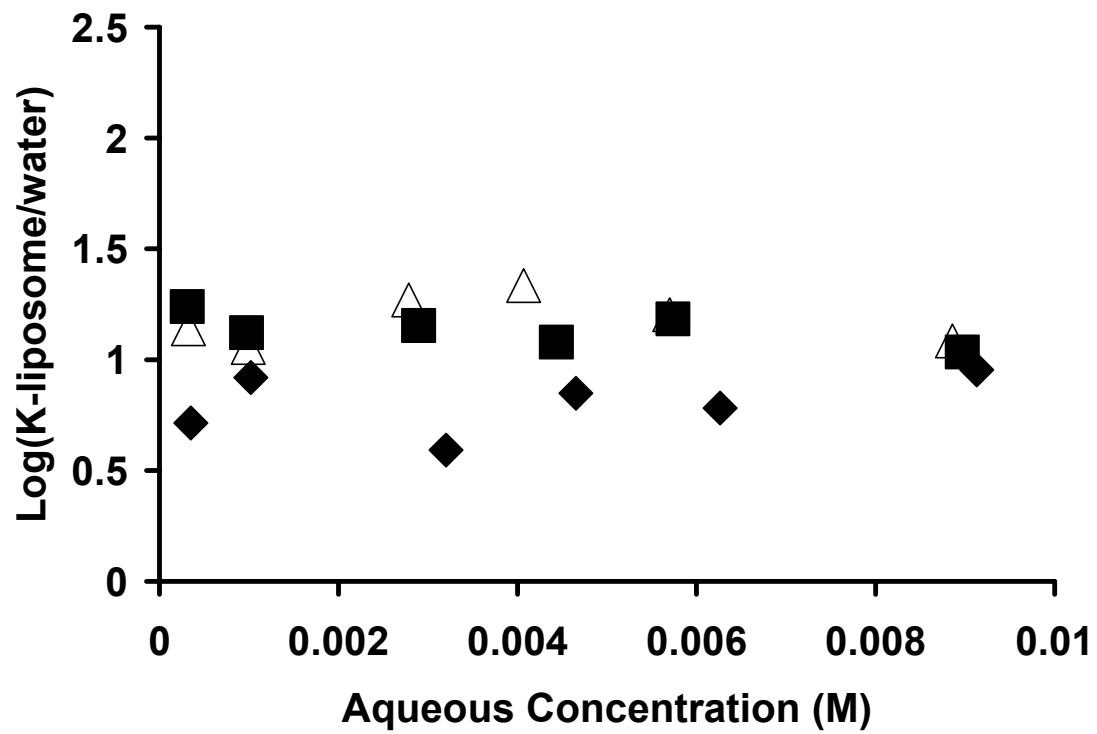


Figure 4-13. Partition coefficient of N-methyltyramine in liposomes.  $\blacklozenge$  = pH 2,  $\blacksquare$  = pH 3, and  $\triangle$  = pH 4.

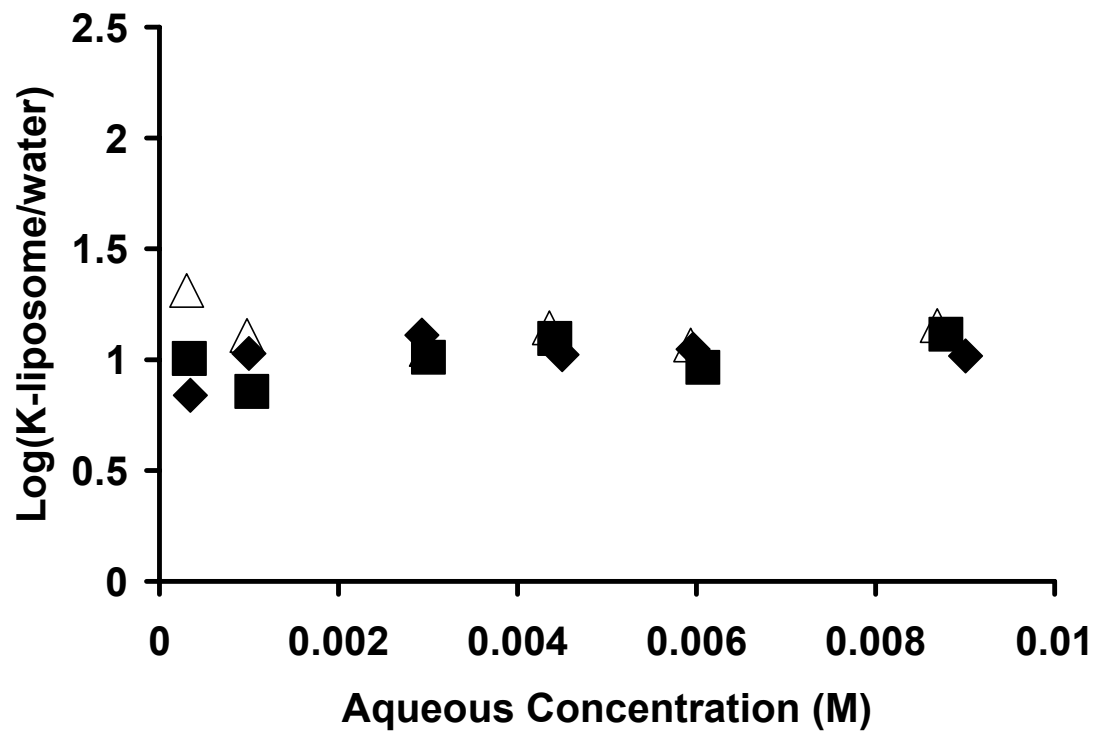


Figure 4-14. Partition coefficient of dimethyltyramine in liposomes. ♦ = pH 2, ■ = pH 3, and Δ = pH 4.

## References

- ABRAHAM, M. H., CHADHA, H. S., WHITING, G. S. & MITCHELL, R. C. (1994) Hydrogen bonding. 32. An analysis of water-octanol and water-alkane partitioning and the  $\Delta \log P$  parameter of seiler. *Journal of Pharmaceutical Sciences*, 83, 1085-1100.
- ACD-PKA (1994-2007) Advanced Chemistry Development / pKa dB. 10.0 ed. Toronto, ON, Canada, Advanced Chemistry Development, Inc.
- ANDERSON, B. D., RYTTING, J. H. & HIGUCHI, T. (1978) Vapor pressure studies of self-association of alcohols in isooctane. I. The effect of chain length. *International Journal of Pharmaceutics*, 1, 15-31.
- ANDERSON, B. D., RYTTING, J. H. & HIGUCHI, T. (1979) Influence of self-association on the solubility of phenol in isooctane and cyclohexane. *Journal of the American Chemical Society*, 101, 5194-7.
- ANDERSON, B. D., RYTTING, J. H. & HIGUCHI, T. (1980) Solubility of polar organic solutes in nonaqueous systems: role of specific interactions. *Journal of Pharmaceutical Sciences*, 69, 676-80.
- ANDERSON, B. D., RYTTING, J. H., LINDENBAUM, S. & HIGUCHI, T. (1975) Calorimetric study of the self-association of primary alcohols in isooctane. *Journal of Physical Chemistry*, 79, 2340-4.
- ARMSTRONG, J. & BARLOW, R. B. (1976) The ionization of phenolic amines, including apomorphine, dopamine, and catecholamines and an assessment of zwitterion constants. *British Journal of Pharmacology*, 57, 501-16.
- ARNETT, E. M., JONES, F. M., TAAGEPERA, M., HENDERSON, W. G., BEAUCHAMP, J. L., HOLTZ, D. & TAFT, R. W. (1972) Complete thermodynamic analysis of the "anomalous order" of amine basicities in solution. *Journal of the American Chemical Society*, 94, 4724-4726.

- AUE, D. H., WEBB, H. M. & BOWERS, M. T. (1972) Quantitative relative gas-phase basicities of alkylamines. Correlation with solution basicity. *Journal of the American Chemical Society*, 94, 4726-4728.
- AUE, D. H., WEBB, H. M. & BOWERS, M. T. (1976) A thermodynamic analysis of solvation effects on the basicities of alkylamines. An electrostatic analysis of substituent effects. *Journal of the American Chemical Society*, 98, 318-329.
- AVEYARD, R. & HAYDON, D. A. (1973) *An Introduction To The Principles Of Surface Chemistry*, Cambridge, UK, Cambridge University Press.
- BAEUERLE, H. D. & SEELIG, J. (1991) Interaction of charged and uncharged calcium channel antagonists with phospholipid membranes. Binding equilibrium, binding enthalpy, and membrane location. *Biochemistry*, 30, 7203-11.
- BARBATO, F., DIMARTINO, G., GRUMETTO, L. & LAROTONDA, M. I. (2004) Prediction of drug-membrane interactions by IAM-HPLC: effects of different phospholipid stationary phases on the partition of bases *European Journal of Pharmaceutical Sciences*, 22, 261-269.
- BJERRUM, N. (1923) Dissociation constants of polybasic acids and their application to the calculation of molecular dimensions. *Zeitschrift fur Physikalische Chemie Stochiometrie und Verwandtschaftslehre*, 106, 219-42.
- BORGMAN, R. J., MCPHILLIPS, J. J., STITZEL, R. E. & GOODMAN, I. J. (1973) Synthesis and pharmacology of centrally acting dopamine derivatives and analogs in relation to Parkinson's disease. *Journal of Medicinal Chemistry*, 16, 630-3.
- BOWERS, M. T., AUE, D. H., WEBB, H. M. & MCIVER, R. T. (1971) Equilibrium constants for gas-phase ionic reactions. Accurate determination of relative proton affinities. *Journal of the American Chemical Society*, 93, 4314-4315.
- BRANDARIZ, I., FIOL, S., HERRERO, R., VILARINO, T. & SASTRE DE VICENTE, M. (1993) Protonation constants of alpha-alanine, gamma-aminobutyric acid, and

- epsilon-aminocaproic acid. *Journal of Chemical and Engineering Data*, 38, 531-533.
- BROWN, H. C., BARTHOLOMAY, H. & TAYLOR, M. D. (1944) Acid-base studies in gaseous systems. II. The anomalous base strength of the methylamines; A new manifestation of steric strain. *Journal of the American Chemical Society*, 66, 435-442.
- CAO, Y. (2008) Application of linear free energy relationships in the prediction of triglyceride/water partition coefficients and lipid bilayer permeability coefficients of small organic molecules and peptides. PhD Thesis. College of Pharmacy, The University of Kentucky, Lexington, KY.
- CAO, Y., MARRA, M. & ANDERSON, B. D. (2004) Predictive relationships for the effects of triglyceride ester concentration and water uptake on solubility and partitioning of small molecules into lipid vehicles. *Journal of Pharmaceutical Sciences*, 93, 2768-79.
- COETZEE, J. F. & PADMANABHAN, G. R. (1965) Properties of bases in acetonitrile as solvent. IV. Proton acceptor power and homoconjugation of mono- and diamines. *Journal of the American Chemical Society*, 87, 5005-5010.
- DEMIRELLI, H. & KOESEGLU, F. (2004) Solvent and substituent effects on the protonation of anilines in dioxane-water mixtures. *Journal of Solution Chemistry*, 33, 1501-1515.
- DIAMOND, J. M. & KATZ, Y. (1974) Interpretation of nonelectrolyte partition coefficients between dimyristoyl lecithin and water. *Journal of Membrane Biology*, 17, 121-54.
- EDSALL, J. T., MARTIN, R. B. & HOLLINGWORTH, B. R. (1958) Ionization of individual groups in dibasic acids, with application to the amino and hydroxyl groups of tyrosine. *Proceedings of the National Academy of Sciences U S A*, 44, 505-18.

- EHRENSON, S. (1976) Transmission of substituent effects. Generalization of the ellipsoidal cavity field effect model. *Journal of the American Chemical Society*, 98, 7510-7514.
- GLUCK, S. J. & CLEVELAND, J. A., JR. (1994) Capillary zone electrophoresis for the determination of dissociation constants. *Journal of Chromatography, A*, 680, 43-8.
- GRANOT, J. (1976) NMR studies of catecholamines, acid dissociation equilibria in aqueous solutions. *FEBS Letters*, 67, 271-5.
- HALL, N. F. & SPRINKLE, M. R. (1932) Relations between the structure and strength of certain organic bases in aqueous solution. *Journal of the American Chemical Society*, 54, 3469-3485.
- HAMMETT, L. P. (1937) Effect of structure upon the reactions of organic compounds. Benzene derivatives. *Journal of the American Chemical Society*, 59, 96-103.
- HARNED, H. S. & OWEN, B. B. (1930) The thermodynamic properties of weak acids and bases in salt solutions, and an exact method of determining their dissociation constants. *Journal of the American Chemical Society*, 52, 5079-5091.
- HARNED, H. S. & ROBINSON, R. A. (1928) The ionic concentrations and activity coefficients of weak electrolytes in certain salt solutions. *Journal of the American Chemical Society*, 50, 3157-3178.
- HENDERSON, W. G., TAAGEPERA, M., HOLTZ, D., MCIVER, R. T., BEAUCHAMP, J. L. & TAFT, R. W. (1972) Methyl substituent effects in protonated aliphatic amines and their radical cations. *Journal of the American Chemical Society*, 94, 4728-4729.
- HINE, J. S. (1975) Equilibrium in hydrogen bonding. *Structural Effects On Equilibria In Organic Chemistry*. New York, John Wiley & Sons, Inc., 200.

- ISHIMITSU, T., HIROSE, S. & SAKURAI, H. (1979) Microscopic acid dissociation constants of 3,4-dihydroxyphenylbutyric acid and 3,4-dihydroxybenzoic acid. *Chemical & Pharmaceutical Bulletin*, 27, 247-51.
- KAPPE, T. & ARMSTRONG, M. D. (1965) Ultraviolet absorption spectra and apparent acidic dissociation constants of some phenolic amines. *Journal of Medicinal Chemistry*, 8, 368-74.
- KIEFER, E. F. (1972) Rapid, convenient preparative procedure for phenethylamines. *Journal of Medicinal Chemistry*, 15, 214.
- KIRKWOOD, J. G. & WESTHEIMER, F. H. (1938) The electrostatic influence of substituents on the dissociation constants of organic acids. I. *Journal of Chemical Physics*, 6, 506-512.
- LAMBERT, W. J., WRIGHT, L. A. & STEVENS, J. K. (1990) Development of a preformulation lipophilicity screen utilizing a C-18-derivatized polystyrene-divinylbenzene high-performance liquid chromatographic (HPLC) column. *Pharmaceutical Research*, 7, 577-86.
- LANGLOIS, M.-H., MONTAGUT, M., DUBOST, J.-P., GRELLET, J. & SAUX, M.-C. (2005) Protonation equilibrium and lipophilicity of moxifloxacin. *Journal of Pharmaceutical and Biomedical Analysis*, 37, 389-393.
- LAZARO, E., RAFOLS, C. & ROSES, M. (2005) Characterization of immobilized artificial membrane (IAM) and XTerra columns by means of chromatographic models. *Journal of Chromatography, A*, 1081, 163-73.
- MACCALLUM, J. L., BENNETT, W. F. & TIELEMAN, D. P. (2008) Distribution of amino acids in a lipid bilayer from computer simulations. *Biophysical Journal*, 94, 3393-404.
- MACK, F. & BOENISCH, H. (1979) Dissociation constants and lipophilicity of catecholamines and related compounds. *Naunyn-Schmiedeberg's Archives of Pharmacology*, 310, 1-9.

- MARTIN, R. B. (1971) Zwitterion formation upon deprotonation in L-3, 4-dihydroxyphenylalanine and other phenolic amines. *Journal of Physical Chemistry*, 75, 2657-61.
- MAYER, P. T., XIANG, T.-X., NIEMI, R. & ANDERSON, B. D. (2003) A hydrophobicity scale for the lipid bilayer barrier domain from peptide permeabilities: Nonadditivities in residue contributions. *Biochemistry*, 42, 1624-1636.
- MELANDRI, S. & MARIS, A. (2004) Intramolecular hydrogen bonds and conformational properties of biogenic amines: A free-jet microwave study of tyramine. *Physical Chemistry Chemical Physics*, 6, 2863-2866.
- MUNSON, M. S. B. (1965) Proton affinities and the methyl inductive effect. *Journal of the American Chemical Society*, 87, 2332-2336.
- N. GULYAEVA, A. Z. P. L. A. C. B. Z. (2003) pH dependence of the relative hydrophobicity and lipophilicity of amino acids and peptides measured by aqueous two-phase and octanol-buffer partitioning. *Journal of Peptide Research*, 61, 71-79.
- NAGY, P. I. & TAKACS-NOVAK, K. (2004) Tautomeric and conformational equilibria of biologically important (hydroxyphenyl)alkylamines in the gas phase and in aqueous solution. *Physical Chemistry Chemical Physics*, 6, 2838-2848.
- NOSZAL, B. & SZAKACS, Z. (2003) Microscopic protonation equilibria of oxidized glutathione. *Journal of Physical Chemistry B*, 107, 5074-5080.
- PEINHARDT, G. & WIESE, M. (2001) Microionization constants: novel approach for the determination of the zwitterionic equilibrium of hydroxyphenylalkylamines by photometric titration. *International Journal of Pharmaceutics*, 215, 83-89.
- PERRIN, D. D., DEMPSEY, B. & SERJEANT, E. P. (1981) *pKa Prediction For Organic Acids And Bases*, London ; New York, Chapman and Hall.



- PLATTS, J. A., ABRAHAM, M. H., BUTINA, D. & HERSEY, A. (2000) Estimation of molecular linear free energy relationship descriptors by a group contribution approach. 2. Prediction of partition coefficients. *Journal of Chemical Information and Computer Sciences*, 40, 71-80.
- RICHARDSON, P. R., BATES, S. P. & JONES, A. C. (2004) A molecular orbital study of the conformational properties of tyramine and phenethylamine. *Journal of Physical Chemistry A*, 108, 1233-1241.
- RIEGELMAN, S., STRAIT, L. A. & FISCHER, E. Z. (1962) Acid dissociation constants of phenylalkanolamines. *Journal of Pharmaceutical Sciences*, 51, 129-33.
- ROBERTSON, E. G., SIMONS, J. P. & MONS, M. (2001) Comment on "Structural and vibrational assignment of *p*-methoxyphenethylamine conformers". *Journal of Physical Chemistry A*, 105, 9990-9992.
- ROGERS, J. A. & DAVIS, S. S. (1980) Functional group contributions to the partitioning of phenols between liposomes and water. *Biochimica et Biophysica Acta*, 598, 392-404.
- RYTTING, J. H., ANDERSON, B. D. & HIGUCHI, T. (1978a) Vapor pressure studies of the self-association of alcohols in isooctane. 2. The effect of chain branching. *Journal of Physical Chemistry*, 82, 2240-5.
- RYTTING, J. H., HUSTON, L. P. & HIGUCHI, T. (1978b) Thermodynamic group contributions for hydroxyl, amino, and methylene groups. *Journal of Pharmaceutical Sciences*, 67, 615-8.
- S. H. YALKOWSKY, S. C. V. G. L. A. (1976) Solubility of nonelectrolytes in polar solvents IV: Nonpolar drugs in mixed solvents. *Journal of Pharmaceutical Sciences*, 65, 1488-1494.
- SZAKACS, Z., BENI, S., VARGA, Z., ORFI, L., KERI, G. & NOSZAL, B. (2005) Acid-base profiling of Imatinib (Gleevec) and its fragments. *Journal of Medicinal Chemistry*, 48, 249-255.

- TAFT, R. W., JR. (1953) The general nature of the proportionality of polar effects of substituent groups in organic chemistry. *Journal of the American Chemical Society*, 75, 4231-8.
- TAKACS-NOVAK, K., NOSZAL, B., HERMECZ, I., KERESZTURI, G., PODANYI, B. & SZASZ, G. (1990) Protonation equilibria of quinolone antibacterials. *Journal of Pharmaceutical Sciences*, 79, 1023-8.
- TEJWANI, R. W. & ANDERSON, B. D. (2004) Unpublished data.
- TEJWANI, R. W. & ANDERSON, B. D. (2008) Influence of intravesicular pH drift and membrane binding on the liposomal release of a model amine-containing permeant. *Journal of Pharmaceutical Sciences*, 97, 381-399.
- VALKO, K., DU, C. M., BEVAN, C. D., REYNOLDS, D. P. & ABRAHAM, M. H. (2000) Rapid-gradient HPLC method for measuring drug interactions with immobilized artificial membrane: comparison with other lipophilicity measures. *Journal of Pharmaceutical Sciences*, 89, 1085-96.
- VAN DE WATERBEEMD, H. & GIFFORD, E. (2003) ADMET in silico modelling: towards prediction paradise? *Nature Reviews*, 2, 192-204.
- WEHRY, E. L. & ROGERS, L. B. (1965) Application of linear free energy relations to electronically excited states of monosubstituted phenols. *Journal of the American Chemical Society*, 87, 4234-4238.
- WESTHEIMER, F. H. & KIRKWOOD, J. G. (1938) The electrostatic influence of substituents on the dissociation constants of organic acids. II. *Journal of Chemical Physics*, 6, 513-517.
- WIMLEY, W. C., CREAMER, T. P. & WHITE, S. H. (1996) Solvation energies of amino acid side chains and backbone in a family of host-guest pentapeptides. *Biochemistry*, 35, 5109-5124.

- WIMLEY, W. C. & WHITE, S. H. (1996) Experimentally determined hydrophobicity scale for proteins at membrane interfaces. *Nature Structural Biology*, 3, 842-848.
- XIANG, T.-X., XU, Y. H. & ANDERSON, B. D. (1998) The barrier domain for solute permeation varies with lipid bilayer phase structure. *Journal of Membrane Biology*, 165, 77-90.
- YAMAZAKI, F., FUJIKI, K. & MURATA, Y. (1965) The ionization constants of organic compounds. I. The microscopic ionization constants of tyrosine and related compounds. *Bulletin of the Chemical Society of Japan*, 38, 8-12.
- ZHANG, J., KLEINODER, T. & GASTEIGER, J. (2006) Prediction of pKa values for aliphatic carboxylic acids and alcohols with empirical atomic charge descriptors. *Journal of Chemical Information and Modeling*, 46, 2256-66.

## **CHAPTER FIVE: Partitioning of solute from water to various locations in the lipid bilayer: A comparison of results from the simulation and the experiment.**

### **Introduction**

As discussed in previous chapters, lipid bilayer membranes consist of multiple regions of widely varying solvation properties. Therefore it is possible that one region preferentially retains a given solute with a high partition coefficient while another acts as a barrier to its transport due to a very low partition coefficient. Since the direct measurement of solute concentration in each of these regions is experimentally difficult, if not impossible, surrogate measurements must be employed similar to those presented in chapter four. While these measurements may account for the observed permeability and binding, additional insight is needed to more readily predict solute transport and retention in the bilayers. Additional insight may be obtained from molecular dynamics simulations that account for the movements and interactions of all atoms in a given system. For example, MD simulations enable visualization of specific (e.g. hydrogen bonding) interactions that contribute to the variation in the solvation environment in a lipid bilayer membrane.

Over the past two decades, atomic-level MD simulations have been used to understand the structure and dynamics of lipid bilayers, and have also been used to probe partitioning and permeation of small molecules (Alper and Stouch, 1995, Bassolino-Klimas et al., 1995, Stouch, 2000, Stouch, 1997, Stouch et al., 1995a, Stouch and Bassolino, 1996, Stouch et al., 1995b, Stouch et al., 1997, Stouch et al., 1996, Xiang and Anderson, 1999, Xiang and Anderson, 2002, Xiang and Anderson, 1994a). A wide variety of solutes have been studied for their interactions with different kinds of lipid bilayer membranes. These solutes include water and ammonia (Marrink and Berendsen, 1994, Shinoda et al., 2004), anesthetics (Pohorille et al., 1996, Tu et al., 1998), CNS agents (Ulander and Haymet, 2003), cholesterol (Pitman et al., 2004), environmental pollutants (Mukhopadhyay et al., 2004), and beta adrenergic blockers (Bemporad et al., 2005).

Questions related to the transport and partitioning of solutes in lipid bilayer membranes that may be accessible by use of MD simulations include: 1) where are the regions of the lowest and the highest partition coefficients?; and 2) what are the energies of transfer of the solutes into these locations? Due to limitations of computational power, earlier studies utilized the technique of thermodynamic integration to compute functional group contributions to the apparent free energy of transfer from water to a single location in the bilayer. More recent studies have however afforded sufficient lengths of simulations to generate free energy profiles across the entire depth of the bilayer. Recent simulations have reported the solute distribution as a function of depth within the lipid bilayer for hexane (MacCallum and Tieleman, 2006), indole (Norman and Nymeyer, 2006), cholesterol (Pandit et al., 2008, Bennett et al., 2009), adamantane derivatives (Chew et al., 2008, Li et al., 2008), and amino acid residues (MacCallum et al., 2007, Johansson and Lindahl, 2008, MacCallum et al., 2008).

In these reports, the shapes of free energy profiles (or solute distribution profiles) vary as vastly as the solutes themselves. These solutes can be classified into six groups based on their chemical nature and size relative to the lipid bilayer thickness: polar small and large, non-polar small and large, dipolar small, and amphiphilic. For the most part, very small polar solutes (or “point solutes”) tend to show profiles consistent with the 4-region model of the lipid bilayer described by Marrink and Berendsen (Marrink and Berendsen, 1994). From these profiles, it has been suggested that polar solutes (e.g. water, methanol, acetic acid) partition least favorably in the hydrocarbon region whereas non-polar solutes (e.g. ethane, benzene, methyl acetate) have their lowest partition coefficients at the interface (Bemporad et al., 2004). As the size of the solute increases, the pre-defined regions tend to smear and more specifics need to be considered in order to interpret the free energy profiles. For example, profiles of hexane (MacCallum and Tieleman, 2006) and ethane (Bemporad et al., 2004) are qualitatively comparable but the middle region (near the center of bilayer) of the profile for hexane is about twice as broad as that of the profile for ethane.

Dipolar and amphiphilic solutes on the other hand exhibit relatively more complex free energy profiles. For example  $\text{CH}_3\text{F}$ ,  $\text{CH}_2\text{F}_2$ , and  $\text{CHF}_3$  show preferred

distribution to the interfacial region whereas CH<sub>4</sub> and CF<sub>4</sub> show preferred distribution to the hydrocarbon region (Pohorille and Wilson, 1996) similar to ethane the profile discussed above. Similar observations of interfacial preference have also been reported in the simulations of relatively larger amphiphilic solutes such as cholesterol (Pasenkiewicz-Gierula et al., 2000, Pandit et al., 2008), pentachlorophenol (Mukhopadhyay et al., 2004), indole (Norman and Nymeyer, 2006), and phenol (Sengupta et al., 2008). Depending on their structure, amphiphiles have shown vastly different partition coefficients in different regions of the lipid bilayer membranes. Such complex profiles are likely to be observed more frequently for drug molecules that tend to have multiple polar functional groups.

Since most drug molecules contain hydrophobic as well as hydrophilic groups, a certain degree of amphiphilicity is always expected and can lead to interfacial binding and complicated distribution profiles. Consequently, the solutes chosen for this study conform to the following criteria: 1) they contain functional groups that are common to many drug molecules; 2) their properties (e.g. functional group contributions) could be determined accurately by experiment; and 3) they are relatively small in size to allow an MD simulation of reasonable length with the computational resources available.

An ongoing objective among the simulation studies published in the literature has been to compare the results of simulations with those from experiments. This validation is an essential step before the additional molecular level information from a given simulation study should be relied upon. The reasonable grounds for comparison of the quantitative results from MD simulations to those from the experiment have been discussed to a limited extent in the literature. Since bulk/solvent water partition coefficients must be used instead of direct measurements of partition coefficients into the various regions of the lipid bilayer, the free energies of solute transfer obtained experimentally are not directly comparable to those obtained in an MD simulation. One could make assumptions about relative volumes of the regions of the bilayer and subsequently obtain the corrected “regional” partition coefficients from the liposome/water partition coefficients. The assumptions made regarding the location of the boundary between adjacent regions would severely limit the utility of such an

approach. In order to avoid such assumptions, and to prevent the impact of choice of standard states in each case, it is best to compare the functional group contributions instead of the solute transfer free energies. Conforming to the discussion by Ben-Naim (Ben-Naim, 1978), molar partition coefficients have been used in this work to calculate the functional group contributions to the apparent free energy of transfer; the quantities obtained from the MD simulation are also calculated to conform to these units.

Comparison of MD simulation results to experimental results has had mixed success in previously reported studies. For example, recent simulations employing amino acid side chains as solutes where the H<sub>2</sub>N-CH-COOH group (the glycine portion) was replaced by a hydrogen atom allowed MacCallum et al (MacCallum et al., 2008, MacCallum et al., 2007) to compute the free energy of transfer of hydroxyl and amino groups from water to the center of a liquid crystalline phase bilayer to be comparable (5.5 and 5.3 kcal per mole, respectively), which is close to the experimentally measured values (5.6 and 5.0 kcal per mole, respectively) determined by Rytting et al (Rytting et al., 1978) for transfer of alkanes, alkylamines, and alkanols from water to heptane. However, simulations conducted by a different laboratory (Bemporad et al., 2004) found that the free energy of transfer of methylamine from water to the center of the bilayer is less than that of methanol by 3.4 kcal per mole. While the first example establishes the free energy of transfer of amino and hydroxyl groups to be about the same, the second one shows that they differ by a significant amount.

In this study, MD simulations were conducted for some of the solutes from chapter four in order to determine the transfer free energy profiles as a function of depth in the bilayer. This allowed the determination of location of the barrier (low partition coefficient) region and the preferred binding region (high partition coefficient) for each solute. Subsequently, values for the free energy of transfer from water to hydrocarbon and from water to the preferred binding region were compared against experimentally measured values for hydroxyl and amino groups from chapter four. The validation of lipid bilayer properties and the merits of the methods of calculating free energy profiles from simulation run data are also reviewed. The intermolecular interactions between the

solutes and the bilayer lipid molecules and their impact on the shapes of the free energy profiles are described in chapter six.

## **Methods and Theoretical**

### ***The systems for MD simulation***

Four molecular systems were studied: a DOPC bilayer devoid of solutes and three bilayers containing tyramine, phenethylamine, or 4-ethylphenol. The chemical structures of the three solutes and DOPC are shown in Figures 5-1 and 5-2, respectively. Each fully hydrated system contained all atoms of 72 DOPC molecules and over 3000 water molecules adding up to over 21000 atoms (Figure 5-3). Three dimensional periodic boundary conditions were applied to the box that was 50.9 angstroms long in the two dimensions of the plane of the bilayer and 83.5 angstroms along the bilayer normal. Initially constructed with all lipid chains in their *trans* conformation, the lipid bilayer was simulated at 600 degrees C to allow for rapid approach to conformational equilibrium. Convergence of the bilayer properties such as order parameters and average number of lipid chain torsions in the *gauche* conformation were monitored. Once an equilibrium conformational structure was obtained, the temperature was reduced and subsequently the structure was allowed to equilibrate for approximately 2 nanoseconds. No data from these runs were used for the calculation of the results, and only the atom coordinates were used as a starting point for further simulation work.

Among the systems containing the solutes, the system with tyramine was constructed first. In order to achieve sufficient sampling while keeping the simulation run to a reasonable length, several copies of solutes were introduced into the lipid bilayer and surrounding water. The impact of solute molecules on the lipid bilayer was assessed by comparing several properties of the lipid bilayer before and after inclusion of the solute. No impact was found with nineteen copies of the solute included. Therefore nineteen tyramine molecules were inserted at various locations in the lipid bilayer and the resulting structure was energy minimized to remove bad contacts. The method was repeated for the 4-ethylphenol and phenylethylamine simulations by starting from one of the tyramine



configurations and deleting appropriate atoms from the solutes and subsequently minimizing the energy.

### ***Force field and the simulation method***

A modified version of the CVFF force field described previously (Alper and Stouch, 1995, Bassolino-Klimas et al., 1993) was employed for the non-bonded interactions of the lipids and solutes. All 1,4 interactions were scaled by a factor of 0.6 which has previously been found to produce good agreement with experiment (Lau et al., 1994). A flexible 3 center SPC-like model for water was used which has been found to produce properties that are in good agreement with experimental as well as with the computational properties calculated using other water potentials. Partial atomic charges needed for the solute molecules were computed using Jaguar 6.0 (Schrodinger, 1991-2000) by employing an HF-SCF type of calculation carried out using 6-31G\* basis set. A single point calculation was carried out for a geometry optimized structure that allowed calculation of the molecular electrostatic potentials (ESPs). The ESP near the van der Waals surface was subsequently used to derive point charges at atomic centers.

The MD simulations were run using a massively parallel simulator, Lammmps 2001 (Plimpton et al., 2001, Plimpton, 1995) operated on an SGI Origin 3000 computer where the number of CPUs varied from 4 to 16 depending on availability. A time step of 1 femtosecond was used, without constraints on any bond lengths, within the velocity Verlet algorithm to integrate Newton's equations of motion. For the NVT ensemble, the Nose-Hoover thermostat implemented in Lammmps 2001 was used to control the temperature of the system at 298 K where the DOPC bilayer is in a liquid crystalline state. The electrostatics were computed using the PPPM method (Luty et al., 1994) with a cutoff of 10 angstroms.

For each of the above mentioned four systems several parallel simulations were run in order to enhance sampling. In the three systems containing solutes, multiple copies of the solute molecules were used in order to provide coverage along the depth of the bilayer and adequate sampling within a reasonable computational time. Nineteen copies of the respective solute molecule were used and were placed inside and around the bilayer such as

to avoid interactions between solute molecules to ensure that the simulation mimicked a dilute system comparable to that of the experiment<sup>‡</sup>. In total over two hundred nanoseconds were simulated, providing almost four microseconds of sampling of the solute trajectories.

### *Constraints and data collection*

In all of the above systems, unrestrained solute molecules would tend to concentrate at low energy locations within the bilayer. This would prevent study of the locations where energy barriers exist, subsequently preventing the derivation of corresponding partitioning probabilities and free energies. In order to provide coverage of sampling across the span of the bilayer, an umbrella sampling technique (Torrie and Valleau, 1977a, Torrie and Valleau, 1977b, Rebertus et al., 1979, Northrup et al., 1982) was employed to constrain the solute molecules at various locations. A quadratic potential was applied to the atom near the center of mass of each solute molecule (aromatic carbon attached to the ethyl group) during the MD simulations to impose a “restoring” force perpendicular to the bilayer plane to maintain it in a particular neighborhood transverse to the plane. Lateral movement and rotation of the solutes were not restricted. The simulation data were recorded every picosecond during the data acquisition segments of the simulation runs where the initial two nanoseconds of the data were discarded to allow the system to equilibrate. These data were subsequently used as described below to calculate the free energy profiles for each solute. Since the simulation box had sufficient space for the nineteen copies of the solute to be present, it was only rarely that the copies of solute molecules approached each other. Any configurations where any atoms of two copies of solutes reached within 5 angstroms of each other were rejected to prevent possible effects of inter-solute interactions on the observed profiles. Since the inter-solute interactions did not occur due to this arrangement, the simulation can be considered similar to the experiment where a low concentration of the solutes was employed.

---

<sup>‡</sup> While nineteen copies of solute were used with 72 copies of DOPC, only nine were inside the lipid bilayer. This results in a tyramine concentration of approximately 0.16 moles per liter in the bilayer. The concentration of DOPC and tyramine in the corresponding experimental studies in Chapter Three and Chapter Four were 0.015 moles and 0.01 moles per liter of water, giving an estimated concentration of tyramine of 0.03 moles per liter in the lipid bilayer. While this concentration differential is significant, the constraints employed in the simulation ensured that the solute copies were well separated thereby simulating the dilute conditions of the experiment.

*A review of post-processing methods typically employed to obtain free energy profiles from MD simulation data*

The data obtained from the MD simulations includes the atom positions, forces, and velocities as a function of time. Since one of the objectives of the simulations is to obtain the position dependent partition coefficients for the solutes, free energy profiles were computed using the data. The methods to compute the free energy difference between two states of a given system include direct counting, integration methods, perturbation approaches, and umbrella sampling (Wilfred F. van Gunsteren, 2002). The following section summarizes a subset of the above techniques that have been applied to the specific case of calculating free energy profiles across a reaction coordinate such as that for transport across a lipid bilayer system.

1. Population density analysis after an unconstrained MD simulation

Since MD simulations allow all the particles in a system to undergo random thermal motions, the general tendency of the system is towards the lowest energy configurations. That is, during an MD simulation (on the order of picoseconds to microseconds) most observed states of the system are those with low energy while high energy states are relatively rare. The information about the relative occurrence of various states along the reaction coordinate can then be used to obtain free energy profile. If  $p(z)$  is the probability distribution of various states along the reaction coordinate  $z$ , the corresponding free energy profile along the reaction coordinate is given as

$$\Delta G(z) = -k_B T \ln(p(z)) + C \quad (5-1)$$

where  $k_B$  is the Boltzmann constant,  $T$  is absolute temperature,  $\Delta G(z)$  is the reversible work required to move the system from the reference state to a state corresponding to a point  $z$  on the reaction coordinate, and  $C$  is a constant related to the choice of the reference state. For transport across the lipid bilayer membrane, the reaction coordinate is along the bilayer normal and the probability distribution of the solutes along the bilayer depth resulting from random thermal motions can allow one to compute the free energy profile using the above equation.

This method is particularly useful for very small solutes and has been used to define the distribution of water across a lipid bilayer by Marrink and Berendsen (Marrink and Berendsen, 1994). The simulation is started with a large number of water molecules uniformly spread across the depth of the lipid bilayer. As simulation progresses, the solute molecules diffuse away from low partition coefficient locations and concentrate in the high partition coefficient locations. The resulting frequency distribution is then used to compute the relative free energy profile. It was found in the case of water that the full energy profile could not be obtained by this method due to very low occurrences at the center of the bilayer leading to a very large uncertainty in this region.

## 2. Population density analysis after a constrained MD simulation

Due to random thermal motion, an unconstrained solute molecule in the bilayer will rapidly translate to a lowest energy location (as discussed above, Equation 5-1) preventing study of the locations within the bilayer where energy barriers exist. While a very long simulation will make it possible to sample these high energy locations, the typical time span of an MD simulation study (picoseconds to microseconds) may not be sufficient to allow gathering of adequate statistics. This is typically overcome by applying a biasing potential during an MD simulation run so that the configurations associated with the high energy locations along the reaction coordinate are *forced* to occur more frequently. This biasing technique was referred to as “umbrella sampling” by Torrie and Valleau (Torrie and Valleau, 1977b, Torrie and Valleau, 1977a). Since the energy required for stabilizing each state along the reaction coordinate is different, the biasing potentials,  $U(z)$ , are separately chosen (based on trial and error) for each “window” along the reaction coordinate. Typically a frequency histogram,  $p^*(z)$ , of the biased occurrence of the states along the reaction coordinate is obtained, and the free energy profile in each window,  $i$ , is recovered as

$$\Delta G_i(z) = -k_B T \ln(p_i^*(z)) + C_i + U_i(z) \quad (5-2)$$

A careful choice of “windows” along the reaction coordinate that typically overlap, allows one to determine the offset constants,  $C_i$ , by requiring that the free energy

profile in adjacent windows be continuous. The offset  $C_i$  for the first window is set such that  $G_i(z)$  is zero. In the lipid bilayer context it can be set to correspond with the solute in the bulk water or at the center of the bilayer. While application of a fixed biasing potential for each “window” requires one to search for an appropriate value for  $U_i(z)$  by trial and error, the choice of a quadratic potential (Pangali et al., 1979) around a desired location ( $z_i$ ) such as the one shown below decreases this effort considerably:

$$U_i(z) = k_i(z - z_{0i})^2 \quad (5-3)$$

During the simulation run, this arrangement allows the applied restoring force to increase in magnitude with increasing distance from the desired position (corresponding to  $z_0$ ). This allows a tuning of the magnitude of the applied constraint force in response to the environment without manual intervention. Additionally, instead of holding a single location on the coordinate, it allows the sampling of other nearby locations thus generating a contiguous profile. The effect of a quadratic biasing potential on a simulation is illustrated in the set of plots in Figure 5-4 where the inherent free energy profiles within the window is either constant or linearly increases with  $z$ . The probability density and free energy profiles for each of the two systems with and without quadratic constraint are also shown.

While the use of a quadratic potential decreases the effort needed for sampling, some *a priori* knowledge of the system and the reaction coordinate being studied is still required. A modification of this approach, called the weighted histogram analysis method (WHAM) is employed for exploring relatively more complex reaction coordinates. In this technique, the population density is analyzed as the simulation progresses to update the umbrella potential for subsequent segments of the simulation (Bartels and Karplus, 1997, Bartels and Karplus, 1998). This technique also referred to as adaptive umbrella sampling, aids in obtaining a more uniform sampling of the states than what would be obtainable otherwise. This method is particularly useful in the case of multidimensional reaction coordinates, such as those exploring multiple dihedrals of a molecule simultaneously.

### 3. Force integration after a constrained MD simulation

In this method, instead of applying a fixed constraint to a full simulation or a segment thereof, the applied constraining potential (or corresponding force) is changed at each time step of the simulation in response to the forces calculated at the penultimate step. This method, employed previously for water transport across the bilayer (Marrink and Berendsen, 1994), relies on the observed forces during a given simulation time step to determine the magnitude of the biasing potential to be applied during the subsequent time step. In the lipid bilayer context, in its simplest form, one can program the MD simulator to ignore the forces acting on a given solute molecule and record them at every time step instead of computing a displacement resulting from such a force. This allows the solute to stay in the desired location and act as a force measurement gauge. After sufficient observations at a given location have been obtained, the solute is moved to another location and the procedure is repeated. The accumulated information on the forces is then used to obtain the free energy profile at a given location as follows

$$\Delta G_z = -N_{Av} \int_0^z \langle F(z) \rangle dz \quad (5-4)$$

where  $N_{Av}$  is Avogadro's number,  $F(z)$  is the force acting on the solute at location  $z$ , and the angle brackets indicate the ensemble average over all configurations. The integral is started from 0 such that  $z=0$  is a chosen point of reference, which can be bulk water or the center of the bilayer.

#### ***Post-processing of the MD simulation data in the current study***

The current study tested both the population density method as well as the force integration method for the calculation of the free energy profiles for tyramine, and only the former was used for 4-ethylphenol and phenylethylamine. Quadratic constraints similar to Equation 5-3 were used in all three cases.

### 1. Population density method

Since the reaction coordinate of interest is the bilayer normal and the locations are interpreted relative to the central plane of the bilayer, the location of the central plane of the bilayer was determined at each time step. The location of the central plane of the bilayer was calculated by taking the average of the locations of the phosphorous atoms of the lipid molecules in each of the two monolayers. The location of each solute (the atom closest to the center of mass) at each time step was then “shifted” from the box coordinates to the relative coordinates to represent the distance of the solute from this central plane. The resulting location information was then used to generate the population density along the bilayer normal ( $p_i(z)$ ) that was used in Equations 5-2 and 5-3 to calculate a free energy profile for a “window” along the reaction coordinate. The offset constant,  $C_i$  for the first window was set to zero (using water as a point of reference) and the offset constants for the rest of the windows were then computed by requiring the overlapping portions of the windows to have the same free energy values. The fragments of profiles obtained from these windows were then joined together using the offset constants to form the continuous profile.

### 2. Force integration method

This method used a combined approach that utilizes the quadratic constraint described in method 2 above, applied to several copies of the solute simultaneously in the bilayer system. The post-processing of data was similar to method 3 above with some modifications. Since the reaction coordinate is along the bilayer normal, only the component of the force along this direction was used in all the calculations. The net displacement force on each solute molecule was determined by adding together the forces on each of the constituent atoms as determined at each time step by the MD simulator. The component of this force along the bilayer normal was then corrected for the applied constraint force (in the same direction) by subtraction. The resulting quantity was taken as the force exerted along the normal by the local chemical environment on the solute and was recorded as a function of time.

The location of the central plane of the bilayer was calculated as described above. The location of each solute at each time step in terms of the distance from this central plane was also calculated. The resulting location information was also stored as a function of simulation time along with the forces. For each 0.3 angstrom slice of the simulation box, the force exerted on the solute across the entire simulation length was averaged. The average forces thus obtained were used in Equation 5-4 above to obtain the free energy profile.

## **Results and Discussion**

### ***The structure of the lipid bilayer membrane in the MD simulation***

The structure and dynamical properties of a variety of lipid bilayer membranes have been reproduced successfully in several MD simulations conducted previously (Stouch et al., 1991, Stouch, 2000, Stouch et al., 1997, Stouch, 1997, Stouch et al., 1996, Stouch and Bassolino, 1996, Stouch et al., 1995b, Stouch et al., 1995a, Bassolino-Klimas et al., 1995, Alper and Stouch, 1995, Bemporad et al., 2004, Bemporad et al., 2005, Xiang and Anderson, 2006, Xiang and Anderson, 2002). In order to verify the current construct and the impact of the inclusion of multiple copies of the solutes, the bilayer properties were calculated from the MD simulation and verified against the experimental results. These properties include the distributions of various atom types and their distance from the central plane of the bilayer, the thickness of the bilayer, order parameters, the fraction of lipid chain torsions in the *gauche* conformation, and the angle made by the phosphocholine chain with the plane of the bilayer.

The distributions of various atoms and functional groups along the depth of the DOPC lipid bilayer are shown in Figure 5-5. The number density of water molecules is constant in the bulk water region that is located at a distance greater than 30 angstroms from the center of the bilayer. Starting at approximately 30 angstroms from the center of the bilayer, the number density decreases to almost zero over the next 20 angstroms. This profile is consistent with that previously observed for MD simulations of DOPC bilayers (Chiu et al., 1999b, Mashl et al., 2001) and other phosphocholine based bilayers (Bemporad et al., 2005); and with the experimental expectation of greater than 30 water



molecules per DOPC molecule (Nagle and Tristram-Nagle, 2000) to maintain a fully hydrated state.

Experimental measurements pertaining to the lipid bilayer dimensions are typically available from lipid crystallography. Unlike solid state crystallography, the atoms in the liquid crystalline state lipid bilayers are present as broad statistical distributions due to their dynamic nature (Nagle and Tristram-Nagle, 2000). As a result of this dynamic distribution of atom locations, X-ray diffraction data yield electron density profiles that only provide the thickness in terms of peak locations of phosphate atoms. Such experiments by Nagle and coworkers (Nagle and Tristram-Nagle, 2000, Tristram-Nagle et al., 1998) show that a fully hydrated DOPC bilayer, such as the one simulated here has a peak to peak distance of about 36.9 Angstroms. The distance between the peaks of phosphorous atoms on the two sides of the bilayer in the current simulation is approximately 37 angstroms (Figure 5-5) and is not altered by inclusion of the solute molecules. Additionally, it fluctuates near this value during the course of the simulation as shown in Figure 5-6.

The lipid chains, sometimes referred to as tails, are known to exhibit relatively greater mobility compared to the head groups, which can influence the barrier properties of the lipid bilayer. The dynamics of this mobility are experimentally measured using the deuterium order parameters ( $S_{CD}$ , measured using NMR spectroscopy) and the average number of alkyl chain torsions in the *gauche* conformation (using vibrational spectroscopy). As one moves along the bilayer normal from the head group region towards the center of the bilayer, the disorder in the alkyl chains is expected to increase and is measured using the order parameter. The order parameters are calculated from the snapshots saved during MD simulation using the following equation (Pastor et al., 2002)

$$S_{CD} = \frac{3\langle \cos^2 \phi \rangle - 1}{2} \quad (5-5)$$

where the angle bracket indicates the average calculated over the observed configurations and  $\phi$  is the angle between a given carbon-hydrogen bond (in the case of NMR experiments, carbon-deuterium bond) and the bilayer normal. The average profile of the

order parameters for each of two chains of the DOPC molecules of the bilayer in this study is shown in Figure 5-7. The rapid decrease in the calculated order parameters near the tenth carbon atom is indicative of the *cis*-double bond at this location and is characteristic of the oleoyl chains and has also been shown in the experimental measurements (Seelig and Waespe-Sarcevic, 1978) of the order parameter. The profile of  $S_{CD}$  values observed across the span of the bilayer is also consistent with the experimental measurements (Seelig and Waespe-Sarcevic, 1978) and those calculated in recently reported MD simulations (Chiu et al., 1999a, Mashl et al., 2001), both of which are shown in Figure 5-7. The difference in the chain order between the regions on the two sides of the double bond in the DOPC bilayer conforms with the description of the last two regions of the four region model of the lipid bilayer proposed by Marrink and Berendsen (Marrink and Berendsen, 1994) comprised of: 1) A low head group density or perturbed water region; 2) A region of high head group density; 3) A region of high tail density; and 4) A region of low tail density near the center of the bilayer.

In the case of the POPC bilayer (Pandit et al., 2007, Pandit et al., 2008), inclusion of 20 to 33 mole percent of cholesterol and ceramide leads to an increase in the order in the bilayer, with the former being more effective at inducing this change. Since cholesterol is located close to the headgroups (Bennett et al., 2009) in the lipid bilayers, the increase in order is attributed to the changes in the headgroup structure. An increase in density of the system has also been observed by these studies suggesting the potential effect through reduction of net free volume necessary for the mobility thereby increasing the order parameters. In this study, nineteen copies of a much smaller solute were spread throughout the water and the bilayer. This leads to a much lower concentration in the headgroups and has a much lower impact on the density. Therefore no significant effect on the order parameters was observed on inclusion of solutes in the lipid bilayer, as shown in Figure 5-8.

The torsions along the lipid chains in the hydrocarbon region frequently change between the *trans* and *gauche* arrangements due to random thermal fluctuations. The proportion of these is generally taken as an indicator of the overall order of the lipid bilayer, and is related to the choice of the area per headgroup in the MD simulations

(Anezo et al., 2003). Using calculations (Holler and Callis, 1989) based on Florey's rotational isomeric state model for chain molecules it has been shown that a normal alkane would have 36% of all bonds in the *gauche* conformation. For sodium dodecyl sulfate micelles, it was shown that about 28% of the bonds in the alkyl chains are in the *gauche* conformation (Haile and O'Connell, 1984, Woods et al., 1986, Holler and Callis, 1989) suggesting that the micelles are slightly more ordered than an isotropic liquid such as an alkane. A fraction of about 30% was calculated during MD simulations by Chiu et al (Chiu et al., 1999b) for both chains of a DOPC bilayer, consistent with approximately 3.5 to 4 *gauche* bonds per chain observed in the current study. As shown in Figure 5-9, the number of torsions in the *gauche* conformation fluctuates around this value during the course of the simulation and is minimally altered by inclusion of multiple copies of solute into the bilayer.

Another measure of the lipid bilayer structure in the head groups is the calculated average of the angle of P-N vector with the plane of the lipid bilayer. Scherer et al (Scherer and Seelig, 1989) pointed out that the  $\text{P-N}^+$  dipole lies almost parallel to the plane of the membrane and that several NMR measurements have shown that the orientation of the choline group is however not consistent. This inconsistency may be because the choline nitrogen atoms are distributed in a bimodal fashion around the phosphorous atom distribution (Figure 5-5), with a slight bias towards the water side. During the simulations conducted in this study, the average angle made by the P→N vectors with the bilayer normal as a function of simulation time (Figure 5-10) suggests that on an average, the choline groups point outwards by about 10 to 15 degrees, similar to the prior studies conducted with phosphocholine bilayers (Xiang and Anderson, 2002).

### ***Convergence of the MD simulations and the comparison of post-processing methods***

#### ***1. Convergence of the simulation and the criteria for the same***

An important part of any method of computing a free energy profile is the assurance that an adequate number of observations were obtained at all parts of the reaction coordinate, and that any other factors affecting the free energy had reached

equilibrium. Since results for this study have been derived from the trajectories of multiple copies of the solute molecules, multiple observations were obtained simultaneously from each “snapshot” of the simulation. These snapshots, referred to as configurations, were recorded at periodic intervals as described in the methods section. Since nineteen copies of solute molecules were used in each simulation, a maximum of nineteen observations were derived from each configuration. A histogram for the number of times a solute copy was observed in each 0.3 angstrom slice of the simulation box was constructed to visualize the extent of coverage obtained during the simulation. This histogram of the number of observations over approximately a 1.5 ms long trajectory as a function of the location along the bilayer normal is shown in Figure 5-11. The total available observations in the vicinity of headgroups and the center of the bilayer are much lower than the other locations despite the use of quadratic constraints on the solutes. Generally, the peaks and valleys in this graph are insignificant as long as an *adequate number* of observations is available in each slice. The number of observations decreases at approximately 35 angstroms from the center of bilayer because no solute copies were positioned near the edges of the simulation box to avoid *wrapping* of atoms between the opposite faces of the unit cell employed to implement the 3-dimensional periodic boundary conditions.

What constitutes an *adequate number* of observations is not known *a priori* without running a simulation because it depends on several factors of the system. While the reaction-coordinate of interest in a lipid bilayer-solute system is the distance along the depth of the bilayer, there can be other independent variables of importance. Some of the obvious ones are the solute orientation, any conformational relaxations in the solute molecule itself, or intermolecular effects such as involvement of water molecules near the interface. Adequate sampling of all effects must be ensured for accuracy. While one could potentially attempt a comprehensive, yet daunting task of obtaining a free energy profile as a function of multiple variables, not all information generated may be of interest in a given situation. In such cases, as in the theory of chemical kinetics (Connors, 1990), the minimum energy path on the hypersurface can be taken as the resulting coordinate. In the illustration of solute orientation as a second variable, the MD simulation must be run for a sufficient time such that the solute at all locations along the

bilayer depth has had sufficient time to reach its equilibrium orientation. As a result, it is not the energetics of all the orientations, but the knowledge of the equilibrium or preferred orientation at each location on the coordinate that may be most instructive.

While not all other variables affecting the free energy can be known, one must still define the criteria for reaching such equilibrium in the MD simulation study such that a “minimum path” is ensured for the chosen reaction coordinate. The choice of such convergence criteria have not consistently been discussed in the MD simulation studies published in the literature.

Berkowitz and coworkers (Bhide and Berkowitz, 2006) found that the decay time for the reorientation correlation functions for water molecules in some regions of the bilayer can be from several tens of picoseconds to hundreds of picoseconds in the MD simulations of the DOPC bilayer. The reorientation correlation times for benzene in MD simulations of a DMPC bilayer were on the order of 25 ps (Bassolino-Klimas et al., 1993), and approximately 100 ps in the ordered chain region of the DPPC bilayer simulated at 50 °C (Bemporad et al., 2005). The reorientation times increase significantly as the solute size increases. For example, in the case of beta blockers in a DPPC bilayer at 50 °C, Bemporad et al (Bemporad et al., 2005) found that the individual flips of the solutes could be separated by nanoseconds. Given these facts, and the significant variation of the reorientation times in different regions of the bilayer for the same solute, it appears that the minimal simulation time needed for convergence of mid sized solutes in this study, may be up to tens of nanoseconds.

As a general rule, the convergence criteria for the simulation are established based on the achievement of self consistency. That is, the simulation is terminated when each additional segment of simulation run produces no further change in the existing result or no further improvement in the standard error of the estimate. While there is no established precedent in the literature, one conceivable method would be to plot a chosen property of interest and the standard error as a function of simulation time. In the initial segment of the simulation run, when the number of observations is *inadequate*, one obtains a significant variation in this property and a relatively large error. As the

configuration space has been sampled over the simulation run time, the estimate of this property becomes more robust and progressively a stage is reached where additional data no longer improve the estimate or reduce the error. This technique is akin to the spectroscopic measurements where the spectra are repeatedly acquired until the signal to noise ratio reaches a point of diminishing returns.

For illustration, a convergence plot is shown in Figure 5-12 where free energy of transfer of phenethylamine from water to the preferred binding region of the bilayer is plotted as a function of MD simulation time. In the first few nanoseconds of the simulation, the free energy estimate changes significantly and shows a large standard error. As the simulation progresses, the estimate becomes more consistent and the relative error decreases. After approximately 25-30 nanoseconds of simulation run no additional improvement in the standard error is seen with additional data. It is apparent in the initial part of the plot (0 to 10 nanoseconds) where there is significant error in the estimated value, illustrating the disadvantage of a shorter simulation time.

To this end, if a simulation were to be conducted with multiple starting points, it may be worthwhile to have fewer longer simulations than to have numerous small simulations if certain processes in the system are expected to converge relatively slowly. Further, for a large solute in a lipid bilayer, the starting points for such simulations are better based on the orientations of solute molecules (Bemporad et al., 2005) rather than on the conformers of the solute molecules (Johansson and Lindahl, 2008). This is because the conformations, like the *gauche-trans* transformations of the lipid chains can interconvert much more rapidly than the solute orientations can. The specifics of each system however may differ and may affect the simulation strategy.

## 2. Free energy profile based on the population density method vs. that based on the force integration method

The free energy profile of tyramine calculated using the population density method is shown in Figure 5-13. It was found that despite using greater than 1.5 ms of total trajectory data, the consistency of the profile with the experiment remains questionable. The free energy of transfer of tyramine from water to the hydrocarbon

region of the bilayer is less than zero, which is inconsistent with that observed experimentally ( $>0$ ). This is likely due to the fact that the population density method utilizes only a portion of information available at each time step of the simulation, which is only the location of the solute. The magnitude of the constraint force applied at each time step can not be removed on a stepwise basis; instead it is only subtracted *after* the solute location data have been accumulated over the entire simulation and have been subjected to two additional manipulations: 1) classification into bilayer slices to generate histograms; and 2) a logarithmic transform to convert the histograms to an energy scale (Equation 5-2). As a result of this indirect method of removal of the constraint force, there is significant accumulation of errors and a potential for inaccuracy.

In contrast to this, the force averaging method utilizes more information available at each time step (forces and solute locations). Further, the exact constraint force is removed at the same time step that it was applied in; allowing accumulation of statistics on the net force exerted by the environment on the solute. This facilitates accurate “book keeping” of the quantities in the simulation and therefore more precise results are encountered. This can be seen from the free energy profile of tyramine in Figure 5-14, where the transfer free energy from water to the hydrocarbon (barrier) region is  $>0$  as expected from the experimental measurements.

### ***Partition coefficient as a function of location in the lipid bilayer***

#### ***1. A review of the profiles in the literature***

The lipid bilayer membrane presents an interesting case of anisotropy: it is heterogeneous in one dimension and almost homogeneous in the other two. During simulation of water transport across the DPPC membrane, Marrink and Berendsen (Marrink and Berendsen, 1994) proposed that the heterogeneity of the bilayer can be represented by four distinct regions starting with bulk water going inwards: low and high head group density, high and low tail density. Here the former two have a relatively high dielectric constant, and the latter two have low dielectric constants. Due to distinct differences in polarity, the relative solubility of a given solute and the partition coefficient vary along the depth of the lipid bilayer membrane. Inspired by this and other

suggestions (Stern and Feller, 2003) of the lipid bilayer heterogeneity, models of the lipid bilayer other than those employed in the MD simulations have also been explored where each region is taken as a continuum solvent having a fixed dielectric constant (Sengupta et al., 2008). While these models provide a reasonable estimate of partition coefficient in a given layer, they have been criticized for their lack of detail in failing to account for chain ordering and fluidity as well as for the involvement of water in the partition coefficients in various regions (MacCallum et al., 2008).

The four regions described above are, on most accounts, broad enough for certain solutes such as methanol, water, ammonia, and methylamine. However, for solutes as large as the regions themselves, smearing effects may hinder the direct application of this model. Additionally, the densities of the regions described above are less likely to impact the partition coefficients of the small solutes (due to the size of available free volume). As a result the partition coefficient profiles of such small solutes exhibit only low and high partition coefficient regions (Marrink and Berendsen, 1994, Shinoda et al., 2004, Bemporad et al., 2004). Partition coefficients of larger solutes on the other hand may be affected by the densities of the regions described in the four region model. The effect of relative density or chain ordering on the partition coefficient has been termed the “non-classical hydrophobic effect” or the “bilayer effect” (Seelig and Ganz, 1991, Wimley and White, 1993, Xiang and Anderson, 1994b, DeVido et al., 1998). As a result of this size selectivity of the *ordered solvent*, larger solutes may show more complex partition coefficient profiles than the smaller solutes. Irrespective of the complexity of the profile, the region of the lowest partition coefficient remains of interest for the transport across the bilayer and the region of the highest partition coefficient remains of interest for liposomal drug delivery applications.

Partition coefficient profiles or corresponding profiles showing the apparent free energies of transfer of a variety of solutes as a function of depth within bilayers have been reported in the literature. Some of the recent ones include the studies of amino acid side chains where the H<sub>2</sub>N-CH-COOH group (the *glycine* portion) of the amino acid was replaced with a hydrogen atom (MacCallum et al., 2008, Johansson and Lindahl, 2008). The transfer free energy profiles of the side chains that show a barrier in the center of the



bilayer include: tyrosine (p-cresol), asparagine (acetamide), glutamine (propionamide), serine (methanol), threonine (ethanol), arginine (propylguanidine), glutamic acid (propionic acid), and aspartic acid (acetic acid). In the same studies, the amino acid side chains that indicate a favorable free energy of transfer to the center of the bilayer include: alanine (methane), valine (propane), leucine (isobutane), isoleucine (n-butane), cysteine (methanethiol), methionine (ethylmethylsulfane), tryptophan (3-methyl-1H-indole), and phenylalanine (toluene). In all cases, the free energy of transfer from water to the center of the bilayer is in the same order as that generated from the hydrocarbon water partition coefficient. The free energy of transfer from water to the interface of the headgroups and the ordered chains for all of these amino acid side chains (Johansson and Lindahl, 2008, MacCallum et al., 2008) is either favorable or neutral. This favorable free energy of transfer to the interface was described by these workers to be due to the complementarity of the amphiphilic nature of the solute and the interface.

## 2. Profiles generated in this study

The free energy profiles calculated for the transfer of tyramine, 4-ethylphenol, and phenylethylamine from water to various locations in the lipid bilayer are shown in Figure 5-14. The location of solute in these profiles is the location of the aromatic atom attached to the ethyl group of each solute. Therefore, the solutes, due to their own size, can span a region of approximately 2 to 5 angstroms on each side of the location indicated on the plot. The free energy difference between any two locations on these profiles (points on the profiles or planes of the bilayer) can be used to obtain the corresponding partition coefficients.

The free energy profiles of all three solutes show similar features, most conspicuous of which is the favorable free energy of transfer to the head group region (minimum in the free energy profile) and the peak or barrier at the center of the bilayer. The three solutes differ from each other significantly in the center of the bilayer and minimally in the head group region.

The minimum in the profiles for each of the three solutes in the head group region occurs near the average location of the carbonyl groups of the DOPC bilayer. It is

conceivable that this region will provide opportunity for hydrogen bonding between the solutes and the polar functional groups of the head groups of the bilayer (including bound water). For 4-ethylphenol and phenethylamine, the simple picture emerges that the hydrophilic groups of solute and bilayer interact with each other thereby increasing solubility near the head groups. However, if the hydrogen bonding were the only underlying reason for the minimum in the free energy profile, tyramine would be expected to show much lower free energy in this region compared to that of the other two solutes due to its two hydrogen bonding functional groups. This suggests other contributors to the local free energy in this region than just the hydrogen bonding potential of the solute.

An additional factor may be the interfacial nature of the carbonyl region, where the interfacial water and the hydrocarbon chains of bilayer are in reasonable proximity to allow a complimentary fit for polar and non-polar sides of 4-ethylphenol and phenethylamine. The solute molecules could preferentially align their polar portions with the carbonyl region and their nonpolar portions with the hydrocarbon regions thus allowing the stabilization to occur. The preferred orientations of solute as a function of depth and corresponding hydrogen bonding interactions are explored in detail in chapter six.

The second prominent feature of the three free energy profiles is the energy barrier in the center of the bilayer. A determinant of this feature could be the hydrophobic effect on the solutes in water that leads to a favorable change in energy upon transfer from water to the center of the bilayer. Since all three solutes contain the same non-polar backbone, this effect is comparable for all three, and the residual difference should be due to the obvious lack of the hydrogen bonding interactions involving the polar functional groups in this region. This barrier is larger for tyramine as compared to that for the other two solutes and suggests a significant role of the polar functionalities in rationalizing the free energy of one solute versus another in this region. A similar explanation was offered for the free energy profile of phenol across a continuum membrane model by Sengupta et al (Sengupta et al., 2008), who deconvoluted the free energy profile into an electrostatic component and a “non-polar” component (work of

cavity formation). They argued that the balance between the two components determines if the free energy of transfer into a given region is favorable or unfavorable.

### ***Free energies of solute transfer and functional group contributions***

Before the free energy profiles are interpreted quantitatively, an additional factor to be considered is the thickness of the lipid bilayer slabs used in the post-processing calculations to average and integrate forces acting on the solute. This can also be referred to as the granularity of the post-processing calculation. While it may be desirable to use an infinitesimally thin slice, the number of observations available in each slice may decrease significantly. The free energy profiles of phenylethylamine calculated using slab thickness of 0.3, 5, and 10 angstrom are shown in Figure 5-15. The general effect of increasing the slab thickness is similar to that obtained from a moving average or a smoothing algorithm, and it appears that an increase in slab thickness above 5 angstroms has a significant impact ( $\sim 1$  kcal) on the estimates of the free energy. Ideally an infinitesimally thin slab should be used for integration. Practically it can be reduced until no further effect is perceived. As a result, a slab thickness of 0.3 angstroms was selected for all the analyses, as it yields a profile similar to that from the slab thickness of 5 Angstroms, and leaves sufficient number of observations available in each slice.

The free energy of transfer ( $\Delta G$ ) of the solute from water to both the center of the bilayer and the preferred binding region is obtained by taking the difference of free energies at the respective locations on the free energy profile in Figure 5-14. The functional group contributions to this quantity ( $\Delta\Delta G$ ) are determined by further taking the difference between the  $\Delta G$  of two compounds. Values for  $\Delta\Delta G$  of aromatic hydroxyl and alkylamino functional groups for each bilayer location were calculated in the same manner and are shown in Figure 5-16. These values for specific locations in the bilayer (preferred binding region or the interface, and the hydrocarbon region or the center of the bilayer) along with those determined from other studies are given in Table 5-1. As expected based on the text in the introduction, the agreement between experiment and simulation for the functional group contributions to the transfer free energy is superior to that for the transfer free energies of entire solutes. The MD simulation overestimates the

preferred binding in the interfacial region for tyramine and 4-ethylphenol and the partition coefficient in the hydrocarbon region for 4-ethylphenol and phenylethylamine (Table 5-1). The hydroxyl and amino group contributions to the apparent free energy of transfer are however quite closely matched by the MD simulations with those from several different studies as discussed in detail below.

### 1. Free energy of transfer from water to the preferred binding region

While it is possible to calculate  $\Delta G_{\text{transfer}}$  from the free energy profile obtained from the simulation, direct experimental estimates of partition coefficients in the slices of bilayer are not possible. Consequently partition coefficients measured in a solvent with chemical selectivity similar to that of the layer of interest have been employed. For example, MacCallum et al (MacCallum et al., 2008) used the octanol/water partition coefficient data of Wimley et al (Wimley et al., 1996) to compare with the MD simulation of the partition coefficient of amino acid side chains in the head group region. In this study, since the solutes show preferred binding to the head group region, the expected concentration in this region overwhelms the contributions from all other regions of the bilayer. As a result, a partition coefficient in the lipid bilayer as a whole largely represents the partition coefficient in the preferred binding region. For example, a partition coefficient multiple of 50 fold between two regions corresponds to an energy differential of 2.5 kcal per mole, leading to a significantly low rate of error with this assumption. The free energy values for transfer to the preferred binding region derived from such partition coefficients (Tejwani and Anderson, 2008) are listed along with the simulation based values in Table 5-1.

The aromatic hydroxyl group contribution for solute transfer from water to the preferred binding region ( $\Delta\Delta G_{\text{OH,w}\rightarrow\text{INT}}$ ) was found to be close to zero kcal per mole from the MD simulation which is close to the values of 0, 1.25, and 1.25 kcal per mole recently reported by MacCallum et al (MacCallum et al., 2008) for MD simulations of amino acid side chain solutes in DOPC bilayers, Johansson et al (Johansson and Lindahl, 2008) for the similar solutes in the DMPC bilayers, and Sengupta et al (Sengupta et al., 2008) for the similar solutes in a continuum dielectric membrane, respectively. The experimental

estimate of the hydroxyl group contribution obtained from the retention factors of phenol and resorcinol in immobilized artificial membrane chromatography (Valko et al., 2000, Lazaro et al., 2005) is 0.3 kcal per mole which is also very close to the MD simulation values reported above.

The amino group contribution to the free energy of transfer from water to the preferred binding region ( $\Delta\Delta G_{\text{NH}_2, \text{w} \rightarrow \text{INT}}$ ) was found to be 1.8 kcal per mole based on the liposome water partition coefficients of tyramine vs. 4-ethylphenol. The corresponding MD simulation estimate for the same quantity based on the same set of solutes was found to be 1 kcal per mole which is within 1 kcal per mole of the experimental value. Corresponding values from the n-butane/n-butylamine pair calculated using MD simulations of MacCallum (MacCallum et al., 2008) and Johansson (Johansson and Lindahl, 2008) are 1.4 and -0.5 kcal per mole, respectively. These values for the transfer free energy of the amino group are not too far from the uncertainty of determination of the experimental and simulation values reported above.

Based on a variety of solutes in this and other experimental studies, a near zero free energy of transfer of the hydroxyl and amino groups from water to the preferred binding region is interesting. Since solvation of the polar functional groups in bulk water is primarily through formation of hydrogen bonds, it is likely that the water available in the head group region maintains the same level of solvation leading to this finding. The microscopic dynamics of hydrogen bonding effects in the MD simulation are discussed in chapter six.

## 2. Free energy of transfer from water to the hydrocarbon region

While it is not feasible to experimentally measure the partition coefficient in the hydrocarbon region of the bilayer, it has been established that the chemical nature of the barrier to transport in liquid crystalline egg phosphatidylcholine and DOPC bilayers is similar to that of a hydrocarbon such as 1,9-decadiene (Mayer et al., 2000, Xiang and Anderson, 1994c). The hydroxyl group contributions for transfer from water to the hydrocarbon ( $\Delta\Delta G_{\text{OH}, \text{w} \rightarrow \text{HC}}$ ) determined from the experimentally measured partition coefficients of a variety of solute pairs are shown in Table 5-1, and range from 2.7 to 5.6

kcal per mole (Xiang and Anderson, 1994c, Abraham et al., 1994, Rytting et al., 1978, Tejwani et al., 2009, Xiang et al., 1998).

The simulation based estimates for  $\Delta\Delta G_{\text{OH},w\rightarrow\text{HC}}$  in a liquid crystalline bilayer (DOPC) range from 4.2 to 5.75 kcal per mole depending on the solutes used. Those for the aromatic hydroxyl trend close to each other and include 5 (this study), 4.5 (MacCallum et al., 2008), and 5.75 (Sengupta et al., 2008) kcal per mole, where the first two studies are MD simulations and the last study is the continuum dielectric model simulation. The values for the aliphatic hydroxyl include 5.5 (MacCallum et al., 2008) and 4.2 (Xiang and Anderson, 2002) kcal per mole, where the former was calculated from a constrained MD simulation followed by force averaging and the latter was calculated by thermodynamic integration in an MD simulation. The latter value corresponds well with the matching experimental measurements (Xiang and Anderson, 1994c) of transport across the same DOPC bilayer (3.9 kcal per mole) and with the same from the partition coefficients in 1,9-decadiene/water system (4.2 kcal per mole).

The experimental value for  $\Delta\Delta G_{\text{OH},w\rightarrow\text{HC}}$  in the liquid crystalline bilayer (3.9 kcal per mole) and that obtained from the partition coefficient in 1,9-decadiene/water system (4.2 kcal/mole) are lower than those obtained from alkane/water partition coefficients of 5.3 kcal per mole (Abraham et al., 1994) and 5.6 kcal per mole (Rytting et al., 1978). This slight difference in the selectivity of the two different hydrocarbon/water systems (alkane/water vs. decadiene/water) has been addressed before and 1,9-decadiene/water has been found to resemble the microenvironment of the barrier in liquid crystalline bilayers containing partially unsaturated lipid chains (Xiang et al., 1998).

The experimental values for  $\Delta\Delta G_{\text{OH},w\rightarrow\text{HC}}$  in solutes with phenol groups on the other hand trend lower (3.9 and 4.4 kcal per mole) than those obtained from the similar solvents (alkane/water) for the aliphatic hydroxyl groups (5.3 and 5.6 kcal per mole). This trend is however not observed in the values obtained from the MD simulations as the aromatic hydroxyl values from various simulation studies range from 4.5 to 5.75 kcal per mole and span the values obtained from the aliphatic solutes in the same studies.

The experimentally measured contribution of the amine group to the free energy of transfer from water to hydrocarbon ( $\Delta\Delta G_{\text{NH}_2, \text{w} \rightarrow \text{HC}}$ ) ranges from 4.3 to 5 kcal per mole for alkylamines except those where partition coefficient values from two different solvents were used in the calculation. The MD simulations of the liquid crystalline bilayer, DOPC, result in comparable values of 4.2 (MacCallum et al., 2008) and 5 (this study) kcal per mole.

The experimental estimates of  $\Delta\Delta G_{\text{OH}, \text{w} \rightarrow \text{HC}}$  and  $\Delta\Delta G_{\text{NH}_2, \text{w} \rightarrow \text{HC}}$  in solute pairs involving tyramine (2.7 and 2.8 kcal per mole, respectively) are consistently lower than the other experimental and simulation estimates for the same value. This lower value has been suggested to be due to an intramolecular interaction (Tejwani et al., 2009) that favors tyramine partitioning into the hydrocarbon region by approximately 1 kcal per mole. It was inferred that this likely involves either a non-classical charge interaction between a hydrogen atom of the amine group and the pi ring system or one or more water molecules bridging between the two polar groups of tyramine. Since this type of NH-pi interaction is not represented in the currently available force fields, it was not represented in the MD simulation involving tyramine. In the MD simulations there is only a very small possibility of obtaining a significant number of configurations where a water molecule would accompany a tyramine molecule to the center of bilayer and where tyramine remains in just the right conformation most of the time. Therefore the MD simulation involving tyramine did not replicate the functional group contributions from the experiments involving tyramine and instead matches more closely the experimental  $\Delta\Delta G$  values obtained from other solutes.

## **Conclusions**

The all atom MD simulations were conducted for three selected solutes to determine the location of the transport barrier region as well as the preferred binding region. The properties of the DOPC lipid bilayer obtained from simulations were found to conform well to those obtained from the published experimental and MD simulation values. The lipid bilayer was stable throughout the simulations of hundreds of nanoseconds and only minor changes in its properties were found after the inclusion of

multiple copies of the solutes. After inclusion of the solutes no change in order parameters was observed but a slight decrease in the number of lipid chain *gauche* torsions occurred. However, the values remained very close to those expected.

Two methods of computing the free energy profiles from constrained MD simulation were compared. The force integration method was found to be more suitable for processing the MD simulation data due to more accurate book keeping of the applied constraint forces and its resulting effect on the accuracy as well as speed of convergence.

The free energy profiles of the three solutes show two distinct regions - one with high partition coefficient (the preferred binding region) near the head group region and another with low partition coefficient (the transport barrier region) at the center of the bilayer. These findings are consistent with the fact that the solutes show a favorable partition coefficient in the liposome/water system, yet there is a barrier to transport across the lipid bilayer membrane. From comparison of the solute profiles it can be discerned that the center of the bilayer discriminates among solutes to a greater extent than does the head group region.

The overall solute transfer free energies or the solute partition coefficients obtained from MD simulations were not in close agreement with those obtained experimentally; however the functional group contributions were predicted more accurately for the liquid crystalline bilayer. The contributions of the hydroxyl and amino groups to the free energies of transfer from water to the head group region are close to zero from the MD simulation and experimental measurements. This suggests that the free energy decrease observed for solutes is more likely due to effects other than just hydrogen bonding (e.g. hydrophobic effect). While solvation of the amphiphilic solutes can be explained near the carbonyl groups of the lipid bilayer, the decrease in the free energy while the solute is located outside of the phosphate groups remains to be explained. The contributions of the hydroxyl and amino groups to the free energies of transfer from water to the center of the bilayer calculated from the MD simulation were found to be consistent with those from experiment and recently published MD



simulations of other solutes. The intramolecular interaction of tyramine favoring its partition coefficient in the hydrocarbon was not detected in the MD simulations.

**Table 5-1.** Free energies of transfer of solutes and functional group contributions. Values less than zero indicate that the transfer is favored. Superscripts and footnotes indicate the source experiment or simulation of the value. When superscripts appear on solutes the free energy values have been calculated from partition coefficients from two different studies and differ in the solvents employed.

Solute or Functional Group	Solute - 1	Solute - 2	Transfer free energy (kcal per mole) from water to:			
			Interface		Hydrocarbon	
			Simulation	Experiment	Simulation	Experiment
Tyramine			-5 <sup>*</sup>	-1.9 <sup>*</sup>	2	1.8
Phenethylamine			-5		-3.5	-0.9
4-Ethylphenol			-6	-3.8 <sup>A</sup>	-3.5	-1
Aromatic hydroxyl	Phenethylamine	Tyramine	0		5	2.7
	Phenol	Resorcinol		0.3 <sup>B</sup>		
	Toluene	p-Cresol	0 <sup>C</sup> 1.25 <sup>D</sup>		4.5 <sup>C</sup>	3.9 <sup>E</sup>
	Benzene	Phenol	1.25 <sup>F</sup>		5.75 <sup>F</sup>	4.4 <sup>E</sup>
	Ethylbenzene <sup>E</sup>	4-Ethylphenol <sup>G</sup>				3.4
Aliphatic hydroxyl	Methane	Methanol	1.4 <sup>C</sup> -1.25 <sup>D</sup>		5.5 <sup>C</sup>	5.3 <sup>E</sup>
	p-Toluic Acid	Hydroxy toluic acid			4.2 <sup>H</sup>	3.9 <sup>I</sup> 4.2 <sup>J</sup> 2.7 <sup>K</sup>
	n-Alkane	n-Alcohol				5.6 <sup>L</sup>
Alkyl amino	4-Ethylphenol	Tyramine	1	1.8	5	2.8
	n-Butane	n-Butylamine	1.4 <sup>C</sup> -0.5 <sup>D</sup>		4.2 <sup>C</sup>	
	n-Alkane	n-Alkylamine				5.0 <sup>L</sup>
	Ethylbenzene <sup>E</sup>	Phenethylamine <sup>G</sup>				3.5
	Methane	Methylamine				4.3 <sup>E</sup>
	4-Ethylanisole <sup>M</sup>	O-Methyltyramine <sup>G</sup>				3.4

A. Calculated from liposome/water partition coefficients measured by Rogers et. al. (Rogers and Davis, 1980)

- B. Calculated from capacity factors in immobilized artificial membrane chromatography from Valko et al (Valko et al., 2000), and Lazaro et al (Lazaro et al., 2005). Both studies lead to the same calculation result.
- C. Calculated from MD simulation in a liquid crystalline lipid bilayer (DOPC) by MacCallum et al (MacCallum et al., 2008)
- D. Calculated from MD simulation in a gel phase lipid bilayer (DMPC) by Johansson et al (Johansson and Lindahl, 2008)
- E. Calculated from hexadecane/water partition coefficients from Abraham et al (Abraham et al., 1994)
- F. Calculated from Continuum dielectric model simulation by Sengupta et al (Sengupta et al., 2008)
- G. Partition coefficient in 1,9-decadiene obtained from Tejwani et al (Tejwani et al., 2009).
- H. Obtained from MD simulation by Xiang et al (Xiang and Anderson, 2002)
- I. Based on transport across egg phosphatidylcholine bilayers (Xiang and Anderson, 1994c)
- J. Based on partition coefficient in 1,9-decadiene/water (Xiang and Anderson, 1994c)
- K. Calculated from transport across DPPC bilayer measured by Xiang et al (Xiang et al., 1998).
- L. Recalculated from alkane and water solubility measurements by Rytting et al (Rytting et al., 1978)
- M. Hydrocarbon/water partition coefficient from Lambert et al (Lambert et al., 1990)

\* It should be noted that while the simulation was conducted for a neutral species, under the experimental conditions employed (Chapters Three and Four) tyramine was in predominantly protonated (positively charged) form. The pH independence of binding (Figures 3-6, 4-12, 4-13, and 4-14) however suggests that the binding and ionization may be determined by two different portions of the tyramine molecule. For details, see text in the two chapters.

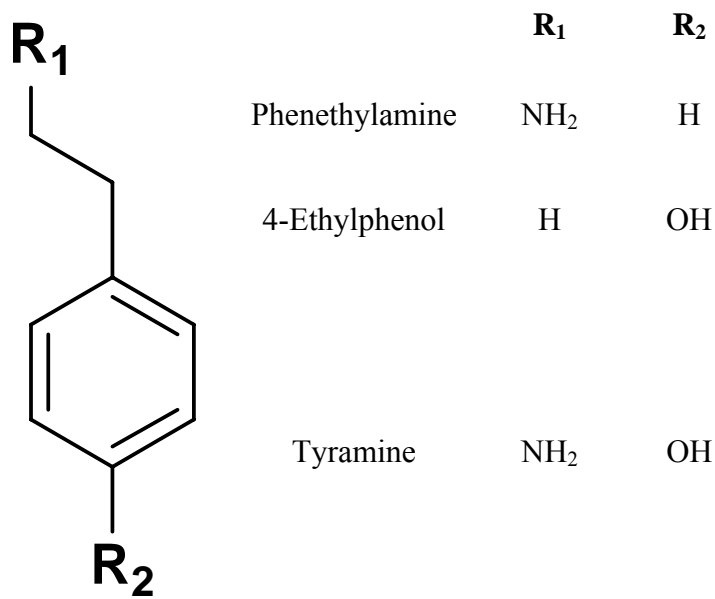
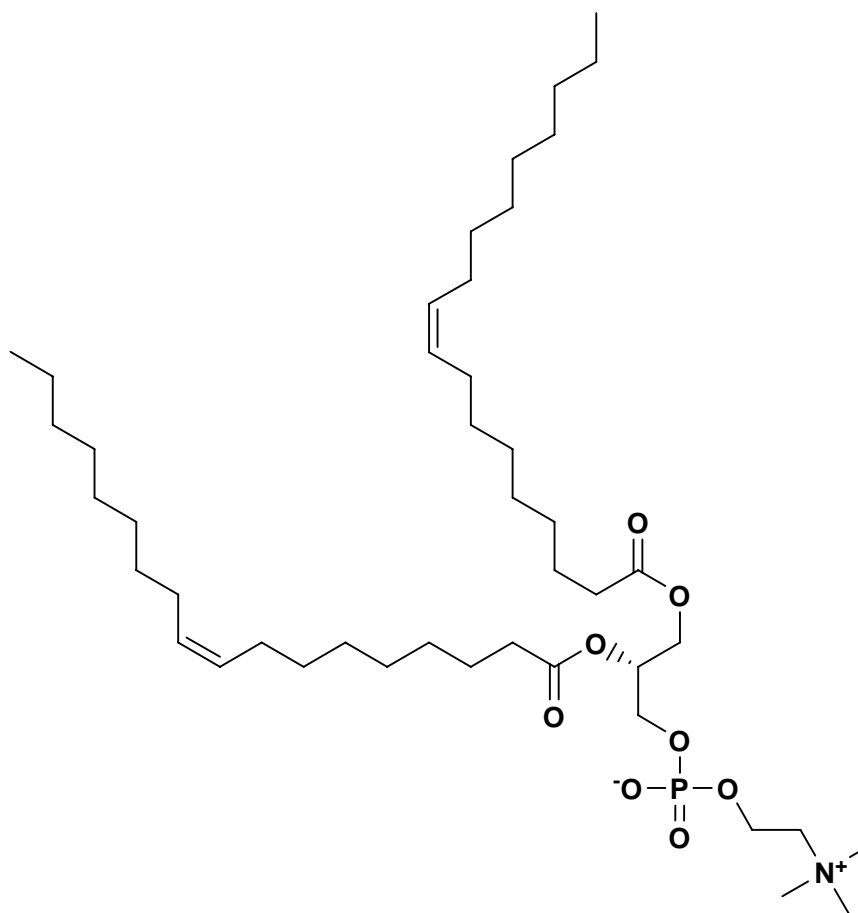


**Figure 5-1.** Chemical structures of the three solutes used in this study



Chemical Formula:  $C_{44}H_{84}NO_8P$   
Molecular Weight: 786.11

**Figure 5-2.** Chemical structure of 1,2-dioleoyl-*sn*-glycero-3-phosphocholine (DOPC).

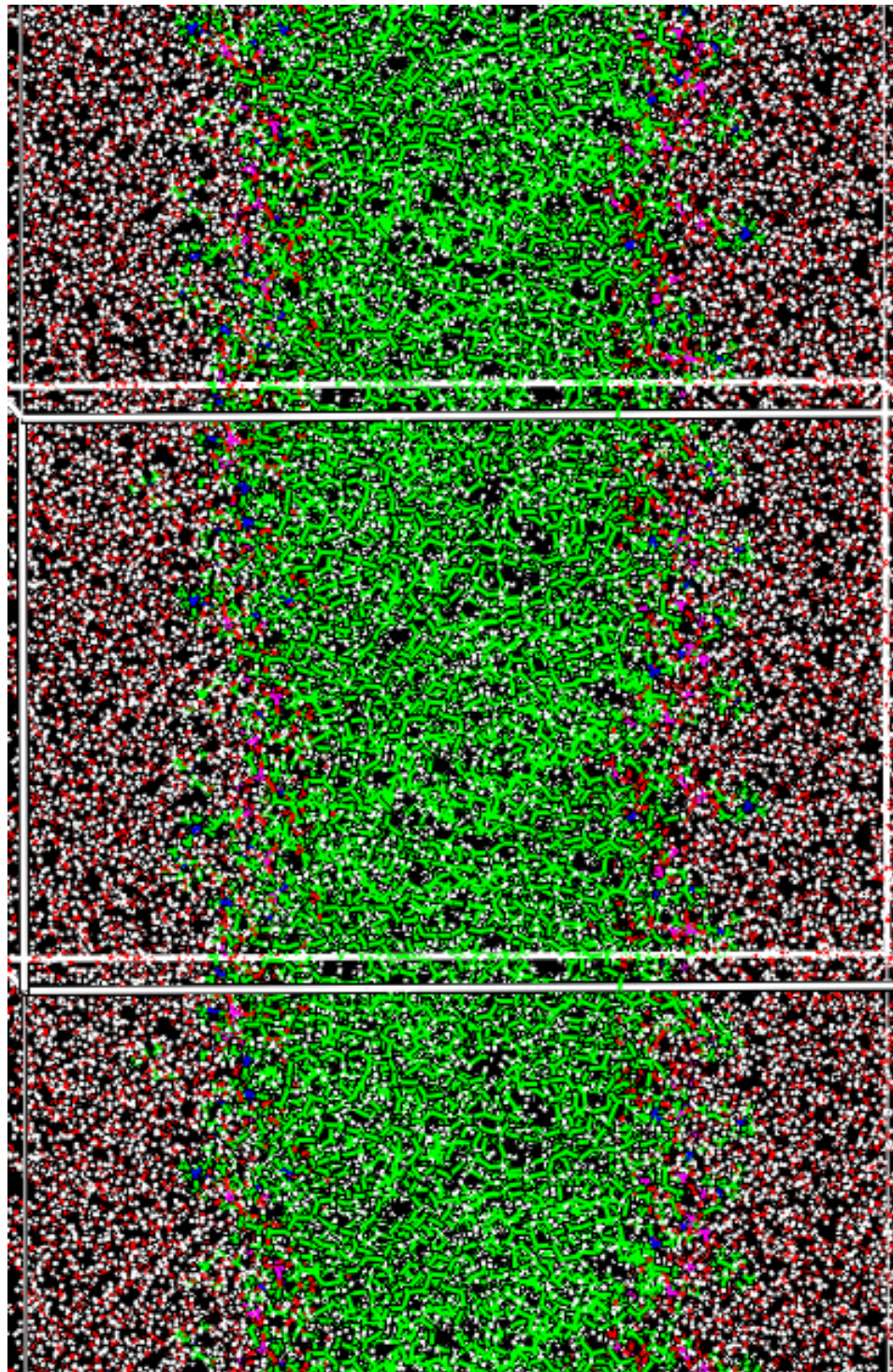


**Figure 5-3.** Structure of the simulated lipid bilayer. Carbon atoms are green, hydrogen atoms are white, oxygen atoms are red, nitrogen atoms are blue, and phosphorous atoms are purple.

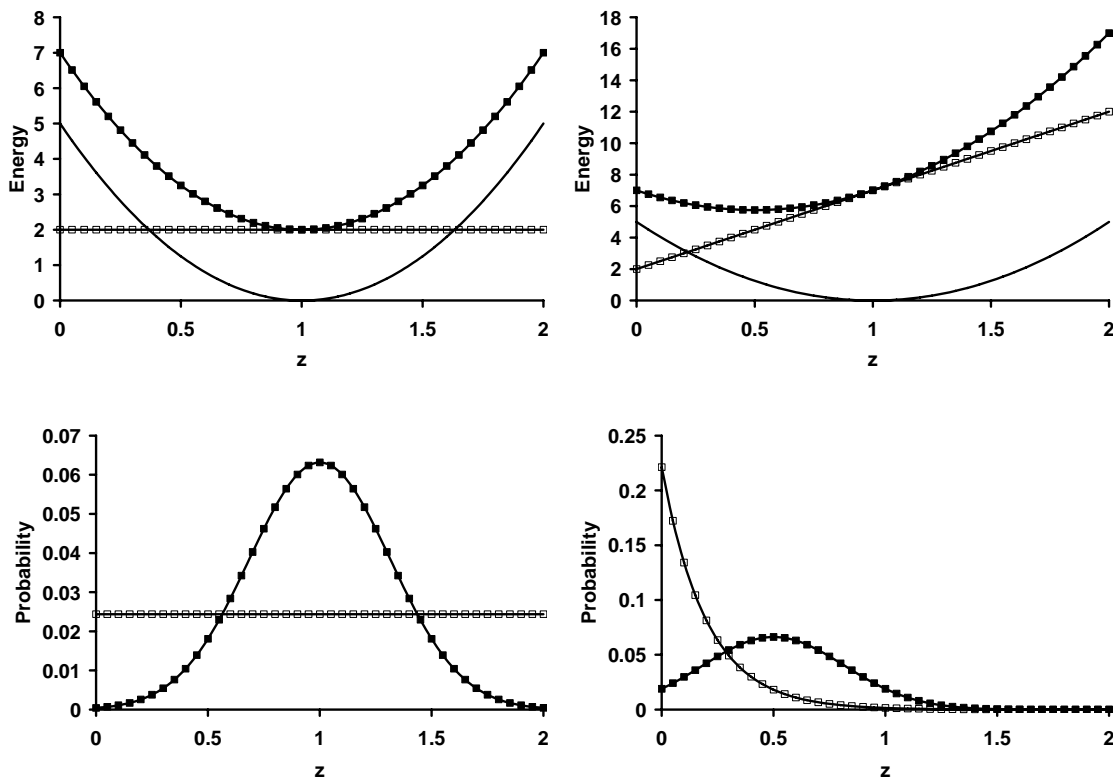


**Figure 5-4.** Illustration showing the use of a quadratic biasing potential in an MD simulation designed to determine a free energy profile. The upper pair of plots shows the energy profiles of two systems: the first has an underlying free energy profile with no slope (left plot,  $\square$ ) and the second has an underlying linear free energy profile with positive slope (right plot,  $\square$ ). A quadratic potential centered at  $z=1$  (—) is applied to each system and the resulting energy profile takes the shape shown ( $\blacksquare$ ) in each plot. The probability distributions of the states for each of the two cases are shown with similar symbols in the lower two plots, the unconstrained system exhibits the probability distribution shown by  $\square$  symbol and the constrained system exhibits the probability distribution shown by  $\blacksquare$  symbol. The benefit of applying the quadratic constraint is apparent in the lower right hand side plot where an otherwise low probability of occurrence ( $z = 0.75$  to  $1$ ) has been improved significantly. In this case the constraint could be relocated to  $z = 1.25$  to further improve sampling of lower probability states on the right side.

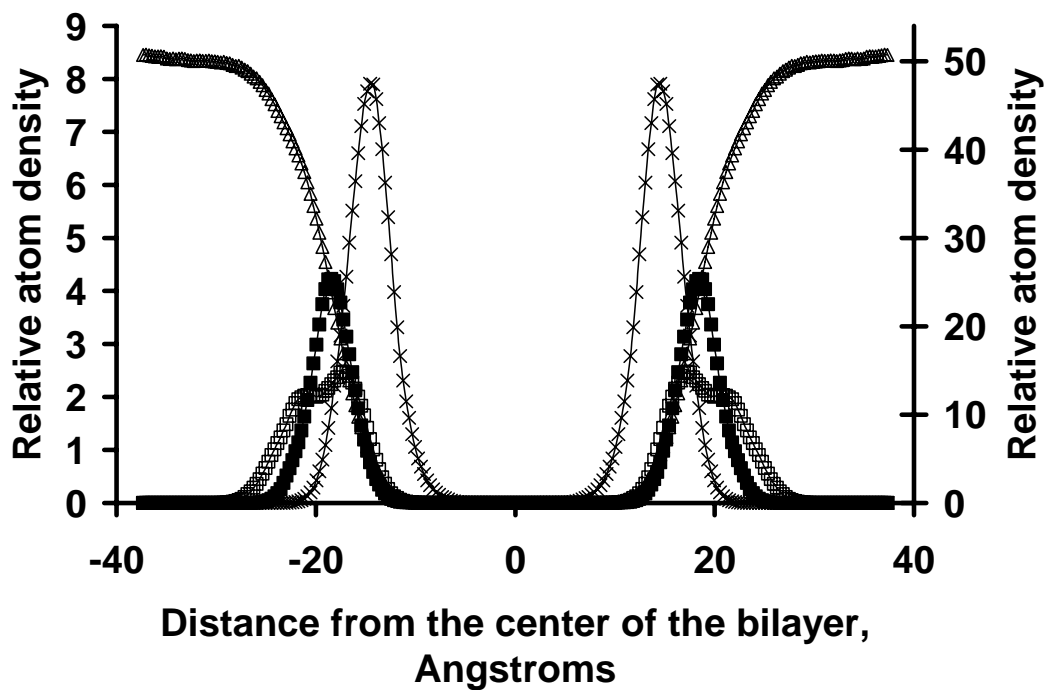


**Figure 5-5.** Average distribution of the atoms of various elements along the depth of the DOPC bilayer. ■: phosphorus, □: nitrogen, ×: carbonyl groups, Δ: oxygen of water. The y-axis on the right hand side has been used for the distribution of the oxygen atoms of water molecules.



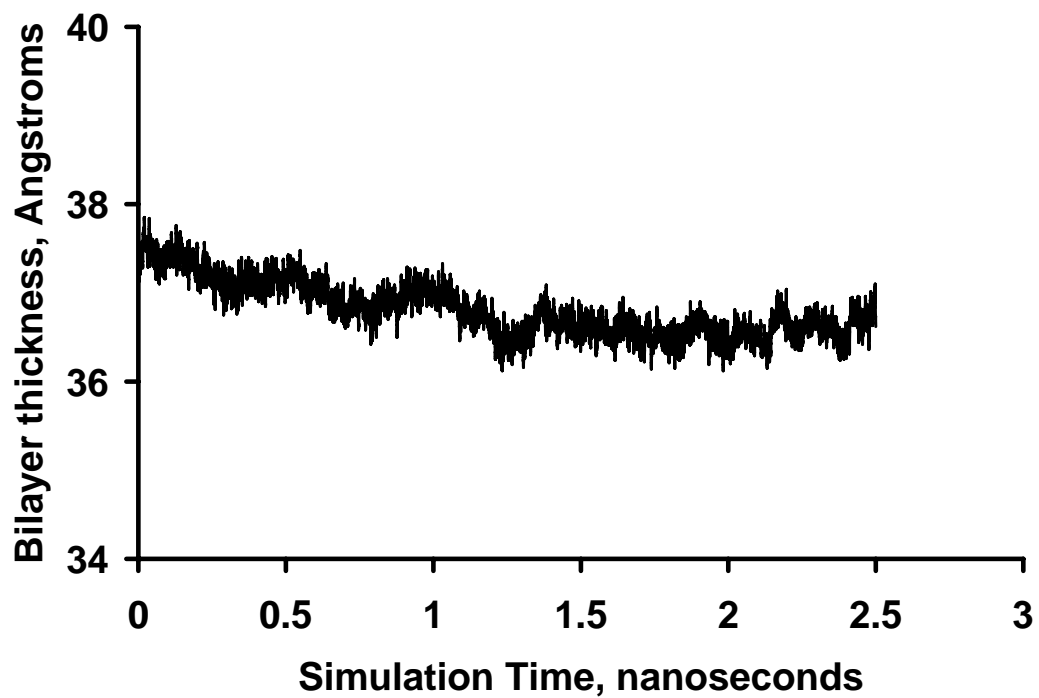


**Figure 5-6.** Thickness of the simulated lipid bilayer as measured by the distance between the average location of phosphorus atoms in the two leaflets over time.

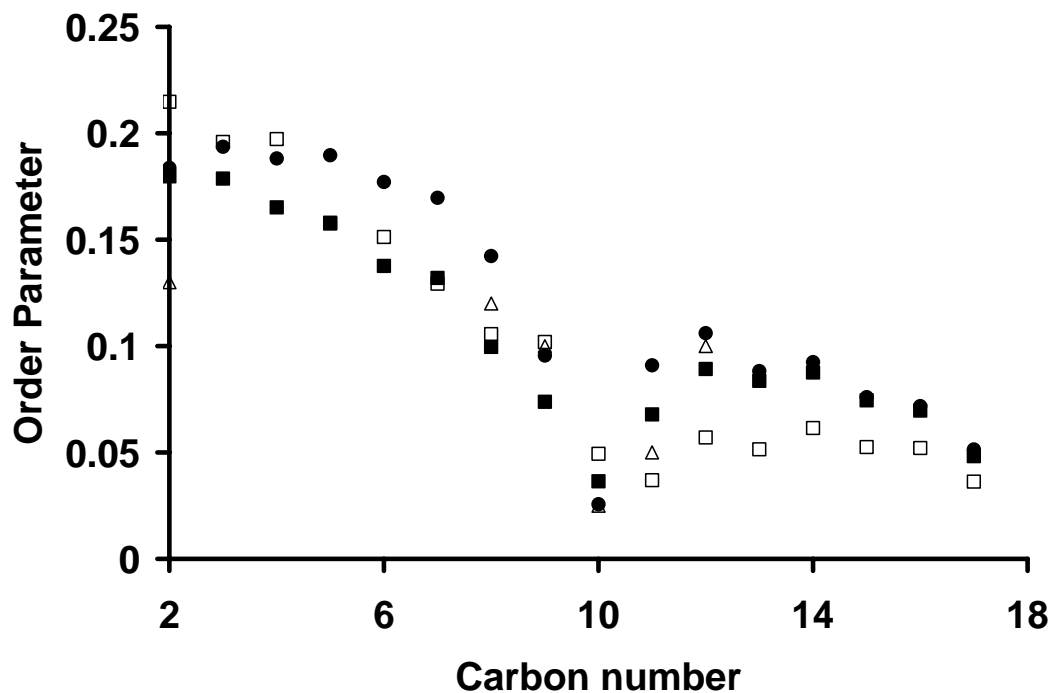


**Figure 5-7.** The order parameters of the two oleoyl chains in the DOPC molecules of the lipid bilayer containing phenethylamine: □ = oleoyl chain at the second carbon of the glycerol, ■ = oleoyl chain at the third carbon of the glycerol. The profiles for the lipid bilayer containing no solute or any of the other two solutes are nearly superimposable with this profile. The experimentally measured order parameters for the oleoyl chain of POPC bilayer are plotted as △ (Seelig and Waespe-Sarcevic, 1978). Average order parameters for both oleoyl chains of DOPC from the MD simulation of Mashl et al are shown as ● (Mashl et al., 2001).

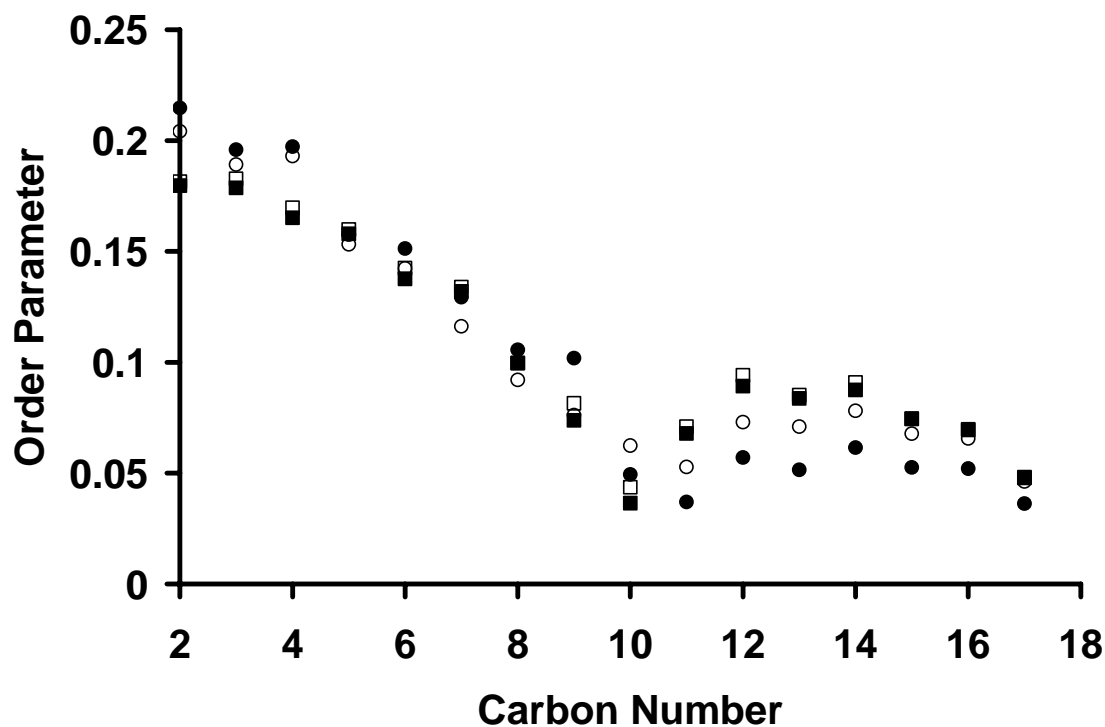


**Figure 5-8.** The order parameters of the two oleoyl chains in the DOPC molecules of the lipid bilayer without solutes (○, □) and that containing phenethylamine (●, ■) as a function of carbon number. The oleoyl chain attached at the second carbon of glycerol is shown as (□, ■) and the chain attached at the third carbon of glycerol is shown as (○, ●).

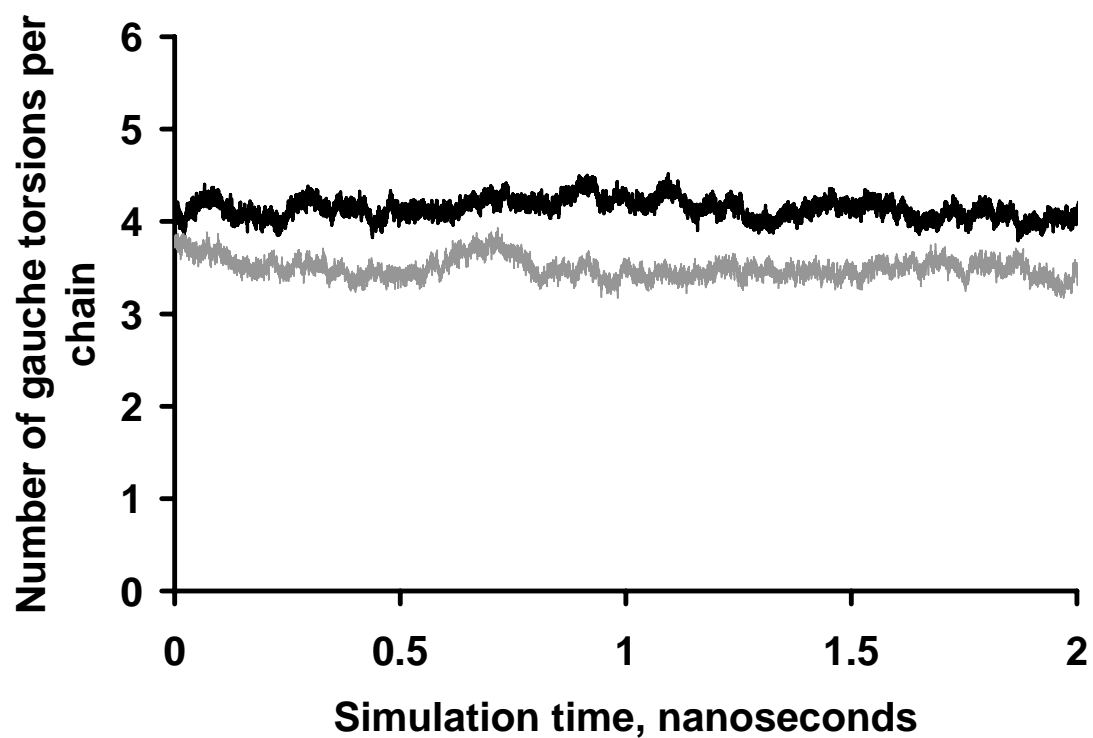


**Figure 5-9.** Average number of oleoyl chain torsions in the *gauche* conformation as a function of simulation time. Upper (dark) and lower (grey) bands are from the simulations for the neat bilayer and that containing tyramine, respectively.

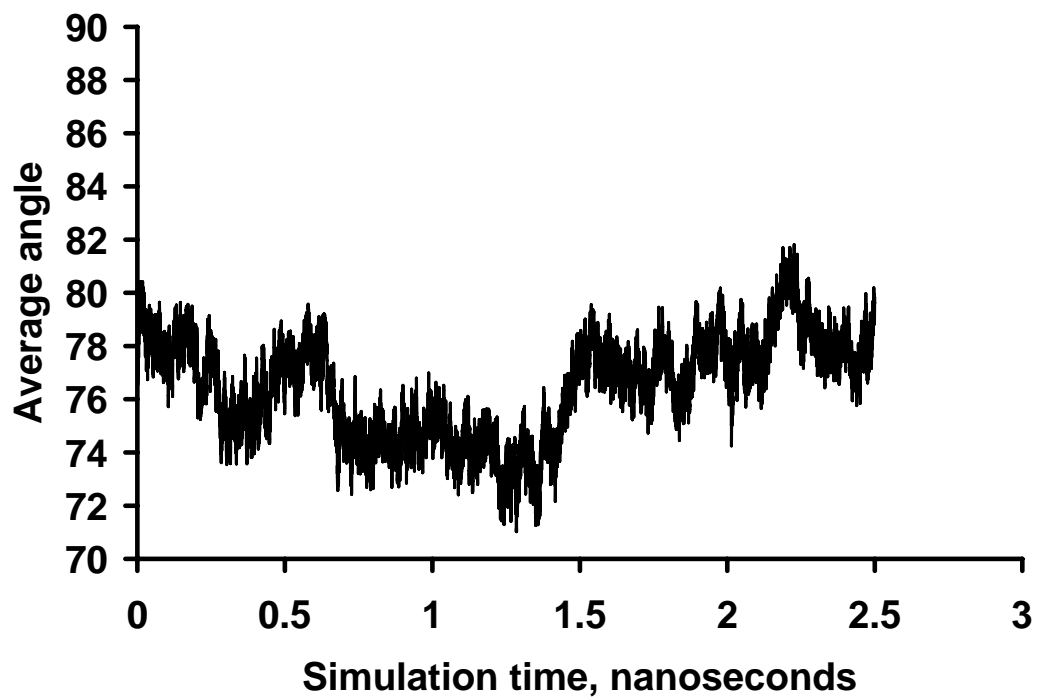


**Figure 5-10.** Average angle of the P→N vector with the bilayer normal as a function of simulation time.

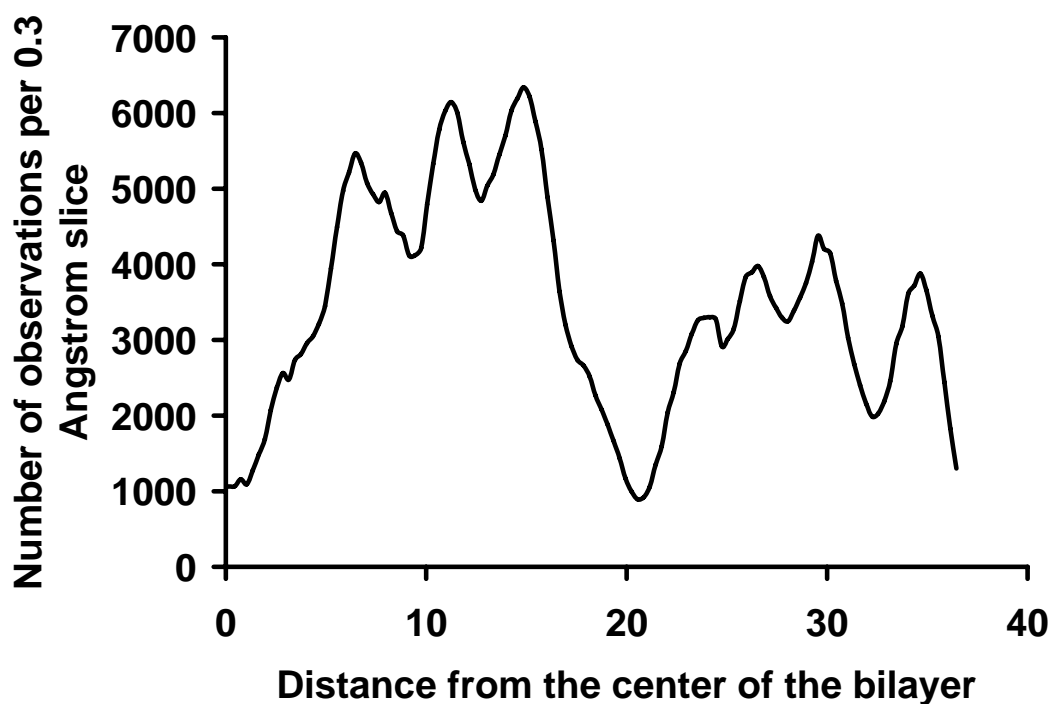


**Figure 5-11.** Number of times tyramine was observed in a given 0.3 angstrom slice of the bilayer as a function of the distance of the mid point of the slice from the center of the bilayer during a representative MD simulation. A solute copy was considered to be present in a 0.3 angstrom slice when the aromatic carbon atom attached to the ethyl chain (the atom closest to the center of mass) was found at this location.

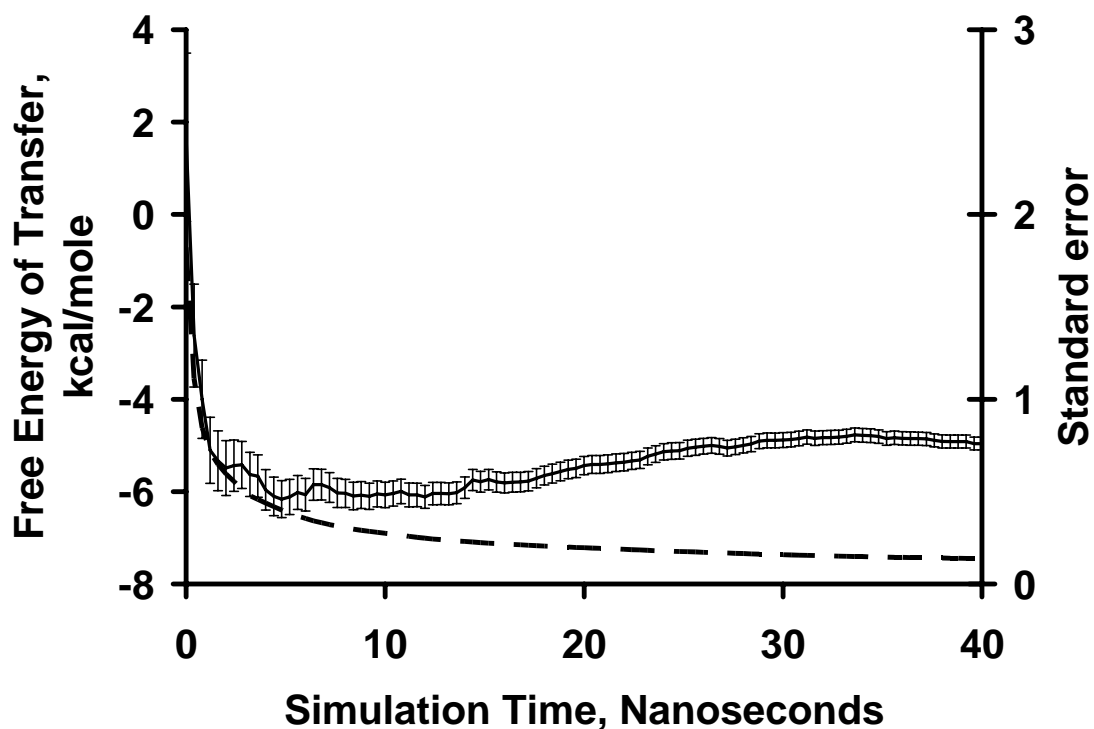


**Figure 5-12.** A representative convergence plot of the evolution of free energy of transfer of phenethylamine from water to the preferred binding region (at about 12 angstroms from the center of bilayer) as data are accumulated during the course of the simulation (—). Error bars indicate the standard error of the estimate. The decrease in the standard error of estimate as the simulation progresses is shown on the right hand side y-axis (- - -).

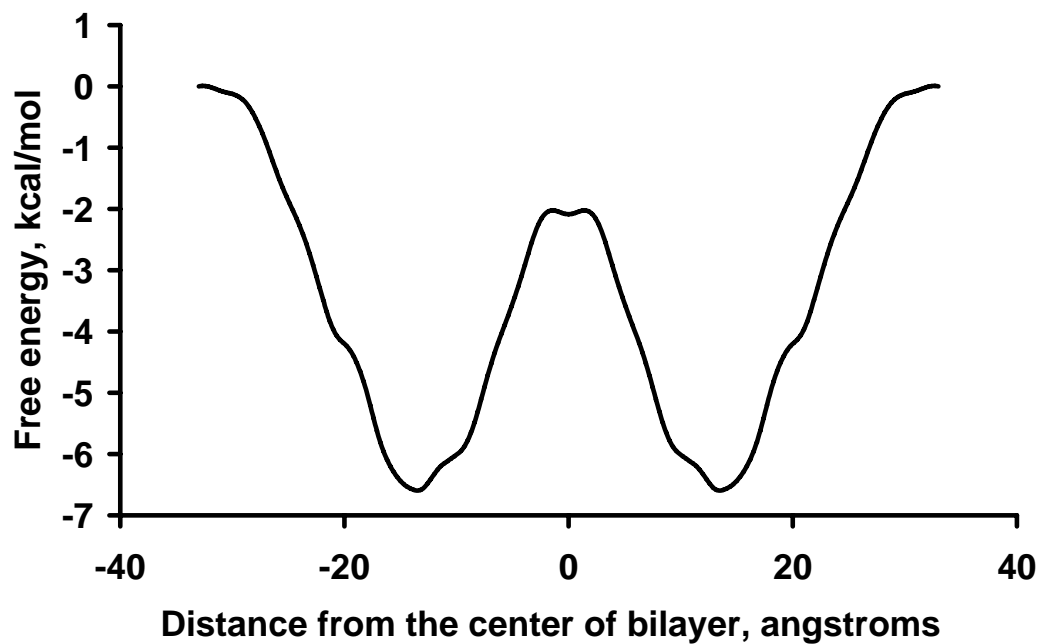


**Figure 5-13.** Free energy of transfer of tyramine from water to various locations within the bilayer, calculated using population density analysis method. Location of tyramine is determined by the location of the aromatic carbon atom attached to the ethyl chain.



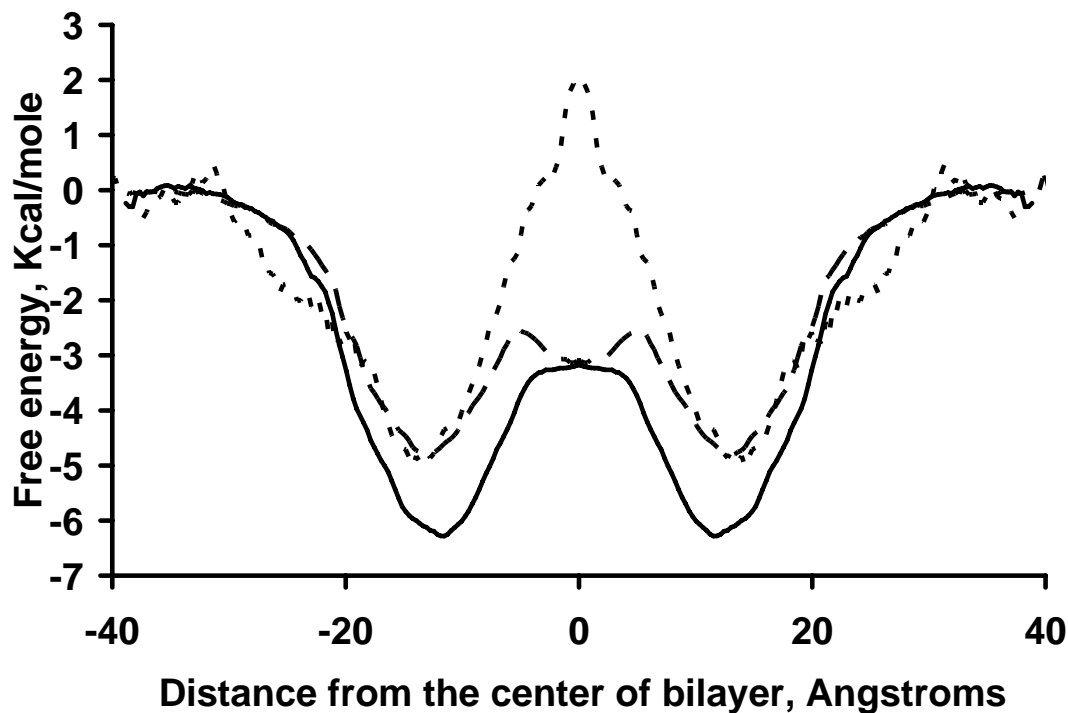


**Figure 5-14.** Free energy of transfer of solute from water to various locations within the bilayer; ••••• = tyramine, - - - - = phenethylamine, — = 4-ethylphenol. The solute position was defined by the location of the aromatic carbon attached to the ethyl chain. Therefore, the solutes, due to their own size, can span a region of approximately 2 to 5 angstroms on each side of the location indicated on the graph.

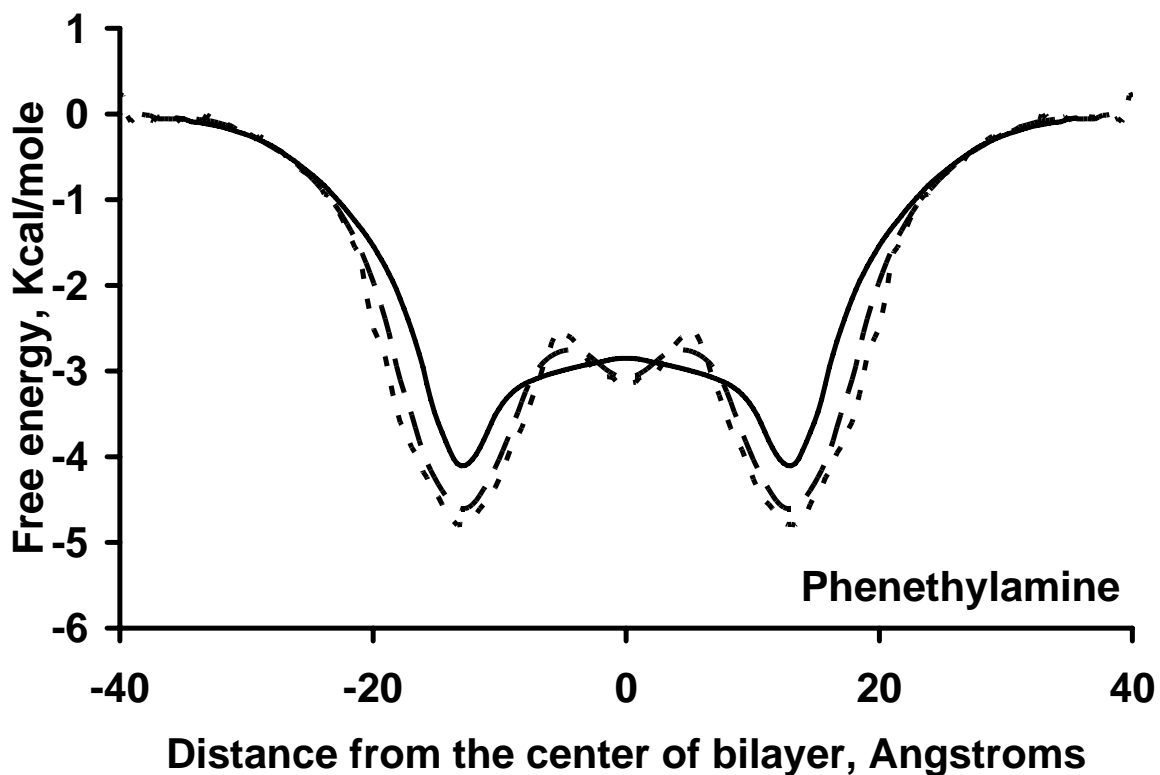


**Figure 5-15.** Effect of slab thickness used for the force integration calculation (0.3 Angstrom = ••••, 5 Angstrom = - - - -, 10 Angstrom = —) on the free energy profile of phenylethylamine. Location of the aromatic carbon attached to ethyl chain is taken as the location of the solute.

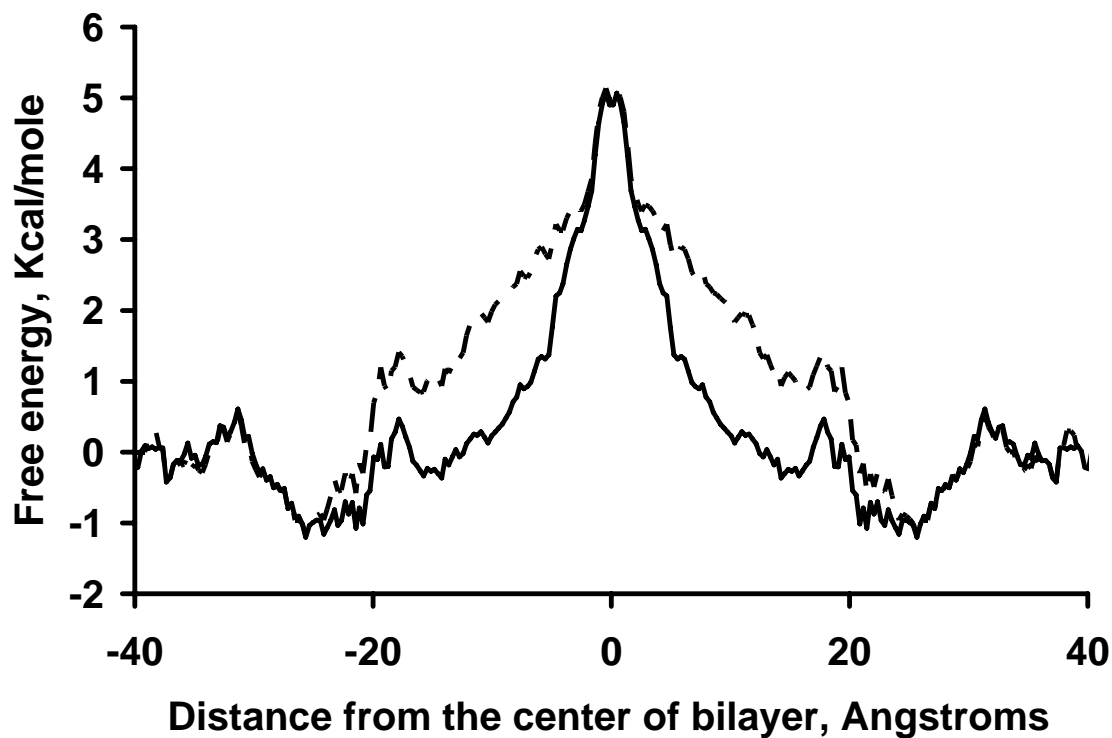


**Figure 5-16.** Hydroxyl (—) and amino (- - -) group contributions to the free energy of solute transfer from water to various locations within the lipid bilayer. The lines were calculated by taking the difference between the profiles of respective solutes from the Figure 5-14. The solute position was defined by the location of the aromatic carbon attached to the ethyl chain. Therefore, the solutes, due to their own size, can span a region of approximately 2 to 5 angstroms on each side of the location indicated on the graph.

## REFERENCES

- ABRAHAM, M. H., CHADHA, H. S., WHITING, G. S. & MITCHELL, R. C. (1994) Hydrogen bonding. 32. An analysis of water-octanol and water-alkane partitioning and the  $\Delta \log P$  parameter of seiler. *Journal of Pharmaceutical Sciences*, 83, 1085-1100.
- ALPER, H. E. & STOUCHE, T. R. (1995) Orientation and diffusion of a drug analog in biomembranes: Molecular dynamics simulations. *Journal of Physical Chemistry*, 99, 5724-31.
- ANEZO, C., DE VRIES, A. H., HOELTJE, H.-D., TIELEMAN, D. P. & MARRINK, S.-J. (2003) Methodological issues in lipid bilayer simulations. *Journal of Physical Chemistry B*, 107, 9424-9433.
- BARTELS, C. & KARPLUS, M. (1997) Multidimensional adaptive umbrella sampling: Applications to main chain and side chain peptide conformations. *Journal of Computational Chemistry*, 18, 1450-1462.
- BARTELS, C. & KARPLUS, M. (1998) Probability distributions for complex systems: Adaptive umbrella sampling of the potential energy. *Journal of Physical Chemistry B*, 102, 865-880.
- BASSOLINO-KLIMAS, D., ALPER, H. E. & STOUCHE, T. R. (1993) Solute diffusion in lipid bilayer membranes: an atomic level study by molecular dynamics simulation. *Biochemistry*, 32, 12624-37.
- BASSOLINO-KLIMAS, D., ALPER, H. E. & STOUCHE, T. R. (1995) Mechanism of solute diffusion through lipid bilayer membranes by molecular dynamics simulation. *Journal of the American Chemical Society*, 117, 4118-29.

- BEMPORAD, D., ESSEX, J. W. & LUTTMANN, C. (2004) Permeation of small molecules through a lipid bilayer: A computer simulation study. *Journal of Physical Chemistry B*, 108, 4875-4884.
- BEMPORAD, D., LUTTMANN, C. & ESSEX, J. W. (2005) Behaviour of small solutes and large drugs in a lipid bilayer from computer simulations. *Biochimica et Biophysica Acta*, 1718, 1-21.
- BEN-NAIM, A. (1978) Standard thermodynamics of transfer. Uses and misuses. *Journal of Physical Chemistry*, 82, 792-803.
- BENNETT, W. F., MACCALLUM, J. L. & TIELEMAN, D. P. (2009) Thermodynamic analysis of the effect of cholesterol on dipalmitoylphosphatidylcholine lipid membranes. *Journal of the American Chemical Society*, 131, 1972-8.
- BHIDE, S. Y. & BERKOWITZ, M. L. (2006) The behavior of reorientational correlation functions of water at the water-lipid bilayer interface. *Journal of Chemical Physics*, 125, 094713.
- CHEW, C. F., GUY, A. & BIGGIN, P. C. (2008) Distribution and dynamics of adamantanes in a lipid bilayer. *Biophysical Journal*, 95, 5627-36.
- CHIU, S. W., CLARK, M. M., JAKOBSSON, E., SUBRAMANIAM, S. & SCOTT, H. L. (1999a) Application of combined Monte Carlo and molecular dynamics method to simulation of dipalmitoyl phosphatidylcholine lipid bilayer. *Journal of Computational Chemistry*, 20, 1153-1164.
- CHIU, S. W., JAKOBSSON, E., SUBRAMANIAM, S. & SCOTT, H. L. (1999b) Combined Monte Carlo and molecular dynamics simulation of fully hydrated dioleoyl and palmitoyl-oleoyl phosphatidylcholine lipid bilayers. *Biophysical Journal*, 77, 2462-2469.
- CONNORS, K. A. (1990) 5. Theory of chemical kinetics. IN CONNORS, K. A. (Ed.) *Chemical Kinetics: The Study Of Reaction Rates In Solution*. New York, John Wiley & Sons, Inc., 187-244.

- DEVIDO, D. R., DORSEY, J. G., CHAN, H. S. & DILL, K. A. (1998) Oil/water partitioning has a different thermodynamic signature when the oil solvent chains are aligned than when they are amorphous. *Journal of Physical Chemistry B*, 102, 7272-7279.
- HAILE, J. M. & O'CONNELL, J. P. (1984) Internal structure of a model micelle via computer simulation. *Journal of Physical Chemistry*, 88, 6363-6.
- HOLLER, F. & CALLIS, J. B. (1989) Conformation of the hydrocarbon chains of sodium dodecyl sulfate molecules in micelles: an FTIR study. *Journal of Physical Chemistry*, 93, 2053-8.
- JOHANSSON, A. C. & LINDAHL, E. (2008) Position-resolved free energy of solvation for amino acids in lipid membranes from molecular dynamics simulations. *Proteins*, 70, 1332-44.
- LAMBERT, W. J., WRIGHT, L. A. & STEVENS, J. K. (1990) Development of a preformulation lipophilicity screen utilizing a C-18-derivatized polystyrene-divinylbenzene high-performance liquid chromatographic (HPLC) column. *Pharmaceutical Research*, 7, 577-86.
- LAU, K. F., ALPER, H. E., THACHER, T. S. & STOUCH, T. R. (1994) Effects of switching functions on the behavior of liquid water in molecular dynamics simulations. *Journal of Physical Chemistry*, 98, 8785-92.
- LAZARO, E., RAFOLS, C. & ROSES, M. (2005) Characterization of immobilized artificial membrane (IAM) and XTerra columns by means of chromatographic models. *Journal of Chromatography, A*, 1081, 163-73.
- LI, C., YI, M., HU, J., ZHOU, H. X. & CROSS, T. A. (2008) Solid-state NMR and MD simulations of the antiviral drug amantadine solubilized in DMPC bilayers. *Biophysical Journal*, 94, 1295-302.
- LUTY, B. A., DAVIS, M. E., TIRONI, I. G. & VAN GUNSTEREN, W. F. (1994) A comparison of particle-particle particle-mesh and Ewald methods for calculating

- electrostatic interactions in periodic molecular systems. *Molecular Simulation*, 14, 11-20.
- MACCALLUM, J. L., BENNETT, W. F. & TIELEMAN, D. P. (2007) Partitioning of amino acid side chains into lipid bilayers: results from computer simulations and comparison to experiment. *Journal of General Physiology*, 129, 371-7.
- MACCALLUM, J. L., BENNETT, W. F. & TIELEMAN, D. P. (2008) Distribution of amino acids in a lipid bilayer from computer simulations. *Biophysical Journal*, 94, 3393-404.
- MACCALLUM, J. L. & TIELEMAN, D. P. (2006) Computer simulation of the distribution of hexane in a lipid bilayer: spatially resolved free energy, entropy, and enthalpy profiles. *Journal of the American Chemical Society*, 128, 125-30.
- MARRINK, S.-J. & BERENDSEN, H. J. C. (1994) Simulation of water transport through a lipid membrane. *Journal of Physical Chemistry*, 98, 4155-4168.
- MASHL, R. J., SCOTT, H. L., SUBRAMANIAM, S. & JAKOBSSON, E. (2001) Molecular simulation of dioleoylphosphatidylcholine lipid bilayers at differing levels of hydration. *Biophysical Journal*, 81, 3005-3015.
- MAYER, P., XIANG, T.-X. & ANDERSON, B. (2000) Independence of substituent contributions to the transport of small-molecule permeants in lipid bilayer. *AAPS Journal*, 2, 40-52.
- MUKHOPADHYAY, P., VOGEL, H. J. & TIELEMAN, D. P. (2004) Distribution of pentachlorophenol in phospholipid bilayers: a molecular dynamics study. *Biophysical Journal*, 86, 337-45.
- NAGLE, J. F. & TRISTRAM-NAGLE, S. (2000) Structure of lipid bilayers. *Biochimica et Biophysica Acta, Reviews on Biomembranes*, 1469, 159-195.
- NORMAN, K. E. & NYMEYER, H. (2006) Indole localization in lipid membranes revealed by molecular simulation. *Biophysical Journal*, 91, 2046-54.

- NORTHRUP, S. H., PEAR, M. R., LEE, C. Y., MCCAMMON, J. A. & KARPLUS, M. (1982) Dynamical theory of activated processes in globular proteins. *Proceedings of the National Academy of Sciences of the United States of America*, 79, 4035-9.
- PANDIT, S. A., CHIU, S. W., JAKOBSSON, E., GRAMA, A. & SCOTT, H. L. (2007) Cholesterol surrogates: a comparison of cholesterol and 16:0 ceramide in POPC bilayers. *Biophysical Journal*, 92, 920-7.
- PANDIT, S. A., CHIU, S. W., JAKOBSSON, E., GRAMA, A. & SCOTT, H. L. (2008) Cholesterol packing around lipids with saturated and unsaturated chains: a simulation study. *Langmuir*, 24, 6858-65.
- PANGALI, C., RAO, M. & BERNE, B. J. (1979) A Monte Carlo simulation of the hydrophobic interaction. *Journal of Chemical Physics*, 71, 2975-81.
- PASENKIEWICZ-GIERULA, M., ROG, T., KITAMURA, K. & KUSUMI, A. (2000) Cholesterol effects on the phosphatidylcholine bilayer polar region: a molecular simulation study. *Biophysical Journal*, 78, 1376-89.
- PASTOR, R. W., VENABLE, R. M. & FELLER, S. E. (2002) Lipid bilayers, NMR relaxation, and computer simulations. *Accounts of Chemical Research*, 35, 438-446.
- PITMAN, M. C., SUITS, F., MACKERELL, A. D., JR. & FELLER, S. E. (2004) Molecular-level organization of saturated and polyunsaturated fatty acids in a phosphatidylcholine bilayer containing cholesterol. *Biochemistry*, 43, 15318-28.
- PLIMPTON, S. (1995) Fast parallel algorithms for short-range molecular dynamics. *Journal of Computational Physics*, 117, 1-19.
- PLIMPTON, S., CROZIER, P. & THOMPSON, A. (2001) Large-scale atomic/molecular massively parallel simulator (Available at <http://lammps.sandia.gov>). IN PLIMPTON, S. (Ed.) 2001 ed. Albuquerque, New Mexico, USA, Sandia National Laboratories, US Department of Energy.



- POHORILLE, A., CIEPLAK, P. & WILSON, M. A. (1996) Interactions of anesthetics with the membrane-water interface. *Chemical Physics*, 204, 337-45.
- POHORILLE, A. & WILSON, M. A. (1996) Excess chemical potential of small solutes across water--membrane and water--hexane interfaces. *Journal of Chemical Physics*, 104, 3760-73.
- REBERTUS, D. W., BERNE, B. J. & CHANDLER, D. (1979) A molecular dynamics and Monte Carlo study of solvent effects on the conformational equilibrium of n-butane in carbon tetrachloride. *Journal of Chemical Physics*, 70, 3395-400.
- ROGERS, J. A. & DAVIS, S. S. (1980) Functional group contributions to the partitioning of phenols between liposomes and water. *Biochimica et Biophysica Acta*, 598, 392-404.
- RYTTING, J. H., HUSTON, L. P. & HIGUCHI, T. (1978) Thermodynamic group contributions for hydroxyl, amino, and methylene groups. *Journal of Pharmaceutical Sciences*, 67, 615-18.
- SCHERER, P. G. & SEELIG, J. (1989) Electric charge effects on phospholipid headgroups. Phosphatidylcholine in mixtures with cationic and anionic amphiphiles. *Biochemistry*, 28, 7720-8.
- SCHRODINGER, L. (1991-2000) Jaguar. 6.0 ed. New York, NY, Schrodinger, LLC.
- SEELIG, J. & GANZ, P. (1991) Nonclassical hydrophobic effect in membrane binding equilibria. *Biochemistry*, 30, 9354-9359.
- SEELIG, J. & WAESPE-SARCEVIC, N. (1978) Molecular order in cis and trans unsaturated phospholipid bilayers. *Biochemistry*, 17, 3310-5.
- SENGUPTA, D., SMITH, J. C. & ULLMANN, G. M. (2008) Partitioning of amino-acid analogues in a five-slab membrane model. *Biochimica et Biophysica Acta*, 1778, 2234-43.

- SHINODA, W., MIKAMI, M., BABA, T. & HATO, M. (2004) Molecular dynamics study on the effects of chain branching on the physical properties of lipid bilayers: 2. Permeability. *Journal of Physical Chemistry B*, 108, 9346-9356.
- STERN, H. A. & FELLER, S. E. (2003) Calculation of the dielectric permittivity profile for a nonuniform system: Application to a lipid bilayer simulation. *Journal of Chemical Physics*, 118, 3401-3412.
- STOUCH, T. R. (1997) Solute transport and partitioning in lipid bilayers. Molecular dynamics simulations. *Progress in Colloid & Polymer Science*, 103, 116-120.
- STOUCH, T. R. (2000) Understanding membrane permeation through simulation. *Book of Abstracts, 219th ACS National Meeting, San Francisco, CA, March 26-30, 2000*, PHYS-174.
- STOUCH, T. R., ALPER, H. E. & BASSOLINO, D. (1995a) Simulations of drug diffusion in biomembranes. *ACS Symposium Series*, 589, 127-38.
- STOUCH, T. R. & BASSOLINO, D. (1996) Movement of small molecules in lipid bilayers: molecular dynamics simulation studies. *Biological Membranes*, 255-278, 1 plate.
- STOUCH, T. R., BASSOLINO, D. & ALPER, H. (1995b) Biomembrane/water interfaces: Water structure and solute transport and partitioning by computer simulation. *Book of Abstracts, 210th ACS National Meeting, Chicago, IL, August 20-24*, COLL-047.
- STOUCH, T. R., BASSOLINO, D. & DAVIS, M. (1996) Chemical functional group contribution to the free energy of membrane permeation by atomic-level molecular dynamics simulation. *Book of Abstracts, 212th ACS National Meeting, Orlando, FL, August 25-29*, COMP-016.
- STOUCH, T. R., BASSOLINO, D. & DAVIS, M. (1997) Molecular dynamics simulation studies of solute permeation of lipid bilayers. *Book of Abstracts, 214th ACS National Meeting, Las Vegas, NV, September 7-11*, PHYS-173.

- STOUCH, T. R., WARD, K. B., ALTIERI, A. & HAGLER, A. T. (1991) Simulations of lipid crystals: characterization of potential energy functions and parameters for lecithin molecules. *Journal of Computational Chemistry*, 12, 1033-46.
- TEJWANI, R. W. & ANDERSON, B. D. (2008) Influence of intravesicular pH drift and membrane binding on the liposomal release of a model amine-containing permeant. *Journal of Pharmaceutical Sciences*, 97, 381-399.
- TEJWANI, R. W., STOUCH, T. R. & ANDERSON, B. D. (2009) Substituent effects on the ionization and partitioning of *p*-(aminoethyl)phenols and structurally related compounds. Electrostatic effects dependent on conformation. *Journal of Pharmaceutical Sciences*, Accepted for publication.
- TORRIE, G. M. & VALLEAU, J. P. (1977a) Monte Carlo study of a phase-separating liquid mixture by umbrella sampling. *Journal of Chemical Physics*, 66, 1402-8.
- TORRIE, G. M. & VALLEAU, J. P. (1977b) Nonphysical sampling distributions in Monte Carlo free energy estimation: Umbrella sampling. *Journal of Computational Physics*, 23, 187-199.
- TRISTRAM-NAGLE, S., PETRACHE, H. I. & NAGLE, J. F. (1998) Structure and interactions of fully hydrated dioleoylphosphatidylcholine bilayers. *Biophysical Journal*, 75, 917-925.
- TU, K., TAREK, M., KLEIN, M. L. & SCHARF, D. (1998) Effects of anesthetics on the structure of a phospholipid bilayer: molecular dynamics investigation of halothane in the hydrated liquid crystal phase of dipalmitoylphosphatidylcholine. *Biophysical Journal*, 75, 2123-34.
- ULANDER, J. & HAYMET, A. D. (2003) Permeation across hydrated DPPC lipid bilayers: simulation of the titrable amphiphilic drug valproic acid. *Biophysical Journal*, 85, 3475-84.
- VALKO, K., DU, C. M., BEVAN, C. D., REYNOLDS, D. P. & ABRAHAM, M. H. (2000) Rapid-gradient HPLC method for measuring drug interactions with

- immobilized artificial membrane: comparison with other lipophilicity measures. *Journal of Pharmaceutical Sciences*, 89, 1085-96.
- WILFRED F. VAN GUNSTEREN, X. D. ALAN E. M. (2002) Computation of free energy. *Helvetica Chimica Acta*, 85, 3113-3129.
- WIMLEY, W. C., CREAMER, T. P. & WHITE, S. H. (1996) Solvation energies of amino acid side chains and backbone in a family of host-guest pentapeptides. *Biochemistry*, 35, 5109-24.
- WIMLEY, W. C. & WHITE, S. H. (1993) Membrane partitioning: distinguishing bilayer effects from the hydrophobic effect. *Biochemistry*, 32, 6307-12.
- WOODS, M. C., HAILE, J. M. & O'CONNELL, J. P. (1986) Internal structure of a model micelle via computer simulation. 2. Spherically confined aggregates with mobile head groups. *Journal of Physical Chemistry*, 90, 1875-1885.
- XIANG, T.-X. & ANDERSON, B. D. (1994a) Molecular distributions in interphases: statistical mechanical theory combined with molecular dynamics simulation of a model lipid bilayer. *Biophysical Journal*, 66, 561-72.
- XIANG, T.-X. & ANDERSON, B. D. (1994b) The relationship between permeant size and permeability in lipid bilayer membranes. *Journal of Membrane Biology*, 140, 111-22.
- XIANG, T.-X. & ANDERSON, B. D. (1994c) Substituent contributions to the transport of substituted *p*-toluic acids across lipid bilayer membranes. *Journal of Pharmaceutical Sciences*, 83, 1511-18.
- XIANG, T.-X. & ANDERSON, B. D. (1999) Molecular dissolution processes in lipid bilayers: A molecular dynamics simulation. *Journal of Chemical Physics*, 110, 1807-1818.

XIANG, T.-X. & ANDERSON, B. D. (2002) A computer simulation of functional group contributions to free energy in water and a DPPC lipid bilayer. *Biophysical Journal*, 82, 2052-66.

XIANG, T.-X. & ANDERSON, B. D. (2006) Liposomal drug transport: A molecular perspective from molecular dynamics simulations in lipid bilayers. *Advanced Drug Delivery Reviews*, 58, 1357-1378.

XIANG, T.-X., XU, Y. H. & ANDERSON, B. D. (1998) The barrier domain for solute permeation varies with lipid bilayer phase structure. *Journal of Membrane Biology*, 165, 77-90.

Copyright © Ravindra W. Tejwani 2009

## **CHAPTER SIX: Specific intermolecular solute-bilayer interactions as determined by MD simulations: Factors responsible for the locations of the transport barrier and the preferred binding regions**

### **Introduction**

In chapter five MD simulations were utilized to identify the locations of the preferred binding and the barrier for the solute transport. Additionally, the functional group contributions to solute transfer from water to these locations in the lipid bilayer were found to coincide with those measured experimentally using either membrane binding or bulk hydrocarbon water partitioning as surrogates for these processes. In this chapter, the microscopic events that underscore these two phenomena are explored with the the aim of understanding the mechanisms of solute retention and transport through the bilayer.

### ***Microscopic environments in the lipid bilayer***

The microscopic dynamics of the lipid bilayer membrane structure have been studied extensively using MD simulations. It has been established that the presence of the lipid bilayer head groups perturbs the structure of the nearby water. This perturbed water has properties different from that of “bulk water”. In the case of fully hydrated bilayers, this perturbed water region extends to approximately 10 angstroms (Alper et al., 1993a, Alper et al., 1993b) from the average location of the phosphorus atoms or the peak of the electron density profile. The functional group and atom distributions as a function of depth within the bilayer reported in various simulation studies (Chiu et al., 1999a, Rosso and Gould, 2008, Chiu et al., 1999b, MacCallum and Tieleman, 2006, Bemporad et al., 2005) have also confirmed that the number of water molecules starts decreasing from its plateau in the bulk water region at approximately 10 angstroms from the interface.

The subsequent region is relatively high in density and contains polar functional groups with hydrogen bond bridging facilitated by water molecules (Pasenkiewicz-Gierula et al., 1997, Bhide and Berkowitz, 2005, Alper et al., 1993b). MD simulations of

DMPC membranes in their liquid crystalline state (Pasenkiewicz-Gierula et al., 1997) have indicated that on average each DMPC molecule forms 5.3 hydrogen bonds with 4.5 water molecules. Of these hydrogen bonds, four are formed by phosphoryl oxygen atoms and one with a carbonyl oxygen atom. Approximately 70% of the head groups are linked to other head groups via water bridges to form clusters of two to seven head groups each. This type of strong interconnected network among the head groups suggests significantly reduced mobility in this region. The choline groups on the other hand are divided between two regions: those located on the outside of the phosphate groups and those located on the inside of the phosphate groups as seen in the NMR experiments by Scherer et al (Scherer and Seelig, 1989). This functional group is interesting in that it carries a net positive charge on the nitrogen atom while it is covered by methyl and methylene groups. This quality probably imparts a character which explains its distribution on both sides of the average phosphate group location.

The high order of the head groups is transmitted to the lipid chains that are covalently bonded to them. This order in the lipid chains gradually drops to a hydrocarbon like environment at the center of the bilayer. The region of the chains close to the carbonyl groups has been referred to as the high density chain region or the ordered chain region. The combined region containing the carbonyl groups and the ordered chains has been proposed as the site of binding for amphiphilic solutes (Xiang and Anderson, 2006) in liposomal drug delivery systems. The ordered chain region tends to be longer in lipids with saturated hydrocarbon tails, while for lipids like DOPC, which contain a double bond, it is truncated. As a result, DOPC bilayers exist in the liquid crystalline state (as opposed to gel state) at relatively low temperatures.

The increased chain ordering in the ordered chain region also leads to an unfavorable contribution to solute partitioning which is also sensitive to the size of the solute. This phenomenon has been termed “non-classical hydrophobicity” or “bilayer effect” (Katz and Diamond, 1974, Seelig and Ganz, 1991, Wimley and White, 1993, Xiang and Anderson, 1994, DeVido et al., 1998). Owing to its proximity to the hydrophilic groups and their hydrating water, this region is also susceptible to the periodic intrusion of water molecules, referred to as “water wires” or “water fingers”.

These strands of water molecules which penetrate the ordered chain region are linked via hydrogen bonds to the polar head group region (Bemporad et al., 2005, Ulander and Haymet, 2003, Venable and Pastor, 2002). Finally, near the center of the bilayer the lipid chains exhibit the most mobility and the least order. This characteristic makes the bilayer center quite similar to a liquid hydrocarbon environment.

### *Solute-bilayer interactions at a microscopic level*

From the above review of the microscopic environments in lipid bilayer membranes and from the partition coefficient profiles of a variety of solutes reported in the literature, some general conclusions can be drawn regarding solute partitioning in various regions of the bilayer. Generally, the hydrophobicity of the solute is one of the determinants. Since some regions of the bilayer are ordered, the additional determinants are the size and shape of the solute. The size effect has been described above as the non-classical hydrophobic effect, whereas the shape effect can be seen from the relative permeability coefficients (indicative of the partition coefficient in the barrier domain) of straight chain and the branched chain carboxylic acids (Xiang and Anderson, 1998). Finally, the polar interactions in the head group region can be conceived to be an additional factor.

Based on the consideration of the determinants above, the solute partitioning profiles can be grouped into different classes. Small and large hydrophobic solutes partition preferentially into the acyl chain regions. Small hydrophobic solutes exhibit a relatively gradual increase in their concentration with depth going from the ordered chain region to the center of the bilayer, whereas the large solutes show a steeper gradient. Examples include the MD simulations of methane, ethane, butane, and hexane (Stouch, 1998, Bemporad et al., 2004, MacCallum et al., 2008). These profiles have been rationalized based on the classical hydrophobic effect giving rise to low solubility in water and high solubility in acyl chains. Small polar solutes on the other hand may show opposite profiles where the barrier is in the hydrocarbon region. An often studied example of this is the profile of water (Marrink and Berendsen, 1994, Shinoda et al., 2004, Bemporad et al., 2004). Finally amphiphilic solutes having both polar and non-



polar regions exhibit concentration versus bilayer depth profiles that reflect the balance of the contributions of their polar and non-polar sides to their relative affinity for various regions, while shape and size determine the steepness of the gradient from the ordered chain region to the bilayer center. Generally, amphiphilic solutes show preferred binding in the head group region as shown by adamantane derivatives (Li et al., 2008, Chew et al., 2008), the camptothecin analog DB-67 (Xiang and Anderson, 2006), and several others (Mukhopadhyay et al., 2004, MacCallum et al., 2008). Most of these studies attribute the preference for this region to the simultaneous solubilization of the hydrophobic and hydrophilic regions of solute in the corresponding two adjacent regions of the bilayer (amphiphilic complementarity). A closer analysis of this region in all studies reporting the partition coefficient profiles shows that while the maximum partition coefficient occurs near the carbonyl groups, the lowering of the free energy profiles begins about 10 to 15 angstroms further away from this region towards water. Therefore, besides amphiphilic complementarity, other microscopic factors may exist that are responsible for the increased partition coefficient.

A contribution of water to the solute bilayer interactions in the interior of the bilayer has been invoked several times in the literature. The presence of water wires was invoked initially in simulations of ion transport (Marrink et al., 1996, Wilson and Pohorille, 1996), but more recently their spontaneous occurrence has been reported in MD simulations of small polar solutes such as acetic acid in the bilayers (Bemporad et al., 2005). While water wires have been reported in several simulations, it is not clear if they significantly impact the partition coefficients in either the ordered chain region or in the center of the bilayer. It remains to be determined if water entry into the bilayer is induced by the solute or if water enters the bilayer irrespective of the presence of the solute.

While the solute size and the shape are widely acknowledged to be determinants of the partitioning profile, the solute orientation in the lipid bilayer has received lesser consideration as a factor in the reported MD simulation studies. The amphiphilic complementarity hypothesis suggested above would require that preferred orientations of the solute exist in the preferred binding region. The idea that unsymmetrical molecules

will orient at an interface is very well accepted in the study of interfacial phenomena (Martin, 1993) and is obviously the underlying mechanism for the structure of the bilayer itself. MD simulations have shown that water has a tendency to orient one of its OH bonds towards the vapor phase (Wilson et al., 1987) while the other points towards the bulk. Since lipid bilayers contain regions of varying environments, the solute orientation at each of these interfaces is explored in this study. Since the approaches to study the solute orientations have not been discussed in the literature a method is proposed for the same. A systematic analysis of how this can impact the partition coefficient profile or a free energy profile has also been presented.

Similar to the solute orientations, the solute conformation may also play an important role in the partitioning into the lipid bilayer. The MD simulations of the beta blockers demonstrate different preferred dihedral angles inside and outside the lipid bilayer (Bemporad et al., 2005). It is conceivable that this can be an important factor for the partitioning of large solutes, and relatively insignificant for small solutes such as butane. Since the solutes used in this study lie between these two examples, this property is also explored to understand if the ethyl chain dihedrals impact the free energy profiles of these solutes.

### **Methods and theoretical**

The description of the systems simulated and the MD simulation method was provided in chapter five along with the post-processing methods to obtain the free energy profiles. The investigations of the specific interactions were carried out using locally written scripts to mine the atom location data saved during the MD simulation runs. The Perl (Wall, 2004) programming language was used for writing these scripts. In order to accomplish the plane and vector geometry related calculations needed for the tasks described below, Perl was supplemented with two additional modules: Math-VectorReal (Thyssen, 2001) and Trigonometric functions (Hietaniemi and Manfredi, 1997).

### ***Hydrogen bond interactions***

For each polar group of each of the solute copies, the hydrogen bond interactions were searched and tabulated for the entire simulation data set. Since there are about 20000 atoms present in each configuration and there are tens of thousands of configurations, the total number of distance computations had to be minimized for efficiency as described below. For each saved configuration, the atoms in the simulation box were classified into smaller 3.2 angstrom cubic boxes. The cubic box containing the heavy atom of the solute polar functional group was identified along with all its neighboring boxes in all 3 dimensions. The atoms inside these cubic boxes were then checked for hydrogen bonding groups and their distances from the heavy atom of the polar functional group of the solute were calculated. If the distance was found to be less than 3.2 angstroms (Stouch, 1998), the interaction was defined as a hydrogen bond and was subsequently tabulated into an appropriate category. In the case of water, the interaction was further classified as a bond with the water oxygen atom or as a bond with the water hydrogen atom. If the hydrogen atom of the polar functional group was found between the heavy atom of the solute and the water oxygen atom, it was classified as a water-O type hydrogen bond. Otherwise it was classified as water H-type of hydrogen bond. The counts were accumulated for each hydrogen bond type occurring in each 0.3 angstrom slice of the simulation box along with the average distance between the heavy atoms to calculate the average bond length.

### ***Solute orientation with respect to the bilayer***

#### ***1. Calculation of the orientation angles***

The angle made by the unit longitudinal vector of the solute with a unit normal vector (a unit vector starting at the central plane of the bilayer and perpendicular to the plane) was calculated for each solute copy at each time step of the simulation. The angle of the longitudinal vector of the solute set to zero when the aromatic carbon attached to the ethyl chain of a solute copy in the bilayer pointed towards the central plane of the bilayer and the opposite carbon on the same ring pointed towards water. Due to symmetry across the central plane of the bilayer, the coordinates of the solute copies

present in the two leaflets were transformed from box coordinates to relative coordinates before the angle was calculated. The solute copies present near the center were assigned to the leaflet that had the central atom of the solute present. The central atom is the aromatic atom of the solute molecule attached to the ethyl chain.

## 2. Calculation of the orientation angle probability

Assume that the unit normal vector and the unit longitudinal vector of the solute are present along the radii of a sphere with their tails at the center and the heads at the surface. The probability of occurrence of an angle of  $0^\circ$  to  $\theta^\circ$  between the two vectors would be proportional to the surface area of the spherical cap that is specified by the rotation of the solute vector around the normal vector (Figure 6-1). The surface area of a spherical cap is given as (Weisstein, 1999)

$$Area = 2\pi R h \quad (6-1)$$

where R is the radius of the sphere and h is the height of the cap. From trigonometry, one obtains

$$h = R - R \cos \theta \quad (6-2)$$

Since both the solute longitudinal vector and the bilayer normal vector are unit vectors, the value of R is 1. The probability of the occurrence of the angle is then given as

$$P(\theta) \propto 1 - \cos \theta \quad (6-3)$$

Therefore the probability of the occurrence of an angle between  $\theta_1$  and  $\theta_2$  is given as

$$P(\theta_2 - \theta_1) \propto |\cos \theta_1 - \cos \theta_2| \quad (6-4)$$

Normalizing to the full range of  $0^\circ$  to  $180^\circ$  angles it can be shown that there is an equal probability of occurrence (20%) for each of the following five windows of angles:

0°-53.1°, 53.1°-78.44°, 78.44°-101.51°, 101.51°-126.84°, and 126.84°-180°. Therefore the solute orientations were tabulated according to these criteria to obtain counts of occurrence in these five classes that would have equal probability of occurrence in an isotropic environment such as bulk water.

### *Measurement of solute dihedral angles*

The first and the second dihedral angles of the ethyl chain of the three solutes were calculated for each solute copy at each time step and were classified into six equal probability bins of 60° width. The angle counts in each bin were stored for each 0.3 angstrom slice of the lipid bilayer over the entire simulation run. The dihedral angles were calculated as the angle between two planes- the first made by the first three atoms of the dihedral and the second made by the last three atoms of the dihedral.

### *Visualization of the simulation coordinates*

The simulation snapshots were visualized using DS ViewerPro (Accelrys, 2005) on a Lenovo T61 computer with Intel T7300 CPU running Windows XP Professional SP2.

## **Results**

The free energies of transfer for each of the three solutes from water to various bilayer locations, obtained in the previous chapter, are shown in Figure 6-2. As a recap, all three solutes show a preferred binding region (approximately 5 to 6 kcal per mole) with a minimum in the free energy located near the location of the carbonyl groups of the oleoyl chains, and a barrier region (approximately -3 to 2 kcal per mole) with a maximum in the free energy located at the center of the bilayer. The relative locations of various functional groups of the lipid bilayer are also shown in Figure 6-3. It is noteworthy that while the number of water molecules present in each 0.3 angstrom slice of the simulation box is significantly less near the head groups as compared to that in the bulk, water molecules still outnumber the lipid head groups. Near the carbonyl groups, there are two water molecules for every molecule of DOPC. The larger scale plot in Figure 6-3 (left hand side) shows that while the distributions of the other lipid head group atoms decrease

to zero as one approaches the center of the bilayer, the number of water molecules asymptotically approaches a very low value of 0.005 per 0.3 angstrom slice. The question as to whether this frequency of water intrusion into the center of the bilayer is a property of water itself or is induced by the solutes is discussed later.

Figure 6-4 shows the entire simulation cell with atoms colored by their respective partial charges. Since the only atoms with charges to the extreme of the scale are the choline nitrogen atoms and the phosphate oxygen atoms, they distinguish the head group region in the picture. Hydrogen atoms of the alkyl groups that carry a slight positive charge appear light pink and the carbon atoms and the oxygen atoms appear pink and red as they carry the incremental levels of negative charges. Overall, it appears that the functional groups with significant charge are limited to the head groups and the interior of the bilayer is slightly positive to negative charged.

### ***Hydrogen bond interactions***

The numbers of hydrogen bonds formed by the polar functional groups of the solutes as a function of the distance from the center of the bilayer are plotted in Figure 6-5. As a guide, the top panel displays the distribution of lipid bilayer functional groups as a function of distance from the center of the bilayer. The number of hydrogen bonds in the bulk water region is at a plateau and then it declines in the head group region before reaching zero at the center of the bilayer for phenylethylamine, tyramine amine, tyramine phenol, and 4-ethylphenol. In general, the tyramine phenol and 4-ethylphenol form a greater number of hydrogen bonds than the tyramine amine and phenylethylamine. Additionally, the variability around the number of bonds is also significant for all four functional groups irrespective of the region in which they are located. Finally, the location of the bond shown in the figures is the location of the aromatic carbon attached to the ethyl chain, whereas the polar functional groups are located at the extremes of the solute molecules. Therefore, the actual hydrogen bond may be located 2 to 5 angstroms away from the location indicated in the plot.

Figure 6-6 through 6-14 show the number of hydrogen bonds formed by each of the four solute functional groups discussed above with: the oxygen atom of the outer

phosphoether, the phosphoryl oxygen atom, the inner phosphoether oxygen atom, the 2-oleoyl ether oxygen atom, the 2-oleoyl carbonyl oxygen atom, the 1-oleoyl ether oxygen atom, 1-oleoyl carbonyl oxygen atom, the water oxygen atom, and the water hydrogen atom. Finally, Figure 6-15 shows the number of configurations observed without any hydrogen bonds for each of the four solute functional groups.

As a general trend, the ether oxygen atoms of the phospholipid form fewer hydrogen bonds with the solutes than the corresponding  $sp^2$  oxygen atoms on the corresponding phosphoryl or carbonyl groups. The phenol functional groups of the solutes form approximately 10 times more hydrogen bonds with the phosphoryl oxygen atoms in the head group region than with the phosphoether oxygen atoms. A similar trend could not be quantified with the amino groups as they do not form a significant number of hydrogen bonds with either type of oxygen atom of the head groups. Similarly, the carbonyl oxygen atoms form a several-fold greater number of hydrogen bonds with the solute polar groups than the corresponding ether oxygen atoms. The solute phenol groups form a greater number of hydrogen bonds than the solute amine groups. The number of hydrogen bonds formed by the amine functional groups of the solutes with the carbonyl oxygen atoms is slightly greater than that with the phosphoryl oxygen atoms.

Finally, the number of hydrogen bonds with oxygen and hydrogen atoms of water shows a trend similar to the number density of water atoms shown in Figure 6-3. Compared with any other type of hydrogen bond interactions described above, the number of hydrogen bonds formed with water is much greater in each of the regions including the bilayer interior. As a reminder, all references to the locations in the bilayer correspond to the location of the aromatic carbon near the center of the solute and the actual hydrogen bond may occur 2 to 5 angstroms away depending on the solute orientation.

Figures 6-16 through 6-25 show the average distances between the heavy atoms (e.g. oxygen to oxygen) for each of the hydrogen bond types described above. While a distance criterion of less than 3.2 angstroms was used for detection of hydrogen bonds,

very few were found to exceed 3.0 angstroms. From a broader perspective, all hydrogen bond types retain their respective characteristic average length through the entire depth of the bilayer and in the water regions. Generally, fluctuations are seen in the lengths of ether oxygen related bonds which could be due to the overall fewer observations for this type of bond, or due to the weakness of the interaction itself.

The lengths of the bonds formed with water molecules are consistent for all four functional groups and show a slight decrease in length in the bilayer interior. The amine functional groups show a longer bond length than the phenol functional groups of the solutes (approximately 3 angstrom vs. 2.8 angstrom).

### ***Solute orientation with respect to the bilayer***

The orientation of each solute copy was measured in reference to the vector perpendicular to the plane of the bilayer (the normal) that has its tail at the center of the bilayer and it points towards the head groups. The angle made by the solute longitudinal vector (head at the benzene ring and tail at the ethyl chain) with the normal was recorded as the orientation angle. The fraction of solute orientations found in each of the following five classes:  $0^{\circ}$ - $53.1^{\circ}$ ,  $53.1^{\circ}$ - $78.44^{\circ}$ ,  $78.44^{\circ}$ - $101.51^{\circ}$ ,  $101.51^{\circ}$ - $126.84^{\circ}$ , and  $126.84^{\circ}$ - $180^{\circ}$  are shown as a function of distance from the center of the bilayer in Figures 6-26, 6-27, and 6-28 for 4-ethylphenol, phenylethylamine, and tyramine, respectively. Unlike other figures, only one leaflet of the bilayer is shown with the center of the bilayer at the left and the water region on the right hand side.

All three solutes show a probability of 20% for each of the five orientations in the bulk water and in the center of the bilayer suggesting that there is free rotation of solutes in these regions. Deviations from equal proportions in water occur near a 30 angstrom distance from the center of the bilayer. This location is consistent with the perturbations observed in the free energy profiles (Figure 6-1) and the number of water molecules per slice in the atom distribution across the unit cell (Figure 6-3).

All three solutes approach the lipid bilayer from bulk water preferably with their aromatic portions pointing towards it, that is, at an angle of about  $180^{\circ}$  with the bilayer



normal. Other similar orientations also occur in significant proportions in this region. In the case of 4-ethylphenol, this occurs at the expense of the opposite orientations, whereas in the case of phenylethylamine it occurs at the expense of the 90° orientation that would be parallel to the bilayer plane. For tyramine, it occurs at the expense of both the opposite as well as the parallel orientations.

All three solutes exhibit an increase in the 90° orientation near the head group region (20 angstroms from the center of the bilayer) close to the average location of phosphorus atoms. This orientation peaks slightly on the inside of the interface for 4-ethylphenol whereas for phenylethylamine and tyramine it almost coincides with the 20 angstrom location of the head groups. In the case of tyramine this 90° orientation, parallel to the bilayer plane, is the most abundant orientation over a brief span at the expense of the 0° and 180° orientations.

On the inside of the head groups and continuing into the ordered chain region, the three solutes differ significantly in their respective orientations. Tyramine and 4-ethylphenol show a strong preference for the 0° orientation (solute aromatic portion pointing towards the lipid head groups) in contrast to phenylethylamine which shows a strong preference for the 180° orientation (solute aromatic portion pointing towards the center of the bilayer). The extent of this preference for the 0° orientation in the hydrocarbon region peaks at 90% for 4-ethylphenol and tyramine. In the same location, the preference of phenylethylamine for the 180° orientation is only 60%. Therefore, in the ordered chain region, a complete flip of phenylethylamine is conceivable however it is much less likely for 4-ethylphenol and tyramine.

Near the center of the bilayer, all solutes again show the convergence of the five orientations to the baseline probability value of 20% suggesting the possibility of free rotation in this region. The values do not quite consistently reach this baseline value as compared with those in the bulk water, but all orientations show an approach towards this value.

In order to demonstrate relative proportions of solute orientations near the center of the bilayer, two representative trajectories from the 4-ethylphenol simulation are

shown in Figure 6-29. The location of solute (as distance from the center of the bilayer) versus the simulation time is shown in the upper panels and the corresponding solute orientation versus the simulation time is shown in the lower panels. It was found that the solute tends to change orientations frequently when in the center of the bilayer whereas it tends to retain the orientation when slightly off the center of the bilayer (in the ordered chain region).

### *Solute dihedral angles*

The  $0^\circ$ ,  $60^\circ$ ,  $120^\circ$ ,  $180^\circ$ ,  $240^\circ$ , and  $300^\circ$  angles for the first dihedral angle of the ethyl chain (shown in Figure 6-30) in each solute copy were monitored for their occurrence throughout the length of the MD simulation. The number of times each solute was found in a  $\pm 30^\circ$  window around this value was counted for each 0.3 angstrom slice of the simulation box. For the first dihedral, the  $0^\circ$  and  $180^\circ$  angles are degenerate and have a very low expectation of occurrence. All other angles are mutually degenerate with equal probability of occurrence. Despite this degeneracy, the conformers were separately monitored in order to capture any evidence of lack of mobility in any of the regions. The populations of each of these 6 angles for 4-ethylphenol, phenylethylamine, and tyramine as a function of distance from the center of the bilayer are shown in Figure 6-31, Figure 6-32, and Figure 6-33, respectively. The angles  $60^\circ$ ,  $120^\circ$ ,  $240^\circ$ , and  $300^\circ$  maintain a little over 20% occurrence in all regions of the simulation box, with the other two angles remaining below 2.5% each. For all solutes, the population of low occurrence angles increases from nearly zero in bulk water to about 2.5% in the head group region.

The  $0^\circ$ ,  $60^\circ$ ,  $120^\circ$ ,  $180^\circ$ ,  $240^\circ$ , and  $300^\circ$  angles for the second dihedral angle of the ethyl chain are shown in Figure 6-34. This set has two pairs that are equivalent or degenerate for tyramine and phenylethylamine:  $60^\circ$  and  $300^\circ$ ; and  $120^\circ$  and  $240^\circ$ . Since there is no amino group present in 4-ethylphenol, one of the hydrogen atoms was chosen for the designation of the angles and three degenerate pairs exist. Again, all dihedral angles were tracked independently irrespective of the degeneracy among them. The populations of each of these 6 angles for 4-ethylphenol, phenylethylamine, and tyramine as a function of distance from the center of the bilayer are shown in Figure 6-35, Figure

6-36, and Figure 6-37, respectively. For 4-ethylphenol, two sets of angles are apparent, those that show abundance of slightly over 30% each and those that show abundance of 0-3%. The occurrence of low abundance angles fluctuates to a higher value in the head group region.

The conformer populations, as expected, coincide for phenylethylamine and tyramine. The major conformer ( $180^\circ$ ) and the minor conformer ( $0^\circ$ ) exist at approximately 80% and 0% abundance. They both show opposite perturbations near the head group region, where the  $0^\circ$  conformer increases by a few percent and the  $180^\circ$  conformer decreases by a few percent. The next most probable abundances are the  $60^\circ$  and  $300^\circ$  angles which are near 5 to 10%. Finally, the  $120^\circ$  and  $240^\circ$  conformers occur at slightly above 0% and do not show a perturbation near the head group region.

## **Discussion**

### ***Transfer of solutes from water to the preferred binding region***

#### ***1. Free energy profiles in the preferred binding region***

The transfer of 4-ethylphenol, phenylethylamine, and tyramine from water to the preferred binding location corresponds to similar changes in the free energy of about -5 to -6 kcal per mole occurring at about 15 angstroms from the center of the bilayer (Figure 6-2). This location in the bilayer is close to the location of the carbonyl groups of the oleoyl chains. This decrease in free energy starts at the center of bilayer for tyramine and at approximately 5 angstroms from the center for 4-ethylphenol and phenylethylamine. On the other side of the head groups, the free energy continues increasing until reaching a plateau at 30 angstroms from the center of the bilayer for all three solutes. As a result, this free energy “well” extends to a greater length on the outside of the head groups than on the inside of the head groups.

#### ***2. Interactions in bulk water and the decrease in the free energy***

In bulk water (locations at a distance of greater than 30 angstroms from the center of the bilayer), all three solutes demonstrate the largest number of hydrogen bonds

compared with other regions of the bilayer (Figure 6-5). While the polar groups of the solutes are solvated with these hydrogen bonds, their non-polar portions remain in a cavity of surrounding water molecules. This classical hydrophobic effect is apparent in the simulation snapshots shown in Figures 6-38 and 6-39. None of the solutes exhibits any preferred orientations or perturbed populations of the dihedral angles in the bulk water region.

While it is conceivable that the strong hydrogen bonding ability of head groups may be one of the reasons for the lower free energy of the solute in this region, the number of hydrogen bonds formed by the solute in the head group region is almost the same as the number formed in bulk water. Additionally, an examination of the hydrogen bond counts by the head group type (Figures 5 through 15) suggests that none of the head group oxygen atoms forms as many hydrogen bonds with any of the solutes as do the water molecules. However, there is a reasonable proportion of configurations in the simulation in which the polar groups of solute formed no hydrogen bonds (Figure 6-15) when located in the head group region. Finally the number of water molecules still exceeds the number of lipid molecules in this region, reaching a value equal to that of the carbonyl groups in the vicinity of the carbonyl groups (Figure 6-3). Therefore the opportunity for the solute to hydrogen bond with water molecules remains relatively high. As a result, hydrogen bonding related changes are less likely to explain the lowering of the free energy (or increase of partition coefficient) in this region.

At 20 to 28 angstroms from the center, the classical hydrophobic effect mentioned above appears to be aided significantly by the presence of choline groups that can shield the hydrophobic parts of the solutes from the surrounding water. These phenomena captured in the MD simulations are shown in Figures 6-40 through 6-42. In each case, the benzene ring of the respective solute is shielded from the surrounding water molecules by choline methyl groups present nearby. This hydrophobic effect aided by the choline groups is probably the primary reason for the decrease in the free energy in this 20-28 angstrom region. Further support for this hypothesis comes from the fact that, irrespective of the presence of a polar group on the benzene ring, all three solutes prefer the 180° orientation in this region as shown in Figures 6-26 through 6-28. In this

orientation the benzene ring points towards the head groups while the rest of the solute is in water. The ethyl chain dihedrals of all three solutes show only small perturbations in this region and appear to have no significant role.

The ratio of populations of the preferred orientations over the disfavored orientations can be used to estimate the relative free energy penalty based on the Boltzmann equation (Adamson and Gast, 1997). For example the preferred orientation of 4-ethylphenol and tyramine is about 10 fold more favorable than the opposite orientation and corresponds to about 1.3 kcal per mole. The ratio for phenylethylamine in this region is about four, which corresponds to approximately 0.8 kcal per mole.

The orientations of 4-ethylphenol and tyramine show significant shuffling in the head group region (20 Angstroms from the center), such that all orientation populations return to approximately 20% for the former (Figures 6-26 and 6-28). Yet the free energies continue to decline monotonically (Figure 6-2). For tyramine, the 90° orientation (parallel to the plane of bilayer) exhibits about a 10% advantage over all others (Figure 6-28). It is in this orientation that both polar groups of tyramine have the opportunity to form hydrogen bonds with the head groups. Given the structured and dense nature of this region, this shuffling of orientations suggests a strong driving force for this effect. It is exactly in this region (near 20 angstroms from the center of the bilayer) that hexane, butane, ethane, and benzene show a slight barrier of 0.5 to 1 kcal (MacCallum and Tieleman, 2006, MacCallum et al., 2008, Bemporad et al., 2005) that has been attributed to the lack of free volume (MacCallum and Tieleman, 2006). Compared to these hydrophobes, the amphiphiles in the current study may be compensating for this barrier with a shift in the proportions of their orientations (almost by the same magnitude of energy). The amphiphiles, by way of re-orientation, also allow a “re-bridging” of the hydrogen bonds of the head group region in contrast to the hydrophobes that must disrupt them. As a result of this, the free energy profiles of the three solutes show a monotonic decline in free energy from bulk water to the minimum at 10 - 15 angstroms, with the exception of a small inflection in the case of tyramine that may indicate an imbalance in these two factors. This inflection in the profile of tyramine

may reflect its two polar functional groups and its slightly reduced non-polar surface area.

A rigid amphiphilic molecule that can not re-orient in this region may suffer a free energy penalty of a magnitude that depends on its size and on the (presumably very low) populations of its disfavored orientations.

### 3. Minimum in the free energy and start of the rise of the free energy barrier

Near the minimum in the free energy profile (i.e. the preferred binding region 15 angstroms from the center of the bilayer), all three solutes show almost equal proportions of two orientations: one that aligns a polar group with the outside polar environment and second that is tilted by approximately 45° from the first. This tilted orientation is actually favored over the aligned orientation in phenylethylamine and tyramine. Both orientations of each of the solutes are conducive to the amphiphilic complementarity of the environment that is frequently cited as a reason for the high partition coefficient in this region (Xiang and Anderson, 2006, MacCallum et al., 2008, Chew et al., 2008, Mukhopadhyay et al., 2004, Dickey and Faller, 2007). From the MD simulations, a snapshot of phenylethylamine in this region is shown in the aligned orientation (Figure 6-43) where it can form a hydrogen bond with the water molecules.

The departure from this region into the ordered chain region within the bilayer interior is energetically disfavored due to the loss of hydrogen bonding and the amphiphilic complementarity with the interface.

### ***Solutes in the hydrocarbon regions***

#### 1. The center of the bilayer

The chemical nature of the center of the bilayer is quite similar to that of a hydrocarbon and as a result relative partition coefficients in this region can usually be predicted using hydrocarbon water partition coefficients. The free energy differential from water to this region for the hydrophobes such as ethane, butane, and hexane is due to the classical hydrophobic effect. That for the amphiphiles is however due to two

opposing effects: the hydrophobic effect and the loss of hydrogen bonds to the polar functional groups. The importance of this balance in determining the partitioning behavior of the compounds has become apparent in the recent use of polar and non-polar surface areas of the solute molecules in construction of predictive LFER equations (S. H. Yalkowsky, 1976, Mayer et al., 2003, Cao, 2008).

Tyramine and 4-ethylphenol exhibit no strongly preferred orientations in this region (Figures 6-26 and 6-28) with only a slight bias towards the  $0^\circ$  orientation that has the aromatic ring pointing outwards. This could be a residual effect of the nearby ordered chain region (discussed below) and the preferred binding region (discussed above) where these orientations outnumber others by a large margin. Phenylethylamine (Figure 6-27) on the other hand shows a greater proportion of the  $0^\circ$  orientation, which is almost non-existent in the nearby ordered chain or the preferred binding regions. These two regions show a very strong preference for the opposite ( $180^\circ$ ) orientation. This complete flip of part of the phenylethylamine population coincides with the slight increase in the free energy on both sides of the central plateau (Figure 6-2).

In all three solutes, this slight preference of the benzene ring to point away from the center could likely be due to its interactions with the double bonds of the DOPC molecules providing some of the stabilization. As seen in Figure 6-44, the solutes located near the center of the bilayer have reasonable access to the double bonds of the oleoyl chains.

The central barrier for the solutes can extend as long as the solute polar groups are away from the influence of the interfacial region. It should be noted that the formation of water wires or any other solvation from intermittent water incursions into this region has a potential to reduce the width of this barrier. These topics are covered separately below.

## 2. The ordered chain region

Outside of the central region (5 to 15 angstroms from the center), the amphiphiles show a favorable free energy change whereas the hydrophobes show the opposite. As discussed above, the ordered chain region exhibits the non-classical hydrophobic effect,

whereby the partition coefficients of larger solutes are lower due to relatively greater entropic exclusion from this region. The tight packing of the acyl chains and the chain ordering effect lead to significantly lower free volume in this region. Again due to the difficulty of creating a cavity, all three solutes show preferred orientations in this region. About 90% of the population of tyramine and 4-ethylphenol exhibit a  $0^\circ$  orientation and the remaining orientations are a slightly tilted version of the same. The fraction of the opposite  $180^\circ$  orientation is virtually zero, however, assuming a 0.1 to 0.01% probability would translate to an energy differential of about 4 to 5 kcal per mole based on the Boltzmann factors. This is suggestive of the rapidity with which these solutes achieve their equilibrium orientation, and the magnitude of the potential penalty for a solute that may not be able to re-orient. Since the preferred orientations are a result of other interactions and not a cause by themselves, this energy estimate can be attributed to other underlying causes. In this case, it corresponds to the loss of hydrogen bonding for the hydroxyl group in going from the preferred orientation to the opposite and corresponds well with the free energy contribution of the hydroxyl group calculated in chapter five.

Phenylethylamine on the other hand is oriented preferentially (60%) in the  $180^\circ$  orientation (which has the polar functional group pointing outwards) with a slightly tilted version of the same having about 15% probability. The  $0^\circ$  orientation that is slightly preferred in the center (30%) is also seen at a 15% probability in this region. It is noteworthy that a sizeable proportion of the phenylethylamine population undergoes a complete flip between the ordered chain and central regions without reaching a significant level of the  $90^\circ$  orientation. This preference for the longitudinal orientations is consistent with the MD simulations by Xiang et al (Xiang and Anderson, 1999) which showed that the free volume in this region is elongated.

### 3. Solute re-orientation in the center and the ordered chain region

While rapid rotation is observed in the bulk water region, it is not certain if the solutes had an opportunity to sample all possible orientations in the ordered chain region. Since solutes were found to move in and out of the lipid bilayer slices (due to a very weak constraint force applied) it becomes difficult to construct correlation functions for



their orientation in a given slice of the bilayer. As an alternative, examination of the trajectories of the solutes in the ordered chain region presents an interesting dynamic (Figure 6-29). When the solutes are present in the center of the bilayer, they demonstrate the occurrence of all possible orientations, whereas, if they move to a location in the ordered chain region they exhibit a preferred orientation. As a result, it can be concluded that while the solute molecules did not demonstrate re-orientation in the ordered chain region, there were sufficient opportunities for all of their orientations to enter the ordered chain region, and only a select few actually entered. The application of a weak quadratic constraint allowed sufficient freedom for the solute molecules to exit the low mobility regions, change orientations, and return thereby providing adequate possibility to sample all orientations at all locations.

#### 4. Water wires and the effect of water entry on solute transfer energetics

Water wires and single water molecule incursions into the lipid bilayer have been shown to occur in the MD simulations by several laboratories (Venable and Pastor, 2002, Ulander and Haymet, 2003, Bemporad et al., 2005, Xiang and Anderson, 2006). Typical water wires of 2-3 water molecules solvating a solute in the bilayer interior are thought to last a few hundred picoseconds to nanoseconds, and re-appear fairly frequently. While the lifetime of such events was not monitored in this study, a review of the snapshots of the simulations did show such occurrences as outlined in Figures 6-45 and 6-46 where a solute molecule is located in the ordered chain region.

While such observations have been reported, it is not clear if the water incursions of this sort are dependent on the presence of the solute or would they have occurred in an independent MD simulation as well. A more important question is how such events impact the net energetics of solute partitioning into the barrier (if at all). The impact of such observations must be carefully interpreted in light of the fact that these studies, including the present study, use constraints to retain the solute in the lipid bilayer interior.

For an illustration, if water wires are assumed to increase the partition coefficient of the solutes in the lipid bilayer, this would increase the partition coefficient of water as well, resulting in a change in the free energy profile of water. Since the number of water

molecules available in each MD simulation run in this study was large and the studies were run for a reasonably long time, tens of thousands of configurations with over 3000 water molecules each enable the construction of a free energy profile for water of a reasonable quality using a population density analysis. These profiles computed from the simulations of 4-ethylphenol, tyramine, and phenylethylamine are shown in Figure 6-47. As can be seen, the three profiles differ only slightly from each other. Tyramine tends to allow greater ingress of water in the ordered chain region than the other two solutes as exemplified by a slightly narrower barrier region for water. Since the profiles are based on the water ingress observations throughout the MD simulation, the number of observations is very high at the extremes of the profile and very low at the center of the bilayer. If these configurations where water was present in the center of the bilayer (in the barrier region) were discarded, the free energy profile of the solute would remain unaltered. As a result, in the current MD simulation water ingress did not contribute significantly to the energy estimates for the solutes, though it may have impacted the width of the barrier region slightly. This however may be part of the normal occurrence and not an aberration.

A profile of water's free energy across a DPPC bilayer computed by Shinoda et al (Shinoda et al., 2004) has also been added to Figure 6-47 and appears to be very close to the profiles from solute MD simulations suggesting no significant impact. Other water profiles reported by Bemporad et al (Bemporad et al., 2004) and Marrink and Berendsen (Marrink and Berendsen, 1994) are also similar to these. Given that these profiles were side products and not the central intent of the MD simulations, it should be stressed the statistics are weak in the center and become weaker as the free energy increases. As a result, the peak shown by 4-ethylphenol at the center may be easily stunted if there were only a few more occurrences. However a possibility of 4-ethylphenol increasing the height of barrier for water can not be ruled out with the current data.

## **Conclusion**

The chemical structure of the solute molecules is expected to impact the location of the transport barrier and the preferred binding domains. In general, hydrophobes

encounter a barrier in the head group region and locate preferentially in the hydrocarbon region. Polar solutes encounter a barrier in the center and may not show a preferred binding region. Amphiphiles on the other hand exhibit preferred binding close to the carbonyl groups and whether they encounter a barrier in the center depends on the balance of the polar and non-polar parts in their structures.

Several specific interactions are important in determining the free energy profiles. Hydrogen bond formation with water is more prevalent even when a solute is present in the head groups. The amphiphiles and the polar molecules re-configure the hydrogen bond network of the head groups and therefore show no change in free energy profile that is attributable to their polar functional groups. Hydrophobic solutes in this region however disrupt the hydrogen bond network and therefore show an increase in the free energy. Partitioning to the center is determined by the balance of hydrogen bonding interactions and the classical hydrophobic effect. The solute size and shape are determinants of the non-classical hydrophobic effect exhibited in the ordered chain region, and are related through the ability of the solute to re-orient to optimize favorable interactions with the water and the polar head groups of the lipid. Therefore, a much larger solute may show reduced retention on the inside of the head groups than a smaller solute. Multiple polar functional groups on the solutes are likely to impact the magnitude of the unfavorable free energy in the barrier region more than they impact the magnitude of the free energy in the preferred binding region.

There is a possibility that unsaturated portions of the solute may have an affinity for the unsaturated portions of the acyl chains in the lipid bilayer. This effect is apparent from the preferred orientations that are opposite those expected from the exclusion effect of the ordered chain region, for all solutes near the center irrespective of the polar group on the benzene ring.

Water wires and other incursions appear to occur throughout the simulations; however, the analyses suggest that the free energy profile of water itself is hardly altered by the solutes constrained throughout the lipid bilayer. As a result, it is reasonable to

conclude that while these events occur, they may be a normal part of the water-bilayer interaction, or if solute induced, are too few to perturb the free energy calculations.

Finally, the solute dihedral angles, while important for much larger solutes are found to be of minimal significance for the three solutes in this study.

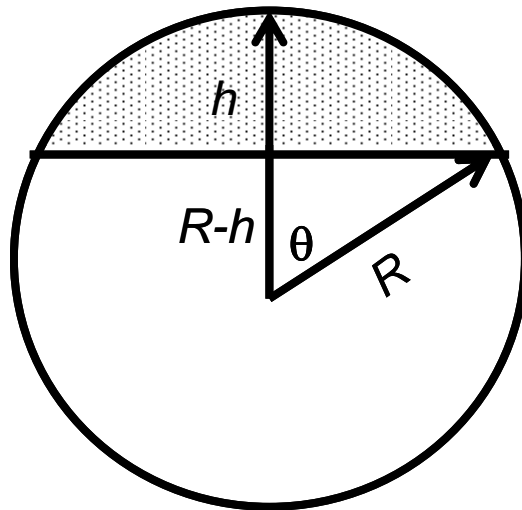


Figure 6-1. The unit normal vector (vertical arrow) and the unit longitudinal vector of the solute (arrow with label  $R$ ) at an angle  $\theta$ .  $R$  is the radius of the sphere and the spherical cap specified by the rotation of the solute vector around the normal vector is shown with dots.

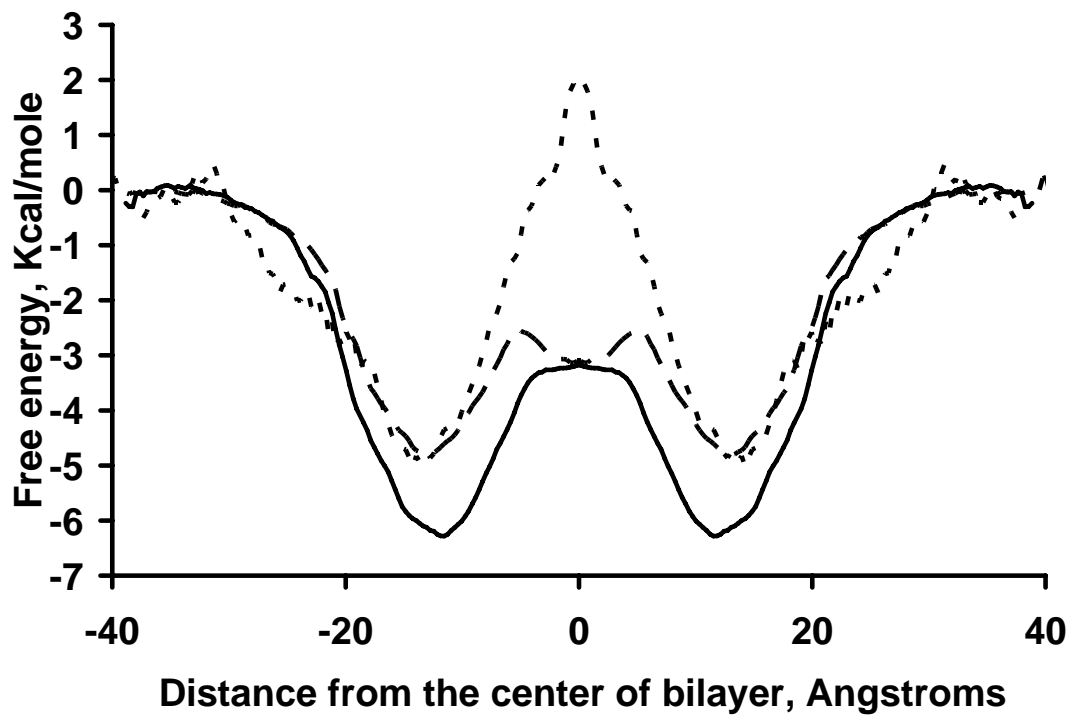


Figure 6-2. Free energy of solute transfer from water to various locations within the bilayer; •••• = tyramine, - - - - = phenylethylamine, — = 4-ethylphenol.

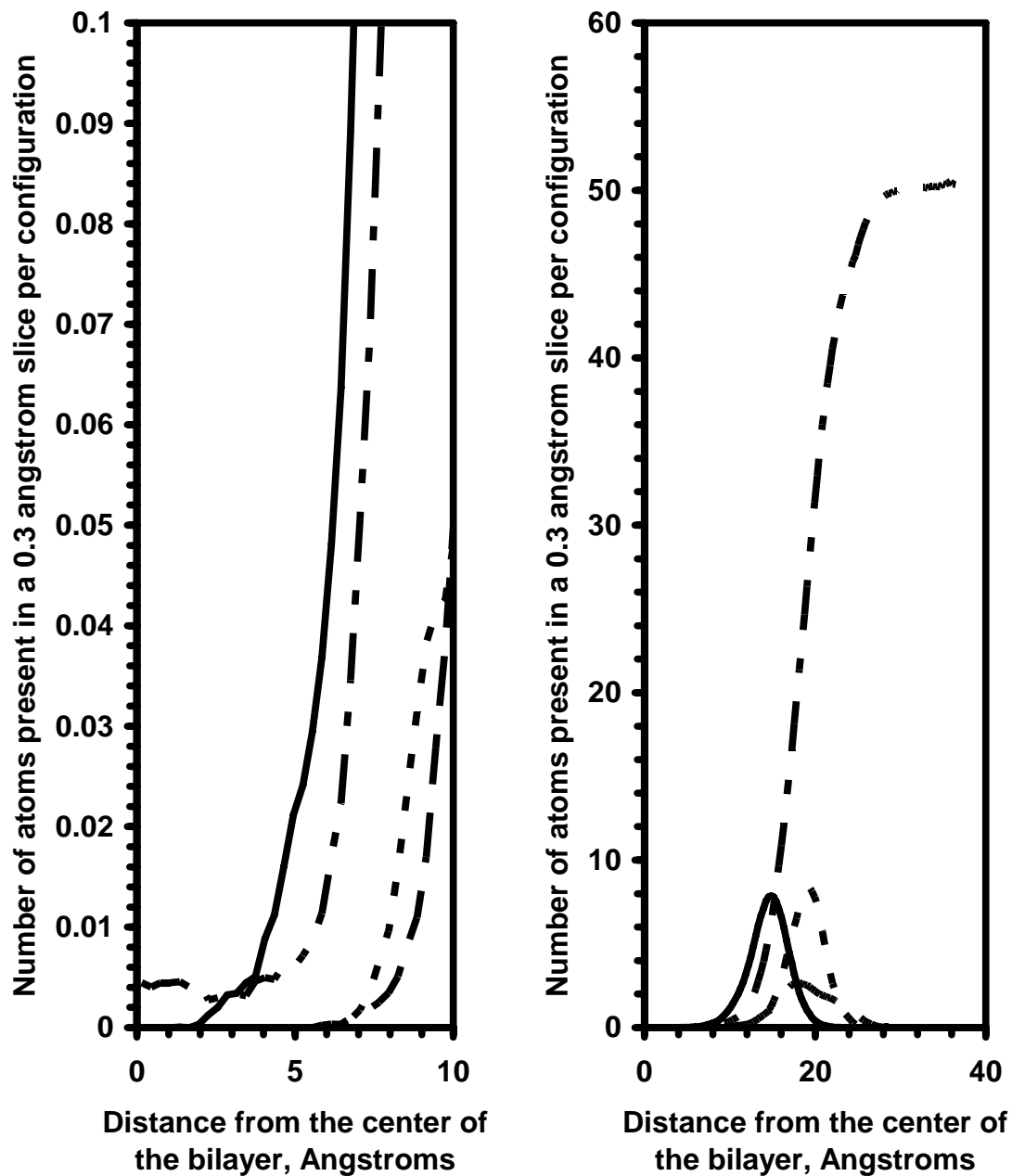


Figure 6-3. Distribution of the lipid bilayer functional groups: — = carbonyl oxygen, - - - = phosphoryl oxygen, - · - · - = choline nitrogen, - · - · - = water. The average number of functional units found in each 0.3 angstrom slice is shown. The left plot shows the presence of carbonyl groups and water near the center of the bilayer. The plateau level of water in the center corresponds to approximately 1/10000 of the concentration in bulk water.

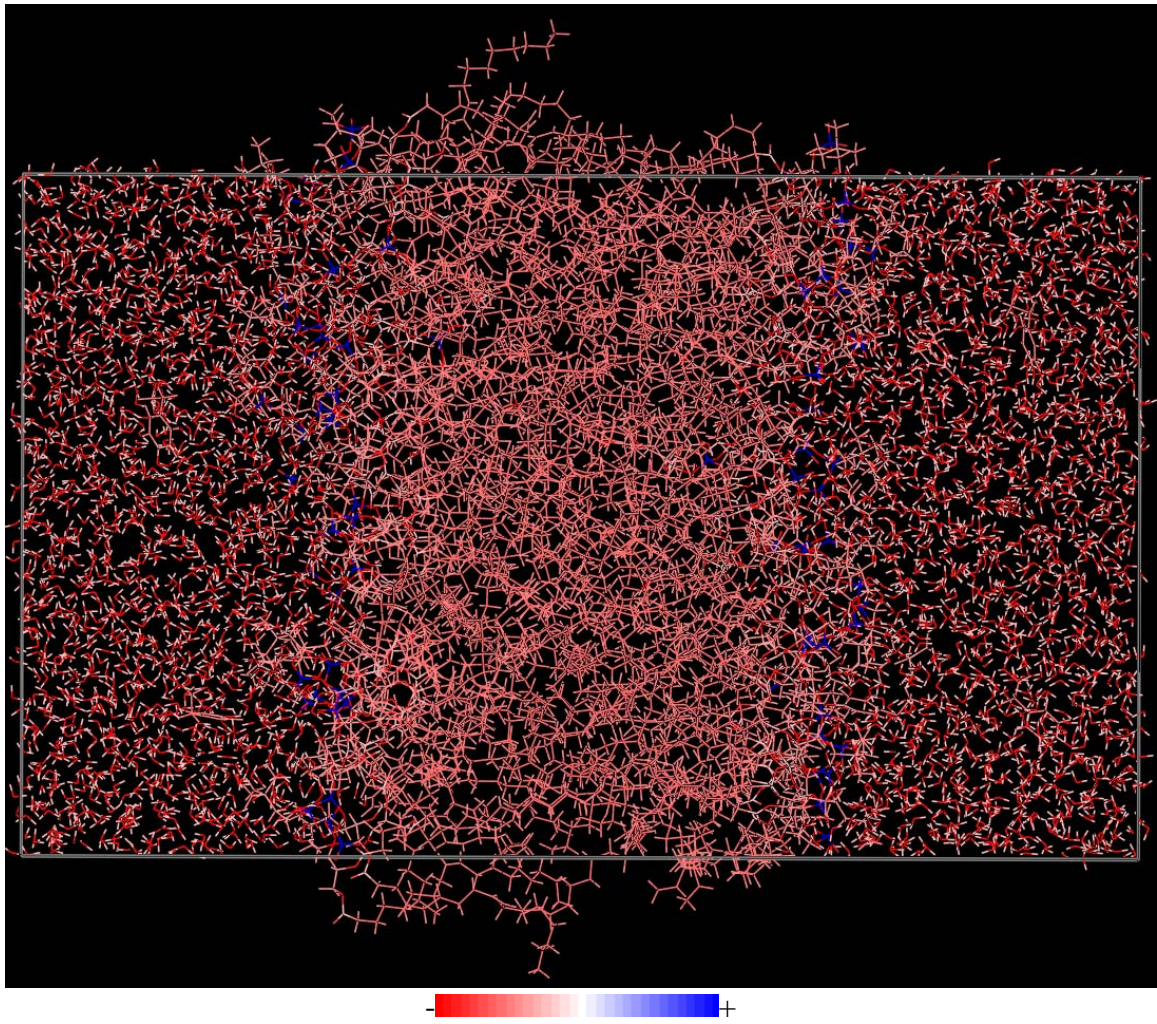


Figure 6-4. Simulation unit cell with the atoms colored by partial charge. Parts of the lipid and water molecules extending out of the unit cell were *relocated* from the opposite face of the unit cell to maintain integrity of the molecules for visualization. The color scale at the bottom has a negative partial charge on the left and positive on the right extreme.



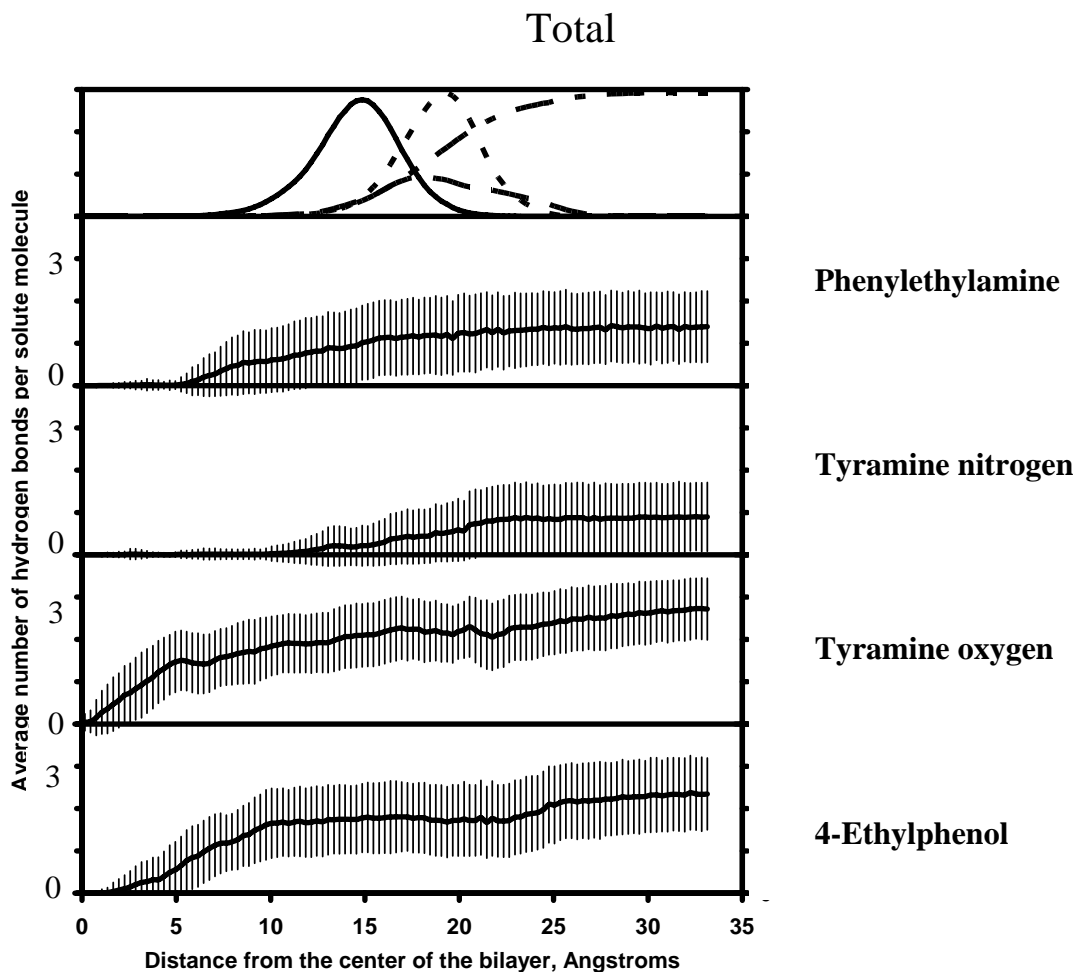


Figure 6-5. Average number of hydrogen bonds per solute functional group as a function of distance from the center of the bilayer. The top panel shows the distribution of the lipid bilayer functional groups: solid line = carbonyl, small dash = phosphoryl, large dash = choline nitrogen, dot dash = water (reduced by 6 fold to match scale). The second to fifth panels show the number of hydrogen bonds per phenylethylamine, tyramine nitrogen, tyramine oxygen, and 4-ethylphenol, respectively. Error bars indicate standard deviations. The plots reflect the location of the aromatic carbon atom of the solute where the ethyl chain is attached. The actual location of the hydrogen bond may depend on the solute orientation.

## Outer phosphoether

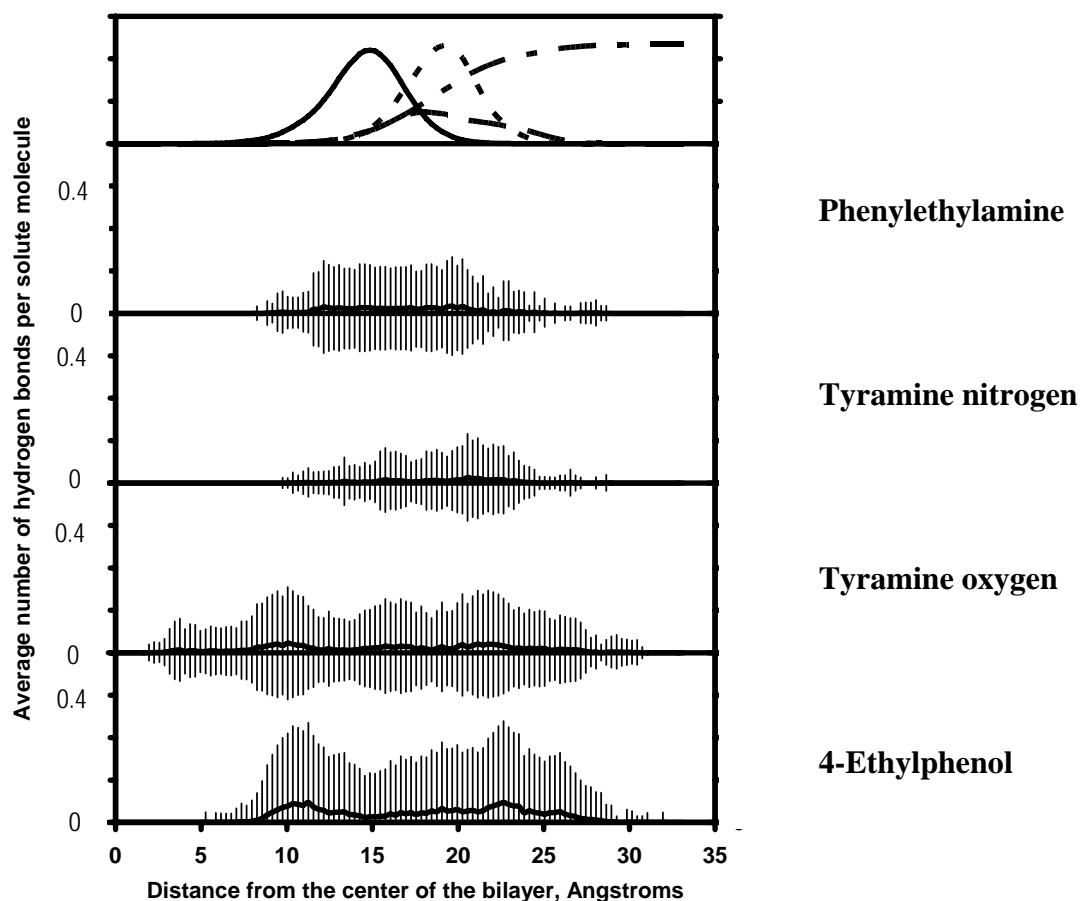


Figure 6-6. Average number of hydrogen bonds with the *outer* phosphoether oxygen by each solute functional group as a function of distance from the center of the bilayer. The top panel shows the distribution of the lipid bilayer functional groups: solid line = carbonyl, small dash = phosphoryl, large dash = choline nitrogen, dot dash = water (reduced by 6 fold to match scale). The second to fifth panels show the number of hydrogen bonds per phenylethylamine, tyramine nitrogen, tyramine oxygen, and 4-ethylphenol, respectively. Error bars indicate standard deviations. The plots reflect the location of the aromatic carbon atom of the solute where the ethyl chain is attached. The actual location of the hydrogen bond may depend on the solute orientation.

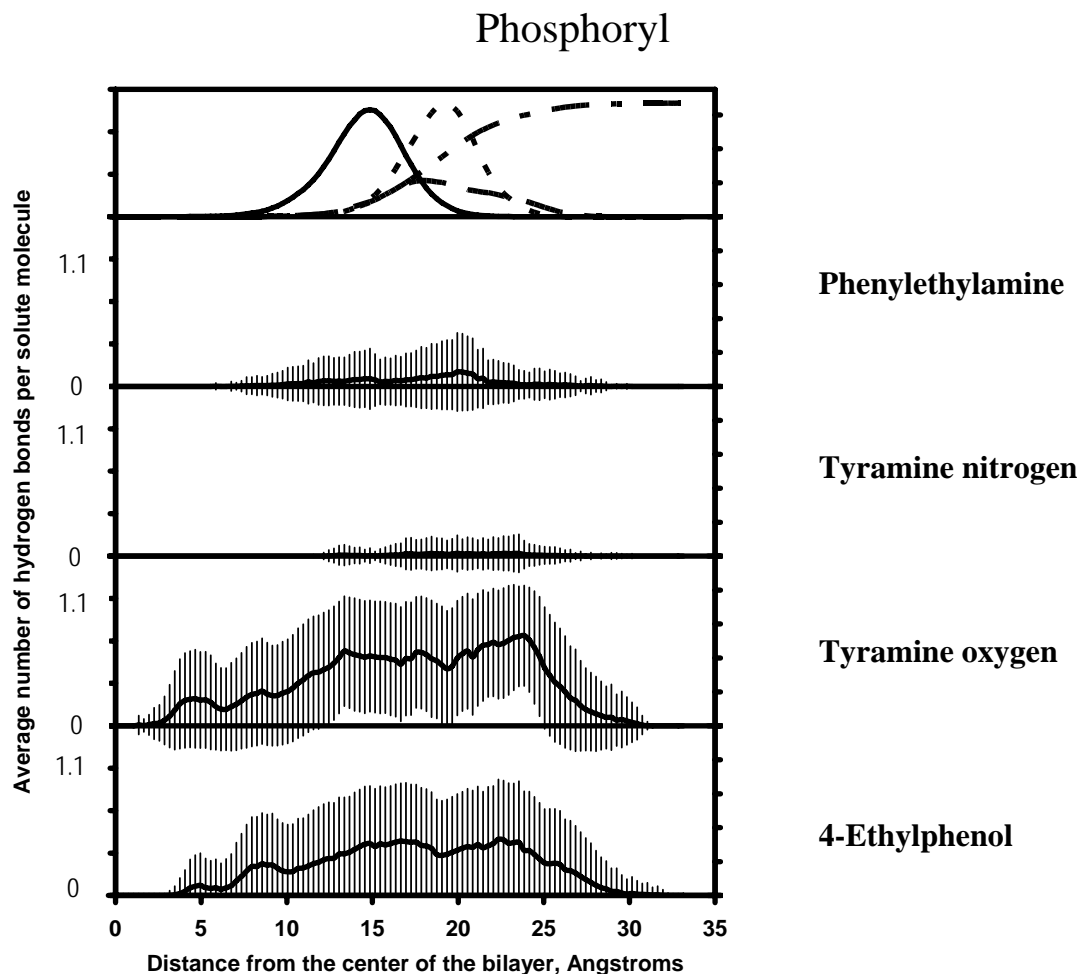


Figure 6-7. Average number of hydrogen bonds with the phosphoryl oxygen by each solute functional group as a function of distance from the center of the bilayer. The top panel shows the distribution of the lipid bilayer functional groups: solid line = carbonyl, small dash = phosphoryl, large dash = choline nitrogen, dot dash = water (reduced by 6 fold to match scale). The second to fifth panels show the number of hydrogen bonds per phenylethylamine, tyramine nitrogen, tyramine oxygen, and 4-ethylphenol, respectively. Error bars indicate standard deviations. The plots reflect the location of the aromatic carbon atom of the solute where the ethyl chain is attached. The actual location of the hydrogen bond may depend on the solute orientation.

## Inner phosphoether

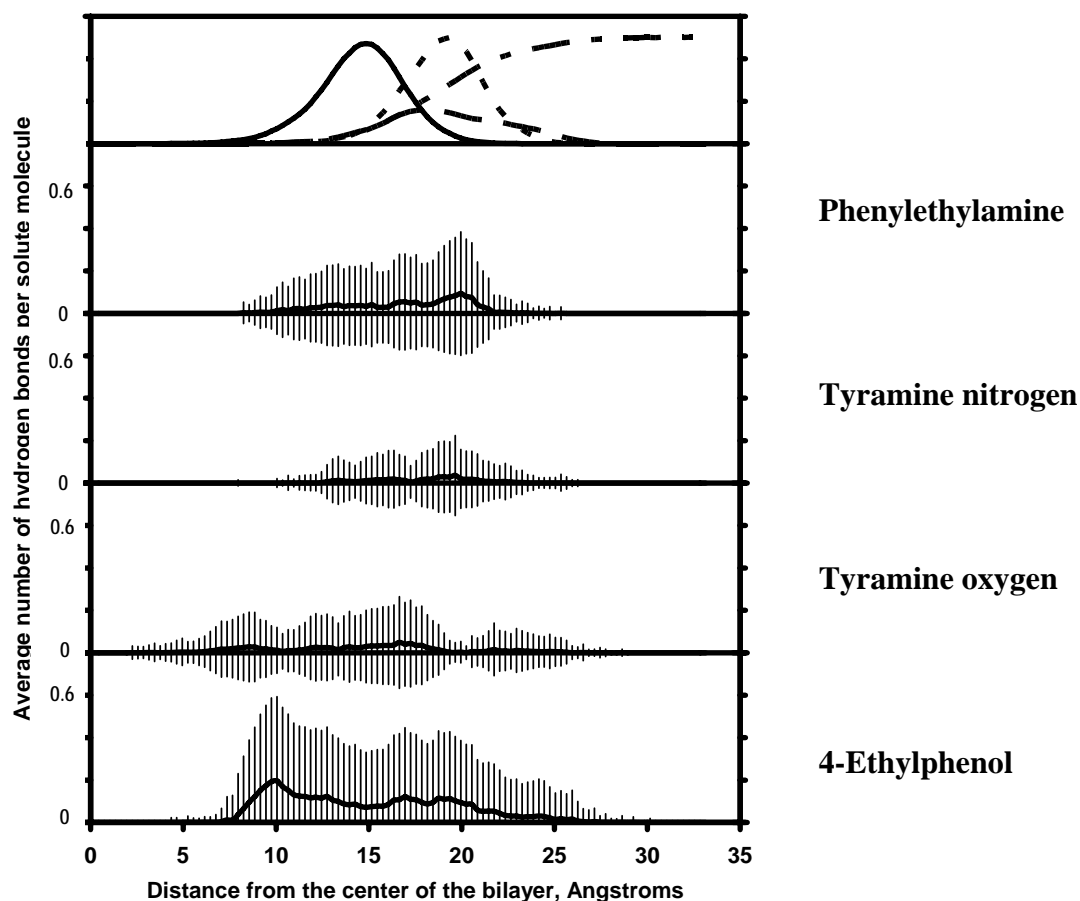


Figure 6-8. Average number of hydrogen bonds with the *inner* phosphoether oxygen by each solute functional group as a function of distance from the center of the bilayer. The top panel shows the distribution of the lipid bilayer functional groups: solid line = carbonyl, small dash = phosphoryl, large dash = choline nitrogen, dot dash = water (reduced by 6 fold to match scale). The second to fifth panels show the number of hydrogen bonds per phenylethylamine, tyramine nitrogen, tyramine oxygen, and 4-ethylphenol, respectively. Error bars indicate standard deviations. The plots reflect the location of the aromatic carbon atom of the solute where the ethyl chain is attached. The actual location of the hydrogen bond may depend on the solute orientation.

## Ether oxygen of 2-oleoyl chain

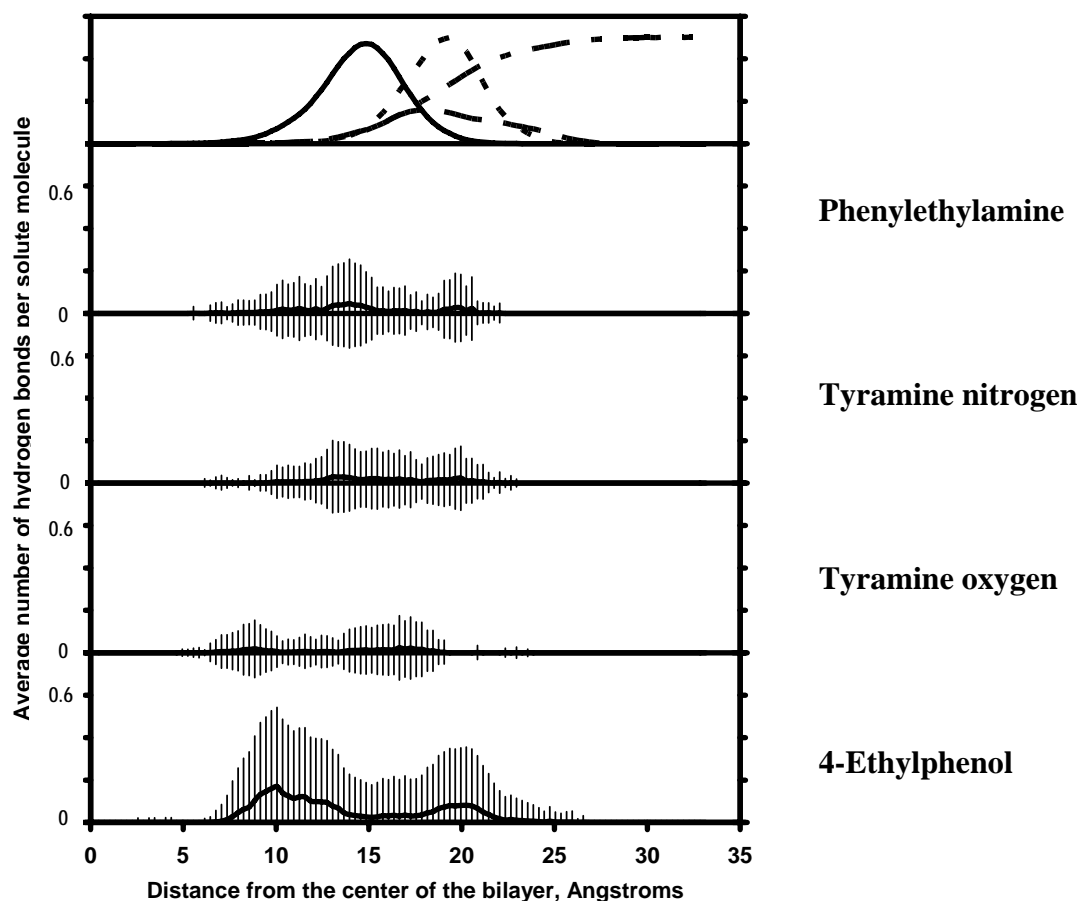


Figure 6-9. Average number of hydrogen bonds with the ether oxygen of 2-oleoyl chain by each solute functional group as a function of distance from the center of the bilayer. The top panel shows the distribution of the lipid bilayer functional groups: solid line = carbonyl, small dash = phosphoryl, large dash = choline nitrogen, dot dash = water (reduced by 6 fold to match scale). The second to fifth panels show the number of hydrogen bonds per phenylethylamine, tyramine nitrogen, tyramine oxygen, and 4-ethylphenol, respectively. Error bars indicate standard deviations. The plots reflect the location of the aromatic carbon atom of the solute where the ethyl chain is attached. The actual location of the hydrogen bond may depend on the solute orientation.

## Carbonyl oxygen of 2-oleoyl chain

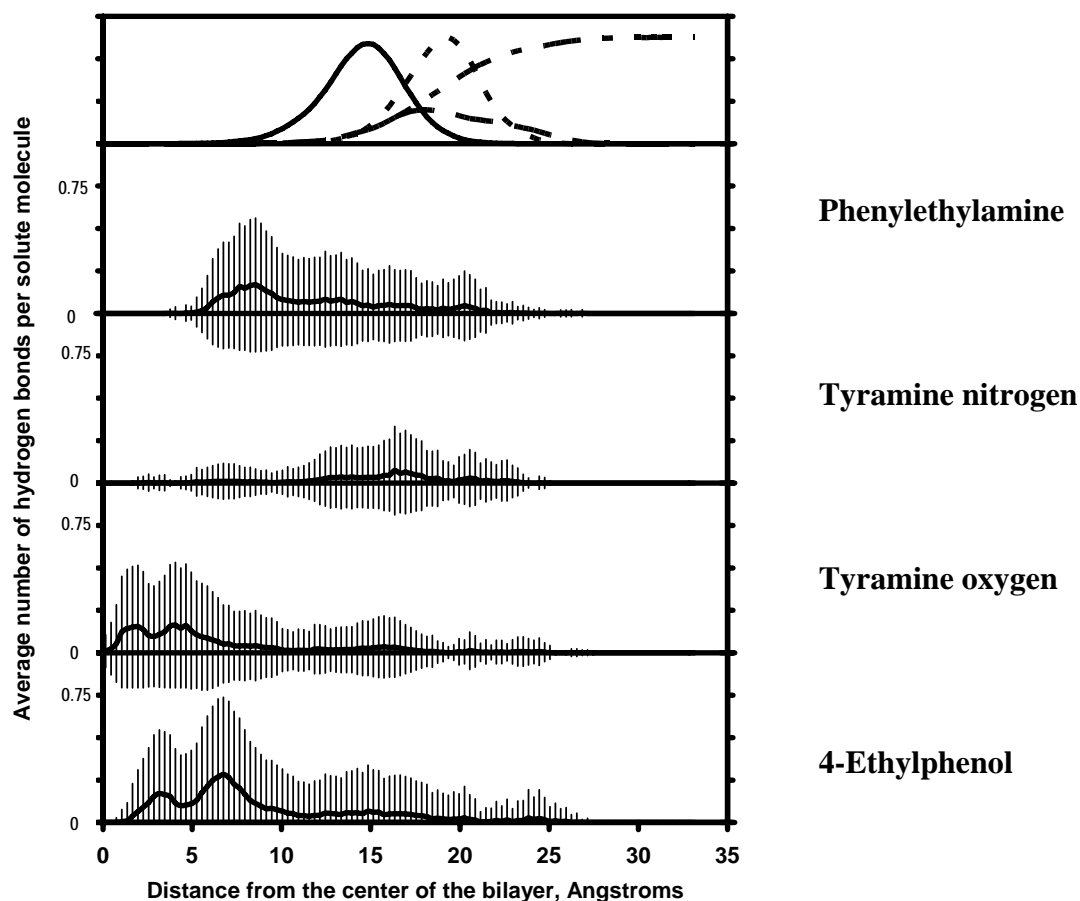


Figure 6-10. Average number of hydrogen bonds with the carbonyl oxygen of 2-oleoyl chain by each solute functional group as a function of distance from the center of the bilayer. The top panel shows the distribution of the lipid bilayer functional groups: solid line = carbonyl, small dash = phosphoryl, large dash = choline nitrogen, dot dash = water (reduced by 6 fold to match scale). The second to fifth panels show the number of hydrogen bonds per phenylethylamine, tyramine nitrogen, tyramine oxygen, and 4-ethylphenol, respectively. Error bars indicate standard deviations. The plots reflect the location of the aromatic carbon atom of the solute where the ethyl chain is attached. The actual location of the hydrogen bond may depend on the solute orientation.

## Ether oxygen of 1-oleoyl chain

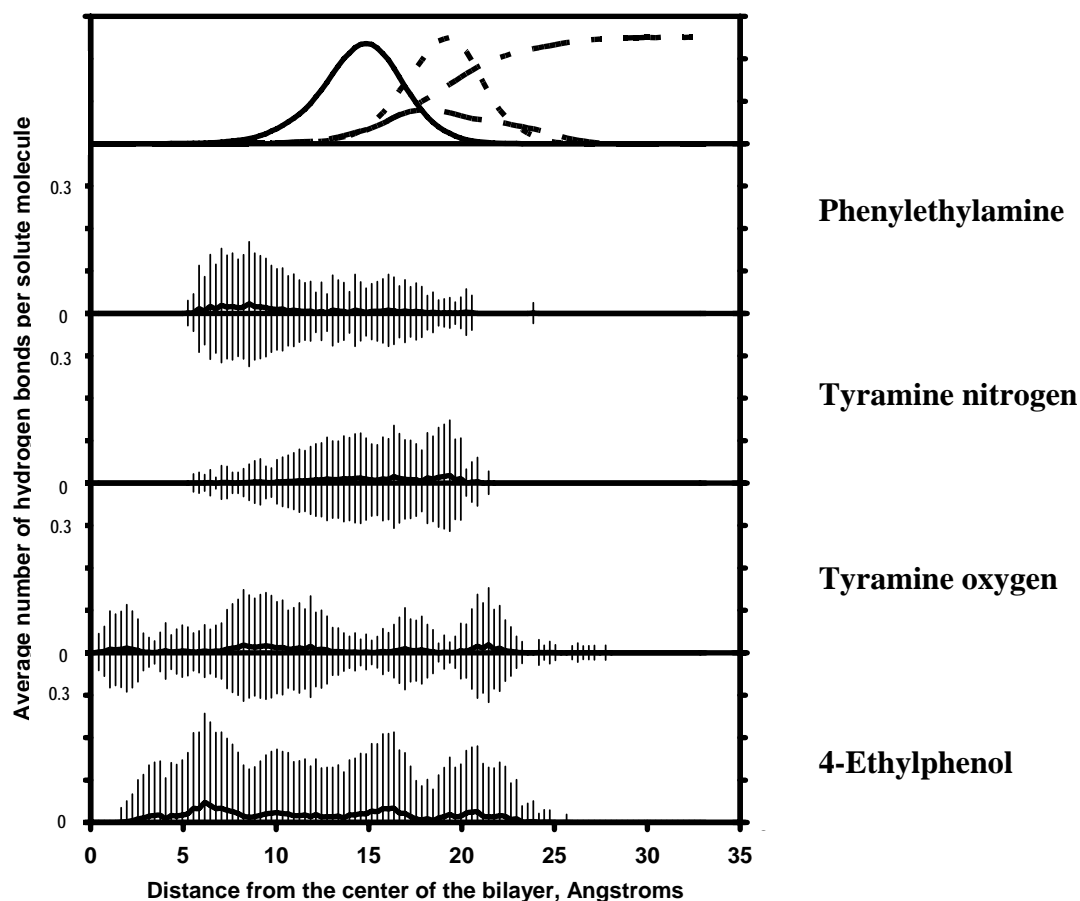


Figure 6-11. Average number of hydrogen bonds with the ether oxygen of 1-oleoyl chain by each solute functional group as a function of distance from the center of the bilayer. The top panel shows the distribution of the lipid bilayer functional groups: solid line = carbonyl, small dash = phosphoryl, large dash = choline nitrogen, dot dash = water (reduced by 6 fold to match scale). The second to fifth panels show the number of hydrogen bonds per phenylethylamine, tyramine nitrogen, tyramine oxygen, and 4-ethylphenol, respectively. Error bars indicate standard deviations. The plots reflect the location of the aromatic carbon atom of the solute where the ethyl chain is attached. The actual location of the hydrogen bond may depend on the solute orientation.

## Carbonyl oxygen of 1-oleoyl chain

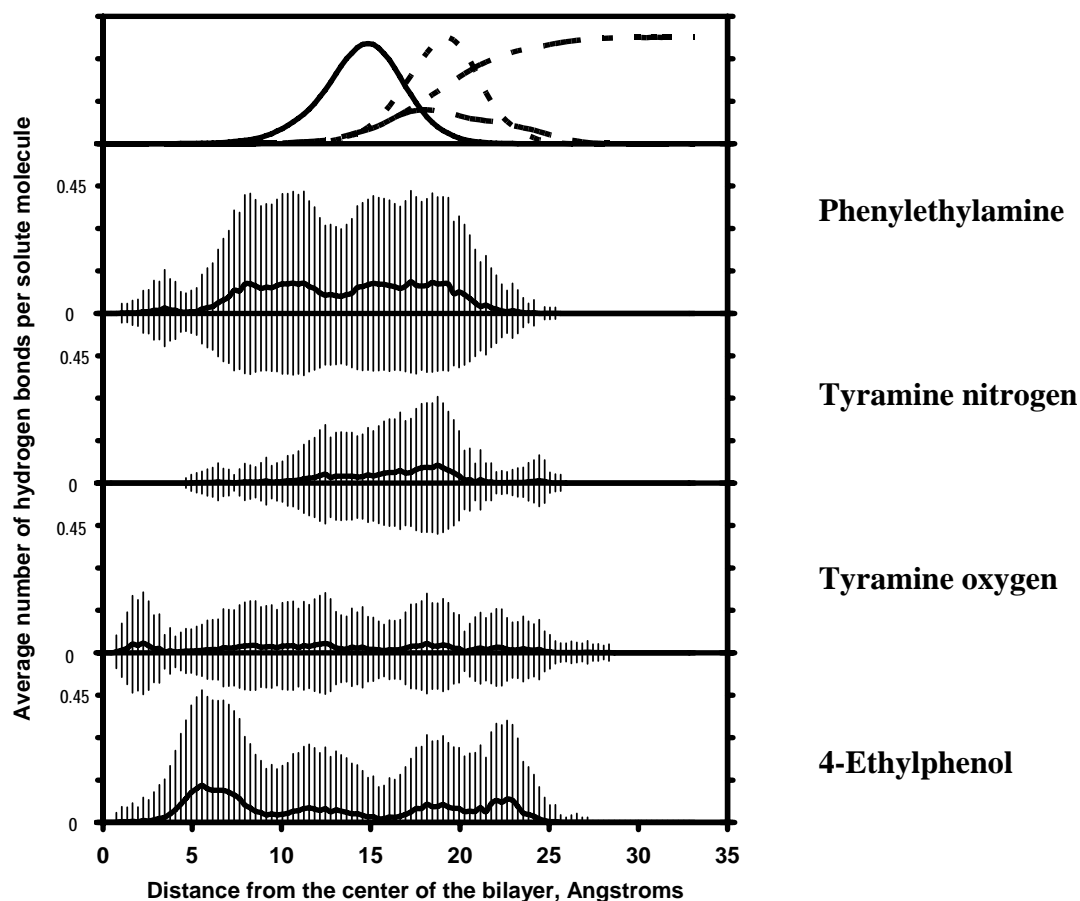


Figure 6-12. Average number of hydrogen bonds with the carbonyl oxygen of 1-oleoyl chain by each solute functional group as a function of distance from the center of the bilayer. The top panel shows the distribution of the lipid bilayer functional groups: solid line = carbonyl, small dash = phosphoryl, large dash = choline nitrogen, dot dash = water (reduced by 6 fold to match scale). The second to fifth panels show the number of hydrogen bonds per phenylethylamine, tyramine nitrogen, tyramine oxygen, and 4-ethylphenol, respectively. Error bars indicate standard deviations. The plots reflect the location of the aromatic carbon atom of the solute where the ethyl chain is attached. The actual location of the hydrogen bond may depend on the solute orientation.



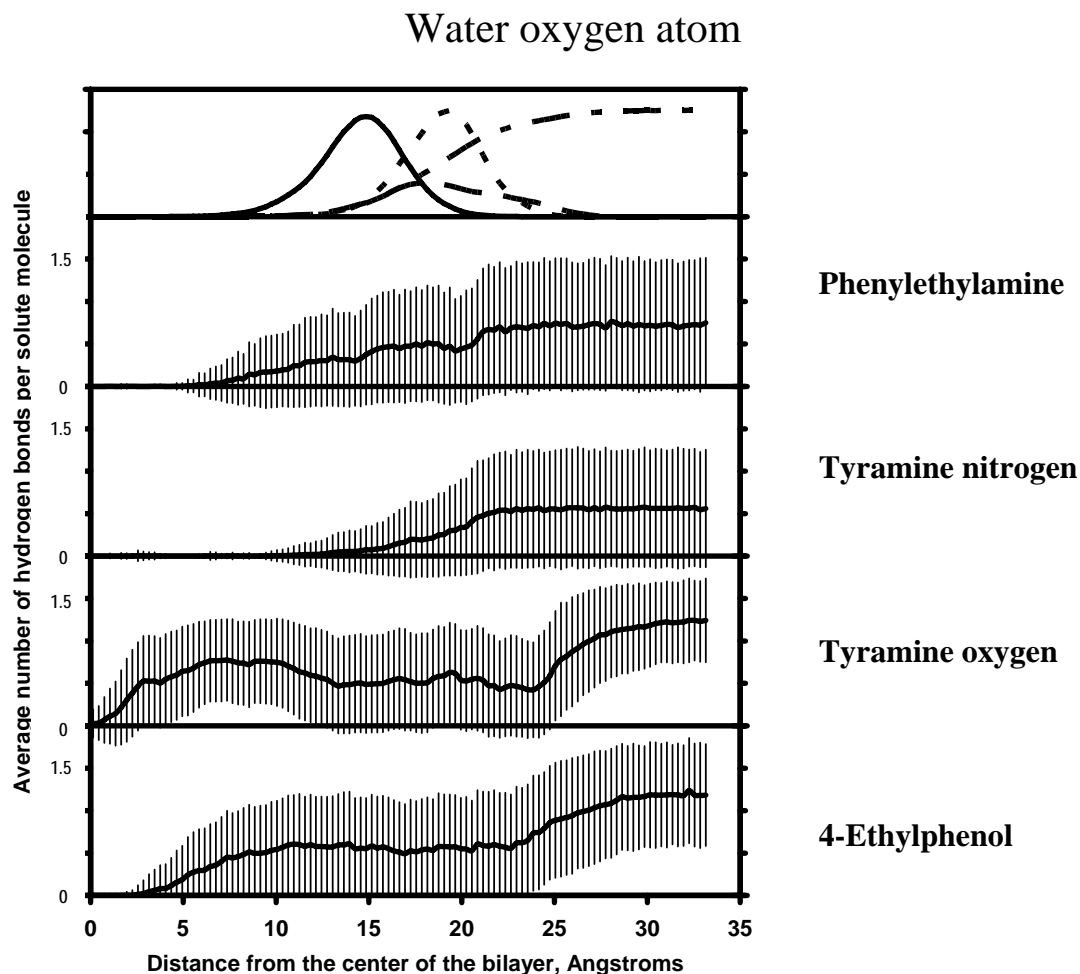


Figure 6-13. Average number of hydrogen bonds with the oxygen atom of water molecules by each solute functional group as a function of distance from the center of the bilayer. The top panel shows the distribution of the lipid bilayer functional groups: solid line = carbonyl, small dash = phosphoryl, large dash = choline nitrogen, dot dash = water (reduced by 6 fold to match scale). The second to fifth panels show the number of hydrogen bonds per phenylethylamine, tyramine nitrogen, tyramine oxygen, and 4-ethylphenol, respectively. Error bars indicate standard deviations. The plots reflect the location of the aromatic carbon atom of the solute where the ethyl chain is attached. The actual location of the hydrogen bond may depend on the solute orientation.

## Water hydrogen atom

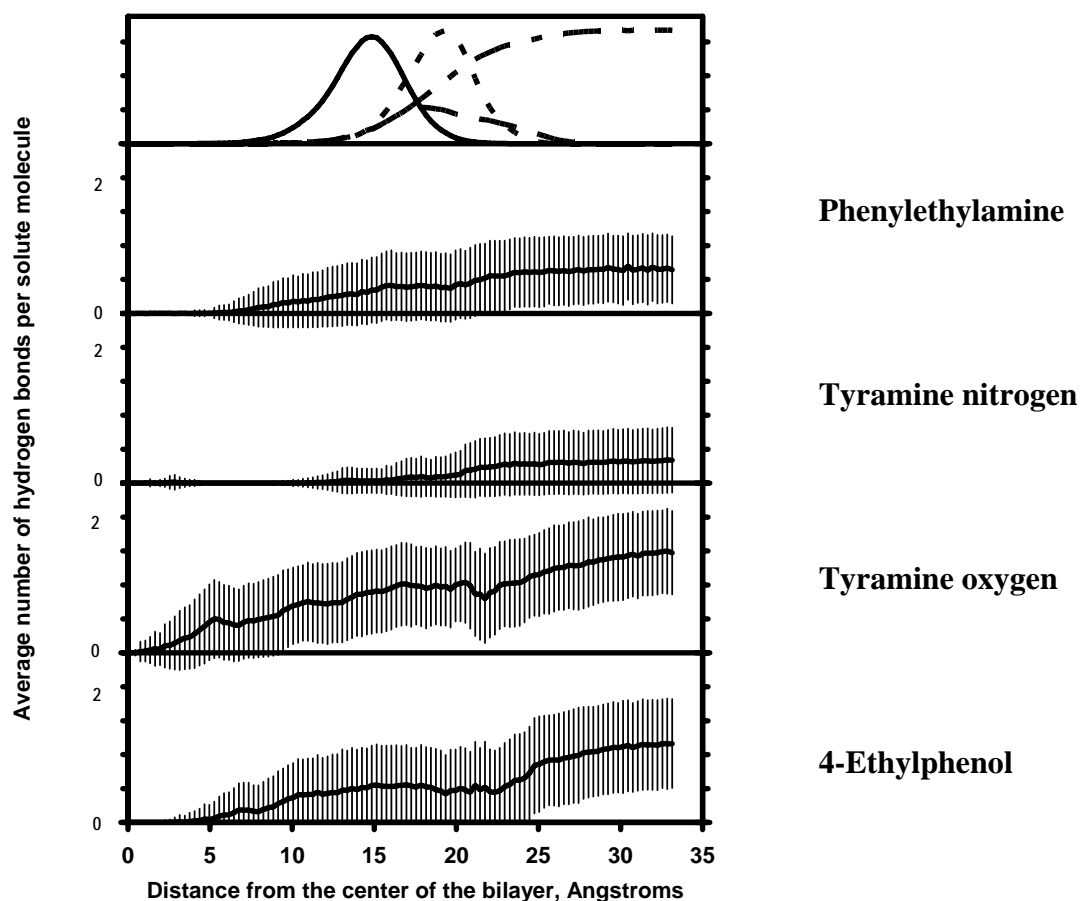


Figure 6-14. Average number of hydrogen bonds with the hydrogen atom of water molecules by each solute functional group as a function of distance from the center of the bilayer. The top panel shows the distribution of the lipid bilayer functional groups: solid line = carbonyl, small dash = phosphoryl, large dash = choline nitrogen, dot dash = water (reduced by 6 fold to match scale). The second to fifth panels show the number of hydrogen bonds per phenylethylamine, tyramine nitrogen, tyramine oxygen, and 4-ethylphenol, respectively. Error bars indicate standard deviations. The plots reflect the location of the aromatic carbon atom of the solute where the ethyl chain is attached. The actual location of the hydrogen bond may depend on the solute orientation.

## No hydrogen bonds

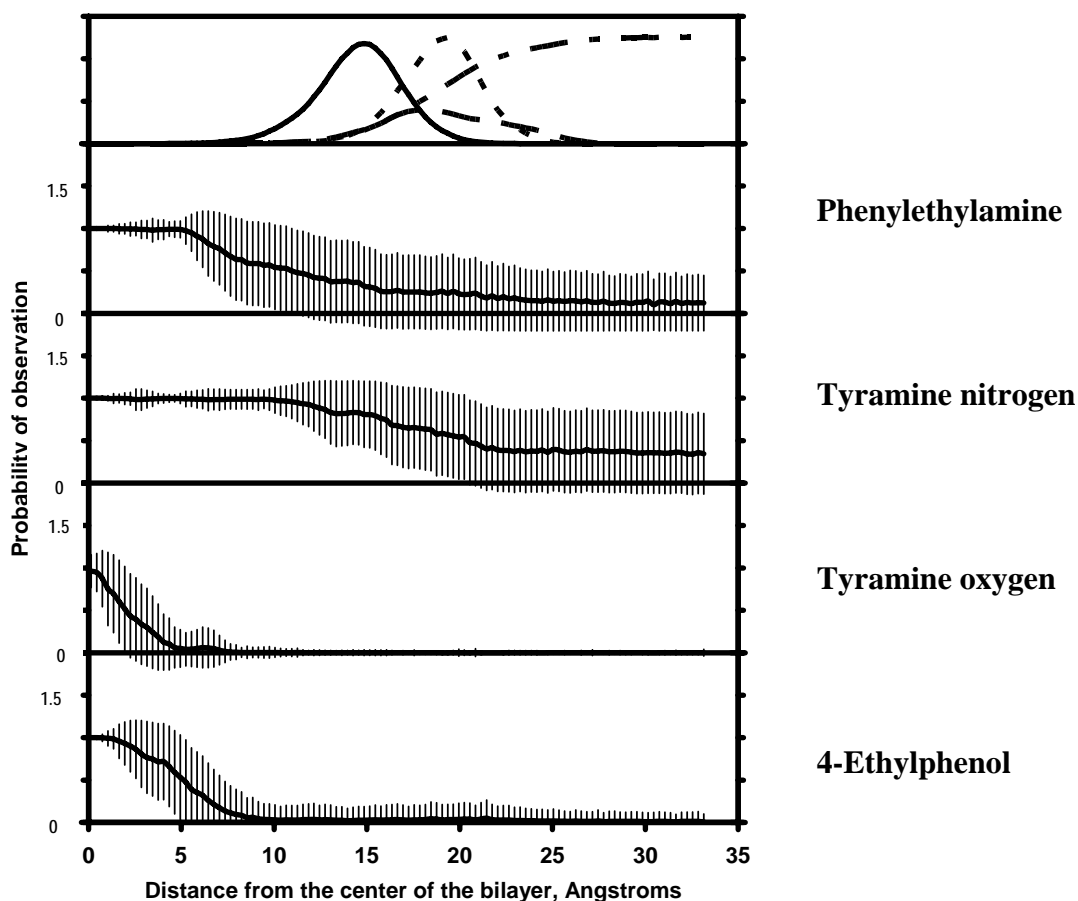


Figure 6-15. Average number of observations where the solute polar functional group is not involved in any hydrogen bonds as a function of distance from the center of the bilayer. The top panel shows the distribution of the lipid bilayer functional groups: solid line = carbonyl, small dash = phosphoryl, large dash = choline nitrogen, dot dash = water (reduced by 6 fold to match scale). Second to fifth panels show the probability of no hydrogen bonds per phenylethylamine, tyramine nitrogen, tyramine oxygen, and 4-ethylphenol, respectively. Error bars indicate standard deviations. The plots reflect the location of the aromatic carbon atom of the solute where the ethyl chain is attached. The actual location of the hydrogen bond may depend on the solute orientation.

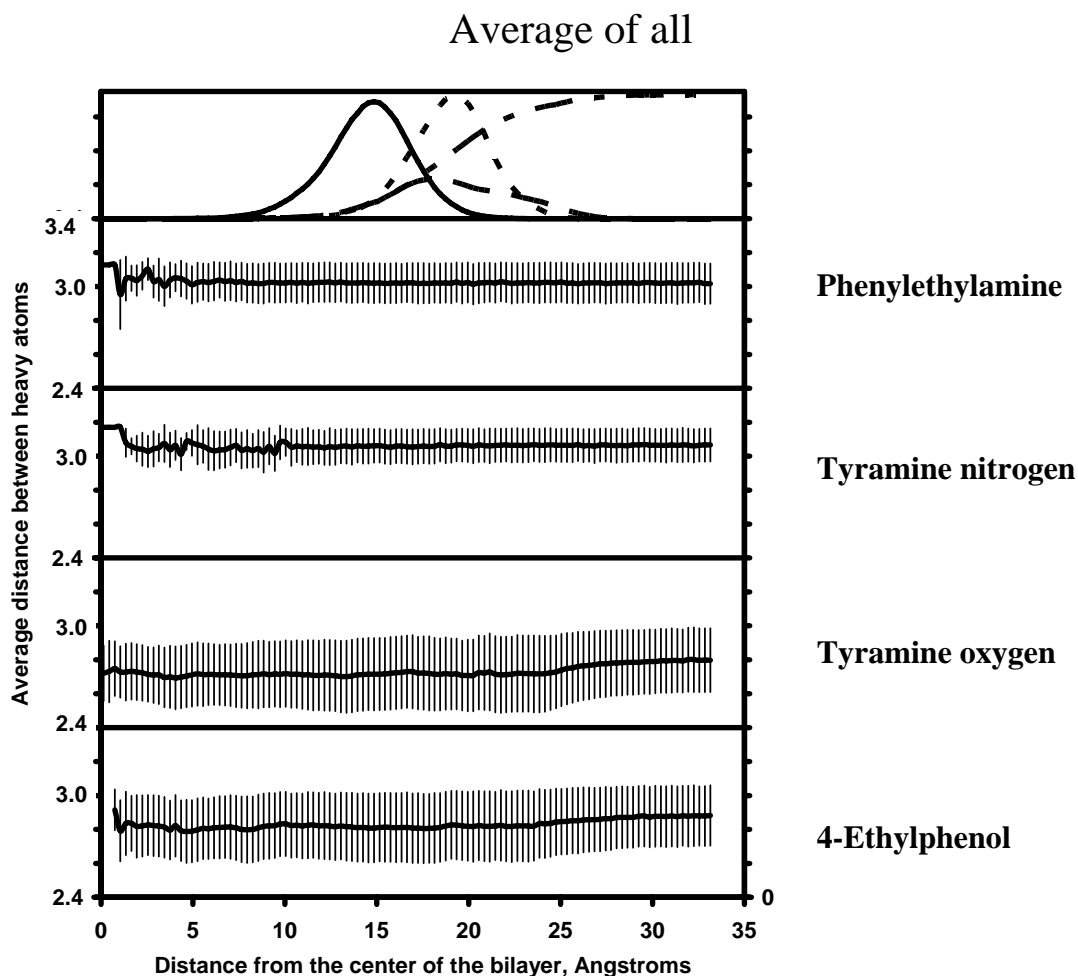


Figure 6-16. Average distance between the heavy (non-hydrogen) atoms of the interacting functional groups of the lipid bilayer and the solute. The top panel shows the distribution of the lipid bilayer functional groups: solid line = carbonyl, small dash = phosphoryl, large dash = choline nitrogen, dot dash = water (reduced by 6 fold to match scale). The second to fifth panels show the distances of the interacting group of the lipid bilayer from the phenylethylamine nitrogen, tyramine nitrogen, tyramine oxygen, and 4-ethylphenol oxygen, respectively. Error bars indicate standard deviations. The plots reflect the location of the aromatic carbon atom of the solute where the ethyl chain is attached. The actual location of the hydrogen bond may depend on the solute orientation.

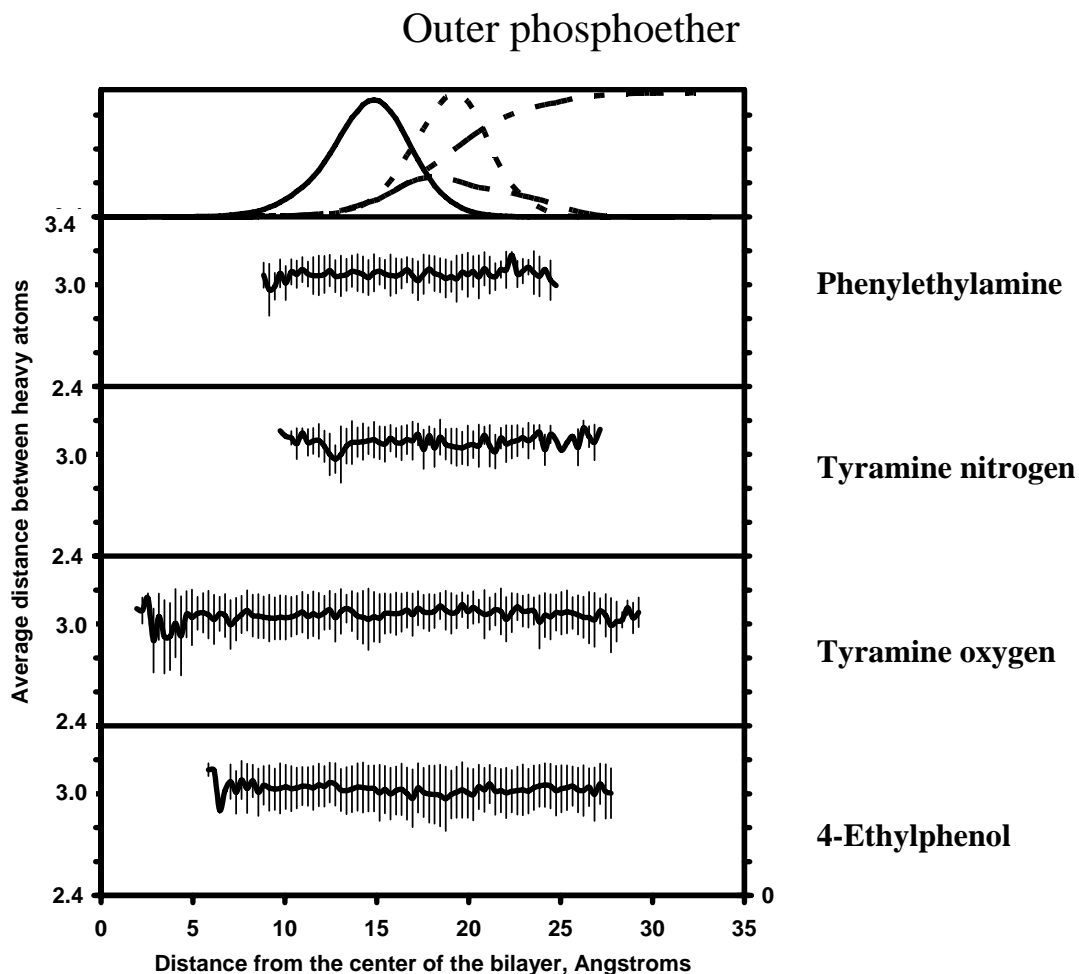


Figure 6-17. Average distance between the outer phosphoether oxygen and the solute polar group. The top panel shows the distribution of the lipid bilayer functional groups: solid line = carbonyl, small dash = phosphoryl, large dash = choline nitrogen, dot dash = water (reduced by 6 fold to match scale). The second to fifth panels show the distances of the lipid functional group from the phenylethylamine nitrogen, tyramine nitrogen, tyramine oxygen, and 4-ethylphenol oxygen, respectively. Error bars indicate standard deviations. The plots reflect the location of the aromatic carbon atom of the solute where the ethyl chain is attached. The actual location of the hydrogen bond may depend on the solute orientation.

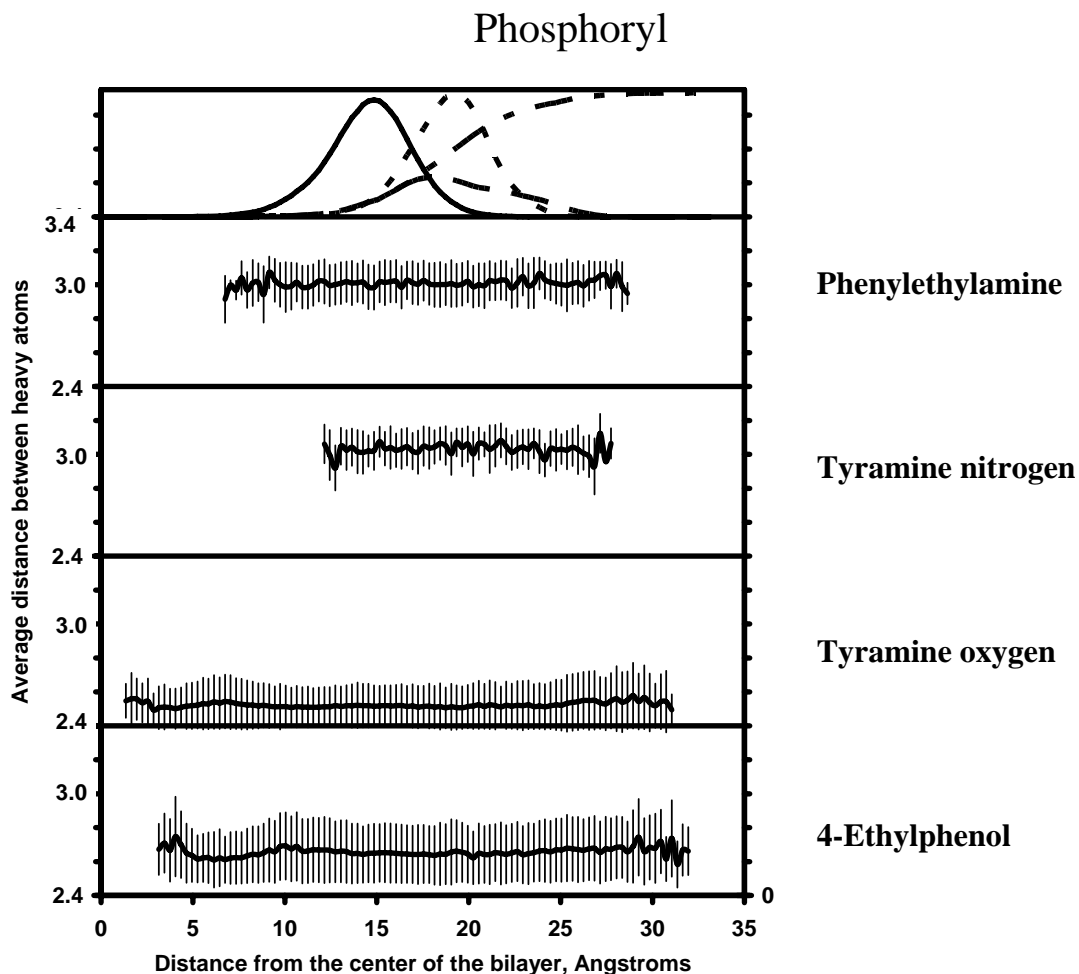


Figure 6-18. Average distance between the phosphoryl oxygen and the solute polar group. The top panel shows the distribution of the lipid bilayer functional groups: solid line = carbonyl, small dash = phosphoryl, large dash = choline nitrogen, dot dash = water (reduced by 6 fold to match scale). The second to fifth panels show the distances of the lipid functional group from the phenylethylamine nitrogen, tyramine nitrogen, tyramine oxygen, and 4-ethylphenol oxygen, respectively. Error bars indicate standard deviations. The plots reflect the location of the aromatic carbon atom of the solute where the ethyl chain is attached. The actual location of the hydrogen bond may depend on the solute orientation.

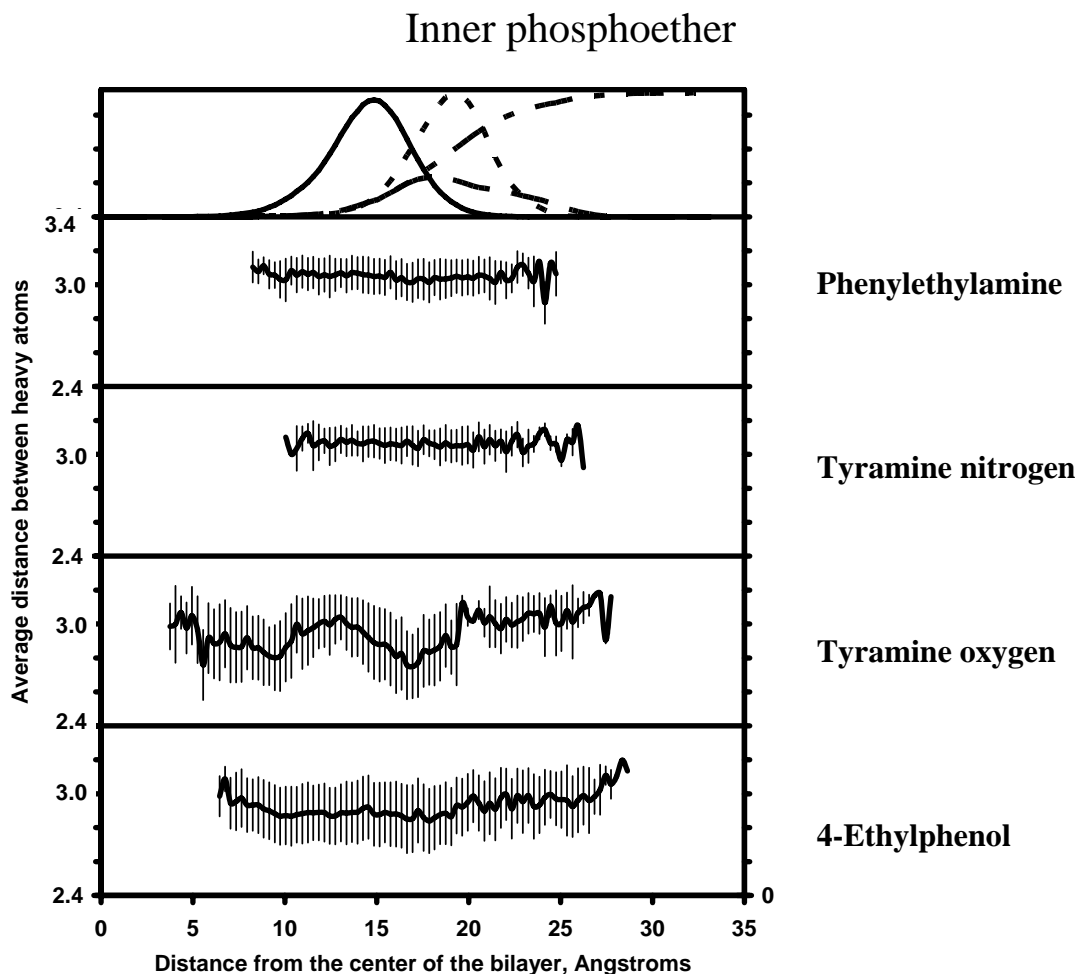


Figure 6-19. Average distance between the inner phosphoether oxygen and the solute polar group. The top panel shows the distribution of the lipid bilayer functional groups: solid line = carbonyl, small dash = phosphoryl, large dash = choline nitrogen, dot dash = water (reduced by 6 fold to match scale). The second to fifth panels show the distances of the lipid functional group from the phenylethylamine nitrogen, tyramine nitrogen, tyramine oxygen, and 4-ethylphenol oxygen, respectively. Error bars indicate standard deviations. The plots reflect the location of the aromatic carbon atom of the solute where the ethyl chain is attached. The actual location of the hydrogen bond may depend on the solute orientation.

## Ether oxygen of 2-oleoyl chain

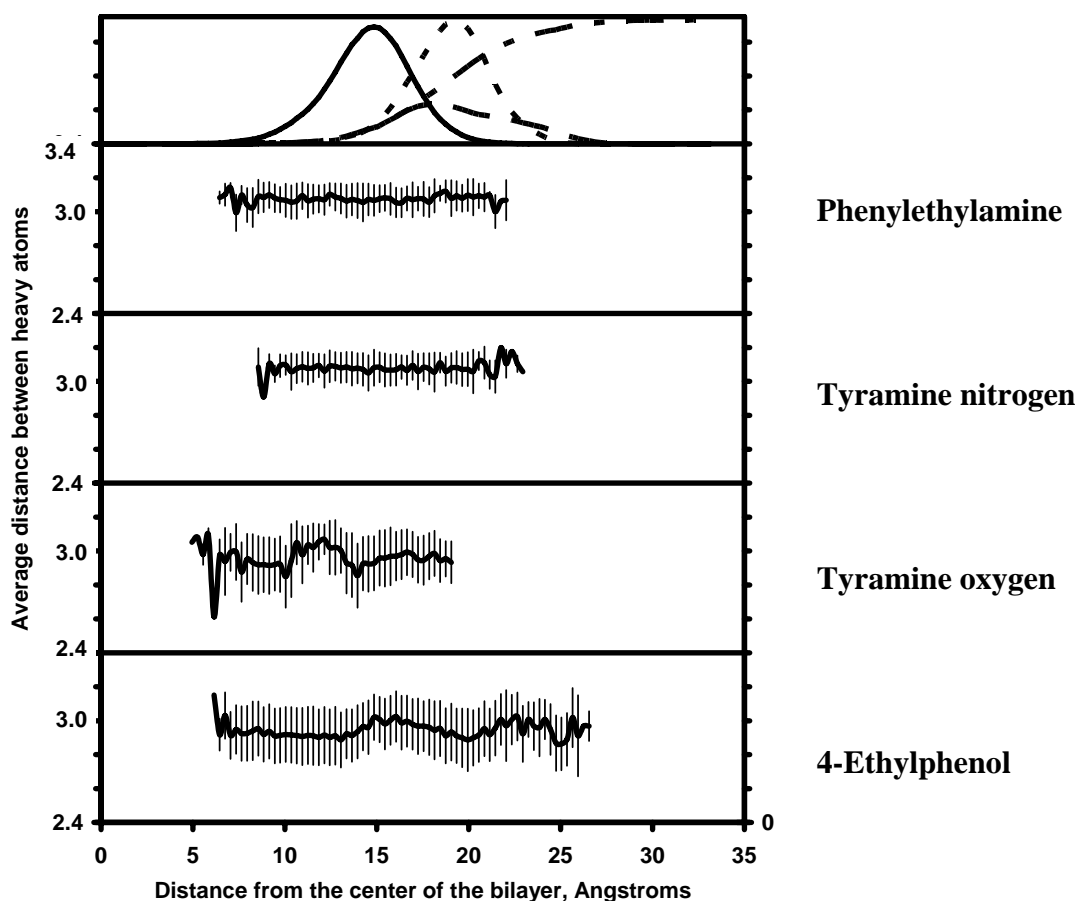


Figure 6-20. Average distance between the ether oxygen of the 2-oleoyl chain and the solute polar group. The top panel shows the distribution of the lipid bilayer functional groups: solid line = carbonyl, small dash = phosphoryl, large dash = choline nitrogen, dot dash = water (reduced by 6 fold to match scale). The second to fifth panels show the distances of the lipid functional group from the phenylethylamine nitrogen, tyramine nitrogen, tyramine oxygen, and 4-ethylphenol oxygen, respectively. Error bars indicate standard deviations. The plots reflect the location of the aromatic carbon atom of the solute where the ethyl chain is attached. The actual location of the hydrogen bond may depend on the solute orientation.



## Carbonyl oxygen of 2-oleoyl chain

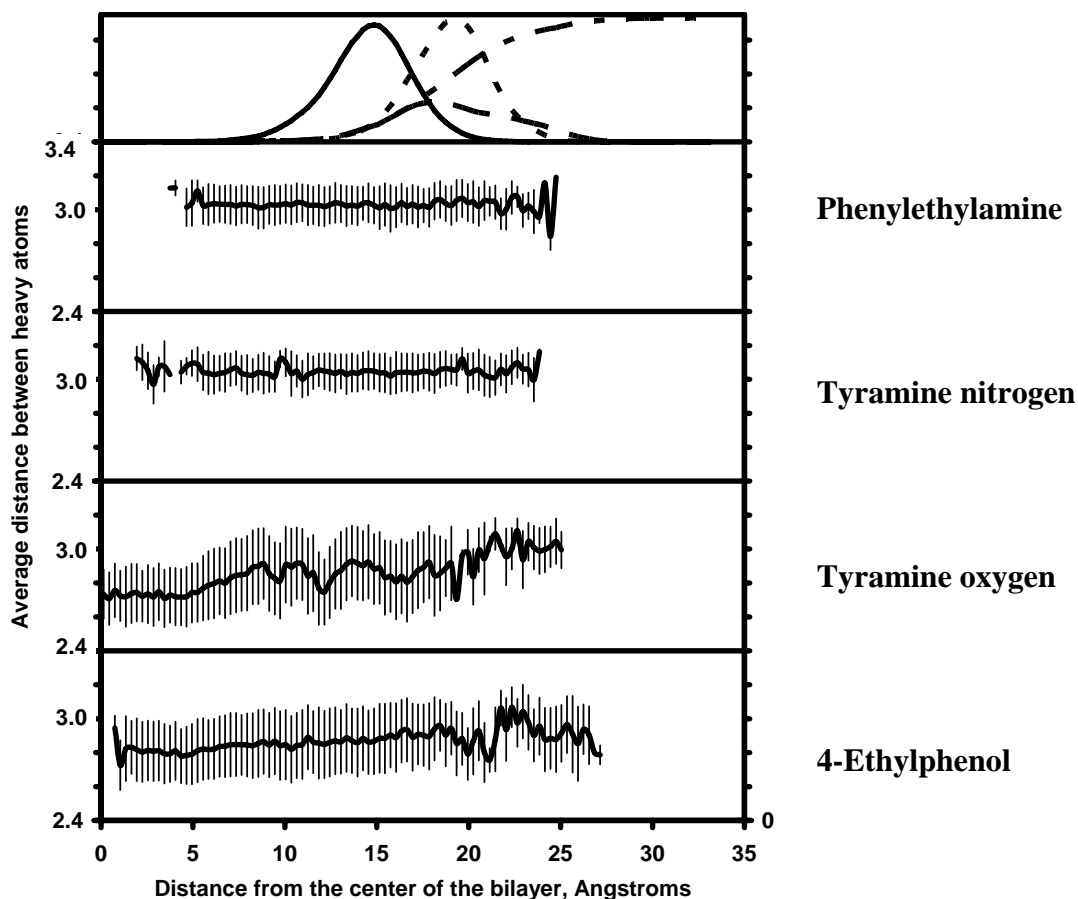


Figure 6-21. Average distance between the carbonyl oxygen of the 2-oleoyl chain and the solute polar group. The top panel shows the distribution of the lipid bilayer functional groups: solid line = carbonyl, small dash = phosphoryl, large dash = choline nitrogen, dot dash = water (reduced by 6 fold to match scale). The second to fifth panels show the distances of the lipid functional group from the phenylethylamine nitrogen, tyramine nitrogen, tyramine oxygen, and 4-ethylphenol oxygen, respectively. Error bars indicate standard deviations. The plots reflect the location of the aromatic carbon atom of the solute where the ethyl chain is attached. The actual location of the hydrogen bond may depend on the solute orientation.

## Ether oxygen of 1-oleoyl chain

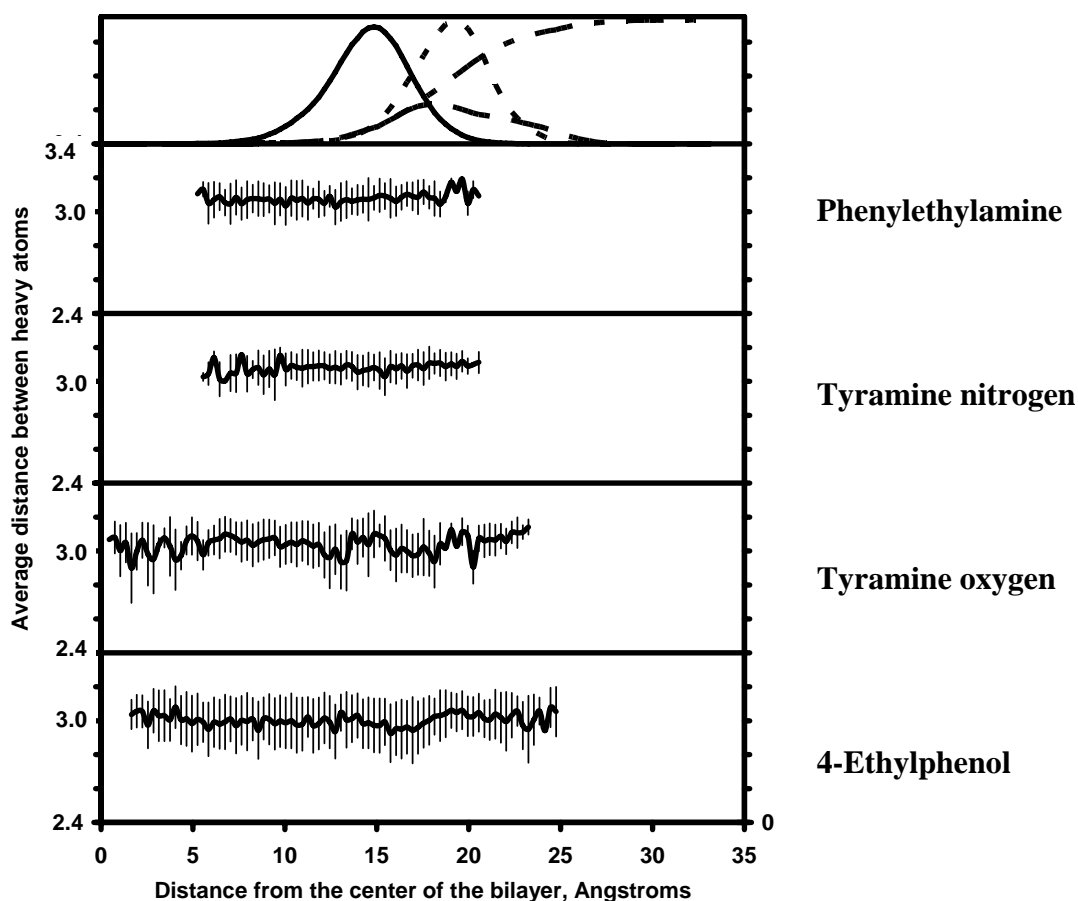


Figure 6-22. Average distance between the ether oxygen of the 1-oleoyl chain and the solute polar group. The top panel shows the distribution of the lipid bilayer functional groups: solid line = carbonyl, small dash = phosphoryl, large dash = choline nitrogen, dot dash = water (reduced by 6 fold to match scale). The second to fifth panels show the distances of the lipid functional group from the phenylethylamine nitrogen, tyramine nitrogen, tyramine oxygen, and 4-ethylphenol oxygen, respectively. Error bars indicate standard deviations. The plots reflect the location of the aromatic carbon atom of the solute where the ethyl chain is attached. The actual location of the hydrogen bond may depend on the solute orientation.

## Carbonyl oxygen of 1-oleoyl chain

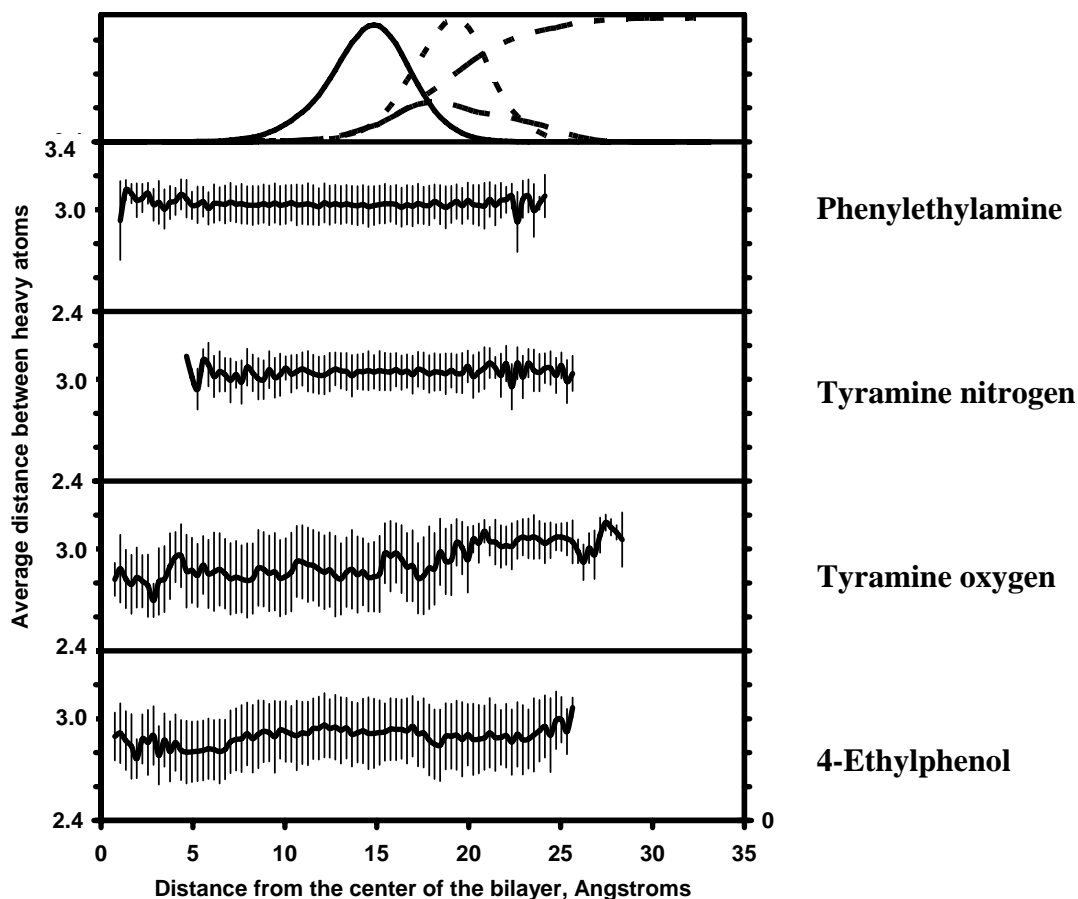


Figure 6-23. Average distance between the carbonyl oxygen of the 1-oleoyl chain and the solute polar group. The top panel shows the distribution of the lipid bilayer functional groups: solid line = carbonyl, small dash = phosphoryl, large dash = choline nitrogen, dot dash = water (reduced by 6 fold to match scale). The second to fifth panels show the distances of the lipid functional group from the phenylethylamine nitrogen, tyramine nitrogen, tyramine oxygen, and 4-ethylphenol oxygen, respectively. Error bars indicate standard deviations. The plots reflect the location of the aromatic carbon atom of the solute where the ethyl chain is attached. The actual location of the hydrogen bond may depend on the solute orientation.

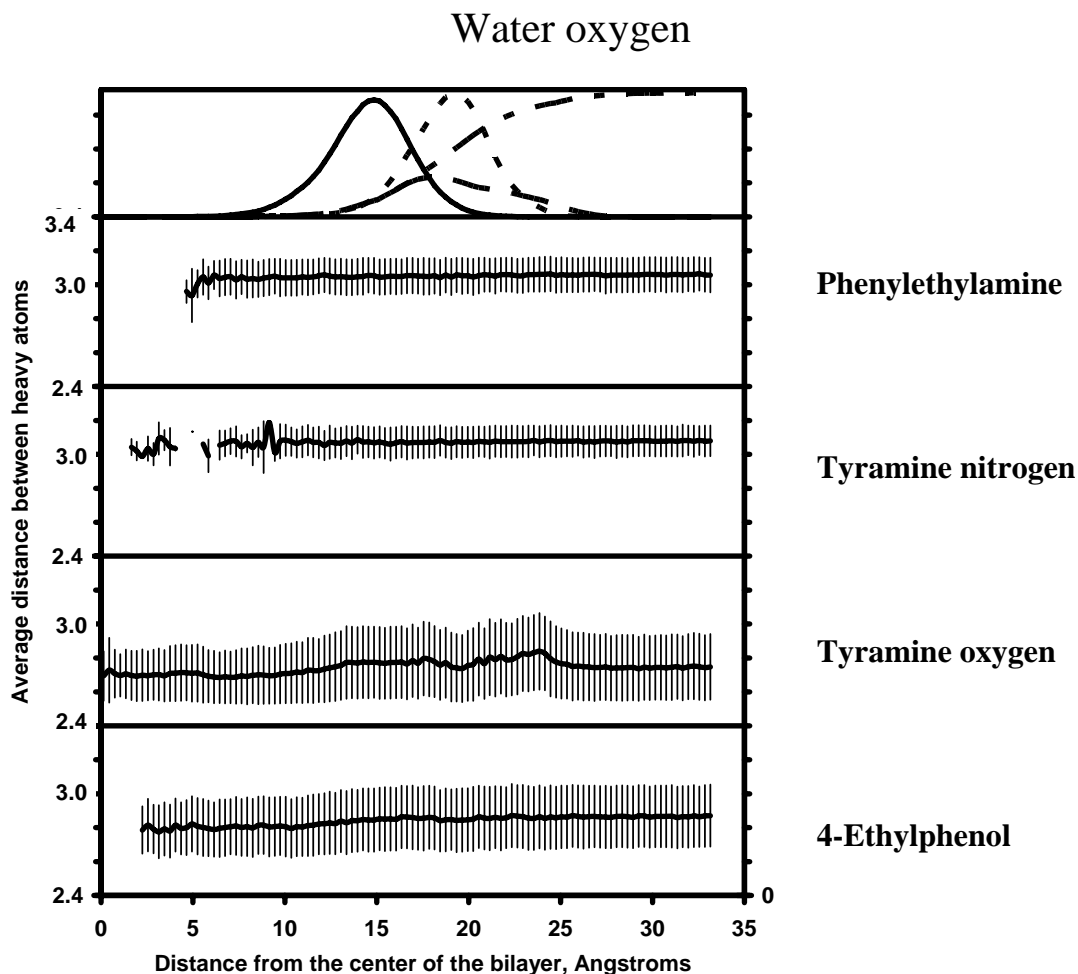


Figure 6-24. Average distance between the oxygen atom of the water molecule and the solute polar group for the water-O type of hydrogen bond. The top panel shows the distribution of the lipid bilayer functional groups: solid line = carbonyl, small dash = phosphoryl, large dash = choline nitrogen, dot dash = water (reduced by 6 fold to match scale). The second to fifth panels show the distances of the water oxygen from the phenylethylamine nitrogen, tyramine nitrogen, tyramine oxygen, and 4-ethylphenol oxygen, respectively. Error bars indicate standard deviations. The plots reflect the location of the aromatic carbon atom of the solute where the ethyl chain is attached. The actual location of the hydrogen bond may depend on the solute orientation.

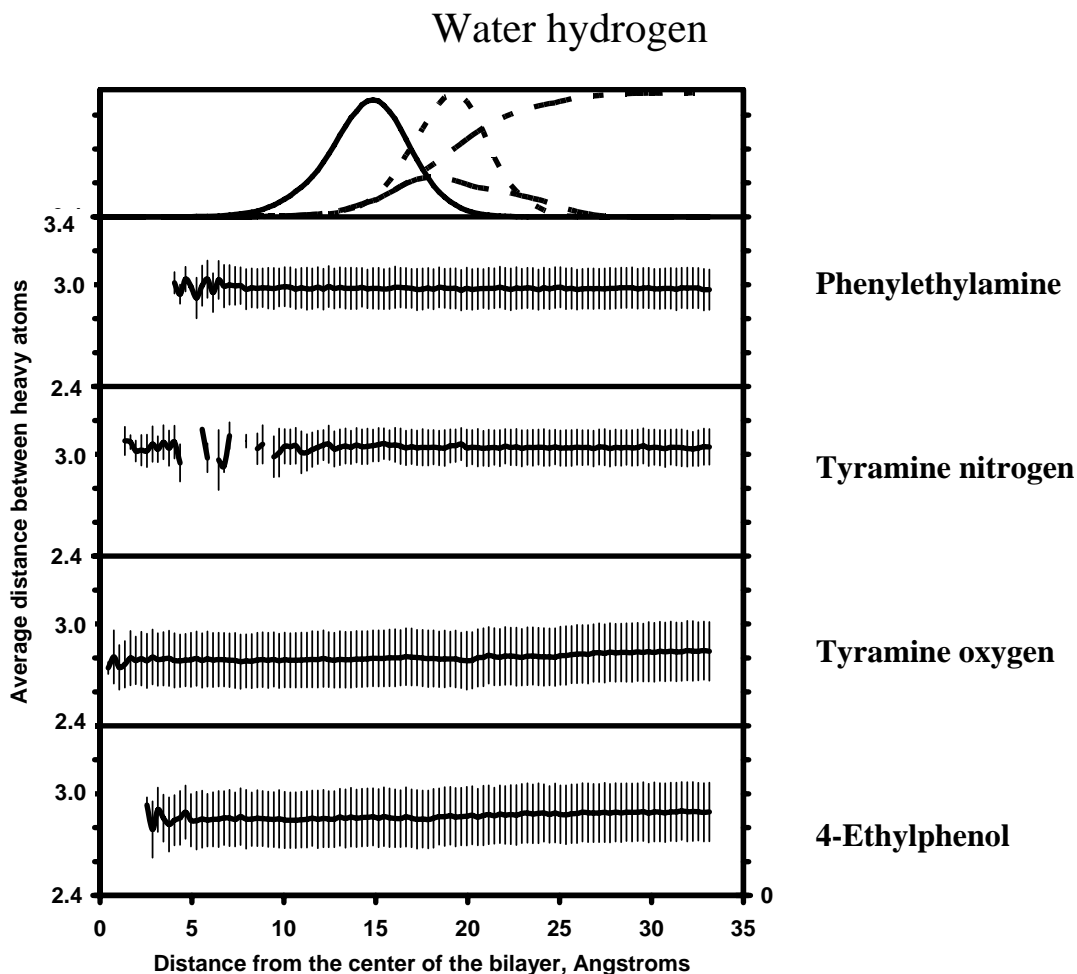


Figure 6-25. Average distance between the oxygen atom of the water molecule and the solute polar group for the water-H type of hydrogen bond. The top panel shows the distribution of the lipid bilayer functional groups: solid line = carbonyl, small dash = phosphoryl, large dash = choline nitrogen, dot dash = water (reduced by 6 fold to match scale). The second to fifth panels show the distances of the water hydrogen from the phenylethylamine nitrogen, tyramine nitrogen, tyramine oxygen, and 4-ethylphenol oxygen, respectively. Error bars indicate standard deviations. The plots reflect the location of the aromatic carbon atom of the solute where the ethyl chain is attached. The actual location of the hydrogen bond may depend on the solute orientation.

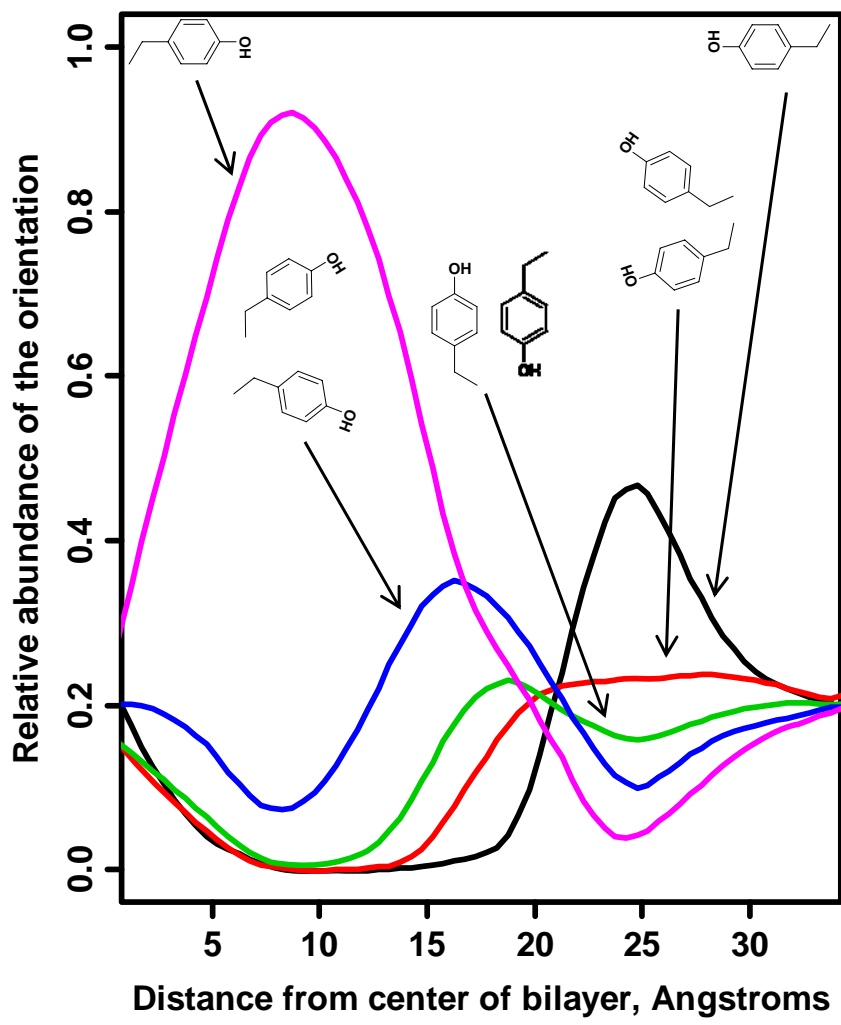


Figure 6-26. Relative distribution of orientations of 4-ethylphenol versus distance from the center of the bilayer

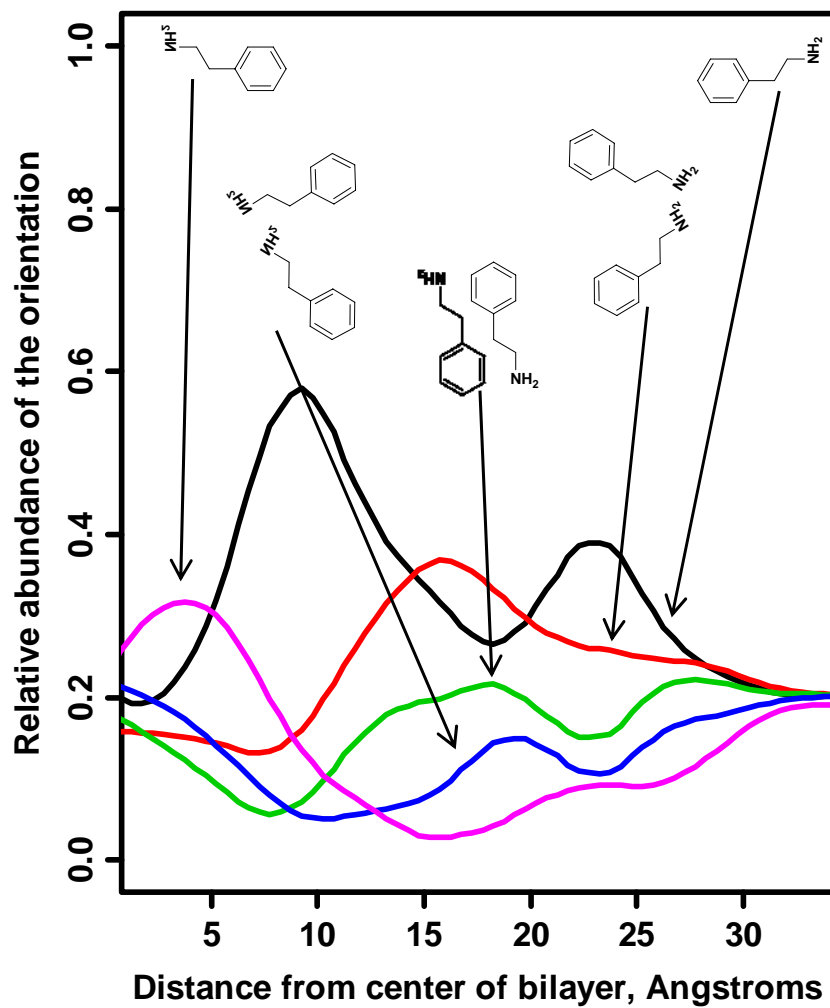


Figure 6-27. Relative distribution of orientations of phenylethylamine versus distance from the center of the bilayer

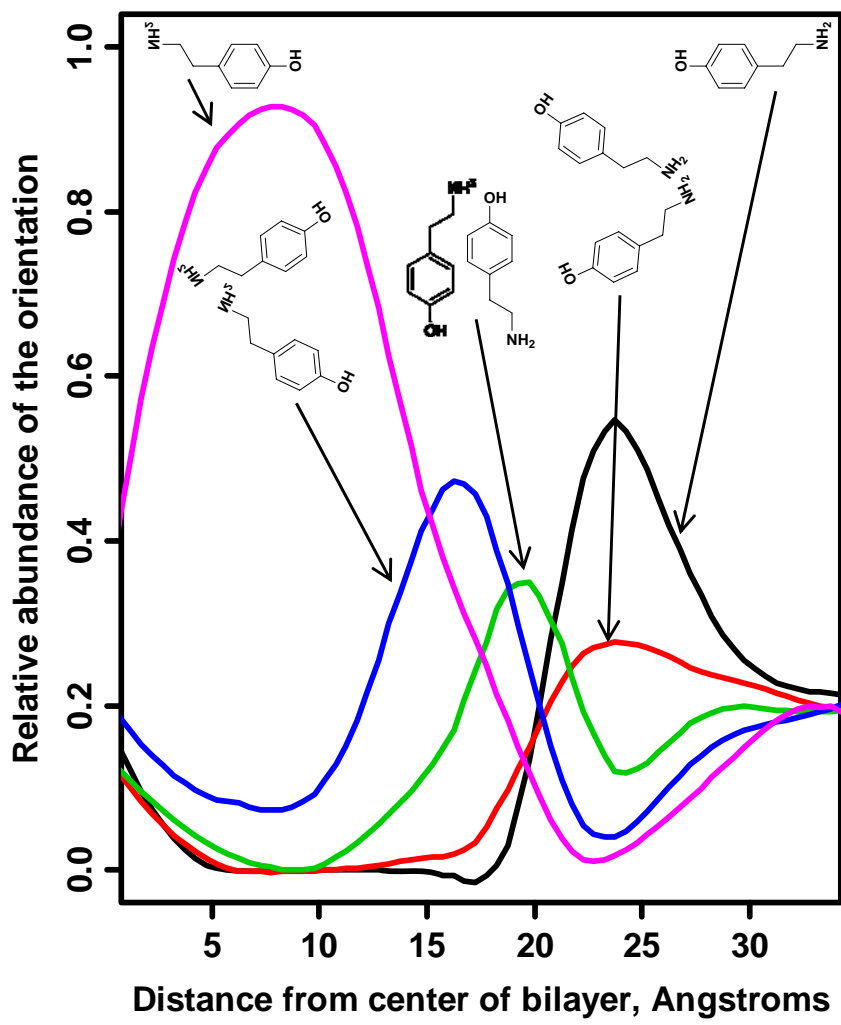


Figure 6-28. Relative distribution of orientations of tyramine versus distance from the center of the bilayer



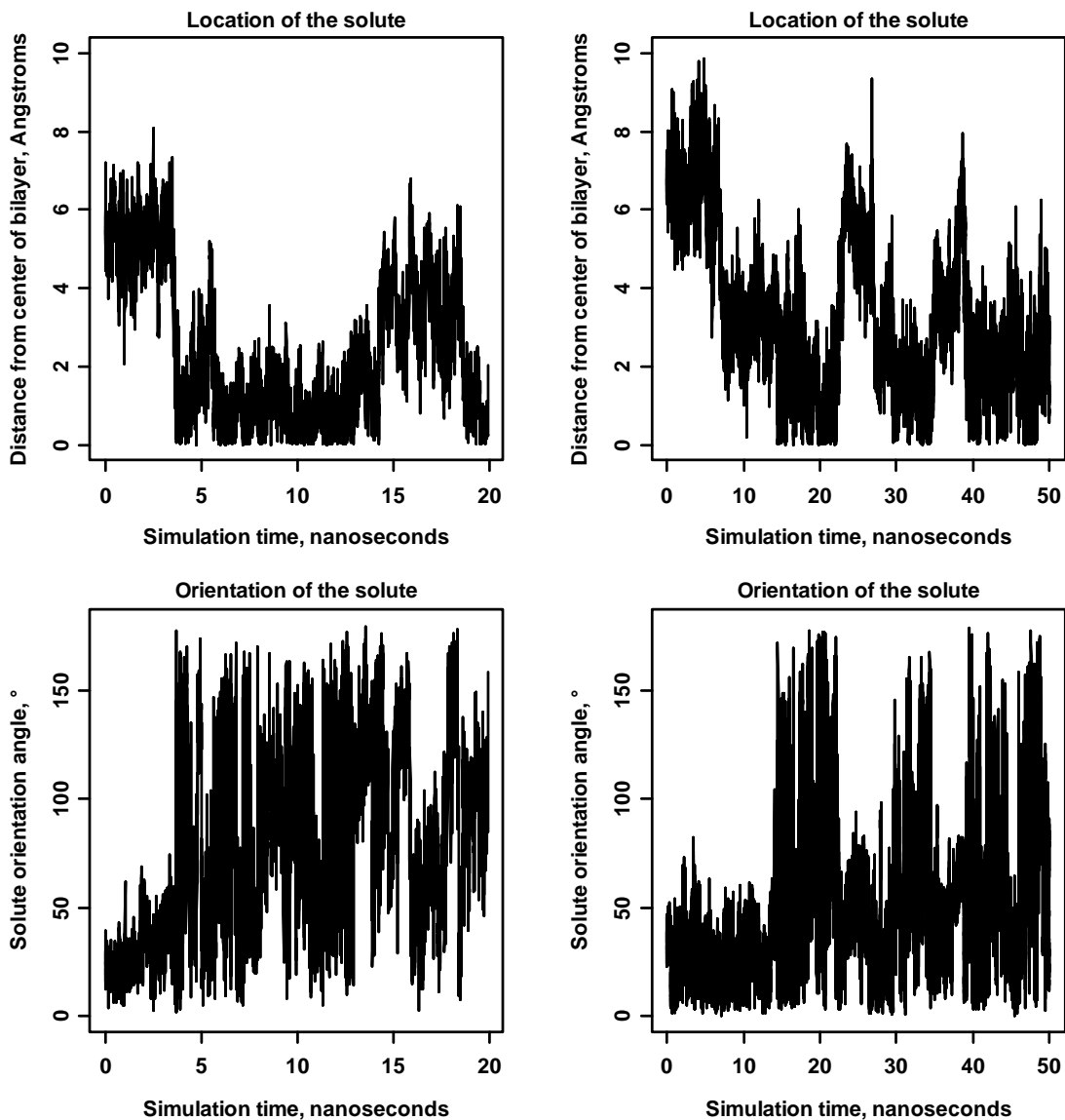


Figure 6-29. Two representative trajectories from the simulation of 4-ethylphenol. Top panels show the location of solute relative to the center of the bilayer versus the simulation time. Bottom panels show the corresponding orientation angle of the solute versus the same time step in the simulation.

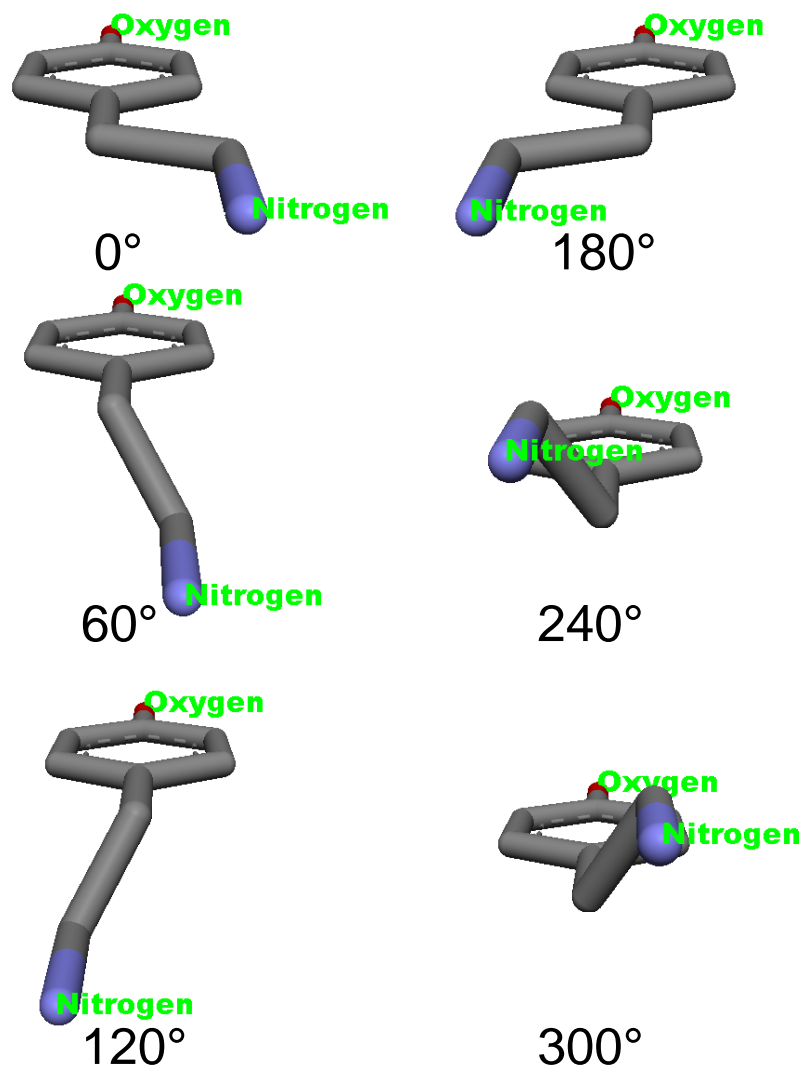


Figure 6-30. Various conformers of tyramine based on the rotation of the first dihedral of the ethylamine chain. The numerical labels assigned for these conformers have been used in the subsequent figures.

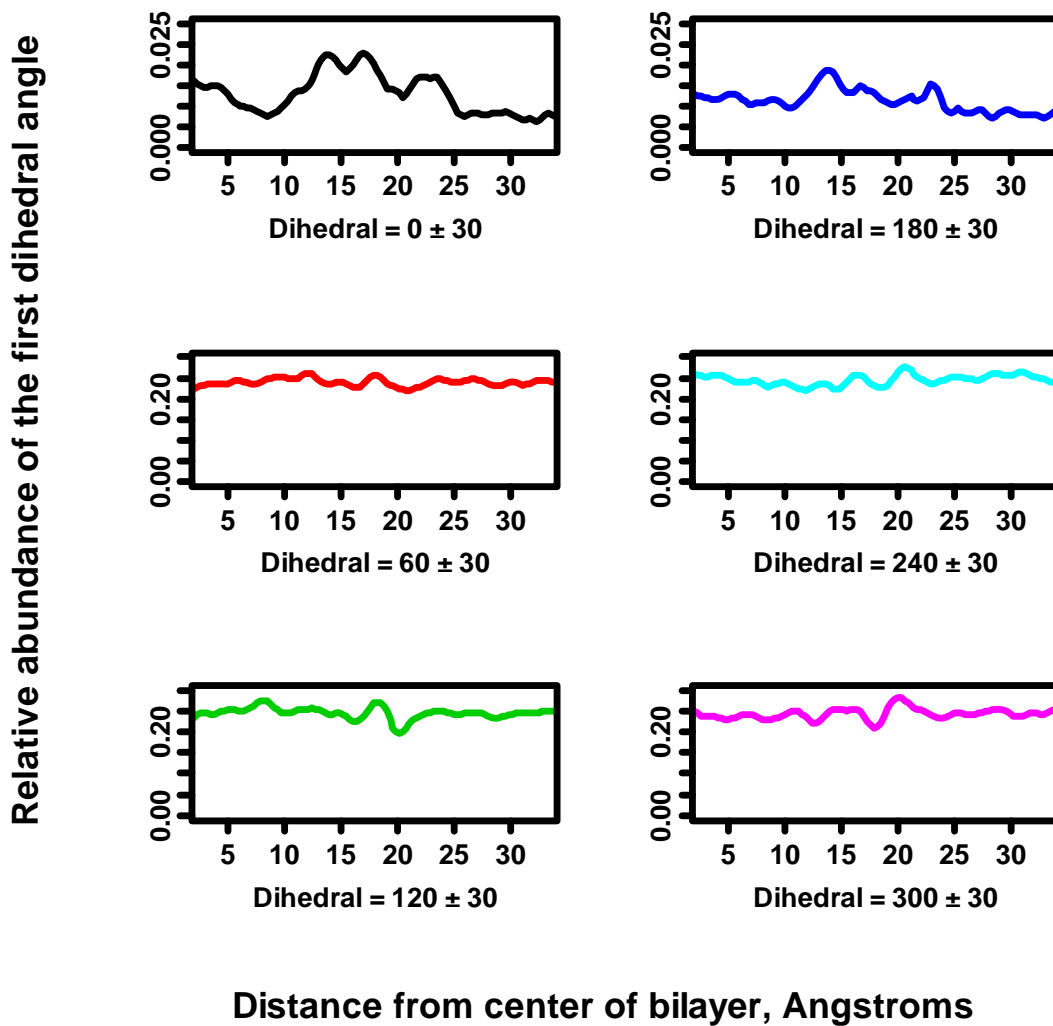


Figure 6-31. Equilibrium distribution of the various conformers of 4-ethylphenol based on the rotation of the first dihedral of the ethyl chain. The conformation labels are as shown in Figure 6-30.

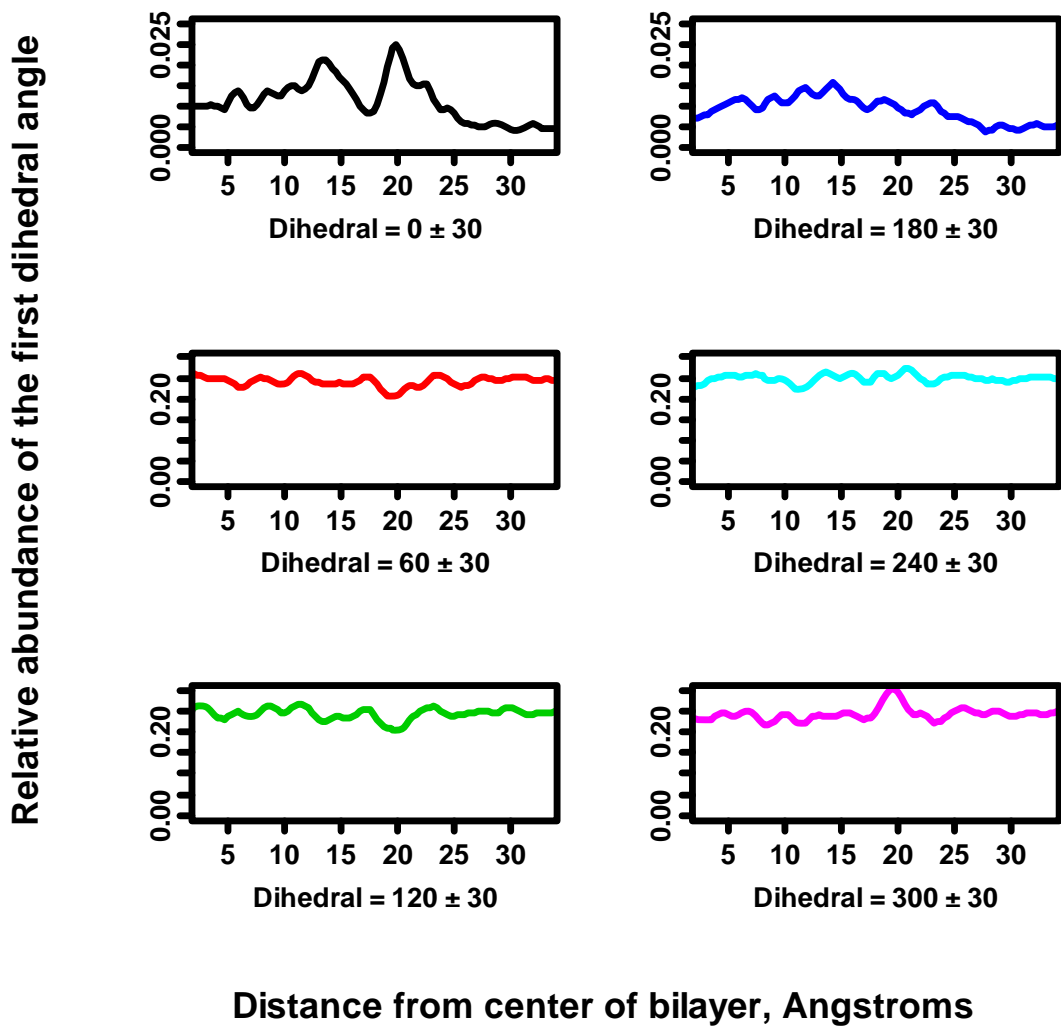


Figure 6-32. Equilibrium distribution of the various conformers of phenylethylamine based on the rotation of the first dihedral of the ethylamine chain. The conformation labels are as shown in Figure 6-30.

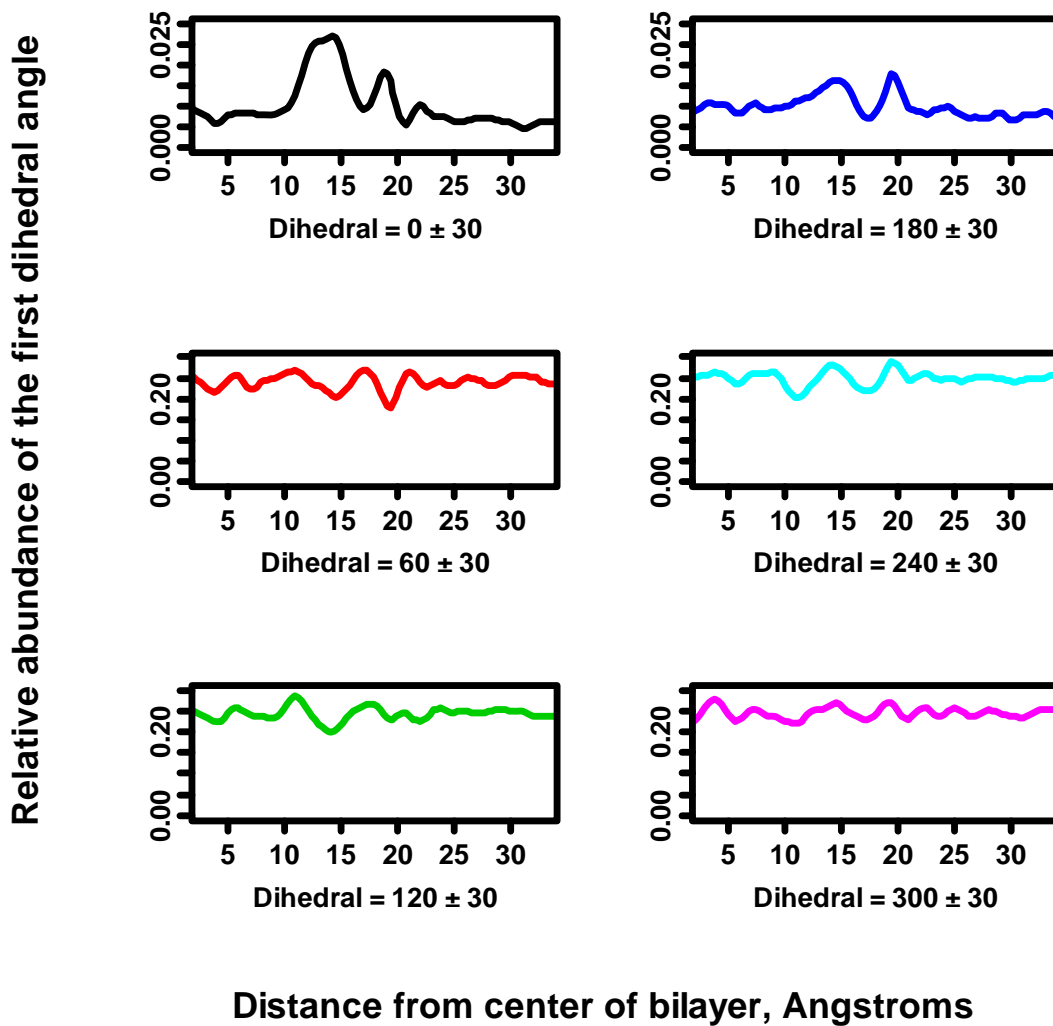


Figure 6-33. Equilibrium distribution of the various conformers of tyramine based on the rotation of the first dihedral of the ethylamine chain. The conformation labels are as shown in Figure 6-30.

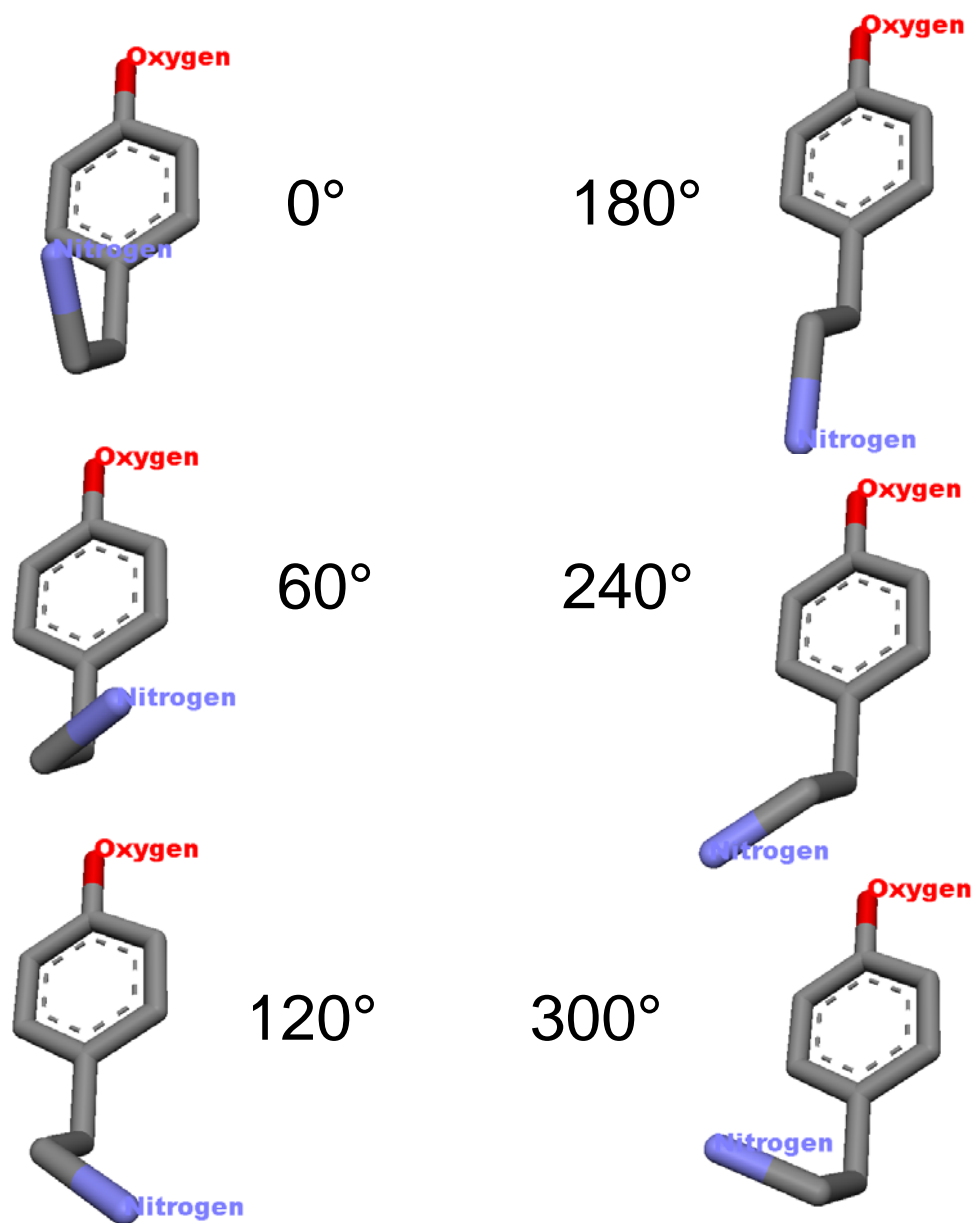


Figure 6-34. Conformers of tyramine based on the rotation of the second dihedral of the ethylamine chain. The numerical labels assigned for these conformers have been used in the subsequent figures.

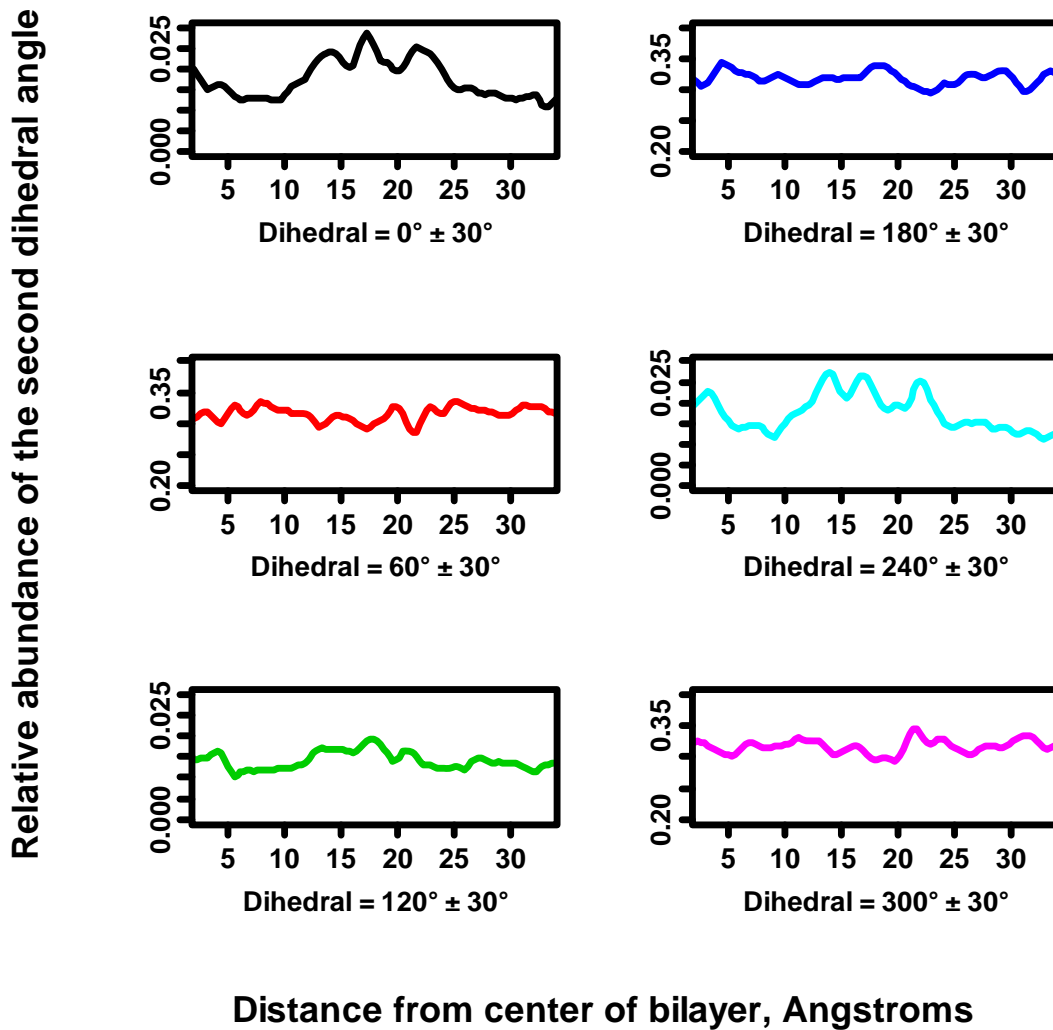


Figure 6-35. Equilibrium distribution of the various conformers of 4-ethylphenol based on the rotation of the second dihedral of the ethyl chain. The conformation labels are as shown in Figure 6-34.

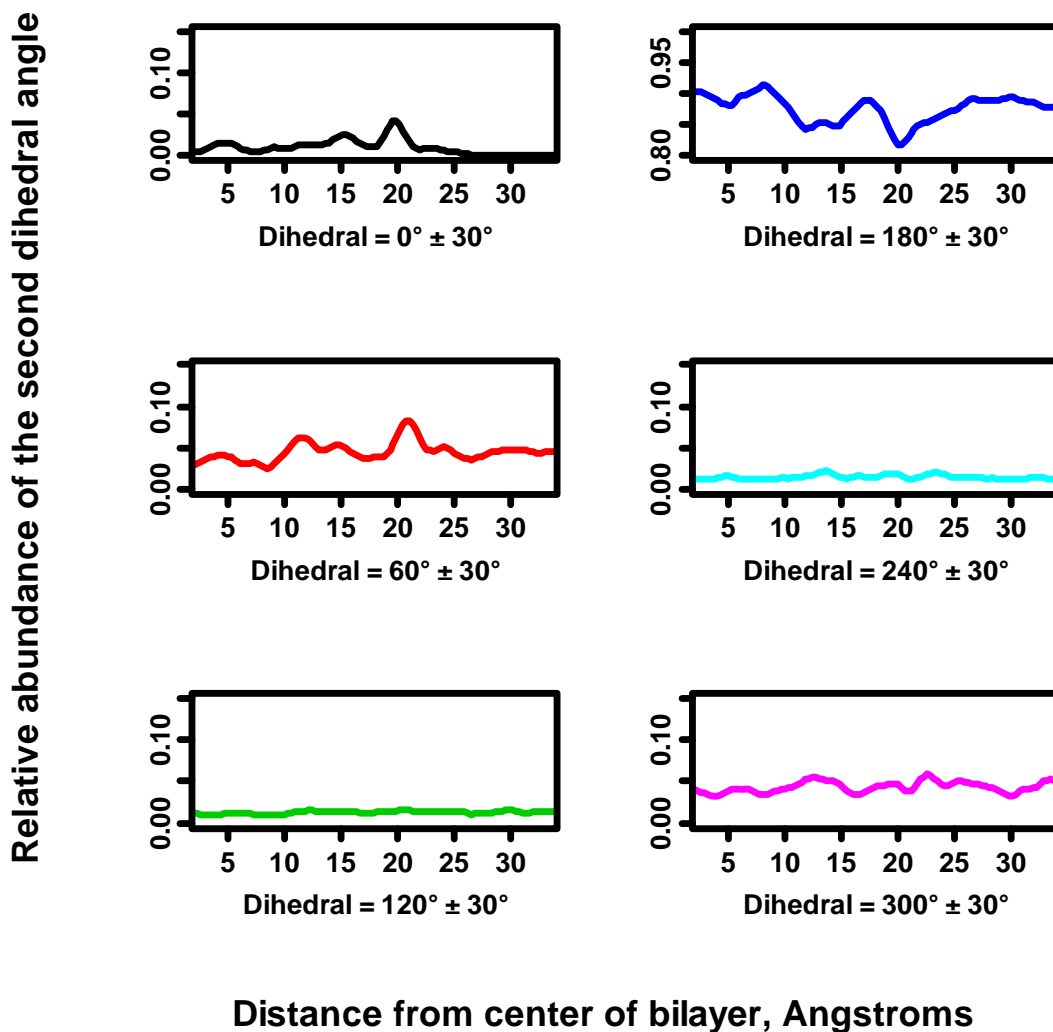


Figure 6-36. Equilibrium distribution of the various conformers of phenylethylamine based on the rotation of the second dihedral of the ethylamine chain. The conformation labels are as shown in Figure 6-34.



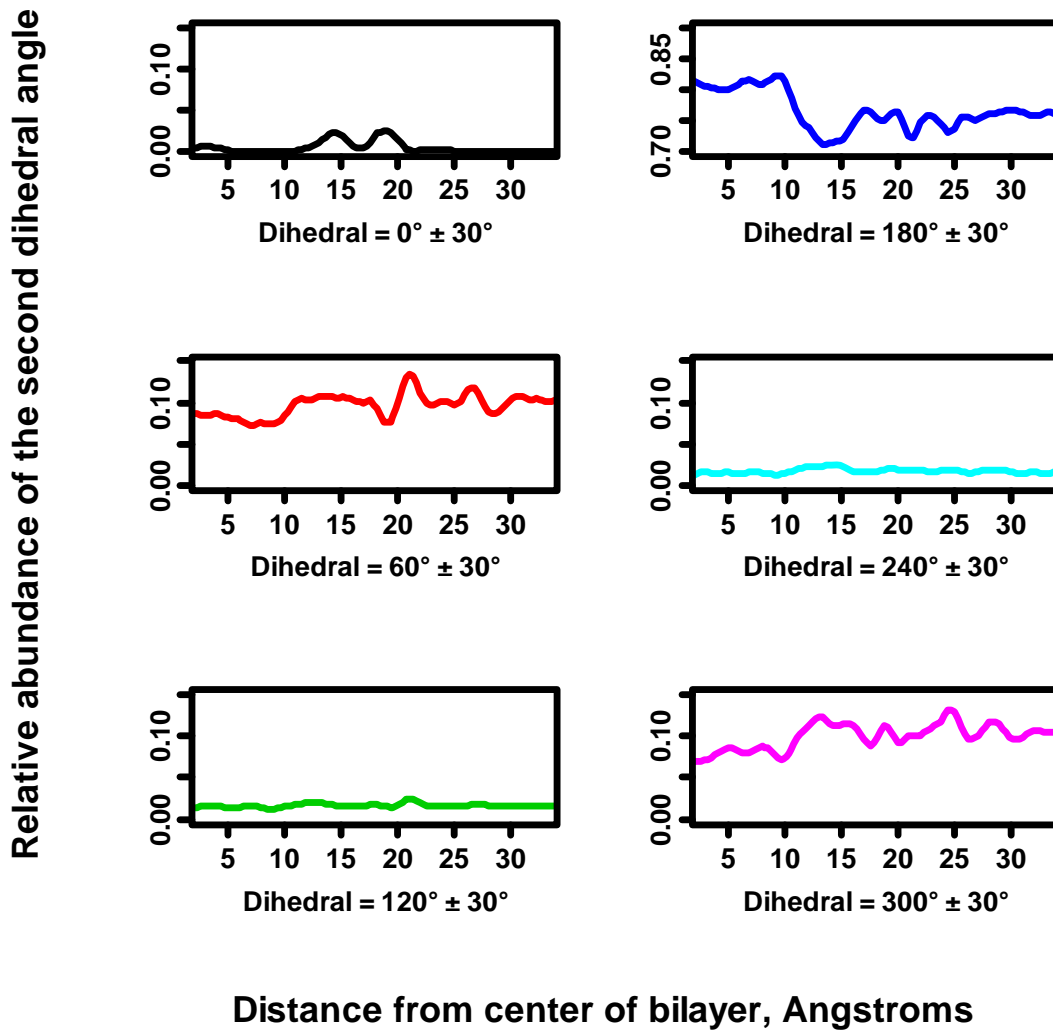


Figure 6-37. Equilibrium distribution of the various conformers of tyramine based on the rotation of the second dihedral of the ethylamine chain. The conformation labels are as shown in Figure 6-34.

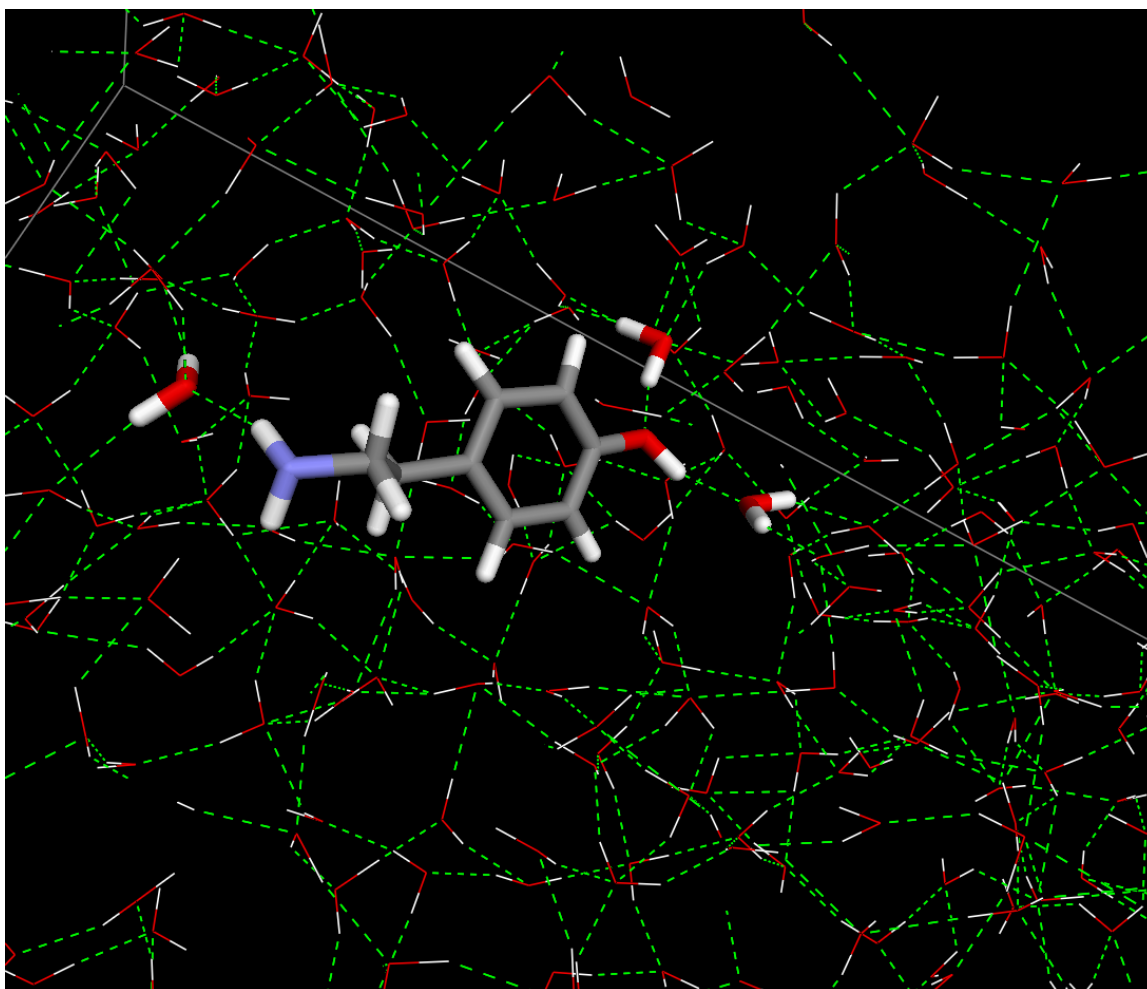


Figure 6-38. Snapshot of a tyramine molecule located in water. Tyramine and the water molecules hydrogen bonded to it are shown as sticks; all other molecules are shown as lines. The dotted lines show the hydrogen bonds detected by the visualization software (Accelrys, 2005). The molecules in the water network on the distal side of the benzene ring appear to be *missing* some of their hydrogen bonds due to the presence of the hydrophobic solute molecule. The faint gray straight lines going through the image are the edges of the unit cell. Atoms are colored by element type: hydrogen=white, carbon=grey, nitrogen = blue, and oxygen = red.

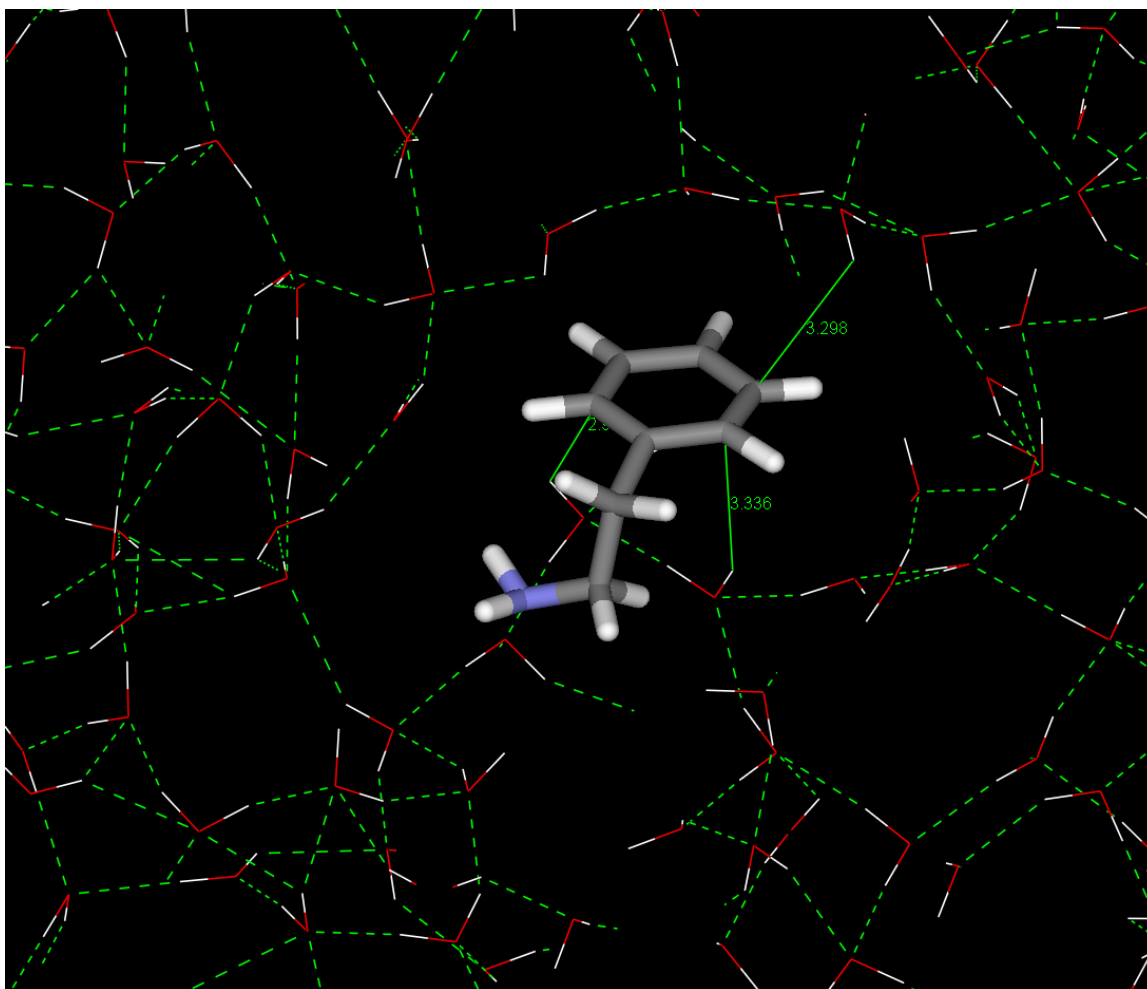


Figure 6-39. Snapshot of a phenylethylamine molecule located in water that does not appear to have any hydrogen bonds with water molecules. The network of water molecules forms an empty cavity around the solute. Distances of the solute atoms from the nearby water molecules that are *missing* some of their hydrogen bonds are shown as solid lines. Water molecules from the proximal and distal side of the plane of the picture were removed for visualization.

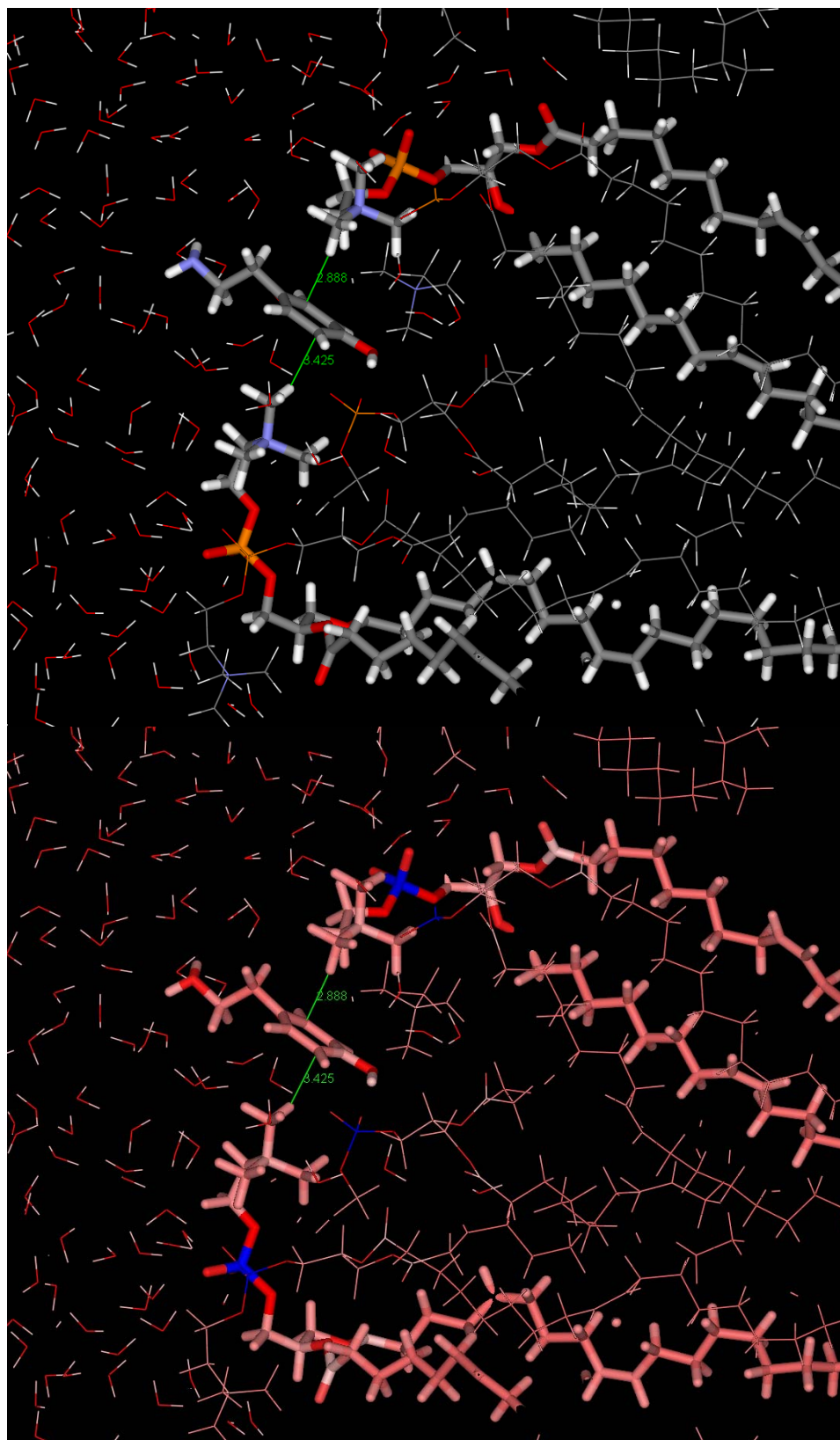


Figure 6-40. Snapshot of a tyramine molecule located on the water side of the water/headgroup interface, viewed from inside the bilayer. Each side of the benzene ring is close to choline methyl groups as if it were solvated by the latter in this relatively polar environment. The phenol group is close to a phosphoryl group (which has been removed for visibility). In the upper image the atoms are colored by element type where all element colors are as before and the phosphorus atoms are orange. In the lower image the atoms are colored by their partial charges. The color scale at the bottom has a negative partial charge on the left and a positive partial charge on the right.

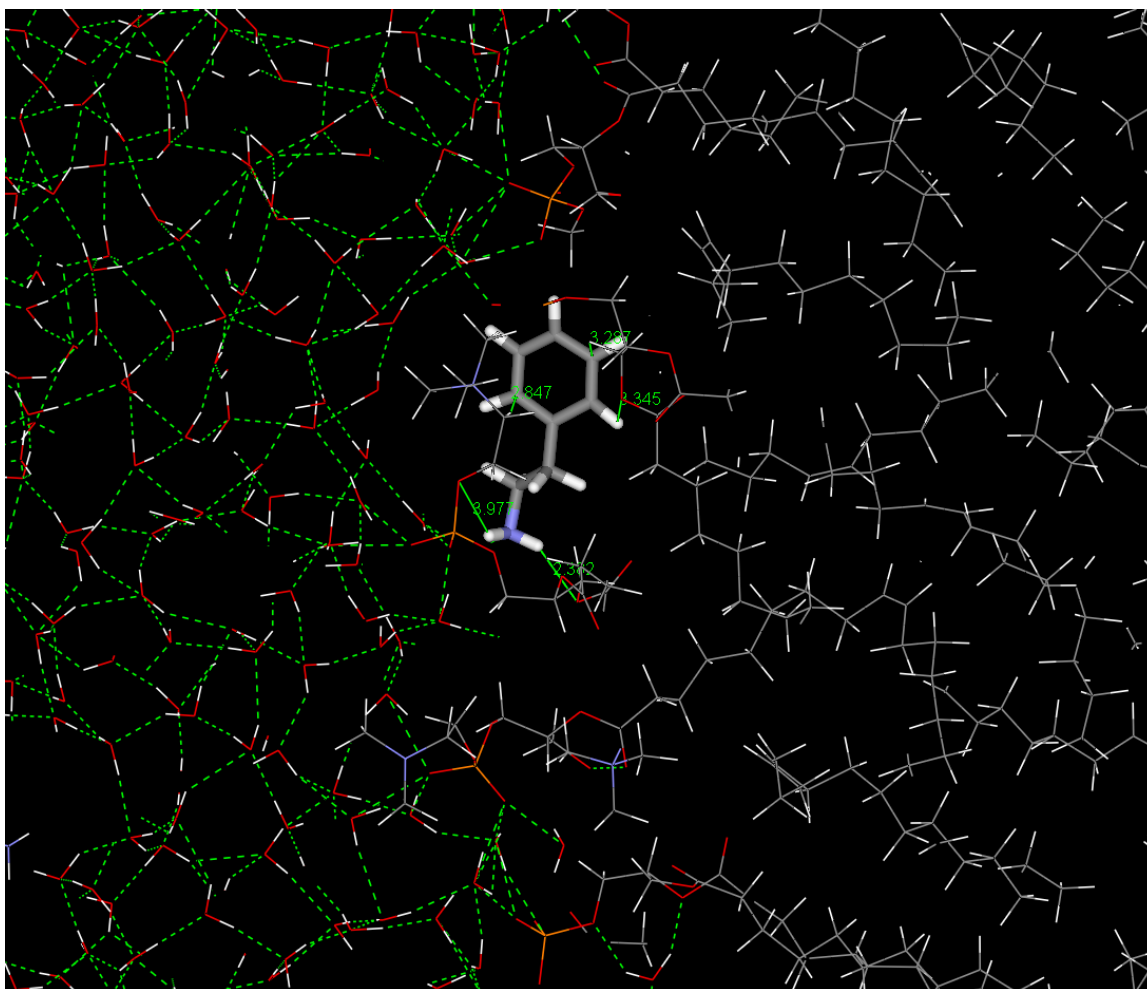


Figure 6-41. Snapshot of a phenylethylamine molecule at the water/headgroup interface as its hydrophobic portion is *shielded* from water by the choline methyl groups. The solid lines with numbers are the distance measurements and the dotted lines indicate hydrogen bonds among various molecules detected by the visualization software (Accelrys, 2005). The atoms are colored by element type.

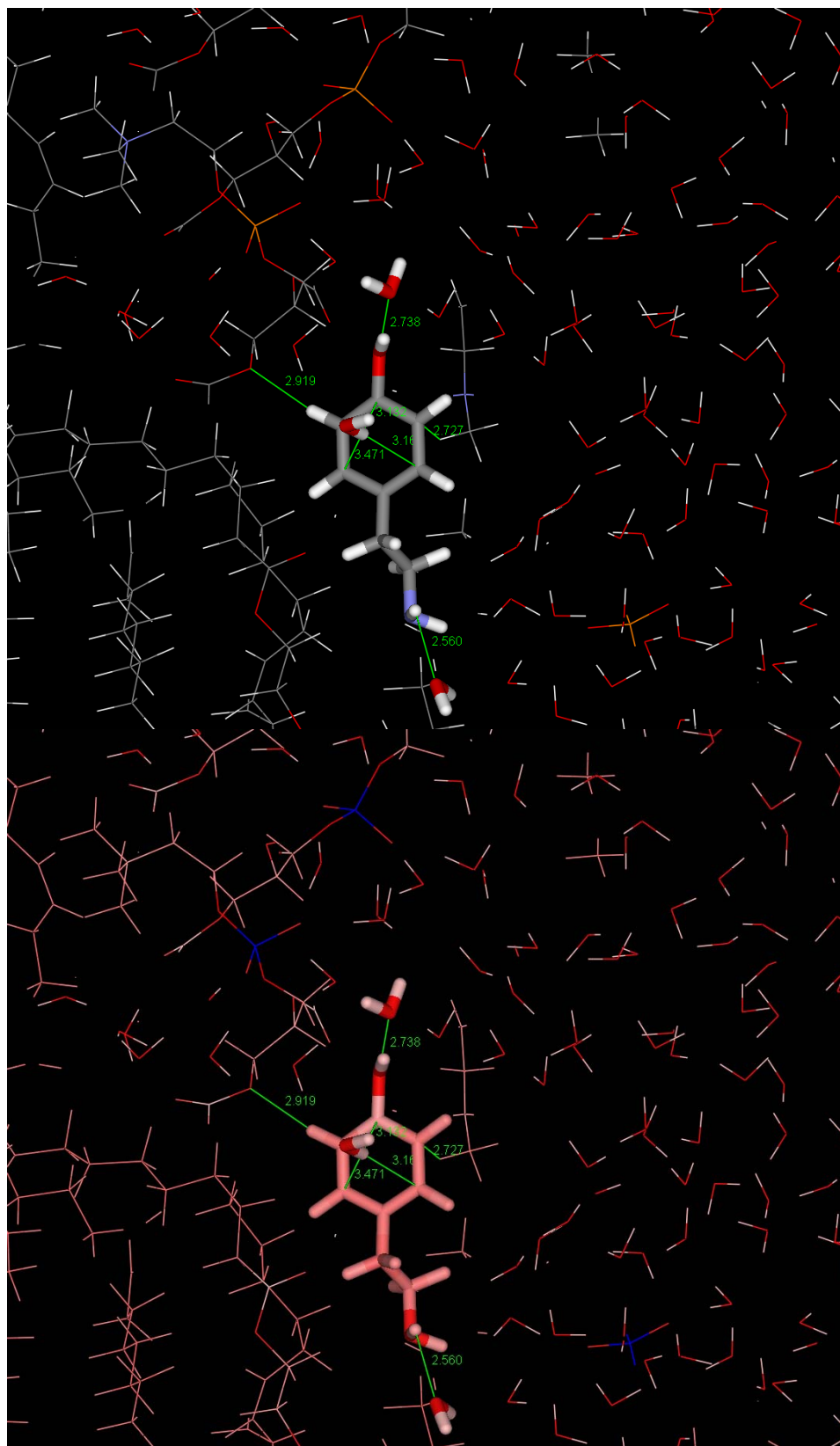


Figure 6-42. Snapshot of a tyramine molecule located at the interface of the bilayer and water. The polar groups are hydrogen bonded with the nearby water molecules. Faces of the benzene ring are close to a water molecule on the proximal side and a choline methyl group on the distal side. The lines with numbers are the measured distances in angstroms. In the upper image the atoms are colored by element type and in the lower image the atoms are colored by their partial charges. The color scale at the bottom has a negative partial charge on the left and a positive partial charge on the right.



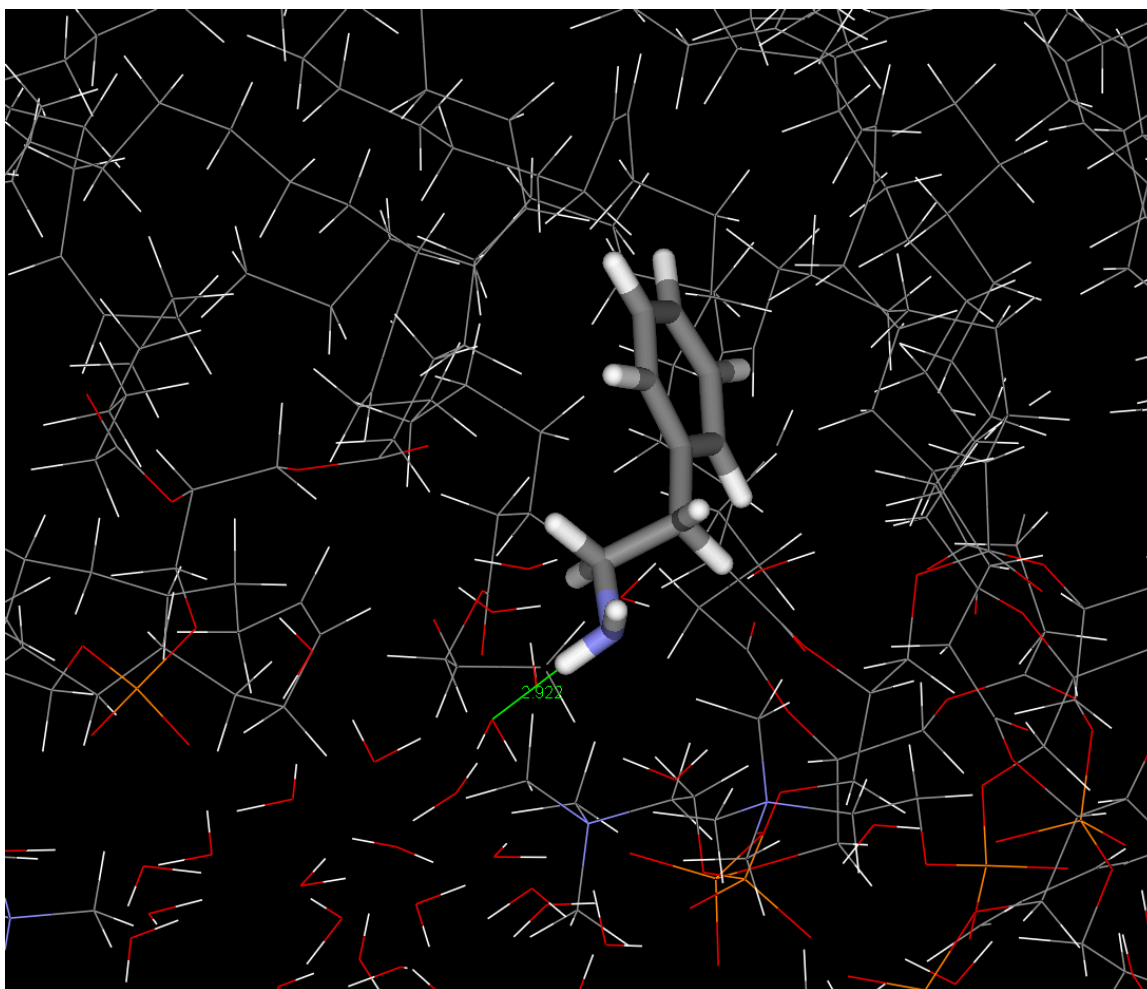


Figure 6-43. Snapshot of a phenylethylamine molecule located on the head group side of the water/head group interface where it forms a hydrogen bond with a nearby water molecule. The line with a number is the distance in angstroms.

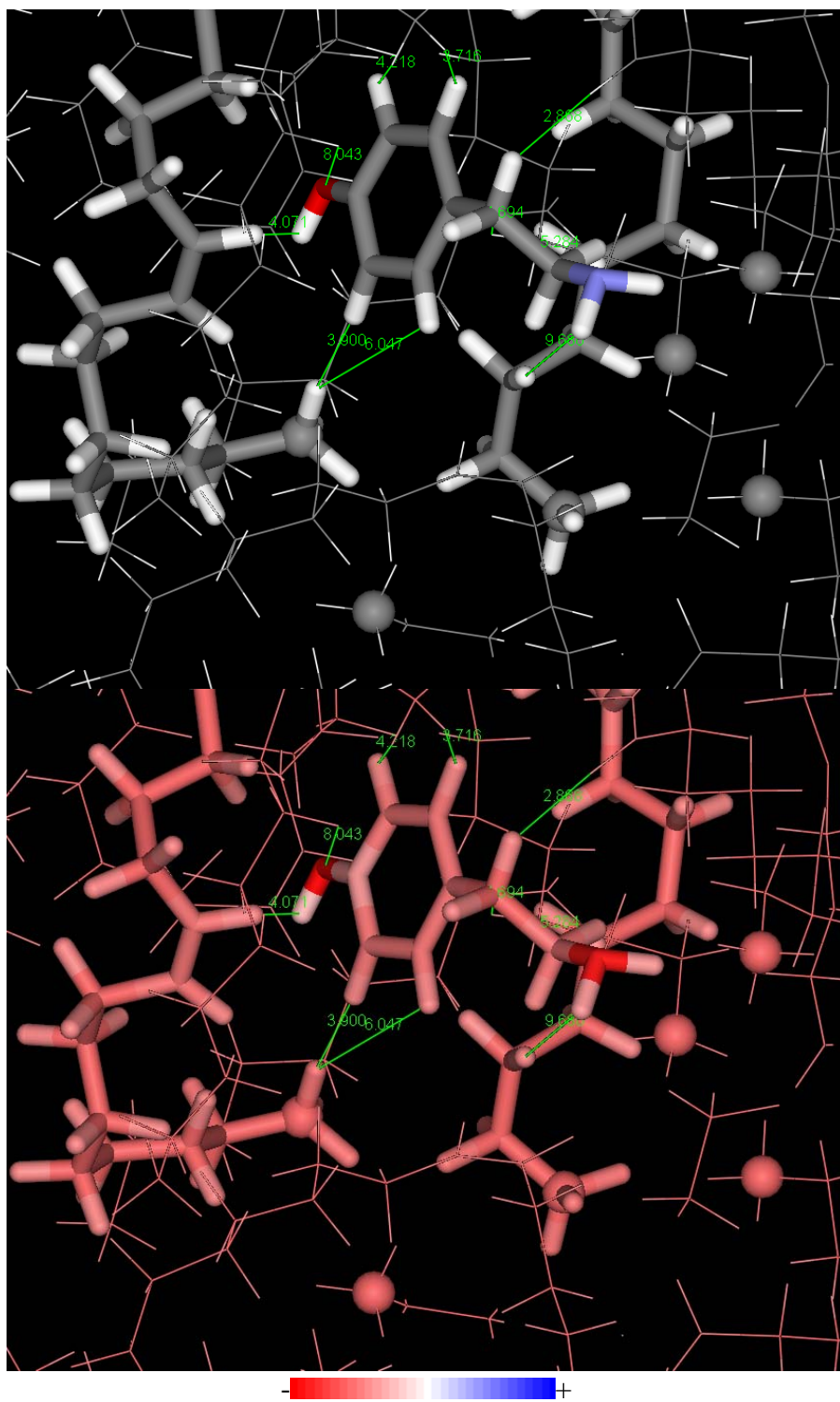


Figure 6-44. Snapshot of a tyramine molecule near the center of the bilayer. The molecules of interest are shown with stick models; others are shown with lines, and the terminal methyl of the oleoyl chains are shown as balls. The lines with numbers are the distance measurements. In the upper image the atoms are colored by element type and in the lower image the atoms are colored by their partial charges. The color scale at the bottom has a negative partial charge on the left and a positive charge on the right.

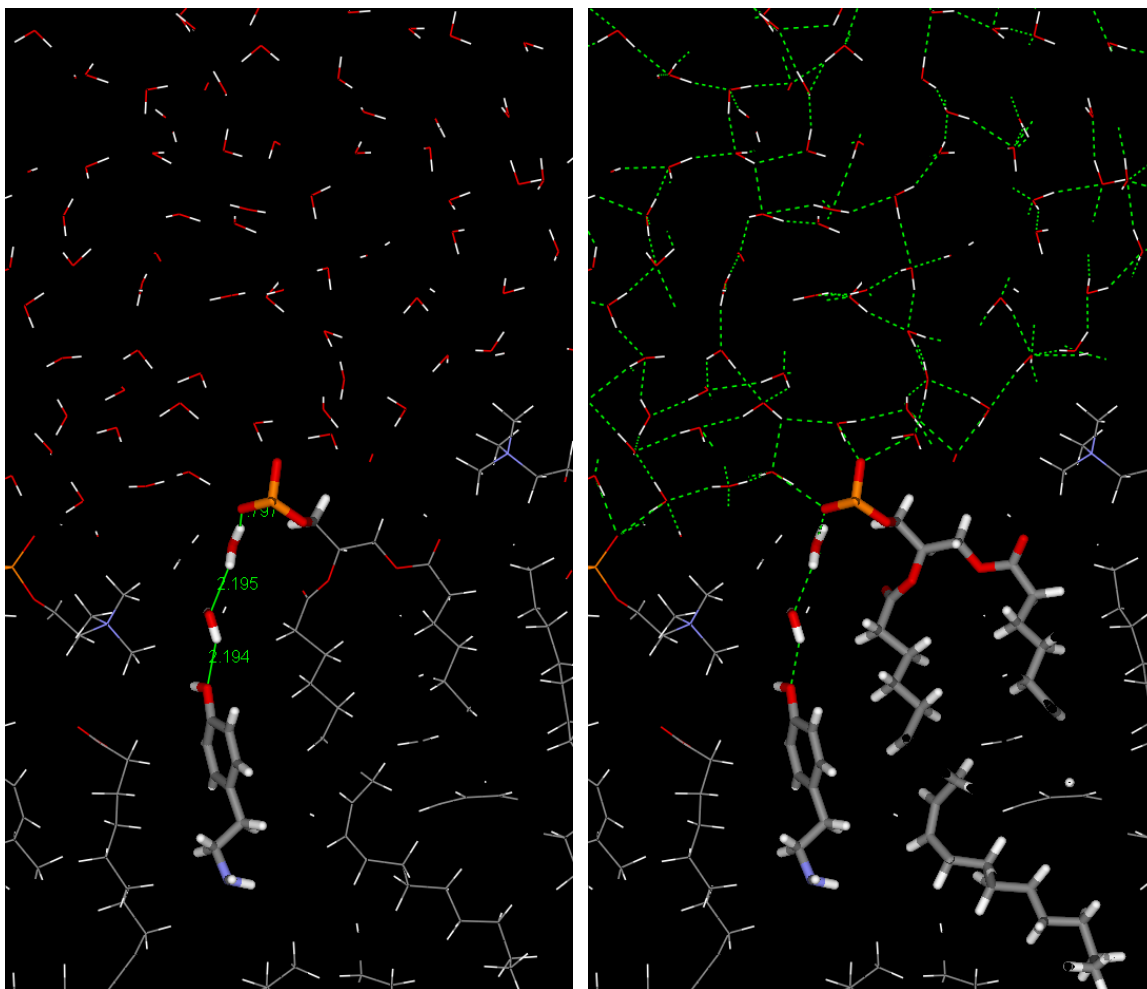


Figure 6-45. Snapshot of a tyramine molecule located at approximately 5 angstroms from the central plane of the bilayer. In the left hand image, lines with numbers show the distance measurements in angstroms. In the right hand image, the dotted lines indicate hydrogen bonds among various molecules detected by the visualization software (Accelrys, 2005).

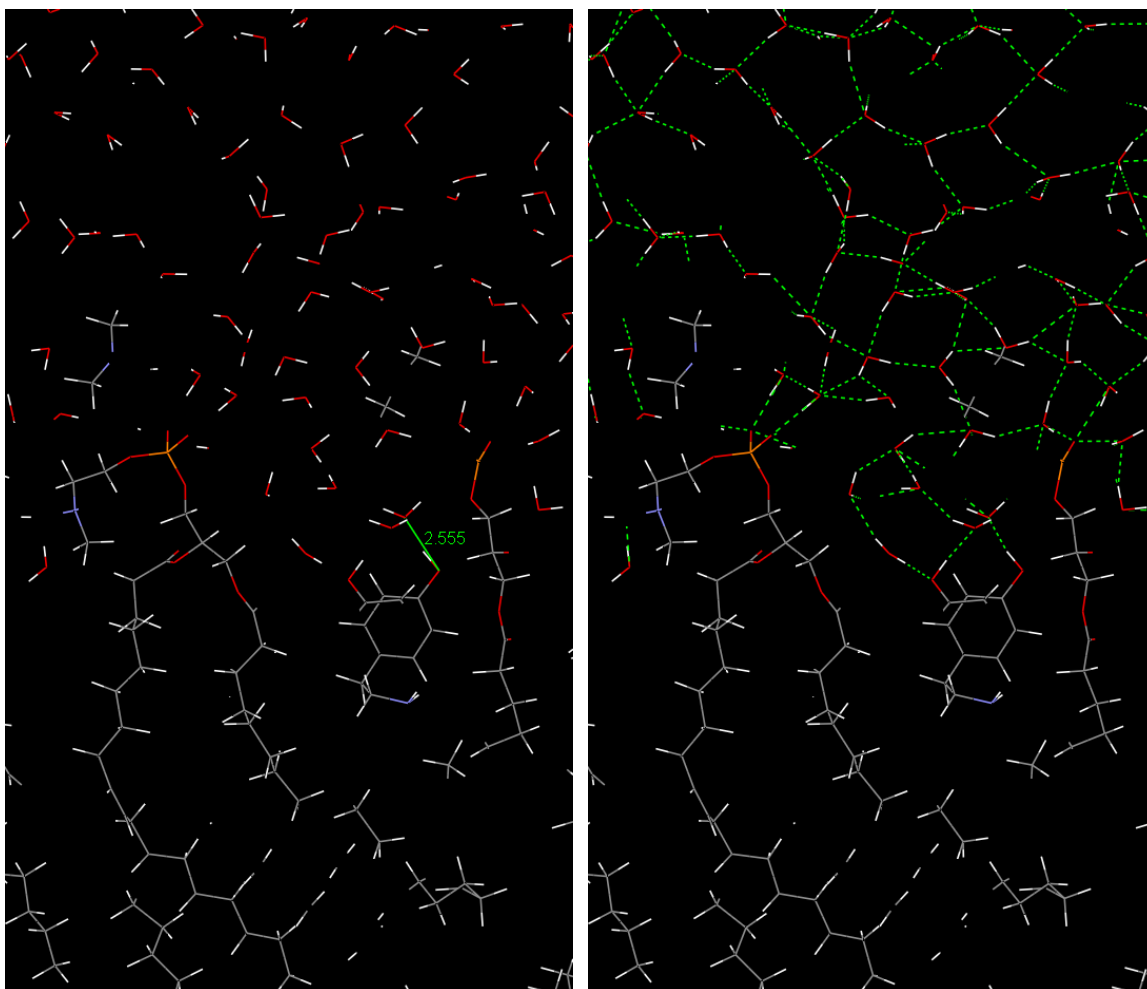


Figure 6-46. Snapshot of a tyramine molecule located at approximately 10 angstroms from the center of the bilayer. While the phenol group appears to participate in the hydrogen bonded network of the water molecules, the ethylamine chain of tyramine located in the hydrocarbon region is in a folded conformation. In the left hand image, lines with numbers are the distance measurements in angstroms. In the right hand image, the dotted lines indicate hydrogen bonds among various molecules detected by the visualization software (Accelrys, 2005).

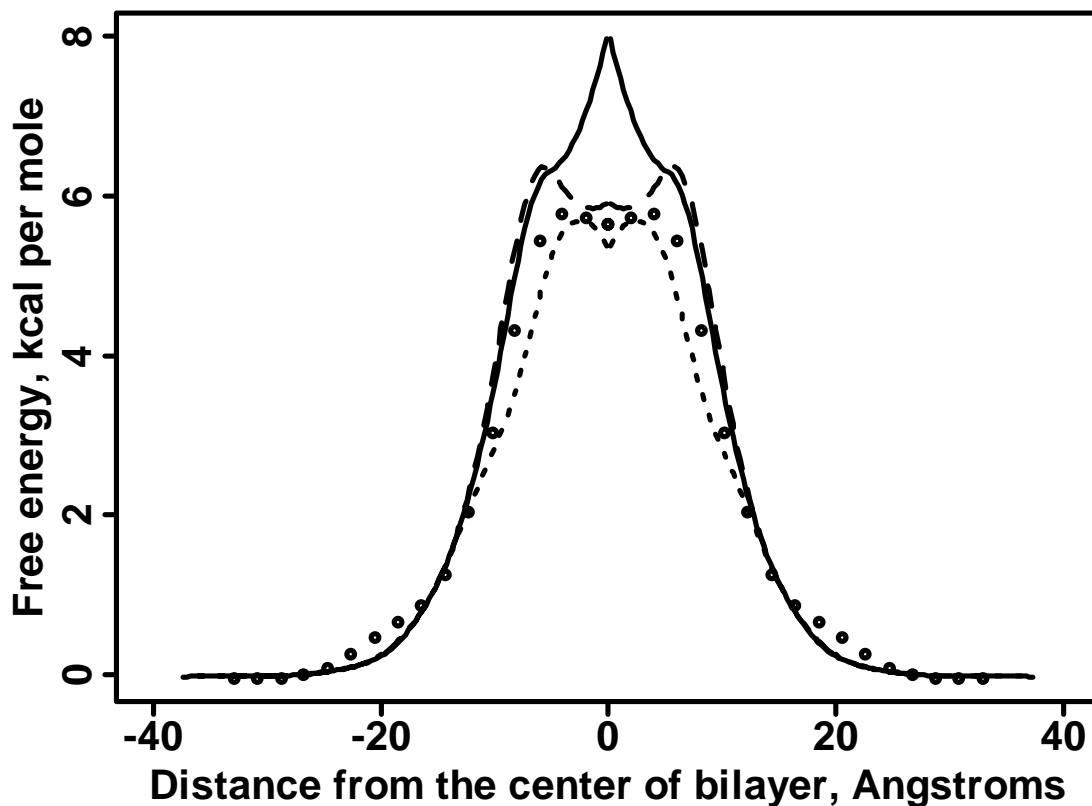


Figure 6-47. Free energy of transfer of water from bulk water to various locations within the simulation cell. The profiles were obtained from the MD simulations of the lipid bilayer containing: 4-ethylphenol (—), phenylethylamine (— —), or tyramine (---). The profiles were computed using the probability density method of post-processing. The lack of a significant number of observations near the center of the bilayer increases the uncertainty in that region. The profile shown with circular symbols (•) has been redrawn from the work of Shinoda et al (Shinoda et al., 2004) for the transfer of water into a DPPC bilayer.

## References

- ACCELRY'S (2005) DS ViewerPro. 6.0 ed., Accelrys Software Incorporated.
- ADAMSON, A. W. & GAST, A. P. (1997) The nature and thermodynamics of liquid interfaces. *Physical Chemistry of Surfaces*. 6 ed. New York, John Wiley and Sons, Inc., 48-100.
- ALPER, H. E., BASSOLINO-KLIMAS, D. & STOUCHE, T. R. (1993a) Computer simulation of a phospholipid monolayer-water system: The influence of long range forces on water structure and dynamics. *Journal of Chemical Physics*, 98, 9798-9807.
- ALPER, H. E., BASSOLINO-KLIMAS, D. & STOUCHE, T. R. (1993b) The limiting behavior of water hydrating a phospholipid monolayer: A computer simulation study. *Journal of Chemical Physics*, 99, 5547-5559.
- BEMPORAD, D., ESSEX, J. W. & LUTTMANN, C. (2004) Permeation of small molecules through a lipid bilayer: A computer simulation study. *Journal of Physical Chemistry B*, 108, 4875-4884.
- BEMPORAD, D., LUTTMANN, C. & ESSEX, J. W. (2005) Behaviour of small solutes and large drugs in a lipid bilayer from computer simulations. *Biochimica et Biophysica Acta*, 1718, 1-21.
- BHIDE, S. Y. & BERKOWITZ, M. L. (2005) Structure and dynamics of water at the interface with phospholipid bilayers. *Journal of Chemical Physics*, 123, 224702.
- CAO, Y. (2008) Application of linear free energy relationships in the prediction of triglyceride/water partition coefficients and lipid bilayer permeability coefficients of small organic molecules and peptides. PhD Thesis. College of Pharmacy, University of Kentucky, Lexington, KY.

- CHEW, C. F., GUY, A. & BIGGIN, P. C. (2008) Distribution and dynamics of adamantanes in a lipid bilayer. *Biophysical Journal*, 95, 5627-36.
- CHIU, S. W., CLARK, M. M., JAKOBSSON, E., SUBRAMANIAM, S. & SCOTT, H. L. (1999a) Application of combined Monte Carlo and molecular dynamics method to simulation of dipalmitoyl phosphatidylcholine lipid bilayer. *Journal of Computational Chemistry*, 20, 1153-1164.
- CHIU, S. W., JAKOBSSON, E., SUBRAMANIAM, S. & SCOTT, H. L. (1999b) Combined Monte Carlo and molecular dynamics simulation of fully hydrated dioleoyl and palmitoyl-oleoyl phosphatidylcholine lipid bilayers. *Biophysical Journal*, 77, 2462-2469.
- DEVIDO, D. R., DORSEY, J. G., CHAN, H. S. & DILL, K. A. (1998) Oil/water partitioning has a different thermodynamic signature when the oil solvent chains are aligned than when they are amorphous. *Journal of Physical Chemistry B*, 102, 7272-7279.
- DICKEY, A. N. & FALLER, R. (2007) How alcohol chain-length and concentration modulate hydrogen bond formation in a lipid bilayer. *Biophysical Journal*, 92, 2366-2376.
- HIETANIEMI, J. & MANFREDI, R. (1997) Math::Trig - trigonometric functions in Perl.
- KATZ, Y. & DIAMOND, J. M. (1974) Thermodynamic constants for nonelectrolyte partition between dimyristoyl lecithin and water. *Journal of Membrane Biology*, 17, 101-20.
- LI, C., YI, M., HU, J., ZHOU, H. X. & CROSS, T. A. (2008) Solid-state NMR and MD simulations of the antiviral drug amantadine solubilized in DMPC bilayers. *Biophysical Journal*, 94, 1295-302.
- MACCALLUM, J. L., BENNETT, W. F. & TIELEMAN, D. P. (2008) Distribution of amino acids in a lipid bilayer from computer simulations. *Biophysical Journal*, 94, 3393-404.

- MACCALLUM, J. L. & TIELEMAN, D. P. (2006) Computer simulation of the distribution of hexane in a lipid bilayer: spatially resolved free energy, entropy, and enthalpy profiles. *Journal of the American Chemical Society*, 128, 125-30.
- MARRINK, S.-J. & BERENDSEN, H. J. C. (1994) Simulation of water transport through a lipid membrane. *Journal of Physical Chemistry*, 98, 4155-4168.
- MARRINK, S. J., JÄHNIG, F. & BERENDSEN, H. J. (1996) Proton transport across transient single-file water pores in a lipid membrane studied by molecular dynamics simulations. *Biophysical Journal*, 71, 632-647.
- MARTIN, A. N. (1993) Interfacial phenomena. *Physical Pharmacy: Physical Chemical Principles In The Pharmaceutical Sciences*. 4 ed. Malvern, PA, Lea and Febiger, 632-392.
- MAYER, P. T., XIANG, T.-X., NIEMI, R. & ANDERSON, B. D. (2003) A hydrophobicity scale for the lipid bilayer barrier domain from peptide permeabilities: Nonadditivities in residue contributions. *Biochemistry*, 42, 1624-1636.
- MUKHOPADHYAY, P., VOGEL, H. J. & TIELEMAN, D. P. (2004) Distribution of pentachlorophenol in phospholipid bilayers: a molecular dynamics study. *Biophysical Journal*, 86, 337-45.
- PASENKIEWICZ-GIERULA, M., TAKAOKA, Y., MIYAGAWA, H., KITAMURA, K. & KUSUMI, A. (1997) Hydrogen bonding of water to phosphatidylcholine in the membrane as studied by a molecular dynamics simulation: location, geometry, and lipid-lipid bridging via hydrogen-bonded water. *Journal of Physical Chemistry A*, 101, 3677-3691.
- ROSSO, L. & GOULD, I. R. (2008) Structure and dynamics of phospholipid bilayers using recently developed general all-atom force fields. *Journal of Computational Chemistry*, 29, 24-37.



- S. H. YALKOWSKY, S. C. V. G. L. A. (1976) Solubility of nonelectrolytes in polar solvents IV: Nonpolar drugs in mixed solvents. *Journal of Pharmaceutical Sciences*, 65, 1488-1494.
- SCHERER, P. G. & SEELIG, J. (1989) Electric charge effects on phospholipid headgroups. Phosphatidylcholine in mixtures with cationic and anionic amphiphiles. *Biochemistry*, 28, 7720-8.
- SEELIG, J. & GANZ, P. (1991) Nonclassical hydrophobic effect in membrane binding equilibria. *Biochemistry*, 30, 9354-9359.
- SHINODA, W., MIKAMI, M., BABA, T. & HATO, M. (2004) Molecular dynamics study on the effects of chain branching on the physical properties of lipid bilayers: 2. Permeability. *Journal of Physical Chemistry B*, 108, 9346-9356.
- STOUCH, T. R. (1998) Permeation of lipid membranes: Molecular dynamics simulations. IN KOLLMAN, P. & ALLINGER, N. (Eds.) *Encyclopedia of Computational Chemistry, Setting the Standards in Computational Chemistry*. 1 ed. New York, NY, John Wiley and Sons, Ltd., 3: 2038-2045.
- THYSSEN, A. (2001) Math::VectorReal - Module to handle 3D vector mathematics in Perl.
- ULANDER, J. & HAYMET, A. D. (2003) Permeation across hydrated DPPC lipid bilayers: simulation of the titrable amphiphilic drug valproic acid. *Biophysical Journal*, 85, 3475-84.
- VENABLE, R. M. & PASTOR, R. W. (2002) Molecular dynamics simulations of water wires in a lipid bilayer and water/octane model systems. *Journal of Chemical Physics*, 116, 2663-2664.
- WALL, L. (2004) Practical extraction and report language. 5.8 ed.
- WEISSTEIN, E. W. (1999) "Spherical cap" from MathWorld - A Wolfram web resource. Wolfram Research, Inc.

- WILSON, M. A. & POHORILLE, A. (1996) Mechanism of unassisted ion transport across membrane bilayers. *Journal of the American Chemical Society*, 118, 6580-7.
- WILSON, M. A., POHORILLE, A. & PRATT, L. R. (1987) Molecular dynamics of the water liquid-vapor interface. *Journal of Physical Chemistry*, 91, 4873-4878.
- WIMLEY, W. C. & WHITE, S. H. (1993) Membrane partitioning: distinguishing bilayer effects from the hydrophobic effect. *Biochemistry*, 32, 6307-12.
- XIANG, T.-X. & ANDERSON, B. D. (1994) The relationship between permeant size and permeability in lipid bilayer membranes. *Journal of Membrane Biology*, 140, 111-22.
- XIANG, T.-X. & ANDERSON, B. D. (1998) Influence of chain ordering on the selectivity of dipalmitoylphosphatidylcholine bilayer membranes for permeant size and shape. *Biophysical Journal*, 75, 2658-2671.
- XIANG, T.-X. & ANDERSON, B. D. (1999) Molecular dissolution processes in lipid bilayers: A molecular dynamics simulation. *Journal of Chemical Physics*, 110, 1807-1818.
- XIANG, T.-X. & ANDERSON, B. D. (2006) Liposomal drug transport: A molecular perspective from molecular dynamics simulations in lipid bilayers. *Advanced Drug Delivery Reviews*, 58, 1357-1378.

## **CHAPTER SEVEN: Conclusions and future directions**

The work presented in this dissertation provides a direct comparison of the experiments and all-atom molecular dynamics (MD) simulations. Additionally, several expected and unexpected findings from the experimental and the MD simulation studies are summarized below.

### **Experimental models for permeation and partitioning**

#### *Methods for obtaining the intrinsic permeability coefficients*

The validity of the experimental measurement of the permeability coefficients has been established in the low pH conditions required for the measurements of the amine containing compounds. The barrier integrity of the bilayer in these conditions was verified using  $^{31}\text{P}$ -NMR, release kinetics of mannitol, and release kinetics of bretylium, a quaternary ammonium compound with very low permeability coefficient.

Quantitative physical models were developed to account for ionization, solute induced pH-drift in the vesicles, solute binding, and the effect of slow permeating proton carriers. While solute induced pH drift should have been expected based on the published method of remote loading of liposomes, no quantitative account is available to ascertain its impact on the release or uptake kinetics. The models developed in this work allow for determination of the intrinsic permeability coefficients from the measurements in the presence of these complicating phenomena.

A relatively large effect of very weak binding of tyramine on the permeability coefficient highlights the importance of the volume contrast between the intra- and extra-vesicular compartments. If the compartment volumes were equal, this effect on the permeability coefficients would have been minimal (a simple multiple of the binding constant) as is the case in side by side diffusion cell studies. The quantitative models derived from these liposomal studies may have a broader application to passive transport processes occurring within cell organelles which tend to have much smaller volumes than their surrounding environment.

The experimental studies employed 4 mole percent DOPA in DOPC in order to impart physical stability to the vesicles. This small charge on the surface of membrane can lead to the Boltzmann distribution of buffer cations near the surface which in turn can affect the binding and transport of the solutes across the lipid bilayer. While this charge on the membrane or the buffer ions were not explicitly modeled in the MD simulations, the inclusion of the solute binding constant in the quantitative model accounts for any effect on the solute concentration gradients (see discussion in Chapter Three). While this small charge on the bilayer membrane can have an impact on the partitioning of ions in the membrane, the simulations employed only the neutral forms of solutes and the experimental studies determined the properties specific to the neutral forms of the solutes. It is however conceivable that this small charge on the membrane could impact the orientations of the solutes in the lipid bilayers in the experiments and such effect may not be represented in the MD simulations.

#### ***Partition coefficients into various regions of the lipid bilayer***

The intrinsic partition coefficients for several compounds in 1,9-decadiene, as a surrogate for the barrier domain, were determined. The microscopic ionization constants needed for the calculation of the intrinsic properties of the *p*-(aminoethyl)-phenols were also determined. The results uncovered a long range intramolecular interaction between the amino and phenol groups of tyramine that caused deviations in the microscopic pKa values and partition coefficient of tyramine from the expected values. Specifically, the interaction led to a decrease in pKa of phenol group when the amino group was protonated and an increase in pKa of amino group when phenol group was ionized. Additionally, the intrinsic partition coefficient of tyramine in 1,9-decadiene was found to be higher than that based on the partition coefficients of related *p*-(aminoethyl)-phenols and well established functional group contributions. The interaction has been reported in spectroscopy literature and can be assigned a free energy value of approximately 1 kcal per mole (favoring the folded conformation of tyramine) based on the shifts in the partition coefficients and the ionization constants. The functional group contributions for partitioning of the phenol and hydroxyl were found to be lower than the expectation from the literature due to this interaction.

Contributions of the solute functional groups to the free energies of transfer to the preferred binding domain were also determined. These values for the aromatic hydroxyl and alkyl amine groups were found to be close to zero and were consistent with the findings from the immobilized artificial membrane (IAM) chromatography measurements as well as the pentapeptide binding experiments reported in the literature.

## **Molecular dynamics simulations for partitioning into DOPC bilayers**

### ***Free energy profiles from the MD-simulation***

The molecular dynamics simulations reproduced the experimental properties of the DOPC bilayer and successfully sustained its structure over the entire simulation run for each of the three solutes. The method of force integration was found to be more robust than the population density analysis for the post-processing of simulation data to obtain the free energy profiles. The improvement in the accuracy was found to be due to the more accurate bookkeeping of the constraint forces at each time step of the simulation.

The MD simulations accurately depicted the experimental finding that a preferred binding domain and a barrier domain exist in the lipid bilayer side-by-side. Functional group contributions to the free energy of transfer were reproduced by the simulations far more accurately than the free energies of transfer of solutes themselves. The hydroxyl and amino group contributions to solute transfer from water to the center of the bilayer were much larger (i.e., more unfavorable) than those to the preferred binding region. All four of these quantities were well corroborated by the experimental determinations.

While the shapes of free energy profiles and the functional group free energy contributions determined from MD simulations were consistent with the corresponding experimental quantities, the free energies of solute transfer to various locations in the bilayer could not be compared with the experiment due to the lack of exactly the same experimental quantity. The specific intramolecular interaction unique to tyramine that was invoked to account for the experimental partition coefficient and ionization constants for this compound could not be reproduced in the MD simulations possibly due to the

known limitations of the force fields which may not accurately account for certain interactions where polarization effects are important, such as the NH- $\pi$  type of interactions. Similarly, the currently available force fields for the simulations only allow representation of atoms as point charges and do not account for effects such as the quadrupolar nature of the benzene ring or a double bond (Vrbancich and Ritchie, 1980, Narten, 1977, Narten, 1968, Cox et al., 1958).

### ***Hydrogen bonding and hydrophobic effect on solute partitioning into the lipid bilayers***

The review of the intermolecular interactions between the solutes and their environments along the transport path led to several interesting findings. First, the head group region is found to have a significant excess of water molecules. Water molecules continue to outnumber the DOPC molecules all the way to the first alkyl carbon. As a result, the majority of hydrogen bonds involving polar functional groups of the solutes were with water even in the head group region.

From the review of the intermolecular interactions as well as the free energy profiles obtained by other workers in the literature, it appears that the characteristic shape of the free energy profile depends on the chemical structure of the solute. Specifically:

a. Polar small solutes such as water, methanol, and ammonia may show only a peak in the center of the bilayer and no change in the free energy in the head groups from that in the bulk water. The latter could be due to solute induced rearrangement of the hydrogen bond network in the head group region resulting in the same number of hydrogen bonds per solute as in the bulk water.

b. Small and large non-polar solutes such as ethane, butane, and hexane may show a small peak in the head group region and a significant reduction in free energy, proportional to their hydrophobicity, in the center of the bilayer. The lowering of the profiles in the center of the bilayer is consistent with the classical hydrophobic effect.

c. Amphiphilic solutes (most drug molecules belong in this class) are very likely to show a preferred binding region. While amphiphilic complementarity on the inside of

the head groups was an expectation, it was found that this explains only half of the profile. Half of the lowering of the free energy profile is external to the head groups where the polar groups of the solutes still have the same number of hydrogen bonds with water as in bulk water. This could be due to partial shielding of the hydrophobic groups of the solutes by relatively nonpolar portions of the head group such as the choline methyl groups. Further, since the number of solute hydrogen bonds is unchanged from bulk water to the head group region, the depth of the free energy profile in this region appears to depend on factors other than the number of hydrogen bonds.

The specific interactions between amphiphilic permeants and other bilayer components give rise to preferred orientations depending on depth within the bilayer. Relative populations of the preferred orientations allow for the calculation of the underlying free energy differences between orientations and therefore their causative intermolecular interactions. This has implications in terms of the size of the solute. If an amphiphile were large enough to never flip inside the lipid bilayer, it would be forced to have an asymmetric orientational profile as it traverses the bilayer. This may give rise to significant energy barriers along the transport path that may perturb the estimates based solely on the polar and non-polar group surface areas. While conformational flexibility was found to be unimportant for the small solutes in the MD simulations, it could become important for the larger solutes. The conformational changes in such large solutes may compensate for the orientational barriers resulting from their size.

Formation of water wires (also known as water defects) appears to be abundant from the snapshot views. However a closer analysis of water distribution suggests that while solutes are constrained to specific locations in the bilayer, water bound to them frequently changes locations. The probability density analysis shows that the free energy barrier of water (in presence of the solutes) in the center of the bilayer has a lower bound that is not significantly different from the free energy profiles reported in the literature. This suggests that the solutes constrained at or near the center of the bilayer do not decrease the free energy barrier of water. As a result, it can be concluded that the free energy estimates obtained for the solutes in the center of the bilayer were also not lowered due to interactions with water.

A preference of the ethyl chain over the benzene ring for the center of the bilayer was consistently found for all three solutes irrespective of the location of the polar functional groups. This may be due to specific interactions between the double bonds of DOPC and the benzene ring but further investigation is required to test this hypothesis.

Finally, real biological membranes contain membrane proteins, including transporters, which have not been included either in the experimental bilayers or the MD simulations. The presence of such components would likely impact passive transport by altering the solvent properties of the bilayer. While this work did not address such complex bilayers, the insights gained from both the experiments and MD simulations will hopefully provide a starting point for studies of biological membrane barriers.

### References

- COX, E. G., CRUICKSHANK, D. W. J. & SMITH, J. A. S. (1958) The crystal structure of benzene at  $-3^{\circ}\text{C}$ . *Proceedings of the Royal Society of London. Series A, Mathematical and Physical Sciences*, 247, 1-21.
- NARTEN, A. H. (1968) Diffraction pattern and structure of liquid benzene. *Journal of Chemical Physics*, 48, 1630-1634.
- NARTEN, A. H. (1977) X-ray diffraction pattern and models of liquid benzene. *Journal of Chemical Physics*, 67, 2102-2108.
- VRBANCICH, J. & RITCHIE, G. L. D. (1980) Quadrupole moments of benzene, hexafluorobenzene and other non-dipolar aromatic molecules. *Journal of the Chemical Society, Faraday Transactions 2: Molecular and Chemical Physics*, 76, 648-659.



## APPENDIX ONE: Additional notes on the volume contrast between intravesicular and extravesicular compartments

### The volume contrast between compartments

The volumetric contrast between the extravesicular and the intravesicular compartments of a liposomal suspension can lead to amplified intravesicular binding effects as well as pH drift. For the case of a vesicular dispersion where approximately 1% of total volume is enclosed in the vesicles, the volume multiple between the compartments is 100 fold.

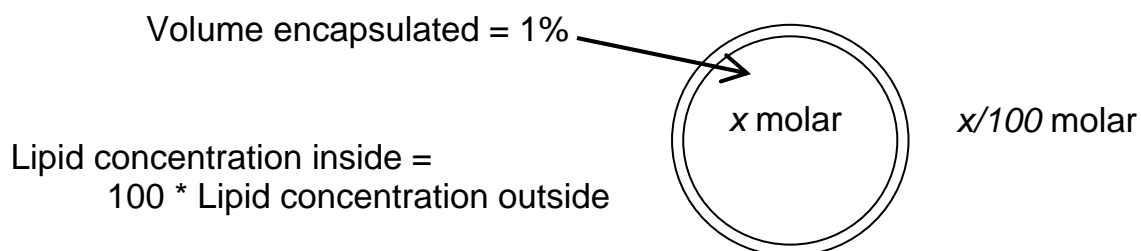


**Figure A1-1.** Intravesicular volume contrast

This volume contrast has several implications:

- 1) For the permeant being released, sink conditions extravesicularly can be assumed in the absence of pH gradients (not assumed in this work).
- 2) The internal reservoir of the buffer species constitutes only 1% of the total capacity. This has implications on the mass balance for the buffer and the buffer capacity.
- 3) For the lipid interactions with the solution, whether treated as interfacial binding or a pseudophase model, the effective intravesicular lipid concentration is approximately 100 times that in the external compartment.

### Magnification of the binding effect due to the volume contrast

The increased intravesicular concentration of the lipid can bind a significant portion of the permeant despite a weak binding constant. The same binding constant however results in an insignificant fraction bound in the extravesicular compartment. This leads to a significant time dependent effect on the concentration gradient of the permeant as demonstrated in Figure 3-15 in chapter three. The resulting altered release profiles are shown in the simulations in Figure 3-14 in chapter three, and show incomplete release at equilibrium. If these simulated data are fit using the classical rate equations (Equations 3-5 or 3-6 in chapter three) they result in an apparently lower permeability coefficient.

If an experimental measurement is carried out in a diffusion apparatus where the volumes of the donor and receiver compartments are comparable, lipid concentrations for both sides would be equal. This would make the bound fractions of permeant to be equal in the two compartments. As a result Equation 3-13 in chapter three (accounting for the binding effect) reduces to

$$\frac{dB_{T(ext)}}{dt} = \frac{6V_{int}}{V_{ext}d} f_{unbound} P_{app} (B_{T(int)} - B_{T(ext)}) \quad (A1-1)$$

For a weak binding compound where fraction unbound can be nearly 1, this equation approaches Equation 3-6 which is the classical transport model that does not account for the binding effect. If, however, binding were strong, the driving force for drug release would be reduced since the fraction unbound would be less.

However, the exact rate law of Equation 3-13 is necessary in the case of diffusion experiments employing different volumes on the donor and receiver side. An example, apart from the liposome suspensions studied here, would be the high throughput cell monolayer permeability experiments in which apical and basolateral compartment volumes may differ by several-fold.

## Volume contrast and the pH drift

The volume contrast effect described above leads to a time dependent effect on the ionization equilibria in the intravesicular compartment. It is expected that over the time scale of the experiments, only the neutral form of the amine containing compound transports across the lipid bilayer. At the low pH conditions of the experiments conducted in this thesis the majority of the amine was present in the protonated form (BH<sup>+</sup>) in equilibrium with a very small amount of the neutral form which is the permeable species (B).

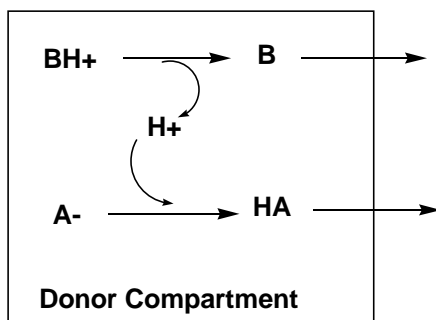


**Figure A1-2.** Schematic showing the generation of a pH gradient in response to the release of a base from the intravesicular space

As the neutral amine (B) transports out of the vesicle, conversion of the protonated amine to the neutral form generates protons that must be neutralized by the buffer system to maintain pH. The buffer system achieves this by consuming the counterion (A<sup>-</sup> in Figure A1-2). The resulting species, HA, remains in equilibrium with the extravesicular components (100 fold greater in the mass balance and hence effectively buffered). The resulting loss of A<sup>-</sup> leads to a shift in the buffer equilibrium (A<sup>-</sup>/HA) giving rise to the pH drift. This unidirectional stress on the buffer capacity can lead to unique situations e.g. for transport of a weak base buffered by a weak acid, the pH drift is much larger if initial pH < pK<sub>a</sub> of buffer than if initial pH > pK<sub>a</sub> of the buffer. This is illustrated in Figures 3-16 and 3-17 in chapter three, and is further detailed in the figures below.

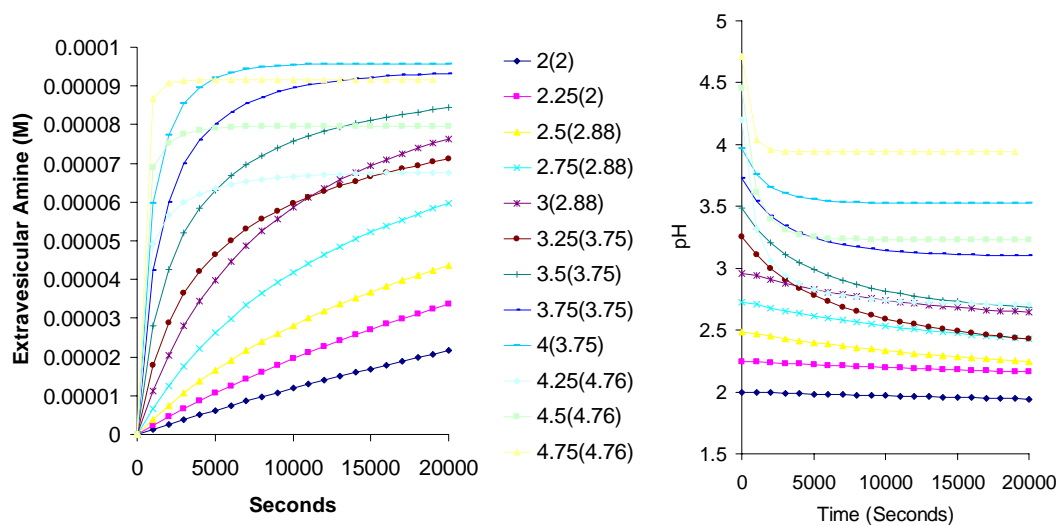


**Figure A1-3.** Left hand side panel shows the simulated release profiles for an initial amine concentration of 0.01 M obtained using various initial pH conditions (numbers in the legend) in presence of various monobasic acid-buffers (0.04 M, pKa values shown in the parentheses in the legend). Corresponding intravesicular pH values are shown in the right hand side panel.

If the pH drift were absent, the left hand side panel of the Figure A1-3 above would have shown non-intersecting curves with each approaching full release at the long time limit. However the apparent permeability coefficient changes with time in each experiment leading to intersection of the profiles due to the pH drift.

Since the major source of intravesicular pH drift is the release of the amine, the extent of drift depends on the concentration of the amine. Therefore 0.01 M amine release will perturb the buffer equilibria by less than 0.01 M equivalents which suggests that the drift should be negligible if initial pH is close to 2 (as seen in Figure A1-3). Similarly, a 0.003 M amine release will perturb the buffer equilibria significantly only if pH is greater than 2.5 as seen in Figure A1-4.

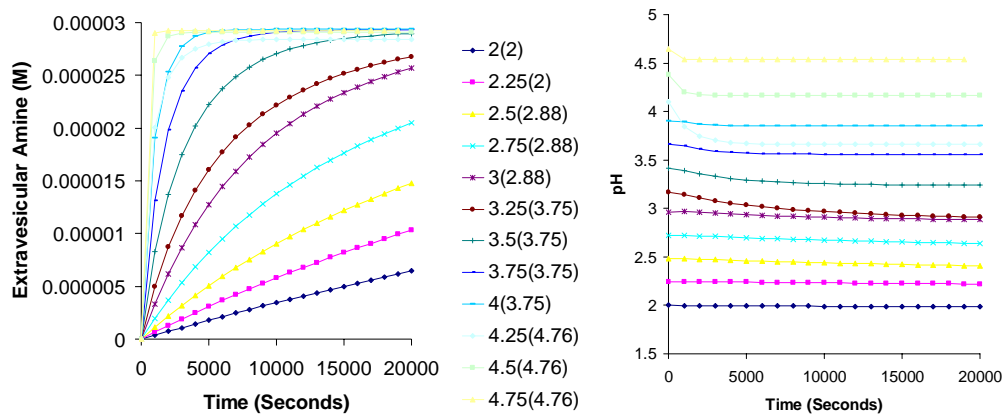


**Figure A1-4.** Left hand side panel shows the simulated release profiles for an initial amine concentration of 0.003 M obtained using various initial pH conditions (numbers in the legend) in presence of various monobasic acid-buffers (0.04 M, pKa values shown in the parentheses in the legend). Corresponding intravesicular pH values are shown in the right hand side panel.

Copyright © Ravindra W. Tejwani 2009

## APPENDIX TWO: Alternative hypotheses evaluated in chapter three

While the intravesicular binding and pH drift were found to be the primary factors affecting the apparent permeability coefficients, other effects, based on the primary observations of the concentration dependence were also considered. Unlike pH drift, the quantitative physical models for these effects can frequently be integrated with valid simplifying assumptions. The models for a permeable ion pair and permeable dimer are given below for information.

### Transport of a permeable ion pair

The transport of an ion pair (between protonated base,  $BH^+$ , and the buffer anion,  $X^-$ ) and a hydrogen bonded complex (between free base,  $B$ , and the buffer,  $HX$ ) are kinetically indistinguishable from each other. Figure A2-1 shows a schematic of the permeation of typical mono-ionizable base accompanied by the permeable ion pair.

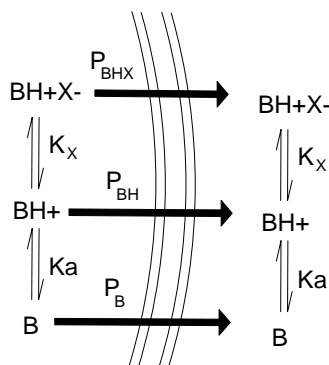


**Figure A2-1.** Transport of a mono-ionizable base along with a permeable ion pair. The symbols have been explained in the text.

The ion pair equilibrium constant,  $K_x$  and the ionization constants of the permeant base and the buffer species are defined using Equation A2-1 through A2-3:

$$K_x = \frac{BH^+X^-}{BH^+X^-} \quad (A2-1)$$

$$K_a = \frac{H^+B}{BH^+} \quad (\text{A2-2})$$

$$K_b = \frac{H^+X^-}{HX} \quad (\text{A2-3})$$

where  $X$  is the concentration of the anionic species of the buffer responsible for formation of the ion pair,  $BHX$  is the concentration of the ion pair,  $BH$  is the concentration of the protonated base and  $B$  is the concentration of the free base. The updated mass balance is then given as:

$$C_T V_T = nV_{in}(B_{in} + BH_{in}^+ + BHX_{in}) + V_{out}(B_{out} + BH_{out}^+ + BHX_{out}) \quad (\text{A2-4})$$

where  $C_T$  is the total concentration of the base,  $n$  is number of vesicles,  $V_{in}$  is the volume of a vesicle,  $V_{out}$  is the volume of the extravascular compartment, and  $V_T$  is the total volume. The subscripts on the species concentrations refer to the intravesicular and extravascular concentrations of the respective species.

The fraction of  $B$  and  $BHX$  in either the donor or the receiver compartment is then calculated as:

$$f_B = \frac{B}{B_T} = \frac{K_a}{K_a + H^+ + K_X H^+ X^-} \quad (\text{A2-5})$$

$$f_{BHX} = \frac{BHX}{B_T} = \frac{K_X H^+ X^-}{K_a + H^+ + K_X H^+ X^-} \quad (\text{A2-6})$$

where  $B_T$  is the total concentration of the base in either compartment. Based on these equations, the rate law for the permeation can be given as

$$\frac{dB_{T(ext)}}{dt} = \frac{6V_{int}}{V_{ext}d} \left[ P_B (f_{B(int)} B_{T(int)} - f_{B(ext)} B_{T(ext)}) + P_{BHX} (f_{BHX(int)} B_{T(int)} - f_{BHX(ext)} B_{T(ext)}) \right] \quad (\text{A2-7})$$

where  $P_B$  and  $P_{BHX}$  are the permeability coefficients of  $B$  and  $BHX$ , respectively. In the above equation, it should be noted that the ion pair binding constant may have to be

determined independent of the transport experiment or fitted as a second parameter besides the intrinsic permeability coefficient,  $P_B$ . If the permeability coefficient of the free form is the only parameter of interest, the ion pair binding constant can be combined into its permeability coefficient as a single parameter for fitting by assuming that the net contribution of such species in the solution is minimal (i.e.  $K_x H^+ X^- \ll H^+$ ). It should be noted that the assumption of charge neutrality in both the compartments is still retained in the case of this quantitative model.

### **Transport of a permeable dimer of the amine**

In Chapter Four, the 1,9-decadiene/water partition coefficients of tyramine were determined for total concentration range from 0.00005 to 0.001 molar. In this range, the partition coefficient of tyramine was found to remain unchanged and followed the pH profile that would be expected of a dilute solution. Based on this argument, it was concluded that the role of dimerization in the passing of tyramine through the barrier domain was negligible. It has been however suggested that the absence of concentration dependence sometimes means the presence of a “persistent dimer” without formation of any higher aggregates. In this situation, the above concentration range could potentially be high enough that dimer was dominant species and no other aggregates were present. Following discussion evaluates the feasibility of this occurrence.

The dimerization constant,  $K_B$ , for a compound can be defined as follows:

$$K_B = \frac{B_2}{B^2} \quad (\text{A2-8})$$

where  $B_2$  is the concentration of the dimer, and  $B$  is the concentration of the free species. The corresponding mass balance for the compound is:

$$B_T = B + 2K_B B^2 \quad (\text{A2-9})$$

If the concentration independence of the partition coefficient in the barrier domain (Figure 4-7) were to be due to the formation of a dimer, the concentration of the dimer would be much larger than the concentration of the monomer. In that case



$$2K_B B^2 \gg B; \text{ and } B_T \approx B_2 \quad (\text{A2-10})$$

therefore,

$$K_B \gg \frac{1}{2B} \quad (\text{A2-11})$$

As a result, considering the concentration range of the solute in Figure 4-7 (0.05 mM to 1 mM), the dimerization constant necessary for a permeable dimer would have to be larger than  $10^4 \text{ M}^{-1}$ . This is much larger magnitude than that can be explained by assuming a 5 kcal per mole of a hydrogen bonded dimer.

Copyright © Ravindra W. Tejwani 2009

## References and Bibliography

- ABRAHAM, M. H., CHADHA, H. S., WHITING, G. S. & MITCHELL, R. C. (1994) Hydrogen bonding. 32. An analysis of water-octanol and water-alkane partitioning and the  $\Delta \log P$  parameter of seiler. *Journal of Pharmaceutical Sciences*, 83, 1085-1100.
- ABRAHAM, M. H., PLATTS, J. A., HERSEY, A., LEO, A. J. & TAFT, R. W. (1999) Correlation and estimation of gas-chloroform and water-chloroform partition coefficients by a linear free energy relationship method. *Journal of Pharmaceutical Sciences*, 88, 670-9.
- ABRAHAM, S. A., WATERHOUSE, D. N., MAYER, L. D., CULLIS, P. R., MADDEN, T. D. & BALLY, M. B. (2005) The liposomal formulation of doxorubicin. *Methods in Enzymology*, 391, 71-97.
- ACCELRY'S (2005) DS ViewerPro. 6.0 ed., Accelrys Software Incorporated.
- ACD-PKA (1994-2007) Advanced Chemistry Development / pKa dB. 10.0 ed. Toronto, ON, Canada, Advanced Chemistry Development, Inc.
- ADAMS, E. Q. (1916) Relations between the constants of basic acids and of amphoteric electrolytes. *Journal of the American Chemical Society*, 38, 1503-1510.
- ADAMSON, A. W. & GAST, A. P. (1997) The nature and thermodynamics of liquid interfaces. *Physical Chemistry of Surfaces*. 6 ed. New York, John Wiley and Sons, Inc., 48-100.
- ADAMSON, A. W. & GAST, A. P. (1997) *Physical Chemistry Of Surfaces*, New York, NY, John Wiley & Sons, Inc.
- ALLEN, T. M. (1997) Liposomes. Opportunities in drug delivery. *Drugs*, 54, 8-14.
- ALPER, H. E., BASSOLINO-KLIMAS, D. & STOUCHE, T. R. (1993) Computer simulation of a phospholipid monolayer-water system: The influence of long range forces on water structure and dynamics. *J Chem Phys*, 98, 9798-9807.
- ALPER, H. E., BASSOLINO-KLIMAS, D. & STOUCHE, T. R. (1993) The limiting behavior of water hydrating a phospholipid monolayer: A computer simulation study. *J Chem Phys*, 99, 5547-5559.
- ALPER, H. E. & STOUCHE, T. R. (1995) Orientation and diffusion of a drug analog in biomembranes: Molecular dynamics simulations. *Journal of Physical Chemistry*, 99, 5724-31.
- ANDERSON, B. D. (1978) Specific interactions in nonaqueous systems: I. Self-association of alcohols and phenol in nonpolar solvents. II. Solubilities of organic compounds in organic solvents and cosolvent mixtures.
- ANDERSON, B. D., RYTTING, J. H. & HIGUCHI, T. (1978) Vapor pressure studies of self-association of alcohols in isooctane. I. The effect of chain length. *International Journal of Pharmaceutics*, 1, 15-31.

- ANDERSON, B. D., RYTTING, J. H. & HIGUCHI, T. (1979) Influence of self-association on the solubility of phenol in isooctane and cyclohexane. *Journal of the American Chemical Society*, 101, 5194-7.
- ANDERSON, B. D., RYTTING, J. H. & HIGUCHI, T. (1980) Solubility of polar organic solutes in nonaqueous systems: role of specific interactions. *Journal of Pharmaceutical Sciences*, 69, 676-80.
- ANDERSON, B. D., RYTTING, J. H., LINDENBAUM, S. & HIGUCHI, T. (1975) Calorimetric study of the self-association of primary alcohols in isooctane. *Journal of Physical Chemistry*, 79, 2340-4.
- ANEZO, C., DE VRIES, A. H., HOELTJE, H.-D., TIELEMAN, D. P. & MARRINK, S.-J. (2003) Methodological issues in lipid bilayer simulations. *Journal of Physical Chemistry B*, 107, 9424-9433.
- ARMSTRONG, J. & BARLOW, R. B. (1976) The ionization of phenolic amines, including apomorphine, dopamine, and catecholamines and an assessment of zwitterion constants. *British Journal of Pharmacology*, 57, 501-16.
- ARNETT, E. M., JONES, F. M., TAAGEPERA, M., HENDERSON, W. G., BEAUCHAMP, J. L., HOLTZ, D. & TAFT, R. W. (1972) Complete thermodynamic analysis of the "anomalous order" of amine basicities in solution. *Journal of the American Chemical Society*, 94, 4724-4726.
- AUE, D. H., WEBB, H. M. & BOWERS, M. T. (1972) Quantitative relative gas-phase basicities of alkylamines. Correlation with solution basicity. *Journal of the American Chemical Society*, 94, 4726-4728.
- AUE, D. H., WEBB, H. M. & BOWERS, M. T. (1976) Quantitative proton affinities, ionization potentials, and hydrogen affinities of alkylamines. *Journal of the American Chemical Society*, 98, 311-317.
- AUE, D. H., WEBB, H. M. & BOWERS, M. T. (1976) A thermodynamic analysis of solvation effects on the basicities of alkylamines. An electrostatic analysis of substituent effects. *Journal of the American Chemical Society*, 98, 318-329.
- AUSTIN, R. P., BARTON, P., DAVIS, A. M., MANNERS, C. N. & STANSFIELD, M. C. (1998) The effect of ionic strength on liposome-buffer and 1-octanol-buffer distribution coefficients. *Journal of Pharmaceutical Sciences*, 87, 599-607.
- AVDEEF, A., BOX, K. J., COMER, J. E. A., HIBBERT, C. & TAM, K. Y. (1998) pH-Metric logP 10. Determination of liposomal membrane-water partition coefficients of ionizable drugs. *Pharmaceutical Research*, 15, 209-215.
- AVEYARD, R. & HAYDON, D. A. (1973) *An Introduction To The Principles Of Surface Chemistry*, Cambridge, UK, Cambridge University Press.
- BAEUERLE, H. D. & SEELIG, J. (1991) Interaction of charged and uncharged calcium channel antagonists with phospholipid membranes. Binding equilibrium, binding enthalpy, and membrane location. *Biochemistry*, 30, 7203-11.
- BALLY, M. B., BOLCSAK, L. E., CULLIS, P. R., JANOFF, A. S., MAYER, L. D., LENK, R. P. & JEDRUSIAK, J. A. (1988) Aminoglycoside phosphates and

- method of preparation of liposomes containing aminoglycoside salts. *PCT Int. Appl.* WO, (Liposome Co., Inc., USA).
- BALLY, M. B., BOLCSAK, L. E., CULLIS, P. R., JANOFF, A. S., MAYER, L. D., LENK, R. P. & JEDRUSIAK, J. A. (1993) Liposomal formulation of aminoglycoside drugs. *Pat. Specif. (Aust.)*. AU, (Liposome Co., Inc., Australia).
- BALLY, M. B., BOMAN, N. L., CULLIS, P. R. & MAYER, L. D. (1997) Liposomal compositions for enhanced retention of bioactive agents. *U.S. US*, (Inex Pharmaceuticals Corporation, Can.; University of British Columbia).
- BALLY, M. B., CULLIS, P. R., HOPE, M. J., JANOFF, A. S. & MAYER, L. D. (1987) Multilamellar liposomes having improved trapping efficiencies. *PCT Int. Appl.* WO, (Liposome Co., Inc., USA).
- BALLY, M. B., CULLIS, P. R., HOPE, M. J., MADDEN, T. D. & MAYER, L. D. (1986) Encapsulation of antineoplastic agents in liposomes. *PCT Int. Appl.* WO, (Liposome Co., Inc., USA).
- BALLY, M. B., LIM, H., CULLIS, P. R. & MAYER, L. D. (1998) Controlling the drug delivery attributes of lipid-based drug formulations. *Journal of Liposome Research*, 8, 299-335.
- BALLY, M. B., MASIN, D., NAYAR, R., CULLIS, P. R. & MAYER, L. D. (1994) Transfer of liposomal drug carriers from the blood to the peritoneal cavity of normal and ascitic tumor-bearing mice. *Cancer Chemotherapy and Pharmacology*, 34, 137-46.
- BALLY, M. B., MAYER, L. D., LOUGHREY, H., REDELMEIER, T., MADDEN, T. D., WONG, K., HARRIGAN, P. R., HOPE, M. J. & CULLIS, P. R. (1988) Dopamine accumulation in large unilamellar vesicle systems induced by transmembrane ion gradients. *Chemistry and Physics of Lipids*, 47, 97-107.
- BALLY, M. B., NAYAR, R., MASIN, D., CULLIS, P. R. & MAYER, L. D. (1990) Studies on the myelosuppressive activity of doxorubicin entrapped in liposomes. *Cancer Chemotherapy and Pharmacology*, 27, 13-19.
- BALLY, M. B., NAYAR, R., MASIN, D., HOPE, M. J., CULLIS, P. R. & MAYER, L. D. (1990) Liposomes with entrapped doxorubicin exhibit extended blood residence times. *Biochimica et Biophysica Acta, Biomembranes*, 1023, 133-9.
- BARBATO, F., DIMARTINO, G., GRUMETTO, L. & LAROTONDA, M. I. (2004) Prediction of drug-membrane interactions by IAM-HPLC: effects of different phospholipid stationary phases on the partition of bases *European Journal of Pharmaceutical Sciences*, 22, 261-269.
- BAR-ON, Z. & DEGANI, H. (1985) Permeability of alkylamines across phosphatidylcholine vesicles as studied by proton NMR. *Biochimica et Biophysica Acta*, 813, 207-12.
- BARTELS, C. & KARPLUS, M. (1997) Multidimensional adaptive umbrella sampling: Applications to main chain and side chain peptide conformations. *Journal of Computational Chemistry*, 18, 1450-1462.

- BARTELS, C. & KARPLUS, M. (1998) Probability distributions for complex systems: Adaptive umbrella sampling of the potential energy. *Journal of Physical Chemistry B*, 102, 865-880.
- BASSOLINO, D., ALPER, H. & STOUCH, T. R. (1996) Drug-membrane interactions studied by molecular dynamics simulation: size dependence of diffusion. *Drug Des Discov*, 13, 135-41.
- BASSOLINO-KLIMAS, D., ALPER, H. E. & STOUCH, T. R. (1993) Solute diffusion in lipid bilayer membranes: An atomic level study by molecular dynamics simulation. *Biochemistry*, 32, 12624-37.
- BASSOLINO-KLIMAS, D., ALPER, H. E. & STOUCH, T. R. (1995) Mechanism of solute diffusion through lipid bilayer membranes by molecular dynamics simulation. *Journal of the American Chemical Society*, 117, 4118-29.
- BEAN, R. C., SHEPHERD, W. C. & CHAN, H. (1968) Permeability of lipid bilayer membranes to organic solutes. *Journal of General Physiology*, 52, 495-508.
- BEMPORAD, D., ESSEX, J. W. & LUTTMANN, C. (2004) Permeation of small molecules through a lipid bilayer: A computer simulation study. *Journal of Physical Chemistry B*, 108, 4875-4884.
- BEMPORAD, D., LUTTMANN, C. & ESSEX, J. W. (2005) Behaviour of small solutes and large drugs in a lipid bilayer from computer simulations. *Biochim Biophys Acta*, 1718, 1-21.
- BEN-NAIM, A. (1978) Standard thermodynamics of transfer. Uses and misuses. *Journal of Physical Chemistry*, 82, 792-803.
- BENNETT, W. F., MACCALLUM, J. L. & TIELEMAN, D. P. (2009) Thermodynamic analysis of the effect of cholesterol on dipalmitoylphosphatidylcholine lipid membranes. *Journal of the American Chemical Society*, 131, 1972-8.
- BERK HESS, H. B. H. J. C. B. J. G. E. M. F. (1997) LINCS: A linear constraint solver for molecular simulations. *Journal of Computational Chemistry*, 18, 1463-1472.
- BHIDE, S. Y. & BERKOWITZ, M. L. (2005) Structure and dynamics of water at the interface with phospholipid bilayers. *J Chem Phys*, 123, 224702.
- BHIDE, S. Y. & BERKOWITZ, M. L. (2006) The behavior of reorientational correlation functions of water at the water-lipid bilayer interface. *J Chem Phys*, 125, 094713.
- BISSON, M. A. & GUTKNECHT, J. (1975) Osmotic regulation in the marine alga, *Codium decortatum*. I. Regulation of turgor pressure by control of ionic composition. *Journal of Membrane Biology*, 24, 183-200.
- BISSON, M. A. & GUTKNECHT, J. (1977) Osmotic regulation in the marine alga, *Codium decortatum*. II. Active chloride influx exerts negative feedback control on the turgor pressure. *Journal of Membrane Biology*, 37, 85-98.
- BISSON, M. A. & GUTKNECHT, J. (1980) Osmotic regulation in algae. *Developments in Plant Biology*, 4, 131-46.

- BJERRUM, N. (1923) Constitution of ampholytes, especially of the amino acids, and their dissociation constants. *Zeitschrift fur Physikalische Chemie Stochiometrie und Verwandtschaftslehre*, 104, 147-73.
- BJERRUM, N. (1923) Dissociation constants of polybasic acids and their application to the calculation of molecular dimensions. *Zeitschrift fur Physikalische Chemie Stochiometrie und Verwandtschaftslehre*, 106, 219-42.
- BJERRUM, N. (1923) Thermodynamics of activity coefficients and osmotic coefficients. *Zeitschrift fur Physikalische Chemie Stochiometrie und Verwandtschaftslehre*, 104, 406-32.
- BOCKRIS, J. O. M. & REDDY, A. K. N. (1998) *Modern Electrochemistry*, New York, Plenum Publishing Corporation.
- BOMAN, N. L., BALLY, M. B., CULLIS, P. R., MAYER, L. D. & WEBB, M. S. (1995) Encapsulation of vincristine in liposomes reduces its toxicity and improves its antitumor efficacy. *Journal of Liposome Research*, 5, 523-41.
- BOMAN, N. L., CULLIS, P. R., BALLY, M. B. & MAYER, L. D. (1995) Preclinical and clinical activity of liposomal doxorubicin. *Drug Targeting and Delivery*, 6, 85-103.
- BOMAN, N. L., CULLIS, P. R., MAYER, L. D., BALLY, M. B. & WEBB, M. S. (1998) Liposomal vincristine: the central role of drug retention in defining therapeutically optimized anticancer formulations. *Long Circulating Liposomes*, 29-49.
- BOMAN, N. L., MASIN, D., MAYER, L. D., CULLIS, P. R. & BALLY, M. B. (1994) Liposomal vincristine which exhibits increased drug retention and increased circulation longevity cures mice bearing P388 tumors. *Cancer Research*, 54, 2830-3.
- BOMAN, N. L., MAYER, L. D. & CULLIS, P. R. (1993) Optimization of the retention properties of vincristine in liposomal systems. *Biochimica et Biophysica Acta, Biomembranes*, 1152, 253-8.
- BORGMAN, R. J., MCPHILLIPS, J. J., STITZEL, R. E. & GOODMAN, I. J. (1973) Synthesis and pharmacology of centrally acting dopamine derivatives and analogs in relation to Parkinson's disease. *Journal of Medicinal Chemistry*, 16, 630-3.
- BOWERS, M. T., AUE, D. H., WEBB, H. M. & MCIVER, R. T. (1971) Equilibrium constants for gas-phase ionic reactions. Accurate determination of relative proton affinities. *Journal of the American Chemical Society*, 93, 4314-4315.
- BRANDARIZ, I., FIOL, S., HERRERO, R., VILARINO, T. & SASTRE DE VICENTE, M. (1993) Protonation constants of alpha-alanine, gamma-aminobutyric acid, and epsilon-aminocaproic acid. *Journal of Chemical and Engineering Data*, 38, 531-533.
- BREYER, E. D., STRASTERS, J. K. & KHALEDI, M. G. (1991) Quantitative retention-biological activity relationship study by micellar liquid chromatography. *Anal. Chem.*, 63, 828-833.

- BROOKS, C. L., KARPLUS, M. & PETTITT, B. M. (1988) *Proteins. A Theoretical Perspective Of Dynamics, Structure, And Thermodynamics*, New York, NY, John Wiley & Sons, Inc.
- BROWN, H. C., BARTHOLOMAY, H. & TAYLOR, M. D. (1944) Acid-base studies in gaseous systems. II. The anomalous base strength of the methylamines; A new manifestation of steric strain. *Journal of the American Chemical Society*, 66, 435-442.
- BROWN, H. C., TAYLOR, M. D. & GERSTEIN, M. (1944) Acid-base studies in gaseous systems. I. Precise dissociation measurements. *Journal of the American Chemical Society*, 66, 431-435.
- BRYANTSEV, V. S., DIALLO, M. S. & GODDARD, W. A. (2007) pKa calculations of aliphatic amines, diamines, and aminoamides via density functional theory with a Poisson-Boltzmann continuum solvent model. *Journal of Physical Chemistry A*, 111, 4422-4430.
- BUTLER, J. A. V. (1934) *The Fundamentals Of Chemical Thermodynamics Part II Thermodynamical Functions And Their Applications*, London, Macmillan And Co. Limited.
- CAO, Y. (2008) Application of linear free energy relationships in the prediction of triglyceride/water partition coefficients and lipid bilayer permeability coefficients of small organic molecules and peptides. PhD Thesis. College of Pharmacy, The University of Kentucky, Lexington, KY.
- CAO, Y., MARRA, M. & ANDERSON, B. D. (2004) Predictive relationships for the effects of triglyceride ester concentration and water uptake on solubility and partitioning of small molecules into lipid vehicles. *Journal of Pharmaceutical Sciences*, 93, 2768-79.
- CAO, Y., XIANG, T.-X. & ANDERSON, B. D. (2008) Development of structure-lipid bilayer permeability relationships for peptide-like small organic molecules. *Mol Pharm*, 5, 371-88.
- CASTRO-ROMAN, F., BENZ, R. W., WHITE, S. H. & TOBIAS, D. J. (2006) Investigation of finite system-size effects in molecular dynamics simulations of lipid bilayers. *Journal of Physical Chemistry B*, 110, 24157-24164.
- CEH, B. & LASIC, D. D. (1995) A rigorous theory of remote loading of drugs into liposomes. *Langmuir*, 11, 3356-68.
- CEH, B. & LASIC, D. D. (1998) Kinetics of accumulation of molecules into liposomes. *Journal of Physical Chemistry B*, 102, 3036-3043.
- CEVC, G., SEDDON, J. M., HARTUNG, R. & EGGERT, W. (1988) Phosphatidylcholine-fatty acid membranes. I. Effects of protonation, salt concentration, temperature and chain-length on the colloidal and phase properties of mixed vesicles, bilayers and nonlamellar structures. *Biochimica et Biophysica Acta, Biomembranes*, 940, 219-40.

- CHAN, E. C. Y., TAN, W. L., HO, P. C. & FANG, L. J. (2005) Modeling Caco-2 permeability of drugs using immobilized artificial membrane chromatography and physicochemical descriptors. *Journal of Chromatography, A*, 1072, 159-168.
- CHANDLER, D. (1987) *Introduction To Modern Statistical Mechanics*, New York, NY, Oxford University Press, Inc.
- CHEW, C. F., GUY, A. & BIGGIN, P. C. (2008) Distribution and dynamics of adamantanes in a lipid bilayer. *Biophysical Journal*, 95, 5627-36.
- CHIU, S. W., CLARK, M. M., JAKOBSSON, E., SUBRAMANIAM, S. & SCOTT, H. L. (1999) Application of combined Monte Carlo and molecular dynamics method to simulation of dipalmitoyl phosphatidylcholine lipid bilayer. *Journal of Computational Chemistry*, 20, 1153-1164.
- CHIU, S. W., JAKOBSSON, E., SUBRAMANIAM, S. & SCOTT, H. L. (1999) Combined Monte Carlo and molecular dynamics simulation of fully hydrated dioleoyl and palmitoyl-oleoyl phosphatidylcholine lipid bilayers. *Biophysical Journal*, 77, 2462-2469.
- CHIU, S. W., PANDIT, S. A., SCOTT, H. L. & JAKOBSSON, E. (2009) An improved united atom force field for simulation of mixed lipid bilayers. *Journal of Physical Chemistry B*.
- CLEVELAND, J. A., JR., MARTIN, C. L. & GLUCK, S. J. (1994) Spectrophotometric determination of ionization constants by capillary zone electrophoresis. *Journal of Chromatography, A*, 679, 167-71.
- COETZEE, J. F. & PADMANABHAN, G. R. (1965) Properties of bases in acetonitrile as solvent. IV. Proton acceptor power and homoconjugation of mono- and diamines. *Journal of the American Chemical Society*, 87, 5005-5010.
- CONDON, F. E. (1965) The influence of hydration on base strength. I. General theory for amines. *Journal of the American Chemical Society*, 87, 4481-4484.
- CONDON, F. E. (1965) The influence of hydration on base strength. II. Aliphatic amines and N-substituted anilines. *Journal of the American Chemical Society*, 87, 4485-4490.
- CONDON, F. E. (1965) The influence of hydration on base strength. III. Alkylhydrazines. *Journal of the American Chemical Society*, 87, 4491-4494.
- CONDON, F. E. (1965) The influence of hydration on base strength. IV. Hindered bases. *Journal of the American Chemical Society*, 87, 4494-4496.
- CONNORS, K. A. (1990) 5. Theory of chemical kinetics. IN CONNORS, K. A. (Ed.) *Chemical Kinetics: The Study of Reaction Rates in Solution*. New York, John Wiley & Sons, Inc., 187.
- CONNORS, K. A. (1990) *Chemical Kinetics. The Study Of Reaction Rates In Solution*, New York, John Wiley & Sons, Inc.



- COX, E. G., CRUICKSHANK, D. W. J. & SMITH, J. A. S. (1958) The crystal structure of benzene at  $-3^{\circ}\text{C}$ . *Proceedings of the Royal Society of London. Series A, Mathematical and Physical Sciences*, 247, 1-21.
- CULLIS, P. R. & HOPE, M. J. (1991) Physical properties and functional roles of lipids in membranes. *New Comprehensive Biochemistry*, 20, 1-41.
- CULLIS, P. R., HOPE, M. J., BALLY, M. B., MADDEN, T. D., MAYER, L. D. & FENSKE, D. B. (1997) Influence of pH gradients on the transbilayer transport of drugs, lipids, peptides and metal ions into large unilamellar vesicles. *Biochimica et Biophysica Acta, Reviews on Biomembranes*, 1331, 187-211.
- DE YOUNG, L. R. & DILL, K. A. (1990) Partitioning of nonpolar solutes into bilayers and amorphous n-alkanes. *Journal of Physical Chemistry*, 94, 801-809.
- DEAMER, D. W. & GUTKNECHT, J. (1986) Proton permeation through model membranes. *Methods in Enzymology*, 127, 471-80.
- DEAMER, D. W. & NICHOLS, J. W. (1983) Proton-hydroxide permeability of liposomes. *Proceedings of the National Academy of Sciences of the United States of America*, 80, 165-8.
- DEAMER, D. W. & NICHOLS, J. W. (1989) Proton flux mechanisms in model and biological membranes. *Journal of Membrane Biology*, 107, 91-103.
- DEAMER, D. W., PRINCE, R. C. & CROFTS, A. R. (1972) Response of fluorescent amines to pH gradients across liposome membranes. *Biochimica et Biophysica Acta, Biomembranes*, 274, 323-35.
- DEMIRELLI, H. & KOESEGLU, F. (2004) Solvent and substituent effects on the protonation of anilines in dioxane-water mixtures. *Journal of Solution Chemistry*, 33, 1501-1515.
- DEVIDO, D. R., DORSEY, J. G., CHAN, H. S. & DILL, K. A. (1998) Oil/water partitioning has a different thermodynamic signature when the oil solvent chains are aligned than when they are amorphous. *Journal of Physical Chemistry B*, 102, 7272-7279.
- DIAMOND, J. M. & KATZ, Y. (1974) Interpretation of nonelectrolyte partition coefficients between dimyristoyl lecithin and water. *Journal of Membrane Biology*, 17, 121-54.
- DIAMOND, J. M. & KATZ, Y. (1974) Interpretation of nonelectrolyte partition coefficients between dimyristoyl lecithin and water. *Journal of Membrane Biology*, 17, 121-54.
- DICKEY, A. N. & FALLER, R. (2007) How alcohol chain-length and concentration modulate hydrogen bond formation in a lipid bilayer. *Biophysical Journal*, 92, 2366-2376.
- EASTMAN, S. J., HOPE, M. J. & CULLIS, P. R. (1991) Transbilayer transport of phosphatidic acid in response to transmembrane pH gradients. *Biochemistry*, 30, 1740-5.

- EDSALL, J. T., MARTIN, R. B. & HOLLINGWORTH, B. R. (1958) Ionization of individual groups in dibasic acids, with application to the amino and hydroxyl groups of tyrosine. *Proceedings of the National Academy of Sciences U S A*, 44, 505-18.
- EDSALL, J. T. & WYMAN, J. (1958) *Biophysical Chemistry*, New York, NY, Academic Press, Inc.
- EHRENSON, S. (1976) Transmission of substituent effects. Generalization of the ellipsoidal cavity field effect model. *Journal of the American Chemical Society*, 98, 7510-7514.
- EMBREE, L., GELMON, K. A., LOHR, A., MAYER, L. D., COLDMAN, A. J., CULLIS, P. R., PALAITIS, W., PILKIEWICZ, F., HUDON, N. J. & ET AL. (1993) Chromatographic analysis and pharmacokinetics of liposome-encapsulated doxorubicin in non-small-cell lung cancer patients. *Journal of Pharmaceutical Sciences*, 82, 627-34.
- EYRING, E. M. & HASLAM, J. L. (1966) Solvent deuterium isotope effects on intramolecularly hydrogen-bonded dicarboxylic acid monoanions. *J Phys Chem A Mol Spectrosc Kinet Environ Gen Theory*, 70, 293-296.
- FERNANDEZ, J. A., UNAMUNO, I. & CASTANO, F. (2001) Reply to the comment on "Structural and vibrational assignment of *p*-methoxyphenethylamine conformers". *Journal of Physical Chemistry A*, 105, 9993-9994.
- FINKELSTEIN, A. (1976) Water and nonelectrolyte permeability of lipid bilayer membranes. *Journal of General Physiology*, 68, 127-35.
- FINKELSTEIN, A. & CASS, A. (1967) Effect of cholesterol on the water permeability of thin lipid membranes. *Nature*, 216, 717-8.
- FINKELSTEIN, A. & CASS, A. (1968) Permeability and electrical properties of thin lipid membranes. *Journal of General Physiology*, 52, 145Suppl+.
- FLORY, P. J. (1953) *Principles Of Polymer Chemistry*, Ithaca, NY, Cornell University Press.
- FORESMAN, J. B. & FRISCH, A. (1993) *Exploring Chemistry With Electronic Structure Methods: A Guide To Using Gaussian*, Pittsburgh, PA, Gaussian, Inc.
- FOYE, W. O. (1989) *Principles Of Medicinal Chemistry*, Bombay, India, Lea & Febiger / Varghese Publishing House.
- GERO, A. (1954) Inductive effect and hydrogen bonding as factors in the base strength of polymethylenediamines. *Journal of the American Chemical Society*, 76, 5159-5160.
- GLUCK, S. J. & CLEVELAND, J. A., JR. (1994) Capillary zone electrophoresis for the determination of dissociation constants. *Journal of Chromatography, A*, 680, 43-8.

- GLUCK, S. J. & CLEVELAND, J. A., JR. (1994) Investigation of experimental approaches to the determination of pKa values by capillary electrophoresis. *Journal of Chromatography, A*, 680, 49-56.
- GRANOT, J. (1976) NMR studies of catecholamines, acid dissociation equilibria in aqueous solutions. *FEBS Lett*, 67, 271-5.
- GRANT, D. J. W. & HIGUCHI, T. (1990) *Solubility Behavior Of Organic Compounds*, New York, Wiley.
- GRAVES, J. S. & GUTKNECHT, J. (1976) Ion transport studies and determination of the cell wall elastic modulus in the marine alga *Halicystis parvula*. *Journal of General Physiology*, 67, 579-97.
- GRAVES, J. S. & GUTKNECHT, J. (1977) Chloride transport and the membrane potential in the marine alga, *Halicystis parvula*. *Journal of Membrane Biology*, 36, 65-81.
- GRAVES, J. S. & GUTKNECHT, J. (1977) Current-voltage relationships and voltage sensitivity of the chloride ion pump in *Halicystis parvula*. *Journal of Membrane Biology*, 36, 83-95.
- GRIT, M. & CROMMELIN, D. J. A. (1992) The effect of aging on the physical stability of liposome dispersions. *Chemistry and Physics of Lipids*, 62, 113-22.
- GRIT, M. & CROMMELIN, D. J. A. (1993) Chemical stability of liposomes: Implications for their physical stability. *Chemistry and Physics of Lipids*, 64, 3-18.
- GUGGINO, S. & GUTKNECHT, J. (1980) Turgor regulation in *Valonia macrophysa* after acute hyposmotic shock. *Developments in Plant Biology*, 4, 495-6.
- GUGGINO, S. & GUTKNECHT, J. (1982) Turgor regulation in *Valonia macrophysa* following acute osmotic shock. *Journal of Membrane Biology*, 67, 155-64.
- GUTKNECHT, J. (1963) Zinc-65 uptake by benthic marine algae. *Limnology and Oceanography*, 8, 31-8.
- GUTKNECHT, J. (1965) Ion distribution, and transport in the red marine alga, *Gracilaria foliifera*. *Biological Bulletin (Woods Hole, MA, United States)*, 129, 495-509.
- GUTKNECHT, J. (1965) Uptake and retention of <sup>137</sup>Cs and <sup>65</sup>Zn by seaweeds. *Limnology and Oceanography*, 10, 58-66.
- GUTKNECHT, J. (1965) Uptake, retention, and loss of zinc-65 and cesium-137 by littoral marine algae.
- GUTKNECHT, J. (1966) Sodium, potassium, and chloride transport and membrane potentials in *Valonia ventricosa*. *Biological Bulletin (Woods Hole, MA, United States)*, 130, 331-44.
- GUTKNECHT, J. (1967) Ion fluxes and short-circuit current in internally perfused cells of *Valonia ventricosa*. *Journal of General Physiology*, 50, 1821-34.
- GUTKNECHT, J. (1968) Permeability of *Valonia* to water and solutes: apparent absence of aqueous membrane pores. *Biochimica et Biophysica Acta*, 163, 20-9.

- GUTKNECHT, J. (1981) Inorganic mercury (Hg<sup>2+</sup>) transport through lipid bilayer membranes. *Journal of Membrane Biology*, 61, 61-6.
- GUTKNECHT, J. (1983) Cadmium and thallos ion permeabilities through lipid bilayer membranes. *Biochimica et Biophysica Acta*, 735, 185-8.
- GUTKNECHT, J. (1984) Proton/hydroxide conductance through lipid bilayer membranes. *Journal of Membrane Biology*, 82, 105-12.
- GUTKNECHT, J. (1984) Proton/hydroxide permeabilities of lipid bilayer membranes. *Hydrogen Ion Transp. Epithelia, [Pap. Conf.]*, 3-12.
- GUTKNECHT, J. (1987) Proton conductance through phospholipid bilayers: water wires or weak acids? *Journal of Bioenergetics and Biomembranes*, 19, 427-42.
- GUTKNECHT, J. (1987) Proton/hydroxide conductance and permeability through phospholipid bilayer membranes. *Proceedings of the National Academy of Sciences of the United States of America*, 84, 6443-6.
- GUTKNECHT, J. (1987) Proton/hydroxide conductance through phospholipid bilayer membranes: effects of phytanic acid. *Biochimica et Biophysica Acta*, 898, 97-108.
- GUTKNECHT, J. (1988) Proton conductance caused by long-chain fatty acids in phospholipid bilayer membranes. *Journal of Membrane Biology*, 106, 83-93.
- GUTKNECHT, J. (1990) Salicylates and proton transport through lipid bilayer membranes: a model for salicylate-induced uncoupling and swelling in mitochondria. *Journal of Membrane Biology*, 115, 253-60.
- GUTKNECHT, J. (1992) Aspirin, acetaminophen and proton transport through phospholipid bilayers and mitochondrial membranes. *Molecular and Cellular Biochemistry*, 114, 3-8.
- GUTKNECHT, J. & BISSON, M. A. (1977) Ion transport and osmotic regulation in giant algal cells. *Water Relat. Membr. Transp. Plants Anim., [Proc. Symp.]*, 3-14.
- GUTKNECHT, J., BISSON, M. A. & TOSTESON, D. C. (1977) Diffusion of carbon dioxide through lipid bilayer membranes. Effects of carbonic anhydrase, bicarbonate, and unstirred layers. *Journal of General Physiology*, 69, 779-94.
- GUTKNECHT, J., BRUNER, L. J. & TOSTESON, D. C. (1972) Permeability of thin lipid membranes to bromide and bromine. *Journal of General Physiology*, 59, 486-502.
- GUTKNECHT, J. & DAINTY, J. (1968) Ionic relations of marine algae. *Oceanography and Marine Biology*, 6, 163-200.
- GUTKNECHT, J., GRAVES, J. S. & TOSTESON, D. C. (1978) Electrically silent anion transport through lipid bilayer membranes containing a long-chain secondary amine. *Journal of General Physiology*, 71, 269-84.
- GUTKNECHT, J., HASTINGS, D. F. & BISSON, M. A. (1978) Ion transport and turgor pressure regulation in giant algal cells. *Membr. Transp. Biol.*, 3, 125-74.

- GUTKNECHT, J. & TOSTESON, D. C. (1970) Ionic permeability of thin lipid membranes. Effects of n-alkyl alcohols, polyvalent cations, and a secondary amine. *Journal of General Physiology*, 55, 359-74.
- GUTKNECHT, J. & TOSTESON, D. C. (1973) Diffusion of weak acids across lipid bilayer membranes. Effects of chemical reactions in the unstirred layers. *Science (Washington, DC, United States)*, 182, 1258-60.
- GUTKNECHT, J. & WALTER, A. (1979) Coupled transport of protons and anions through lipid bilayer membranes containing a long-chain secondary amine. *Journal of Membrane Biology*, 47, 59-76.
- GUTKNECHT, J. & WALTER, A. (1980) Transport of auxin (indoleacetic acid) through lipid bilayer membranes. *Journal of Membrane Biology*, 56, 65-72.
- GUTKNECHT, J. & WALTER, A. (1981) Histamine, theophylline and tryptamine transport through lipid bilayer membranes. *Biochimica et Biophysica Acta*, 649, 149-54.
- GUTKNECHT, J. & WALTER, A. (1981) Hydrofluoric and nitric acid transport through lipid bilayer membranes. *Biochimica et Biophysica Acta*, 644, 153-6.
- GUTKNECHT, J. & WALTER, A. (1981) Hydroxyl ion permeability of lipid bilayer membranes. *Biochimica et Biophysica Acta*, 645, 161-2.
- GUTKNECHT, J. & WALTER, A. (1981) Transport of protons and hydrochloric acid through lipid bilayer membranes. *Biochimica et Biophysica Acta*, 641, 183-8.
- GUTKNECHT, J. & WALTER, A. (1982) Anion and proton transport through lipid bilayers and red cell membranes. *Chloride Transp. Biol. Membr., [Symp.]*, 91-109.
- GUTKNECHT, J. & WALTER, A. (1982) Thiocyanate ion and thiocyanic acid transport through lipid bilayer membranes. A model for thiocyanate ion inhibition of gastric acid secretion. *Biochimica et Biophysica Acta*, 685, 233-40.
- HAILE, J. M. & O'CONNELL, J. P. (1984) Internal structure of a model micelle via computer simulation. *Journal of Physical Chemistry*, 88, 6363-6.
- HALL, N. F. & SPRINKLE, M. R. (1932) Relations between the structure and strength of certain organic bases in aqueous solution. *Journal of the American Chemical Society*, 54, 3469-3485.
- HAMMETT, L. P. (1937) Effect of structure upon the reactions of organic compounds. Benzene derivatives. *Journal of the American Chemical Society*, 59, 96-103.
- HARNED, H. S. & OWEN, B. B. (1930) The thermodynamic properties of weak acids and bases in salt solutions, and an exact method of determining their dissociation constants. *Journal of the American Chemical Society*, 52, 5079-5091.
- HARNED, H. S. & ROBINSON, R. A. (1928) The ionic concentrations and activity coefficients of weak electrolytes in certain salt solutions. *Journal of the American Chemical Society*, 50, 3157-3178.

- HARRIGAN, P. R., WONG, K. F., REDELMEIER, T. E., WHEELER, J. J. & CULLIS, P. R. (1993) Accumulation of doxorubicin and other lipophilic amines into large unilamellar vesicles in response to transmembrane pH gradients. *Biochimica et Biophysica Acta, Biomembranes*, 1149, 329-38.
- HASTINGS, D. F. & GUTKNECHT, J. (1976) Ionic relations and the regulation of turgor pressure in the marine alga, *Valonia macrophysa*. *Journal of Membrane Biology*, 28, 263-75.
- HASTINGS, D. F. & GUTKNECHT, J. (1978) Potassium and turgor pressure in plants. *Journal of Theoretical Biology*, 73, 363-6.
- HENDERSON, W. G., TAAGEPERA, M., HOLTZ, D., MCIVER, R. T., BEAUCHAMP, J. L. & TAFT, R. W. (1972) Methyl substituent effects in protonated aliphatic amines and their radical cations. *Journal of the American Chemical Society*, 94, 4728-4729.
- HIETANIEMI, J. & MANFREDI, R. (1997) Math::Trig - trigonometric functions in Perl.
- HIGUCHI, T. & BROCHMANN-HANSEN, E. (1961) *Pharmaceutical Analysis*, New York, NY, Interscience Publishers / John Wiley & Sons, Inc.
- HIGUCHI, W. I. & HIESTAND, E. N. (1963) Dissolution rates of finely divided drug powders. I. Effect of a distribution of particle sizes in a diffusion-controlled process. *Journal of Pharmaceutical Sciences*, 52, 67-71.
- HIGUCHI, W. I., ROWE, E. L. & HIESTAND, E. N. (1963) Dissolution rates of finely divided drug powders. II. Micronized methylprednisolone. *Journal of Pharmaceutical Sciences*, 52, 162-4.
- HILDEBRAND, J. H. & SCOTT, R. L. (1950) *The Solubility Of Nonelectrolytes*, New York, NY, Reinhold Publishing Corporation.
- HINE, J. S. (1975) Equilibrium in hydrogen bonding. *Structural Effects On Equilibria In Organic Chemistry*. New York, John Wiley & Sons, Inc., 200.
- HINE, J. S. (1975) *Structural Effects On Equilibria In Organic Chemistry*, New York, NY, John Wiley & Sons, Inc.
- HOLLER, F. & CALLIS, J. B. (1989) Conformation of the hydrocarbon chains of sodium dodecyl sulfate molecules in micelles: an FTIR study. *Journal of Physical Chemistry*, 93, 2053-8.
- HOPE, M. J. & CULLIS, P. R. (1987) Lipid asymmetry induced by transmembrane pH gradients in large unilamellar vesicles. *Journal of Biological Chemistry*, 262, 4360-6.
- HOPE, M. J., NAYAR, R., MAYER, L. D. & CULLIS, P. R. (1993) Reduction of liposome size and preparation of unilamellar vesicles by extrusion techniques. *Liposome Technol. (2nd Ed.)*, 1, 123-39.
- HOPE, M. J., REDELMEIER, T. E., WONG, K. F., RODRIGUEZA, W. & CULLIS, P. R. (1989) Phospholipid asymmetry in large unilamellar vesicles induced by transmembrane pH gradients. *Biochemistry*, 28, 4181-7.

- HOU, T. J. & XU, X. J. (2003) ADME evaluation in drug discovery. 2. Prediction of partition coefficient by atom-additive approach based on atom-weighted solvent accessible surface areas. *J Chem Inf Comput Sci*, 43, 1058-67.
- HOU, T. J. & XU, X. J. (2003) ADME evaluation in drug discovery. 3. Modeling blood-brain barrier partitioning using simple molecular descriptors. *J Chem Inf Comput Sci*, 43, 2137-52.
- HOWE, D. & GUTKNECHT, J. (1978) Role of urinary bladder in osmoregulation in marine teleost, *Opsanus tau*. *American Journal of Physiology*, 235, R48-R54.
- HRISTOVA, K. & WHITE, S. H. (2005) An experiment-based algorithm for predicting the partitioning of unfolded peptides into phosphatidylcholine bilayer interfaces. *Biochemistry*, 44, 12614-12619.
- HUQUE, F. T. T., BOX, K., PLATTS, J. A. & COMER, J. (2004) Permeability through DOPC/dodecane membranes: measurement and LFER modelling. *European Journal of Pharmaceutical Sciences*, 23, 223-232.
- ISHIHAMA, Y., NAKAMURA, M., MIWA, T., KAJIMA, T. & ASAKAWA, N. (2002) A rapid method for pKa determination of drugs using pressure-assisted capillary electrophoresis with photodiode array detection in drug discovery. *Journal of Pharmaceutical Sciences*, 91, 933-942.
- ISHIMITSU, T., FUJIWARA, Y. & HIROSE, S. (1979) Study of the tautomeric forms of 3,4-dihydroxyphenylacetic acid by carbon-13 nuclear magnetic resonance spectroscopy. *Talanta*, 26, 67-9.
- ISHIMITSU, T., HIROSE, S. & SAKURAI, H. (1976) Acid dissociation of tyrosine and its related compounds. *Chemical & pharmaceutical bulletin*, 24, 3195-8.
- ISHIMITSU, T., HIROSE, S. & SAKURAI, H. (1977) Microscopic acid dissociation constants of 3,4-dihydroxyphenylpropionic acid and related compounds, and 3,4-dihydroxyphenylalanine (DOPA). *Talanta*, 24, 555-60.
- ISHIMITSU, T., HIROSE, S. & SAKURAI, H. (1978) Microscopic acid dissociation constants of 3,4-dihydroxyphenethylamine (dopamine). *Chemical & pharmaceutical bulletin*, 26, 74-78.
- ISHIMITSU, T., HIROSE, S. & SAKURAI, H. (1979) Microscopic acid dissociation constants of 3,4-dihydroxyphenylbutyric acid and 3,4-dihydroxybenzoic acid. *Chemical & pharmaceutical bulletin*, 27, 247-51.
- JACOBS, R. E. & WHITE, S. H. (1984) Behavior of hexane dissolved in dimyristoylphosphatidylcholine bilayers: an NMR and calorimetric study. *Journal of the American Chemical Society*, 106, 915-920.
- JACOBS, R. E. & WHITE, S. H. (1984) Behavior of hexane dissolved in dioleoylphosphatidylcholine bilayers: an NMR and calorimetric study. *Journal of the American Chemical Society*, 106, 6909-6912.
- JACOBS, R. E. & WHITE, S. H. (1986) Mixtures of a series of homologous hydrophobic peptides with lipid bilayers: a simple model system for examining the protein-lipid interface. *Biochemistry*, 25, 2605-2612.

- JACOBS, R. E. & WHITE, S. H. (1987) Lipid bilayer perturbations induced by simple hydrophobic peptides. *Biochemistry*, 26, 6127-6134.
- JACOBS, R. E. & WHITE, S. H. (1989) The nature of the hydrophobic binding of small peptides at the bilayer interface: implications for the insertion of transbilayer helices. *Biochemistry*, 28, 3421-3437.
- JANOFF, A. S., KURTZ, C. L., JABLONSKI, R. L., MINCHEY, S. R., BONI, L. T., GRUNER, S. M., CULLIS, P. R., MAYER, L. D. & HOPE, M. J. (1988) Characterization of cholesterol hemisuccinate and  $\alpha$ -tocopherol hemisuccinate vesicles. *Biochimica et Biophysica Acta, Biomembranes*, 941, 165-75.
- JOGUPARTHI, V. (2007) Physicochemical approaches to enhance the liposomal loading and retention of hydrophobic weak acids. PhD Thesis. College of Pharmacy, The University of Kentucky, Lexington, KY.
- JOHANSSON, A. C. & LINDAHL, E. (2008) Position-resolved free energy of solvation for amino acids in lipid membranes from molecular dynamics simulations. *Proteins*, 70, 1332-44.
- KANTER, P. M., BULLARD, G. A., GINSBERG, R. A., PILKIEWICZ, F. G., MAYER, L. D., CULLIS, P. R. & PAVELIC, Z. P. (1993) Comparison of the cardiotoxic effects of liposomal doxorubicin (TLC D-99) versus free doxorubicin in beagle dogs. *In Vivo*, 7, 17-26.
- KANTER, P. M., BULLARD, G. A., PILKIEWICZ, F. G., MAYER, L. D., CULLIS, P. R. & PAVELIC, Z. P. (1993) Preclinical toxicology study of liposome-encapsulated doxorubicin (TLC D-99): comparison with doxorubicin and empty liposomes in mice and dogs. *In Vivo*, 7, 85-95.
- KAPPE, T. & ARMSTRONG, M. D. (1965) Ultraviolet absorption spectra and apparent acidic dissociation constants of some phenolic amines. *Journal of Medicinal Chemistry*, 8, 368-74.
- KATZ, Y. & DIAMOND, J. M. (1974) Method for measuring nonelectrolyte partition coefficients between liposomes and water. *Journal of Membrane Biology*, 17, 69-86.
- KATZ, Y. & DIAMOND, J. M. (1974) Nonsolvent water in liposomes. *Journal of Membrane Biology*, 17, 87-100.
- KATZ, Y. & DIAMOND, J. M. (1974) Thermodynamic constants for nonelectrolyte partition between dimyristoyl lecithin and water. *Journal of Membrane Biology*, 17, 101-20.
- KATZ, Y., HOFFMAN, M. E. & BLUMENTHAL, R. (1983) Parametric analysis of membrane characteristics and membrane structure. *Journal of Theoretical Biology*, 105, 493-510.
- KIEFER, E. F. (1972) Rapid, convenient preparative procedure for phenethylamines. *Journal of Medicinal Chemistry*, 15, 214.



- KIRKWOOD, J. G. & WESTHEIMER, F. H. (1938) The electrostatic influence of substituents on the dissociation constants of organic acids. I. *Journal of Chemical Physics*, 6, 506-512.
- KOTYK, A., JANACEK, K. & KORYTA, J. (1988) *Biophysical Chemistry Of Membrane Functions*, New York, NY, John Wiley & Sons, Inc.
- LAIDLER, K. J. & MEISER, J. H. (1995) *Physical Chemistry*, Boston, MA, Houghton Mifflin Company.
- LAMBERT, W. J., WRIGHT, L. A. & STEVENS, J. K. (1990) Development of a preformulation lipophilicity screen utilizing a C-18-derivatized polystyrene-divinylbenzene high-performance liquid chromatographic (HPLC) column. *Pharm Res*, 7, 577-86.
- LANGLOIS, M.-H., MONTAGUT, M., DUBOST, J.-P., GRELLET, J. & SAUX, M.-C. (2005) Protonation equilibrium and lipophilicity of moxifloxacin. *Journal of Pharmaceutical and Biomedical Analysis*, 37, 389-393.
- LASIC, D. D., CEH, B., STUART, M. C. A., GUO, L., FREDERIK, P. M. & BARENHOLZ, Y. (1995) Transmembrane gradient driven phase transitions within vesicles: lessons for drug delivery. *Biochimica et Biophysica Acta, Biomembranes*, 1239, 145-56.
- LAU, K. F., ALPER, H. E., THACHER, T. S. & STOUCHE, T. R. (1994) Effects of switching functions on the behavior of liquid water in molecular dynamics simulations. *Journal of Physical Chemistry*, 98, 8785-92.
- LAZARO, E., RAFOLS, C. & ROSES, M. (2005) Characterization of immobilized artificial membrane (IAM) and XTerra columns by means of chromatographic models. *Journal of Chromatography, A*, 1081, 163-73.
- LEE, R. J., WANG, S., TURK, M. J. & LOW, P. S. (1998) The effects of pH and intraliposomal buffer strength on the rate of liposome content release and intracellular drug delivery. *Bioscience Reports*, 18, 69-78.
- LEO, A., HANSCH, C. & ELKINS, D. (1971) Partition coefficients and their uses. *Chemical Reviews (Washington, DC, United States)*, 71, 525-616.
- LI, C., YI, M., HU, J., ZHOU, H. X. & CROSS, T. A. (2008) Solid-state NMR and MD simulations of the antiviral drug amantadine solubilized in DMPC bilayers. *Biophysical Journal*, 94, 1295-302.
- LIEN, E. J. (1987) *SAR: Side Effects And Drug Design*, New York, NY, Marcel Dekker, Inc.
- LUAN, F., MA, W., ZHANG, H., ZHANG, X., LIU, M., HU, Z. & FAN, B. (2005) Prediction of pK(a) for neutral and basic drugs based on radial basis function Neural networks and the heuristic method. *Pharm Res*, 22, 1454-60.
- LUTY, B. A., DAVIS, M. E., TIRONI, I. G. & VAN GUNSTEREN, W. F. (1994) A comparison of particle-particle particle-mesh and Ewald methods for calculating electrostatic interactions in periodic molecular systems. *Molecular Simulation*, 14, 11-20.

- MACCALLUM, J. L., BENNETT, W. F. & TIELEMAN, D. P. (2007) Partitioning of amino acid side chains into lipid bilayers: results from computer simulations and comparison to experiment. *Journal of General Physiology*, 129, 371-7.
- MACCALLUM, J. L., BENNETT, W. F. & TIELEMAN, D. P. (2008) Distribution of amino acids in a lipid bilayer from computer simulations. *Biophysical Journal*, 94, 3393-404.
- MACCALLUM, J. L. & TIELEMAN, D. P. (2006) Computer simulation of the distribution of hexane in a lipid bilayer: spatially resolved free energy, entropy, and enthalpy profiles. *Journal of the American Chemical Society*, 128, 125-30.
- MACDONALD, P. M. & SEELIG, J. (1988) Anion binding to neutral and positively-charged lipid membranes. *Biochemistry*, 27, 6769-75.
- MACK, F. & BOENISCH, H. (1979) Dissociation constants and lipophilicity of catecholamines and related compounds. *Naunyn-Schmiedeberg's Archives of Pharmacology*, 310, 1-9.
- MADDEN, T. D., HARRIGAN, P. R., TAI, L. C. L., BALLY, M. B., MAYER, L. D., REDELMEIER, T. E., LOUGHREY, H. C., TILCOCK, C. P. S., REINISH, L. W. & CULLIS, P. R. (1990) The accumulation of drugs within large unilamellar vesicles exhibiting a proton gradient: a survey. *Chemistry and Physics of Lipids*, 53, 37-46.
- MADDEN, T. D., HOPE, M. J., TILCOCK, C. P. S., CULLIS, P. R., HARRIGAN, P. R., MUI, B. S., BALLY, M. B., TAI, L. & MAYER, L. D. (1990) Accumulation of drugs into liposomes by a proton gradient. *PCT Int. Appl.* WO, (Liposome Co., Inc., USA).
- MARRINK, S. J., JÄHNIG, F. & BERENDSEN, H. J. (1996) Proton transport across transient single-file water pores in a lipid membrane studied by molecular dynamics simulations. *Biophysical Journal*, 71, 632-647.
- MARRINK, S.-J. & BERENDSEN, H. J. C. (1994) Simulation of water transport through a lipid membrane. *Journal of Physical Chemistry*, 98, 4155-4168.
- MARTIN, A. N. (1993) Interfacial phenomena. *Physical Pharmacy: Physical Chemical Principles In The Pharmaceutical Sciences*. 4 ed. Malvern, PA, Lea and Febiger, 632-392.
- MARTIN, R. B. (1971) Zwitterion formation upon deprotonation in L-3, 4-dihydroxyphenylalanine and other phenolic amines. *Journal of Physical Chemistry*, 75, 2657-61.
- MASHL, R. J., SCOTT, H. L., SUBRAMANIAM, S. & JAKOBSSON, E. (2001) Molecular simulation of dioleoylphosphatidylcholine lipid bilayers at differing levels of hydration. *Biophysical Journal*, 81, 3005-3015.
- MAYER, L., BALLY, M. B., CULLIS, P. R., GINSBERG, R. S. & MITILENES, G. N. (1988) Pharmaceutical liposomes containing antineoplastic agents and buffers. *PCT Int. Appl.* WO, (Liposome Co., Inc., USA).

- MAYER, L. D., BALLY, M. B. & CULLIS, P. R. (1986) Uptake of adriamycin into large unilamellar vesicles in response to a pH gradient. *Biochimica et Biophysica Acta, Biomembranes*, 857, 123-6.
- MAYER, L. D., BALLY, M. B. & CULLIS, P. R. (1990) Strategies for optimizing liposomal doxorubicin. *Journal of Liposome Research*, 1, 473-90.
- MAYER, L. D., BALLY, M. B., HOPE, M. J. & CULLIS, P. R. (1985) Uptake of antineoplastic agents into large unilamellar vesicles in response to a membrane potential. *Biochimica et Biophysica Acta, Biomembranes*, 816, 294-302.
- MAYER, L. D., BALLY, M. B., HOPE, M. J. & CULLIS, P. R. (1985) Uptake of dibucaine into large unilamellar vesicles in response to a membrane potential. *Journal of Biological Chemistry*, 260, 802-8.
- MAYER, L. D., BALLY, M. B., HOPE, M. J. & CULLIS, P. R. (1986) Techniques for encapsulating bioactive agents into liposomes. *Chemistry and Physics of Lipids*, 40, 333-45.
- MAYER, L. D., BALLY, M. B., LOUGHREY, H., MASIN, D. & CULLIS, P. R. (1990) Liposomal vincristine preparations which exhibit decreased drug toxicity and increased activity against murine L1210 and P388 tumors. *Cancer Research*, 50, 575-9.
- MAYER, L. D., CULLIS, P. R. & BALLY, M. B. (1994) The use of transmembrane pH gradient-driven drug encapsulation in the pharmacodynamic evaluation of liposomal doxorubicin. *Journal of Liposome Research*, 529-53.
- MAYER, L. D., NAYAR, R., THIES, R. L., BOMAN, N. L., CULLIS, P. R. & BALLY, M. B. (1993) Identification of vesicle properties that enhance the antitumor activity of liposomal vincristine against murine L1210 leukemia. *Cancer Chemotherapy and Pharmacology*, 33, 17-24.
- MAYER, L. D., TAI, L. C. L., BALLY, M. B., MITILENES, G. N., GINSBERG, R. S. & CULLIS, P. R. (1990) Characterization of liposomal systems containing doxorubicin entrapped in response to pH gradients. *Biochimica et Biophysica Acta, Biomembranes*, 1025, 143-51.
- MAYER, L. D., TAI, L. C. L., KO, D. S. C., MASIN, D., GINSBERG, R. S., CULLIS, P. R. & BALLY, M. B. (1989) Influence of vesicle size, lipid composition, and drug-to-lipid ratio on the biological activity of liposomal doxorubicin in mice. *Cancer Research*, 49, 5922-30.
- MAYER, L. D., WONG, K. F., MENON, K., CHONG, C., HARRIGAN, P. R. & CULLIS, P. R. (1988) Influence of ion gradients on the transbilayer distribution of dibucaine in large unilamellar vesicles. *Biochemistry*, 27, 2053-60.
- MAYER, P., XIANG, T.-X. & ANDERSON, B. D. (2000) Independence of substituent contributions to the transport of small molecule permeants in lipid bilayers. *AAPS PharmSci*, 2(2) article 14 (<http://www.pharmsci.org/>), 1-13.
- MAYER, P. T. (2001) Functional group contributions to peptide permeability in lipid bilayer membranes: The role of peptide conformation and length. PhD Thesis.

Department of Pharmaceutics and Pharmaceutical Chemistry, The University of Utah, Salt Lake City, UT.

- MAYER, P. T., XIANG, T.-X., NIEMI, R. & ANDERSON, B. D. (2003) A hydrophobicity scale for the lipid bilayer barrier domain from peptide permeabilities: Nonadditivities in residue contributions. *Biochemistry*, 42, 1624-1636.
- MCCAMMON, J. A. & HARVEY, S. (1989) *Dynamics Of Proteins And Nucleic Acids*, Cambridge, United Kingdom, Cambridge University Press.
- MELANDRI, S. & MARIS, A. (2004) Intramolecular hydrogen bonds and conformational properties of biogenic amines: A free-jet microwave study of tyramine. *Physical Chemistry Chemical Physics*, 6, 2863-2866.
- MICROMATH, I. (1995) Micromath Scientist for Windows. 2.01 Compiled 7/21/1995 1:55 PM ed. Saint Louis, Missouri, 63144, Micromath Scientific Software.
- MILLER, G. P., HANNA, I. H., NISHIMURA, Y. & GUENGERICH, F. P. (2001) Oxidation of phenethylamine derivatives by cytochrome P450 2D6: The issue of substrate protonation in binding and catalysis. *Biochemistry*, 40, 14215-14223.
- MORGAN, M. E., LIU, K. & ANDERSON, B. D. (1998) Microscale titrimetric and spectrophotometric methods for determination of ionization constants and partition coefficients of new drug candidates. *Journal of Pharmaceutical Sciences*, 87, 238-245.
- MUKHOPADHYAY, P., VOGEL, H. J. & TIELEMAN, D. P. (2004) Distribution of pentachlorophenol in phospholipid bilayers: a molecular dynamics study. *Biophysical Journal*, 86, 337-45.
- MUNSON, M. S. B. (1965) Proton affinities and the methyl inductive effect. *Journal of the American Chemical Society*, 87, 2332-2336.
- MYSELS, K. J. (1967) *Introduction To Colloid Chemistry*, New York, Interscience Publishers, Inc.
- N. GULYAEVA, A. Z. P. L. A. C. B. Z. (2003) pH dependence of the relative hydrophobicity and lipophilicity of amino acids and peptides measured by aqueous two-phase and octanol-buffer partitioning. *Journal of Peptide Research*, 61, 71-79.
- NAGLE, J. F. & TRISTRAM-NAGLE, S. (2000) Structure of lipid bilayers. *Biochimica et Biophysica Acta, Reviews on Biomembranes*, 1469, 159-195.
- NAGY, P. I. & TAKACS-NOVAK, K. (2004) Tautomeric and conformational equilibria of biologically important (hydroxyphenyl)alkylamines in the gas phase and in aqueous solution. *Physical Chemistry Chemical Physics*, 6, 2838-2848.
- NAGY, P. I., VOELGYI, G. & TAKACS-NOVAK, K. (2005) Tautomeric and conformational equilibria of tyramine and dopamine in aqueous solution. *Molecular Physics*, 103, 1589-1601.

- NARTEN, A. H. (1968) Diffraction pattern and structure of liquid benzene. *Journal of Chemical Physics*, 48, 1630-1634.
- NARTEN, A. H. (1977) X-ray diffraction pattern and models of liquid benzene. *Journal of Chemical Physics*, 67, 2102-2108.
- NAYAR, R., MAYER, L. D., HOPE, M. J. & CULLIS, P. R. (1984) Phosphatidic acid as a calcium ionophore in large unilamellar vesicle systems. *Biochimica et Biophysica Acta, Biomembranes*, 777, 343-6.
- NEUFELDT, V. (1997) Webster's new world college dictionary. IN NEUFELDT, V. & GURALNIK, D. B. (Eds.) *Webster's New World College Dictionary*. 3 ed. Cleveland, OH, Simon & Schuster, Inc.
- NICHOLS, J. W. & DEAMER, D. W. (1976) Catechol amine uptake and concentration by liposomes maintaining pH gradients. *Biochimica et Biophysica Acta, Biomembranes*, 455, 269-71.
- NICHOLS, J. W. & DEAMER, D. W. (1978) Proton and hydroxyl permeability coefficients measured for unilamellar liposomes. *Front. Biol. Energ., [Pap. Int. Symp.]*, 2, 1273-83.
- NICHOLS, J. W. & DEAMER, D. W. (1980) Net proton-hydroxyl permeability of large unilamellar liposomes measured by an acid-base titration technique. *Proceedings of the National Academy of Sciences of the United States of America*, 77, 2038-42.
- NICHOLS, J. W., HILL, M. W., BANGHAM, A. D. & DEAMER, D. W. (1980) Measurement of net proton-hydroxyl permeability of large unilamellar liposomes with the fluorescent pH probe, 9-aminoacridine. *Biochimica et Biophysica Acta, Biomembranes*, 596, 393-403.
- NORMAN, K. E. & NYMEYER, H. (2006) Indole localization in lipid membranes revealed by molecular simulation. *Biophysical Journal*, 91, 2046-54.
- NORTHRUP, S. H., PEAR, M. R., LEE, C. Y., MCCAMMON, J. A. & KARPLUS, M. (1982) Dynamical theory of activated processes in globular proteins. *Proceedings of the National Academy of Sciences of the United States of America*, 79, 4035-9.
- NOSZAL, B. & SZAKACS, Z. (2003) Microscopic protonation equilibria of oxidized glutathione. *Journal of Physical Chemistry B*, 107, 5074-5080.
- PANDIT, S. A., CHIU, S. W., JAKOBSSON, E., GRAMA, A. & SCOTT, H. L. (2007) Cholesterol surrogates: a comparison of cholesterol and 16:0 ceramide in POPC bilayers. *Biophysical Journal*, 92, 920-7.
- PANDIT, S. A., CHIU, S. W., JAKOBSSON, E., GRAMA, A. & SCOTT, H. L. (2008) Cholesterol packing around lipids with saturated and unsaturated chains: a simulation study. *Langmuir*, 24, 6858-65.
- PANDIT, S. A., VASUDEVAN, S., CHIU, S. W., MASHL, R. J., JAKOBSSON, E. & SCOTT, H. L. (2004) Sphingomyelin-cholesterol domains in phospholipid membranes: atomistic simulation. *Biophysical Journal*, 87, 1092-100.

- PANGALI, C., RAO, M. & BERNE, B. J. (1979) A Monte Carlo simulation of the hydrophobic interaction. *Journal of Chemical Physics*, 71, 2975-81.
- PARTHASARATHI, R., PADMANABHAN, J., ELANGO, M., CHITRA, K., SUBRAMANIAN, V. & CHATTARAJ, P. K. (2006) pKa prediction using group philicity. *Journal of Physical Chemistry A*, 110, 6540-4.
- PASENKIEWICZ-GIERULA, M., ROG, T., KITAMURA, K. & KUSUMI, A. (2000) Cholesterol effects on the phosphatidylcholine bilayer polar region: a molecular simulation study. *Biophysical Journal*, 78, 1376-89.
- PASENKIEWICZ-GIERULA, M., TAKAOKA, Y., MIYAGAWA, H., KITAMURA, K. & KUSUMI, A. (1997) Hydrogen bonding of water to phosphatidylcholine in the membrane as studied by a molecular dynamics simulation: location, geometry, and lipid-lipid bridging via hydrogen-bonded water. *Journal of Physical Chemistry A*, 101, 3677-3691.
- PASTOR, R. W., VENABLE, R. M. & FELLER, S. E. (2002) Lipid bilayers, NMR relaxation, and computer simulations. *Accounts of Chemical Research*, 35, 438-446.
- PATAI, S. (1968) *The Chemistry Of The Amino Group*, Surrey, England, John Wiley & Sons Ltd.
- PECSAR, R. E. & MARTIN, J. J. (1966) Solution thermodynamics from gas-liquid chromatography. *Analytical Chemistry*, 38, 1661-1669.
- PEINHARDT, G. & WIESE, M. (2001) Microionization constants: novel approach for the determination of the zwitterionic equilibrium of hydroxyphenylalkylamines by photometric titration. *International Journal of Pharmaceutics*, 215, 83-89.
- PERRIN, C. L. & THOBURN, J. D. (1992) Symmetries of hydrogen bonds in monoanions of dicarboxylic acids. *Journal of the American Chemical Society*, 114, 8559-8565.
- PERRIN, D. D., DEMPSEY, B. & SERJEANT, E. P. (1981) *pKa Prediction For Organic Acids And Bases*, New York, NY, Chapman and Hall.
- PITMAN, M. C., SUITS, F., MACKERELL, A. D., JR. & FELLER, S. E. (2004) Molecular-level organization of saturated and polyunsaturated fatty acids in a phosphatidylcholine bilayer containing cholesterol. *Biochemistry*, 43, 15318-28.
- PLATTS, J. A., ABRAHAM, M. H., BUTINA, D. & HERSEY, A. (2000) Estimation of molecular linear free energy relationship descriptors by a group contribution approach. 2. Prediction of partition coefficients. *J Chem Inf Comput Sci*, 40, 71-80.
- PLIMPTON, S. (1995) Fast parallel algorithms for short-range molecular dynamics. *Journal of Computational Physics*, 117, 1-19.
- PLIMPTON, S., CROZIER, P. & THOMPSON, A. (2001) Large-scale atomic/molecular massively parallel simulator (Available at <http://lammps.sandia.gov>). IN PLIMPTON, S. (Ed.) 2001 ed. Albuquerque, New Mexico, USA, Sandia National Laboratories, US Department of Energy.

- POHORILLE, A., CIEPLAK, P. & WILSON, M. A. (1996) Interactions of anesthetics with the membrane-water interface. *Chem Phys*, 204, 337-45.
- POHORILLE, A. & WILSON, M. A. (1996) Excess chemical potential of small solutes across water--membrane and water--hexane interfaces. *J Chem Phys*, 104, 3760-73.
- PRAUSNITZ, J. M. (1969) *Molecular Thermodynamics Of Fluid-Phase Equilibria*, Englewood Cliffs, NJ, Prantice-Hall, Inc.
- QUINN, P. J. & CHERRY, R. J. (1992) *Structural And Dynamic Properties Of Lipids And Membranes*, Chapel Hill, NC, Portland Press Ltd.
- REBERTUS, D. W., BERNE, B. J. & CHANDLER, D. (1979) A molecular dynamics and Monte Carlo study of solvent effects on the conformational equilibrium of n-butane in carbon tetrachloride. *Journal of Chemical Physics*, 70, 3395-400.
- REDELMEIER, T. E., HOPE, M. J. & CULLIS, P. R. (1990) On the mechanism of transbilayer transport of phosphatidylglycerol in response to transmembrane pH gradients. *Biochemistry*, 29, 3046-53.
- REDELMEIER, T. E., MAYER, L. D., WONG, K. F., BALLY, M. B. & CULLIS, P. R. (1989) Proton flux in large unilamellar vesicles in response to membrane potentials and pH gradients. *Biophysical Journal*, 56, 385-93.
- REICHARD, K. & JOHNSON, E. F. (1995) *Teach Yourself - Unix*, New York, NY, MIS Press / Henry Holt and Company, Inc.
- RICHARDS, R. L., HABBERSETT, R. C., SCHER, I., JANOFF, A. S., SCHIEREN, H. P., MAYER, L. D., CULLIS, P. R. & ALVING, C. R. (1986) Influence of vesicle size on complement-dependent immune damage to liposomes. *Biochimica et Biophysica Acta, Biomembranes*, 855, 223-30.
- RIEGELMAN, S., STRAIT, L. A. & FISCHER, E. Z. (1962) Acid dissociation constants of phenylalkanolamines. *Journal of Pharmaceutical Sciences*, 51, 129-33.
- ROBERTSON, E. G., SIMONS, J. P. & MONS, M. (2001) Comment on "Structural and vibrational assignment of *p*-methoxyphenethylamine conformers". *Journal of Physical Chemistry A*, 105, 9990-9992.
- ROCK, P. A. (1983) *Chemical Thermodynamics*, Mill Valley, CA, University Science Books.
- ROGERS, J. A. & DAVIS, S. S. (1980) Functional group contributions to the partitioning of phenols between liposomes and water. *Biochimica et Biophysica Acta, Biomembranes*, 598, 392-404.
- ROSSO, L. & GOULD, I. R. (2008) Structure and dynamics of phospholipid bilayers using recently developed general all-atom force fields. *Journal of Computational Chemistry*, 29, 24-37.
- RYCKAERT, J.-P., CICCOTTI, G. & BERENDSEN, H. (1977) Numerical integration of the cartesian equations of motion of a system with constraints: molecular dynamics of n-alkanes. *Journal of Computational Physics*, 23, 327-341.

- RYTTING, J. H., ANDERSON, B. D. & HIGUCHI, T. (1978) Vapor pressure studies of the self-association of alcohols in isoctane. 2. The effect of chain branching. *Journal of Physical Chemistry*, 82, 2240-5.
- RYTTING, J. H., HUSTON, L. P. & HIGUCHI, T. (1978) Thermodynamic group contributions for hydroxyl, amino, and methylene groups. *Journal of Pharmaceutical Sciences*, 67, 615-8.
- S. H. YALKOWSKY, S. C. V. G. L. A. (1976) Solubility of nonelectrolytes in polar solvents IV: Nonpolar drugs in mixed solvents. *Journal of Pharmaceutical Sciences*, 65, 1488-1494.
- SAKURAI, H. & ISHIMITSU, T. (1975) Acid dissociation of serotonin(5-hydroxytryptamine) and 5-hydroxytryptophan. *Yakugaku Zasshi*, 95, 1384-7.
- SCHERER, P. G. & SEELIG, J. (1989) Electric charge effects on phospholipid headgroups. Phosphatidylcholine in mixtures with cationic and anionic amphiphiles. *Biochemistry*, 28, 7720-8.
- SCHLICK, T., BARTH, E. & MANDZIUK, M. (1997) Biomolecular dynamics at long timesteps: bridging the timescale gap between simulation and experimentation. *Annu Rev Biophys Biomol Struct*, 26, 181-222.
- SCHRODINGER, L. (1991-2000) Jaguar. 6.0 ed. New York, NY, Schrodinger, LLC.
- SEELIG, J. & GANZ, P. (1991) Nonclassical hydrophobic effect in membrane binding equilibria. *Biochemistry*, 30, 9354-9359.
- SEELIG, J. & WAESPE-SARCEVIC, N. (1978) Molecular order in cis and trans unsaturated phospholipid bilayers. *Biochemistry*, 17, 3310-5.
- SENGUPTA, D., SMITH, J. C. & ULLMANN, G. M. (2008) Partitioning of amino-acid analogues in a five-slab membrane model. *Biochim Biophys Acta*, 1778, 2234-43.
- SHANMUGASUNDARAM, V., MAGGIORA, G. M. & LAJINESS, M. S. (2005) Hit-directed nearest-neighbor searching. *Journal of Medicinal Chemistry*, 48, 240-248.
- SHINODA, W., MIKAMI, M., BABA, T. & HATO, M. (2004) Molecular dynamics study on the effects of chain branching on the physical properties of lipid bilayers: 2. Permeability. *Journal of Physical Chemistry B*, 108, 9346-9356.
- SIMON, S. A. & GUTKNECHT, J. (1980) Solubility of carbon dioxide in lipid bilayer membranes and organic solvents. *Biochimica et Biophysica Acta*, 596, 352-8.
- STENBERG, P. (2001) Computational models for the prediction of intestinal membrane permeability. Dissertation. Pharmaceutics, Uppsala University, Uppsala, Sweden.
- STENBERG, P., LUTHMAN, K., ELLENS, H., LEE, C. P., SMITH, P., LAGO, A., ELLIOTT, J. D. & ARTURSSON, P. (1999) Prediction of the intestinal absorption of endothelin receptor antagonists using three theoretical methods of increasing complexity. *Pharmaceutical Research*, 16, 1520-1526.



- STERN, H. A. & FELLER, S. E. (2003) Calculation of the dielectric permittivity profile for a nonuniform system: Application to a lipid bilayer simulation. *J Chem Phys*, 118, 3401-3412.
- STEWART, B. H. & CHAN, O. H. (1998) Use of immobilized artificial membrane chromatography for drug transport applications. *Journal of Pharmaceutical Sciences*, 87, 1471-1478.
- STEWART, B. H., CHUNG, F. Y., TAIT, B., JOHN, C. & CHAN, O. H. (1998) Hydrophobicity of HIV protease inhibitors by immobilized artificial membrane chromatography: application and significance to drug transport. *Pharmaceutical Research*, 15, 1401-1406.
- STOUCH, T. R. (1997) Solute transport and partitioning in lipid bilayers. Molecular dynamics simulations. *Progress in Colloid & Polymer Science*, 103, 116-120.
- STOUCH, T. R. (1998) Permeation of lipid membranes: Molecular dynamics simulations. IN KOLLMAN, P. & ALLINGER, N. (Eds.) *Encyclopedia of Computational Chemistry, Setting the Standards in Computational Chemistry*. 1 ed., John Wiley and Sons, Ltd., Molecular Mechanics: 3580.
- STOUCH, T. R. (2000) Understanding membrane permeation through simulation. *Book of Abstracts, 219th ACS National Meeting, San Francisco, CA, March 26-30, 2000*, PHYS-174.
- STOUCH, T. R., ALPER, H. E. & BASSOLINO, D. (1995) Simulations of drug diffusion in biomembranes. *ACS Symposium Series*, 589, 127-38.
- STOUCH, T. R. & BASSOLINO, D. (1996) Movement of small molecules in lipid bilayers: molecular dynamics simulation studies. *Biological Membranes*, 255-278, 1 plate.
- STOUCH, T. R., BASSOLINO, D. & ALPER, H. (1995) Biomembrane/water interfaces: Water structure and solute transport and partitioning by computer simulation. *Book of Abstracts, 210th ACS National Meeting, Chicago, IL, August 20-24*, COLL-047.
- STOUCH, T. R., BASSOLINO, D. & DAVIS, M. (1996) Chemical functional group contribution to the free energy of membrane permeation by atomic-level molecular dynamics simulation. *Book of Abstracts, 212th ACS National Meeting, Orlando, FL, August 25-29*, COMP-016.
- STOUCH, T. R., BASSOLINO, D. & DAVIS, M. (1997) Molecular dynamics simulation studies of solute permeation of lipid bilayers. *Book of Abstracts, 214th ACS National Meeting, Las Vegas, NV, September 7-11*, PHYS-173.
- STOUCH, T. R., WARD, K. B., ALTIERI, A. & HAGLER, A. T. (1991) Simulations of lipid crystals: characterization of potential energy functions and parameters for lecithin molecules. *Journal of Computational Chemistry*, 12, 1033-46.
- SUGANO, K., NABUCHI, Y., MACHIDA, M. & ASO, Y. (2003) Prediction of human intestinal permeability using artificial membrane permeability. *International Journal of Pharmaceutics*, 257, 245.

- SUGANO, K., TAKATA, N., MACHIDA, M., SAITOH, K. & TERADA, K. (2002) Prediction of passive intestinal absorption using bio-mimetic artificial membrane permeation assay and the paracellular pathway model. *International Journal of Pharmaceutics*, 241, 241.
- SUN, J., ZHANG, T.-H. & HE, Z.-G. (2005) Profiling drug membrane transport via immobilized artificial membrane chromatography. *Current Pharmaceutical Analysis*, 1, 273-282.
- SZAKACS, Z., BENI, S., VARGA, Z., ORFI, L., KERI, G. & NOSZAL, B. (2005) Acid-base profiling of Imatinib (Gleevec) and its fragments. *Journal of Medicinal Chemistry*, 48, 249-255.
- TAFT, R. W., JR. (1953) The general nature of the proportionality of polar effects of substituent groups in organic chemistry. *Journal of the American Chemical Society*, 75, 4231-8.
- TAKACS-NOVAK, K., NOSZAL, B., HERMECZ, I., KERESZTURI, G., PODANYI, B. & SZASZ, G. (1990) Protonation equilibria of quinolone antibacterials. *Journal of Pharmaceutical Sciences*, 79, 1023-8.
- TANFORD, C. (1957) The location of electrostatic charges in Kirkwood's model of organic ions. *Journal of the American Chemical Society*, 79, 5348-5352.
- TANFORD, C. (1957) Theory of protein titration curves. II. Calculations for simple models at low ionic strength. *Journal of the American Chemical Society*, 79, 5340-5347.
- TANFORD, C. & KIRKWOOD, J. G. (1957) Theory of protein titration curves. I. General equations for impenetrable spheres. *Journal of the American Chemical Society*, 79, 5333-5339.
- TEJWANI, R. W. & ANDERSON, B. D. (2004) Unpublished data.
- TEJWANI, R. W. & ANDERSON, B. D. (2006) Passive permeability-pH profile of tyramine across a 1,2-dioleoyl-*sn*-glycero-3-phosphocholine (DOPC) bilayer. *AAPS Annual Meeting*. San Antonio, TX, American Association Of Pharmaceutical Scientists.
- TEJWANI, R. W. & ANDERSON, B. D. (2008) Influence of intravesicular pH drift and membrane binding on the liposomal release of a model amine-containing permeant. *Journal of Pharmaceutical Sciences*, 97, 381-399.
- TEJWANI, R. W., DAVIS, M. E. & STOUCH, T. R. (2004) Large scale molecular dynamics simulation of a drug like molecule In 1,2-dioleoyl-*sn*-glycero-3-phosphocholine (DOPC) bilayer. *AAPS Annual Meeting*. Baltimore, MD, American Association Of Pharmaceutical Scientists.
- TEJWANI, R. W., DAVIS, M. M. & STOUCH, T. R. (2004) Large scale molecular dynamics simulation of a drug like molecule in 1,2-dioleoyl-*sn*-glycero-3-phosphocholine (DOPC) bilayer. *AAPS Journal*, 6, T2271.
- TEJWANI, R. W., STOUCH, T. R. & ANDERSON, B. D. (2009) Substituent effects on the ionization and partitioning of *p*-(aminoethyl)phenols and structurally related

- compounds. Electrostatic effects dependent on conformation. *Journal of Pharmaceutical Sciences*, Accepted for publication.
- THIES, R. L., COWENS, D. W., CULLIS, P. R., BALLY, M. B. & MAYER, L. D. (1990) Method for rapid separation of liposome-associated doxorubicin from free doxorubicin in plasma. *Analytical Biochemistry*, 188, 65-71.
- THOMAS, G. B. J. & FINNEY, R. L. (1984) *Calculus And Analytic Geometry*, Reading, MA, Addison-Wesley Publishing Company.
- THYSSEN, A. (2001) Math::VectorReal - Module to handle 3D vector mathematics in Perl.
- TINOCO, I. J., SAUER, K. & WANG, J. C. (1995) *Physical Chemistry Principles And Applications In Biological Sciences*, Upper Saddle River, NJ, Prantice Hall.
- TORRIE, G. M. & VALLEAU, J. P. (1977) Monte Carlo study of a phase-separating liquid mixture by umbrella sampling. *Journal of Chemical Physics*, 66, 1402-8.
- TORRIE, G. M. & VALLEAU, J. P. (1977) Nonphysical sampling distributions in Monte Carlo free energy estimation: Umbrella sampling. *Journal of Computational Physics*, 23, 187-199.
- TRISTRAM-NAGLE, S., PETRACHE, H. I. & NAGLE, J. F. (1998) Structure and interactions of fully hydrated dioleoylphosphatidylcholine bilayers. *Biophysical Journal*, 75, 917-925.
- TU, K., TAREK, M., KLEIN, M. L. & SCHARF, D. (1998) Effects of anesthetics on the structure of a phospholipid bilayer: molecular dynamics investigation of halothane in the hydrated liquid crystal phase of dipalmitoylphosphatidylcholine. *Biophysical Journal*, 75, 2123-34.
- ULANDER, J. & HAYMET, A. D. (2003) Permeation across hydrated DPPC lipid bilayers: simulation of the titrable amphiphilic drug valproic acid. *Biophysical Journal*, 85, 3475-84.
- URBAN, J. J., CRAMER, C. J. & FAMINI, G. R. (1992) A computational study of solvent effects on the conformation of dopamine. *Journal of the American Chemical Society*, 114, 8226-8231.
- VALKO, K., DU, C. M., BEVAN, C. D., REYNOLDS, D. P. & ABRAHAM, M. H. (2000) Rapid-gradient HPLC method for measuring drug interactions with immobilized artificial membrane: comparison with other lipophilicity measures. *Journal of Pharmaceutical Sciences*, 89, 1085-96.
- VAN DE WATERBEEMD, H. & GIFFORD, E. (2003) ADMET in silico modelling: towards prediction paradise? *Nat Rev Drug Discov*, 2, 192-204.
- VARHANICKOVA, D., SHIU, W.-Y. & MACKAY, D. (1995) Aqueous solubilities of alkylphenols and methoxyphenols at 25 °C. *Journal of Chemical and Engineering Data*, 40, 448-51.

- VENABLE, R. M. & PASTOR, R. W. (2002) Molecular dynamics simulations of water wires in a lipid bilayer and water/octane model systems. *J Chem Phys*, 116, 2663-2664.
- VRBANCICH, J. & RITCHIE, G. L. D. (1980) Quadrupole moments of benzene, hexafluorobenzene and other non-dipolar aromatic molecules. *Journal of the Chemical Society, Faraday Transactions 2: Molecular and Chemical Physics*, 76, 648-659.
- WALL, L. (2004) Practical Extraction And Report Language. 5.8 ed.
- WALTER, A. & GUTKNECHT, J. (1984) Monocarboxylic acid permeation through lipid bilayer membranes. *Journal of Membrane Biology*, 77, 255-64.
- WALTER, A. & GUTKNECHT, J. (1986) Permeability of small nonelectrolytes through lipid bilayer membranes. *Journal of Membrane Biology*, 90, 207-17.
- WALTER, A., HASTINGS, D. & GUTKNECHT, J. (1982) Weak acid permeability through lipid bilayer membranes. Role of chemical reactions in the unstirred layer. *Journal of General Physiology*, 79, 917-33.
- WATERHOUSE, D. N., MADDEN, T. D., CULLIS, P. R., BALLY, M. B., MAYER, L. D. & WEBB, M. S. (2005) Preparation, characterization, and biological analysis of liposomal formulations of vincristine. *Methods in Enzymology*, 391, 40-57.
- WEBB, M. S., SARRIS, A. H., CABANILLAS, F., MAYER, L. D., BALLY, M. B., BURGE, C. & CULLIS, P. R. (2000) Clinical and preclinical pharmacology of liposomal vincristine. *Journal of Liposome Research*, 10, 501-512.
- WEBB, M. S., SAXON, D., WONG, F. M. P., LIM, H. J., WANG, Z., BALLY, M. B., CHOI, L. S. L., CULLIS, P. R. & MAYER, L. D. (1998) Comparison of different hydrophobic anchors conjugated to poly(ethylene glycol): effects on the pharmacokinetics of liposomal vincristine. *Biochimica et Biophysica Acta, Biomembranes*, 1372, 272-282.
- WEHRY, E. L. & ROGERS, L. B. (1965) Application of linear free energy relations to electronically excited states of monosubstituted phenols. *Journal of the American Chemical Society*, 87, 4234-4238.
- WEISSTEIN, E. W. (1999) "Spherical cap" from MathWorld - A Wolfram web resource. Wolfram Research, Inc.
- WESTHEIMER, F. H. & KIRKWOOD, J. G. (1938) The electrostatic influence of substituents on the dissociation constants of organic acids. II. *Journal of Chemical Physics*, 6, 513-517.
- WILFRED F. VAN GUNSTEREN, X. D. ALAN E. M. (2002) Computation of free energy. *Helvetica Chimica Acta*, 85, 3113-3129.
- WILSON, M. A. & POHORILLE, A. (1996) Mechanism of unassisted ion transport across membrane bilayers. *Journal of the American Chemical Society*, 118, 6580-7.

- WILSON, M. A., POHORILLE, A. & PRATT, L. R. (1987) Molecular dynamics of the water liquid-vapor interface. *Journal of Physical Chemistry*, 91, 4873-4878.
- WIMLEY, W. C., CREAMER, T. P. & WHITE, S. H. (1996) Solvation energies of amino acid side chains and backbone in a family of host-guest pentapeptides. *Biochemistry*, 35, 5109-5124.
- WIMLEY, W. C. & WHITE, S. H. (1992) Partitioning of tryptophan side-chain analogs between water and cyclohexane. *Biochemistry*, 31, 12813-12818.
- WIMLEY, W. C. & WHITE, S. H. (1993) Membrane partitioning: Distinguishing bilayer effects from the hydrophobic effect. *Biochemistry*, 32, 6307-6312.
- WIMLEY, W. C. & WHITE, S. H. (1996) Experimentally determined hydrophobicity scale for proteins at membrane interfaces. *Nature Structural Biology*, 3, 842-848.
- WINER, B. J. (1971) *Statistical Principles In Experimental Design*, New York, McGraw Hill, Inc.
- WOODS, M. C., HAILE, J. M. & O'CONNELL, J. P. (1986) Internal structure of a model micelle via computer simulation. 2. Spherically confined aggregates with mobile head groups. *Journal of Physical Chemistry*, 90, 1875-1885.
- XIANG, T. X., JIANG, Z. Q., SONG, L. & ANDERSON, B. D. (2006) Molecular dynamics simulations and experimental studies of binding and mobility of 7-tert-butyltrimethylsilyl-10-hydroxycamptothecin and its 20(S)-4-aminobutyrate ester in DMPC membranes. *Mol Pharm*, 3, 589-600.
- XIANG, T.-X. & ANDERSON, B. D. (1994) Molecular distributions in interphases: statistical mechanical theory combined with molecular dynamics simulation of a model lipid bilayer. *Biophysical Journal*, 66, 561-72.
- XIANG, T.-X. & ANDERSON, B. D. (1994) The relationship between permeant size and permeability in lipid bilayer membranes. *J Membr Biol*, 140, 111-22.
- XIANG, T.-X. & ANDERSON, B. D. (1994) Substituent contributions to the transport of substituted *p*-toluic acids across lipid bilayer membranes. *Journal of Pharmaceutical Sciences*, 83, 1511-18.
- XIANG, T.-X. & ANDERSON, B. D. (1995) Development of a combined NMR paramagnetic ion-induced line-broadening/dynamic light scattering method for permeability measurements across lipid bilayer membranes. *Journal of Pharmaceutical Sciences*, 84, 1308-15.
- XIANG, T.-X. & ANDERSON, B. D. (1997) Permeability of acetic acid across gel and liquid-crystalline lipid bilayers conforms to free-surface-area theory. *Biophysical Journal*, 72, 223-237.
- XIANG, T.-X. & ANDERSON, B. D. (1998) Influence of chain ordering on the selectivity of dipalmitoylphosphatidylcholine bilayer membranes for permeant size and shape. *Biophysical Journal*, 75, 2658-2671.

- XIANG, T.-X. & ANDERSON, B. D. (1999) Molecular dissolution processes in lipid bilayers: A molecular dynamics simulation. *Journal of Chemical Physics*, 110, 1807-1818.
- XIANG, T.-X. & ANDERSON, B. D. (2002) A computer simulation of functional group contributions to free energy in water and a DPPC lipid bilayer. *Biophysical Journal*, 82, 2052-66.
- XIANG, T.-X. & ANDERSON, B. D. (2006) Liposomal drug transport: A molecular perspective from molecular dynamics simulations in lipid bilayers. *Advanced Drug Delivery Reviews*, 58, 1357-1378.
- XIANG, T.-X., CHEN, X. & ANDERSON, B. D. (1992) Transport methods for probing the barrier domain of lipid bilayer membranes. *Biophysical Journal*, 63, 78-88.
- XIANG, T.-X., XU, Y. H. & ANDERSON, B. D. (1998) The barrier domain for solute permeation varies with lipid bilayer phase structure. *Journal of Membrane Biology*, 165, 77-90.
- YAMAZAKI, F., FUJIKI, K. & MURATA, Y. (1965) The ionization constants of organic compounds. I. The microscopic ionization constants of tyrosine and related compounds. *Bull Chem Soc Jpn*, 38, 8-12.
- YOON, I., SEO, K., LEE, S., LEE, Y. & KIM, B. (2007) Conformational study of tyramine and its water clusters by laser spectroscopy. *Journal of Physical Chemistry A*, 111, 1800-1807.
- ZHANG, J., KLEINODER, T. & GASTEIGER, J. (2006) Prediction of pKa values for aliphatic carboxylic acids and alcohols with empirical atomic charge descriptors. *J Chem Inf Model*, 46, 2256-66.

## Vita

Ravindra Wadhmal Tejwani (Ravi Tejwani)

Year of birth: 1971

Place of birth: Jalgaon, Maharashtra, India

### Educational Institutions and Degrees

- 1993 - 1996 Master of Science, Pharmaceutical Sciences, University of Mississippi  
Thesis: Effect of cyclodextrin complexation on solution and solid-state stability of cholecalciferol. Thesis Advisor: Christy M. Wyandt
- 1988 - 1992 Bachelor of Pharmacy, University of Poona

### Professional Positions Held

- 2007 - Present Senior Research Scientist, Bristol-Myers Squibb R&D, New Brunswick, NJ
- 2001 - 2007 Research Scientist, Bristol-Myers Squibb R&D, New Brunswick, NJ and Princeton, NJ
- 1997 - 2001 Associate Research Scientist, Bristol-Myers Squibb R&D, New Brunswick, NJ
- 1997 Analytical Chemist, Wyeth-Ayerst Lederle Laboratories, Perl River, NY
- 1994 - 1996 Research and Teaching Assistant, College of Pharmacy, University of Mississippi, University, MS; and Computer Consultant, Mississippi Center for Supercomputing Research, University, MS
- 1992 - 1993 Registered Pharmacist, Vikram Pharmacy, Jalgaon, Maharashtra, India
- 1991 Intern, Hoechst (India) Limited, Bombay, India

### Scholastic and Professional Honors

- 2007 AAPS Graduate Symposium in Drug Delivery and Pharmaceutical Technologies
- 2002 - 2006 Member, New York Academy of Sciences (NYAS)
- 1999 American Mensa Society
- 1996 The Rho Chi Pharmacy Honor Society
- 1996 Sigma Xi, The Scientific Research Society
- 1996 - Present Member, American Association of Pharmaceutical Scientists (AAPS)
- 1995 The Honor Society of Phi Kappa Phi
- 1995 Graduate Student Achievement Award, University of Mississippi
- 1995 and 1996 The National Deans List
- 1992 Registered Pharmacist, Maharashtra State Pharmacy Council
- 1989 - 1992 Mahindra Search For Talent Scholarships
- 1988 - 1992 Valedictorian of the class, College of Pharmacy
- Several Reviewer for abstract screening for the AAPS Annual Meeting
- Several Reviewer for the pharmaceutical journals: Journal of Pharmaceutical Sciences, International Journal of Pharmaceutics, and Pharmaceutical Research

### Professional Publications

- 2009 Ravi W. Tejwani, Terry R. Stouch, Bradley D. Anderson, "Substituent Effects on the Ionization and Partitioning of p-(Aminoethyl)phenols and Structurally Related Compounds. Electrostatic Effects Dependent on Conformation" *Journal of Pharmaceutical Sciences*, Accepted for publication (2009).
- 2008 Dilbir S. Bindra, Mandar V. Dali, Prakash V. Parab, Jatin M. Patel, Li Tao, Ravi W. Tejwani and Nipa Vatsaraj, "Pharmaceutical Formulation Containing An SGLT2 Inhibitor", filed on March 21, 2008 (Application numbers: WO/2008/116179 and PCT/US2008/057888).
- 2008 Johnson B.M., Kamath, A.V., Leet, J.E., Liu X., Bhide, R.S., Tejwani, R.W., Zhang, Y., Qian, L., Wei, D.D., Lombardo, L.J., Shu, Y.Z., "Metabolism of 5-Isopropyl-6-(5-methyl-1,3,4-oxadiazol-2-yl)-N-(2-methyl-1H-pyrrolo[2,3-b]pyridin-5-yl)pyrrolo[2,1-f][1,2,4]triazin-4-amine (BMS-645737): Identification of an Unusual N-Acetylglucosamine Conjugate in the Cynomolgus Monkey" *Drug Metabolism and Disposition*, Vol. 36, No. 12, p2475-2483 (2008).
- 2008 Rejean Ruel et. al. "Discovery and preclinical studies of 5-isopropyl-6-(5-methyl-1,3,4-oxadiazol-2-yl)-N-(2-methyl-1H-pyrrolo[2,3-b]pyridin-5-yl)pyrrolo[2,1-f][1,2,4]triazin-4-amine (BMS-645737), an in vivo active potent VEGFR-2 inhibitor" *Bioorganic and Medicinal Chemistry Letters*, Vol. 19, No. 9, p2985-2989 (2008).
- 2008 Ravi W. Tejwani, Bradley D. Anderson, "Influence of Intravesicular pH Drift and Membrane Binding on the Liposomal Release of a Model Amine-Containing Permeant" *Journal of Pharmaceutical Sciences*, Vol. 97, No. 1, p381-399 (2008).
- 2006 Potin, Dominique et. al. "Discovery and Development of 5-[(5S,9R)-9-(4-Cyanophenyl)-3-(3,5-dichlorophenyl)-1-methyl-2,4-dioxo-1,3,7-triazaspiro[4.4]non-7-yl-methyl]-3-thiophenecarboxylic Acid (BMS-587101) - A Small Molecule Antagonist of Leukocyte Function Associated Antigen-1" *Journal of Medicinal Chemistry*, Vol. 49, No. 24, p6946-6949 (2006).
- 2004 Hemant N. Joshi, Martha Davidovich, Ravi W. Tejwani, Vaishali P. Sahasrabudhe, Mohammed Jemal, Mohinder S. Bathala, Sailesh A. Varia, Abu T. Serajuddin, "Bioavailability Enhancement of a Poorly Water-Soluble Drug by Solid Dispersion in Polyethylene Glycol-Polysorbate 80 Mixture" *International Journal of Pharmaceutics*, Vol. 269, No. 1, p251-258 (2004).
- 2003 Yasutsugu Ueda, et. al. "Phosphonooxymethyl Prodrugs of the Broad Spectrum Antifungal Azole, Ravuconazole: Synthesis and Biological Properties" *Bioorganic & Medicinal Chemistry Letters*, Vol. 13, No. 21, p3669-3672 (2003).



- 2002 John J. Venit, Mandar V. Dali, Manisha M. Dali, Yande Huang, Charles E. Dahlheim, Ravi W. Tejwani, "Combretastatin A-4 Phosphate Prodrug Mono- and Di- Organic Amine Salts, Mono- and Di- Amino Acid Salts, and Mono- and Di- Amino Acid Ester Salts" Provisional United States Patent Application #60/251,921 filed on December 7, 2000, PCT International Application (2002), Patent number: WO 2002022626.
- 2000 Ravi W. Tejwani, Hemant N. Joshi, Sailesh A. Varia, and Abu T. Serajuddin, "Phase Behavior Of Polyethylene Glycol-Polysorbate 80 Mixtures And Polyethylene Glycol-Polysorbate 80-Water Mixtures" Journal of Pharmaceutical Sciences, Vol. 89, No. 7, p946-950 (2000).

Ravindra W. Tejwani